IRRIGATION MANAGEMENT AND SOILS AS CONTROLS ON DEEP PERCOLATION AND NITRATE LEACHING IN AGRICULTURAL SYSTEMS

by

Meghan Marie Robinson

A thesis submitted in partial fulfillment
of the requirements for the degree

of

Master of Science

in

Land Resources and Environmental Sciences

MONTANA STATE UNIVERSITY
Bozeman, Montana

August 2025

©COPYRIGHT

by

Meghan Marie Robinson

2025

All Rights Reserved

ACKNOWLEDGEMENTS

I am deeply grateful to my advisor Dr. Adam Sigler for his thoughtful and encouraging guidance from my undergrad days through the completion of this degree. His mentorship in designing research that answers interesting questions, thinking critically about data, and communicating to broader audiences has helped me grow as a scientist. I appreciate committee member Dr. Clain Jones whose insights on nutrient management and detailed feedback strengthened this work, and committee members Dr. Kent McVay and Dr. Jasmine Neupane for their questions, feedback, and perspectives on data that were beneficial in analyzing and interpreting results. Dr. Rob Payn's feedback was very helpful for modeling components of this work. Toby Koffman and Aneliya Cox (Environmental Analytical Lab) conducted water sample analysis that was critical for this project. Cooperating producers Mitch Konen, Bill Lee, and Travis Stuber made this research possible, and their curiosity to understand findings has made this work so much stronger. I also appreciate the NWARC faculty and staff, particularly Dr. Jessica Torrion and Jordan Penney, for being accommodating and supportive of our research. I appreciate the excellent support and general comradery from the MSUEWQ team: Bridget Warrenfeltz, Hendrick Moore, and Mathilda Haddock made the 2023 and 2024 field seasons successful and enjoyable; fellow grad students Hezekiah Afolabi, Raeya Gordon, and Nick Kiekover were all great helps with everything from field work to coding sessions; Gabrielle Jawer, Kyla Schrauben, Eric Castro, Jack Swanson, and Isaac Buttery all contributed to field and lab projects as well. This work was funded by the Montana Fertilizer Advisory Committee and the MSU College of Agriculture, with additional support from the Montana Water Center. I am extremely grateful to Mom, Dad, Erin, Ally, and friends for their constant love and support.

TABLE OF CONTENTS

1. INTRODUCTION 1
1.1: Background and Motivation for Work 1
Literature Cited 4
2. METHODS 6
2.1: Study Areas 6
2.1.1: Fairfield 6
2.1.2: Gallatin 8
2.1.3: Creston 9
2.2: Field Selections, Instrumentation, and General Methods 9
2.2.1: Field Location Selections 9
2.2.2: Instrumentation Overview 11
2.2.3: Hydrometer Analysis 13
2.3: Soil Water Sensor Assessment and Corrections 15
2.3.1: Gravimetric Water Comparisons 15
2.3.2: In-Field Sensor Comparisons 17
2.4: Lysimeters and Nitrate Measurements 19
2.4.1: Controls on Lysimeter Sample Success 19
2.4.2: Lysimeter and Soil Nitrate Comparison 21
2.5: Modeling Methods 25
2.5.1: Single Porosity Models 26
2.5.2: Dual Porosity and Dual Permeability Models 28
Literature Cited 44
3. PERCOLATION METRIC TO QUANTIFY SOIL WATER RESPONSE TO WATER INPUT ON IRRIGATED AGRICULTURAL FIELDS 48
Contribution of Authors and Co-Authors 48
Manuscript Information 49
Abstract 50
3.1: Introduction 51
3.2: Methods 54
3.2.1: Site Locations and Descriptions 54
3.2.2: Site Instrumentation and Irrigation Events 56
3.2.3: Percolation Metric Calculation 57
3.2.4: Precipitation Event Delineation 59
3.3: Results 60
3.3.1: Site Weather Context 60
3.3.2: Soil Water Content and Metric Results Across Soil Types 61

TABLE OF CONTENTS CONTINUED

3.3.3: Results Within Soil Types 63

3.4: Discussion 63
3.4.1: Irrigation Response Variability Across Soil Textures 63
3.4.2: Other Controls on Water Responses 65

3.5: Conclusions and Future Work 66

Literature Cited 81

4. SEASONAL SOIL CRACKING AND DYNAMIC NITRATE CONCENTRATIONS CONTROL DEEP PERCOLATION AND LEACHING IN AN IRRIGATED SYSTEM: IMPLEMENTING TIME VARIABLE SOIL HYDROLOGICAL PARAMETERS FOR PROBABILISTIC MODELING 86

Contribution of Authors and Co-Authors 86

Manuscript Information 87

Abstract 88

4.1: Introduction 89

4.2: Methods 95
4.2.1: Site Description and Field Management 95
4.2.2: Field Instrumentation and Sampling 97
4.2.3: Model Inputs and Time Variable Model Framework 99
4.2.4: Modeling Deep Percolation and Quantifying Nitrate Leaching 103

4.3: Results 105
4.3.1: Weather Context 105
4.3.2: Patterns in Soil Water Content 106
4.3.3: Lysimeter Nitrate Concentrations 107
4.3.4: Soil Nitrate Inventories 108
4.3.5: Inverse Modeling Parameter Distributions and Model Fits 110
4.3.6: Modeled Deep Percolation Results 112
4.3.7: Nitrate Leaching Estimates 113

4.4: Discussion 114
4.4.1: Seasonal Development of Soil Cracks Drives Variable Deep Percolation Risk 114
4.4.2: Time Variable Modeling Assessment 115
4.4.3: Deep Percolation Patterns and Implications for Water Use Efficiency 117
4.4.4: Variability in Nitrate Leaching Risk 118

4.5: Conclusions 121

Literature Cited 141

TABLE OF COTENTS CONTINUED

5. WATER AND NITROGEN USE EFFICIENCY IN LOW LEACHING RISK SYSTEMS- A GALLATIN VALLEY CASE STUDY 150
Contribution of Authors and Co-Authors 150
Manuscript Information 151
Abstract 152
5.1: Introduction 153
5.2: Methods 154
5.2.1: Site Descriptions, Equipment, and Field Visits 154
5.2.2: Modeling Methods 156
5.2.3: Water Use Efficiency and Nitrate Leaching 156
5.3: Results 157
5.3.1: Field Results 157
5.3.2: Modeling Results 160
5.4: Discussion 162
5.4.1: Limited Nitrate Leaching Risk in Silt Soil 162
5.5: Conclusions 165
Literature Cited 185
6. CONCLUSION 187
REFERENCES CITED 190
APPENDICES 206
SITE EQUIPMENT SUMMARIES 207
FAIRFIELD WEATHER PARAMETER VARIABILITY ASSESSMENT 210
GALLATIN WEATHER PARAMETER VARIABILITY ASSESSMENT 215

LIST OF TABLES

Table Page

1. Chp 2 - Table 1: Sites Instrumentation and Issues..... 32
2. Chp 2 - Table 2: Lysimeter sample relationship to VWC 33
3. Chp 3 - Table 1: Soils Across Sites. 68
4. Chp 3 - Table 2: Irrigation Summary Across Sites. 69
5. Chp 3 - Table 3: Precipitation Event Summary for NWARC 71
6. Chp 4 - Table 1: Mapped Soil Summary. 123
7. Chp 4 -Table 2: Irrigation Management Summary. 124
8. Chp 4 - Table 3: Inverse Modeling Summary.. 126
9. Chp 5 - Table 1: Monitoring Periods and Growing Season..... 167
10. Chp 5 -Table 2: Site Summary..... 168

LIST OF FIGURES

Figure Page

1. Chp 2 - Figure 1: Field and Sensor VWC Comparison.. 34

2. Chp 2 - Figure 2: RIR Field Sensor Comparison..... 35

3. Chp 2 - Figure 3: GSP Field Sensor Comparison. 36

4. Chp 2 - Figure 4: F121 Field Sensor Comparison.. 37

5. Chp 2 - Figure 5: Lysimeter Sample Successes.. 38

6. Chp 2 - Figure 6: Lysimeter Responses to VWC.. 39

7. Chp 2 - Figure 7: Lysimeter Installation Photos 40

8. Chp 2 - Figure 8: Comparison of Lysimeter and Nitrate Soil Pools..... 41

9. Chp 2 - Figure 9: Lysimeter and Nitrate Soil Pools by Depth 42

10. Chp 2 - Figure 10: Lysimeter Sphere of Influence. 43

11. Chp 3 - Figure 1: Site Map. 72

12. Chp 3 - Figure 2 Site Soil Textures.. 73

13. Chp 3 - Figure 3: Irrigation Response Example. 74

14. Chp 3 - Figure 4: Precipitation Event Delineation..... 75

15. Chp 3 - Figure 5: Monthly Precipitation and ET.. 76

16. Chp 3 - Figure 6: Study Location Comparison of VWC by Depth. 77

17. Chp 3 - Figure 7: All Sites 15 cm Comparison..... .78

18. Chp 3 - Figure 8: Metric Values Across Sites. 79

19. Chp 3 - Figure 9: Fairfield Metric by Antecedent Soil Water Content. 80

LIST OF FIGURES CONTINUED

20. Chp 4 - Figure 1: Fairfield Site Maps. 127

21. Chp 4 - Figure 2: Crop Coefficient Ratios Over 2024 Growing Season. 128

22. Chp 4 - Figure 3: Monthly Precipitation and Evapotranspiration..... 129

23. Chp 4 - Figure 4: Soil Water Content Irrigation Responses. 130

24. Chp 4 - Figure 5: Lysimeter Nitrate, No F121..... 131

25. Chp 4 - Figure 6: Lysimeter Nitrate, Including F121.. 132

26. Chp 4 - Figure 7: Soil Nitrate Profiles to 66 cm.. 133

27. Chp 4 - Figure 8: Inverse Model Predictions Over Time. 134

28. Chp 4 - Figure 9: Inverse Model Predictions Across Sites. 135

29. Chp 4 - Figure 10: Model Fit Summary..... 136

30. Chp 4 - Figure 11: Ranges of Deep Percolation Estimates..... 137

31. Chp 4 - Figure 12: Nitrate Leaching Estimates.. 138

32. Chp 4 - Figure 13: Licor and OpenET Compare.. 139

33. Chp 4 - Figure 14: Conceptual Water and Nitrate Movement..... 140

34. Chp 5 - Figure 1: Gallatin Field Sites.. 169

35. Chp 5 - Figure 2: Map of Gallatin Valley Silt Loams and Irrigation. 170

36. Chp 5 - Figure 3: Soil Water Content Responses for B23. 171

37. Chp 5 - Figure 4: Soil Water Content Responses for B24.. 172

38. Chp 5 - Figure 5: Soil Water Content Responses for T23. 173

39. Chp 5 - Figure 6: Soil Water Content Responses for T24. 174

40. Chp 5 - Figure 7: 2023 Lysimeter Nitrate Patterns. 175

41. Chp 5 - Figure 8: 2024 Lysimeter Patterns. 176

LIST OF FIGURES CONTINUED

42. Chp 5 - Figure 9: 2023 Soil Samples. 177

43. Chp 5 - Figure 10: 2024 Biweekly Soil Sampling. 178

44. Chp 5 - Figure 11: 2024 Early and Late Season Soil Samples. 179

45. Chp 5 - Figure 12: B23 Model Calibrations.. 180

46. Chp 5 - Figure 13: B24 Model Calibration and Deep Percolation.. 181

47. Chp 5 - Figure 14: T23 Model Calibration and Deep Percolation..... 182

48. Chp 5 - Figure 15: T24 Model Calibration and Deep Percolation..... 183

49. Chp 5 - Figure 16: B23 Runoff Assessment. 184

ABSTRACT

Water and nitrogen are critical resources for agricultural production, and managing for efficient water and nitrogen use has benefits for sustainable water resource management and water quality in addition to agricultural productivity. Deep percolation and nitrate leaching limit water and nitrogen use efficiency, and in irrigated systems, sustained periods with high soil water content result in higher risk of deep percolation and leaching losses. In this thesis, I address the question of how soil properties, weather, and irrigation management interact to control risk of deep percolation and leaching. Research was conducted in four fields of cooperating irrigators in western and central Montana. Soil water sensors and suction lysimeters were installed in fields to monitor water content and soil water nitrate concentrations. Modeling work with Hydrus 1D predicted deep percolation for study fields. Findings suggest that structured clay loam soils and sandy loam soils with high sand content had the highest infiltration rates across soil types studied. For clay loam soils, risk of deep percolation was variable throughout a growing season, controlled by the development of soil desiccation cracks. Peak periods of nitrate leaching varied based on how temporal patterns in nitrate concentrations interacted with deep percolation timing controlled by desiccation crack development. Leaching losses of 0.5-3 kg ha^{-1} were estimated for the clay loam study field in 2023, when nitrate concentrations were low during periods of peak deep percolation. Leaching losses were 5-17 kg ha^{-1} during 2024, when a slow-release fertilizer application resulted in prolonged periods with high nitrate concentrations. In silt loam soils cultivated for potatoes, infiltration was limited, and leaching risk was low. Runoff may present a larger challenge for water and nitrogen use efficiency than leaching, and fertilizer application timing appears to influence risk of non-growing season nitrate leaching. These results suggest that soil properties including texture and structure as well as irrigation and fertilizer management control water and nitrogen use efficiency. Temporal variability in soil structure is important to consider both for modeling efforts and for management to reduce the risk of deep percolation and leaching.

CHAPTER ONE

INTRODUCTION

1.1: Background and Motivation for Work

Water is a crucial resource that governs agricultural productivity and ecosystem processes while supporting human populations. Water management across uses is critical for supporting the growing population, and agricultural water management for adequate crop production is a particularly high priority (Mancosu et al., 2015). As the global population grows and diets shift, demands on agricultural productivity are increasing (van Dijk et al., 2021). Irrigated agriculture contributes approximately 40% of the food supply, and the Food and Agriculture Organization of the United Nations (FAO) estimates that over 250 million ha of land are irrigated globally (FAO, 2021). In Montana and many regions of the world, irrigation accounts for the largest consumptive water use, so understanding water use efficiency in irrigated systems is necessary to meet production demands within constraints of the limited water supply (Montana Department of Natural Resources and Conservation, 2015; Zhang et al., 2022). Erratic precipitation, changing patterns of rainfall and snow accumulation, and increased tendency towards drought all incentivize improved understanding of water management that is more efficient and resilient in the face of climate change (Wang, 2005).

Nitrogen is a limiting nutrient for crop productivity, and global nitrogen fertilizer applications have been estimated to exceed 100 Tg, with enhanced crop yields from synthetic fertilizers providing food for as much as half of the global population (Erisman et al., 2008).

Nitrate is mobile in soils and vulnerable to leaching losses with deep percolation, and agricultural nitrate leaching has been tied to climbing nitrate concentrations in groundwater (Puckett et al., 2011) and high nitrate concentrations in streams and rivers (Stets et al., 2015). In addition to water quality challenges resulting from nitrate leaching, high annual fertilizer expenses for producers creates an economic incentive for efficient nitrogen use and prevention of nitrate leaching. Understanding irrigation management controls on nitrate leaching risk can help preserve water quality and increase nitrogen use efficiency to benefit agricultural producers (Quemada et al., 2013).

Work presented in this thesis explores patterns and relative risk of deep percolation and nitrate leaching across a range of Montana's irrigated agricultural systems, with the goal of understanding controls on water and nitrogen use efficiency. This work is further motivated by Extension goals surrounding irrigation decision making support for producers. A 2019 United States Department of Agriculture (USDA) survey found that less than 5% of Montana irrigators use data sources such as soil water sensors for making irrigation decisions (USDA NASS, 2019). While irrigation and agricultural monitoring technologies can be marketed as though they inherently improve water use efficiency, new technologies can also be managed poorly, and positive outcomes are dependent on understanding data and implications for decisions (Levidow et al., 2014). Adoption of irrigation technologies that could improve water and nitrogen use efficiency is generally limited. Identified barriers include producers' lack of confidence in interpreting data relative to their observational knowledge and personal experience (Berthold et al., 2021), and a lack of adoption within communities that shows that new approaches may be beneficial (Genius et al., 2014). In this work, I hope to develop an

understanding of water and nitrogen dynamics across diverse systems, and to connect findings with statewide contexts irrigators work in to assist in decision making processes.

In this thesis, I aim to better understand drivers of deep percolation and nitrate leaching, particularly combinations of soil characteristics, weather, and irrigation management decisions that lead to the highest risk of leaching. I develop a readily calculatable metric for quantifying soil water content response patterns to identify when and where risk of deep percolation may be highest. I then asked how spatial and temporal patterns of deep percolation and nitrate leaching in a high-risk system can be identified and modeled to provide insights about periods of highest potential for losses. Finally, I examine a low nitrate leaching risk system and assess what other opportunities for water and nitrogen losses may exist, and what management controls may be most important for mitigating against leaching losses.

Literature Cited

Berthold, T. A., Ajaz, A., Olsovsky, T., & Kathuria, D. (2021). Identifying barriers to adoption of irrigation scheduling tools in Rio Grande Basin. *Smart Agricultural Technology*, *1*, 100016. https://doi.org/10.1016/j.atech.2021.100016

Erisman, J. W., Sutton, M. A., Galloway, J., Klimont, Z., & Winiwarter, W. (2008). How a century of ammonia synthesis changed the world. *Nature Geoscience*, *1*(10), 636–639. https://doi.org/10.1038/ngeo325

FAO. (2021). AQUASTAT- FAO's Global Information System on Water and Agriculture. Food and Agriculture Organization of the United Nations.

Genius, M., Koundouri, P., Nauges, C., & Tzouvelekas, V. (2014). Information Transmission in Irrigation Technology Adoption and Diffusion: Social Learning, Extension Services, and Spatial Effects. *American Journal of Agricultural Economics*, *96*(1), 328–344. https://doi.org/10.1093/ajae/aat054

Levidow, L., Zaccaria, D., Maia, R., Vivas, E., Todorovic, M., & Scardigno, A. (2014). Improving water-efficient irrigation: Prospects and difficulties of innovative practices. *Agricultural Water Management*, *146*, 84–94. https://doi.org/10.1016/j.agwat.2014.07.012

Mancosu, N., Snyder, R. L., Kyriakakis, G., & Spano, D. (2015). Water Scarcity and Future Challenges for Food Production. *Water*, *7*(3), Article 3. https://doi.org/10.3390/w7030975

Montana Department of Natural Resources and Conservation. (2015). *State Water Plan Regional Basin Plans*. https://dnrc.mt.gov/Water-Resources/Water-Planning-Implementation-and-Communications/State-Water-Plan-Regional-Basin-Plans/

Puckett, L. J., Tesoriero, A. J., & Dubrovsky, N. M. (2011). Nitrogen Contamination of Surficial Aquifers—A Growing Legacy. *Environmental Science & Technology*, *45*(3), 839–844. https://doi.org/10.1021/es1038358

Quemada, M., Baranski, M., Nobel-de Lange, M. N. J., Vallejo, A., & Cooper, J. M. (2013). Meta-analysis of strategies to control nitrate leaching in irrigated agricultural systems and their effects on crop yield. *Agriculture, Ecosystems & Environment*, *174*, 1–10. https://doi.org/10.1016/j.agee.2013.04.018

Stets, E. g., Kelly, V. j., & Crawford, C. g. (2015). Regional and Temporal Differences in Nitrate Trends Discerned from Long-Term Water Quality Monitoring Data. *JAWRA Journal of the American Water Resources Association*, *51*(5), 1394–1407. https://doi.org/10.1111/1752-1688.12321

USDA NASS 2019. 2018 Irrigation Water and Management Survey (United States Department of Agriculture). https://www.nass.usda.gov/Publications/AgCensus/2017/Online_Resources/Farm_and_Ranch_Irrigation_Survey/fris.pdf

van Dijk, M., Morley, T., Rau, M. L., & Saghai, Y. (2021). A meta-analysis of projected global food demand and population at risk of hunger for the period 2010–2050. *Nature Food*, *2*(7), Article 7. https://doi.org/10.1038/s43016-021-00322-9

Wang, G. (2005). Agricultural drought in a future climate: Results from 15 global climate models participating in the IPCC 4th assessment. *Climate Dynamics*, *25*(7), 739–753. https://doi.org/10.1007/s00382-005-0057-9

Zhang, K., Li, X., Zheng, D., Zhang, L., & Zhu, G. (2022). Estimation of Global Irrigation Water Use by the Integration of Multiple Satellite Observations. *Water Resources Research*, *58*(3), e2021WR030031. https://doi.org/10.1029/2021WR030031

CHAPTER TWO

METHODS

2.1: Study Areas

2.1.1: Fairfield

Extensive previous work on the Moccasin Terrace of the Judith River Watershed in central Montana identified nitrate leaching risk in dryland agricultural production systems. On the Moccasin terrace, thin cultivated soils over a shallow aquifer led to a steady increase in groundwater nitrate between 1994 and 2014 (Sigler et al., 2018, 2020, 2022). The Fairfield Bench in the Sun River Watershed was identified as a geologically parallel landform with relatively thin clay loam soils over a gravel layer and shallow aquifer (Vuke et al., 2002), with extensive irrigation rather than dryland farming as the primary contrast to the Moccasin Terrace study area. The Fairfield Bench, located in Teton County, is home to an 33,590 ha irrigation district that has supported primarily small grain production for over 100 years (Coleman et al., 2022). Top crops grown in Teton County were winter wheat (68,696 ha), barley (41,821 ha) alfalfa (28,715 ha), spring wheat (13,839 ha), and chickpeas (8,980 ha) in 2024 (USDA CropScape, 2024).

In contrast with the Moccasin Terrace, where mean nitrate-N concentrations of 20.4 mg L^{-1} have been reported (Sigler et al., 2018), groundwater nitrate concentrations on the Fairfield Bench are not as consistently and intensely elevated. Montana Department of Agriculture monitoring wells have detected nitrate in approximately 95% of water samples, with a median nitrate concentration of 5 mg L^{-1} and concentrations as high as 20 mg L^{-1} (Montana Department

of Agriculture, 2015). Relatively low groundwater nitrate concentrations likely do not reflect a lack of nitrate leaching, but rather that the augmented water inputs from irrigation dilute nitrate concentrations. Annual cycles in groundwater levels find that the water table is consistently highest during summer months, supporting the influence of irrigation on groundwater (Montana Bureau of Mines and Geology Research Well F-1). Landform nitrate exports may be higher relative to the Moccasin Terrace despite lower groundwater nitrate concentrations, due to larger water fluxes with irrigation water input.

Evidence of nitrate leaching is supported by signals of high nitrate in downstream surface water networks fed by springs generated on the Fairfield Bench (Water Quality Planning Bureau, Watershed Managment Section, 2004). The Sun River Watershed Group has conducted twenty years of stream monitoring in the Sun River Watershed and identified that nitrate-N concentrations near the Sun River's emergence from the mountain front and upstream of anthropogenic activities are consistently too low for detection (<0.1 mg L^{-1}). Muddy Creek, which drains the Fairfield Bench, has notably high nitrate-N concentrations including a median of 2.75 mg L^{-1} during baseflow periods when groundwater contributions are highest (Sigler, 2019). Muddy Creek has been estimated to contribute approximately 50% of the annual load of nitrate entering the Sun River each year (Sigler, 2011). The finding of high downstream nitrate concentrations, the geological similarities to a landform with previously identified high leaching risk, and the large community of irrigators in the irrigation district motivated work assessing questions around controls on nitrate leaching on the Fairfield Bench.

2.1.2: Gallatin

In the Gallatin Valley of southwestern Montana, rapid urbanization and the need to balance supporting residential, industrial, and agricultural activities creates challenges for water resource management and preservation of water quality. The USDA estimates that there are approximately 32,780 ha of irrigated lands in Gallatin County (USDA NASS, 2017), with top crops produced in the county including alfalfa (13,321 ha), winter wheat (8,244 ha), spring wheat (7,956 ha), barley (7,689 ha), and potatoes (1,940 ha) in 2024 (USDA CropScape, 2024). Irrigation return flows and ditch infrastructure have also been found to contribute to groundwater recharge and augment stream flow year-round (Kendy & Bredehoeft, 2006). Efforts to characterize groundwater nitrate in the Gallatin Valley suggest regions of heightened nitrate concentrations, with residential developments on septic systems implicated as the likely source in at least some areas (Sigler et al., 2024). While a variety of land uses likely contribute to groundwater nitrate in the Gallatin, understanding risk of agricultural leaching will support the preservation of groundwater resources needed by a growing population. The Montana Department of Environmental Quality has recognized total nitrogen impairments on Godfrey and Camp Creek watersheds, both of which drain irrigated landscapes where this research took place (Water Quality Planning Bureau, Watershed Managment Section, 2013). Work conducted in the Gallatin also provides the benefit of including silt loam soil textures, which differ from Fairfield Bench clay loams. Working in a broader range of soil and cropping system conditions is useful in accomplishing Extension goals of producing guidance that benefits a more diverse population of irrigators. This research and associated Extension work benefits from engagement with the Association of Gallatin Agricultural Irrigators, which advocates for acknowledgement of the

important role of irrigation in the watershed and creates connection to a network of local irrigators.

2.1.3: Creston

Research conducted in Creston takes advantage of the opportunity to work at Montana State University's Northwestern Agricultural Research Center (NWARC) with center pivot irrigation and active irrigation research. Top crops grown in Flathead County in 2024 were alfalfa (4,977 ha), winter wheat (3,753 ha), canola (3,270 ha), barley (1,626 ha) and spring wheat (1,362 ha) (USDA CropScape, 2024). Work at Creston was further motivated by its location in the Columbia River Basin, where the University of Montana recently received a grant from the US Environmental Protection Agency (EPA) to study pesticides in surface water and promote best management practices that reduce pesticide transport. Pesticide leaching questions are not specifically addressed in this thesis, but research on drivers of nitrate leaching have direct implications for controls on leaching risk of agrichemicals more broadly. Creston soils are sandy loams, and the only sand dominated soil across study locations, providing a range of soil textures that extends relevance of this work to more irrigators statewide.

2.2: Field Selections, Instrumentation, and General Methods

2.2.1: Field Location Selections

Research presented in this thesis was conducted in irrigated fields of cooperating producers and at NWARC. Across the 2023 and 2024 growing seasons, a total of six fields managed by four separate cooperators and spanning three watersheds of western and central Montana were instrumented and regularly visited for data collection. Broadly, the site locations

were chosen to represent a diverse subset of Montana's varied soil, climate, and agricultural systems. Field selections were motivated by locations that were relevant and interesting to our cooperators and broader networks of irrigators in local areas. Site locations within fields sought to replicate equipment within mapped soil units and irrigation treatments. All equipment was installed under center pivot irrigation systems.

Detailed descriptions for each study area are presented in chapters specific to locations and only a brief overview is provided here. The Fairfield study field was proposed by our cooperator as it is a consistently high yielding field with generally homogenous soils that might be most conducive for research. Soils at the field are mapped as Rothiemay-Niart clay loams or Varney-Rothiemay clay loams (map units 123B and 124B), which together account for roughly 35% of the area of the Fairfield Bench. A total of approximately 70% of all Fairfield Bench soils are clay loams, suggesting that field soils at the selected site are representative of the area's soils (Chp 4 - Figure 1). A total of six monitoring sites were installed at Fairfield, three under our cooperator's standard practice irrigation (grower standard practice, GSP), and three under a reduced, experimental irrigation rate (reduced irrigation rate, RIR). Gallatin Valley sites were installed in potato fields, as potatoes are the most economically lucrative crop for our cooperators and understanding in-field water and nitrogen dynamics in potato fields were of highest interest to them. Study sites were selected for fields where potatoes were grown in silt loam soils. Silt loam soils were prioritized because I estimated that roughly 55% of irrigated agricultural lands in the Gallatin Valley are on silt loams (Chp 5 - Figure 2). Potatoes are rotated in four- to five-year rotations to mitigate against disease risk, and equipment was moved between the 2023 and 2024 growing seasons to follow the potato rotations. Nine monitoring sites were

installed in the four fields instrumented over two years. The field at NWARC was chosen for its location under a center pivot and the ability to work in ‘production’ spring wheat, or wheat that is grown based on the farm manager’s standard management practices and is not part of any research station field trials. Four sites were installed, two of which were on sandy loam soils with 65% sand content, and which received the farm manager’s standard practice irrigation. The other two sites were installed on sandy loam soils with 75% sand content that were irrigated based on spatially variable evapotranspiration loss replacements under a research project conducted by the MSU Precision Agriculture Program.

2.2.2: Instrumentation Overview

At each field site, arrays of soil water sensors at 15, 30, and 90 cm below the ground surface were installed. For installations during 2024, 60-cm soil water sensors were also included. Soil water sensors used at all Fairfield sites that were installed during 2023 and Gallatin sites in both 2023 and 2024 were HOBO Decagon 10HS capacitance sensors connected to HOBO USB Microstations (Onset Computer Corp., Bourne, MA, USA). Sensors installed at two Fairfield sites in 2024 and all NWARC sites were METER Teros 12 (T12) volumetric water content, temperature, and electrical conductivity sensors connected to ZL6 Cellular Data Loggers (METER Inc, Pullman, WA, USA). Summaries of soil water sensors used at each site are included in Chp 2 - Table 1. Additionally, each monitoring site included suction lysimeters at 30 and 60 cm, installed with silica slurry to ensure direct soil contact (Prenart Equipment, Frederiksberg, Denmark). Manual rain gauges were mounted at a height of approximately one meter above ground surface on wood posts and were installed at most monitoring sites. Rain gauges were checked and emptied at each field visit, and mineral oil was added to prevent

evaporation. One off-field manual or tipping bucket (Onset Computer Corp., Bourne, MA, USA) rain gauge was also installed at Fairfield and Gallatin sites to provide a precipitation-only reading, enabling the partitioning of rain and irrigation from gauges under pivots. A weather station immediately adjacent to the study field at NWARC collected precipitation data which was used for this work. Plant cameras were installed at select monitoring locations in each field to track crop growth and irrigation events for the duration of growing seasons. In 2024 in Fairfield, a Licor-710 sensor (LI-COR Inc., Lincoln, NE, USA) tracked actual evapotranspiration (AET) at 30-minute intervals and was installed from May until November.

All field monitoring sites were installed based on methods from Sigler et al. (2020), to facilitate farmers' abilities to seed crops over equipment and to attain canopy closure over instruments. In small grain fields, soil pits were excavated, and equipment was installed before seeding to minimize crop disturbance. All data loggers were then stored in five-gallon buckets buried below the depth of expected disturbance from tillage and seeding operations. After seeding, buckets were dug out, and a second five-gallon bucket was attached to the top of the first to extend above the soil surface and allow equipment access throughout the season. The bucket system allowed other management such as fertilizer or pesticide application, irrigation, and harvest to occur with minimal disruption for cooperators. In potato fields, depths of soil disturbance for seeding and harvest were not conducive to presence of equipment, so equipment was installed after seeding and removed before harvest. Total numbers of monitoring sites per field ranged from two to six (Chp 2- Table 1).

Primary objectives during field visits were to collect lysimeter samples and soil samples, to download data from all loggers, and to make observations on crop rooting depth. Lysimeters

were evacuated to -60 kPa vacuum, then allowed to sit for 20-24 hours before samples were collected. Samples were filtered through 0.45-μm nylon syringe filters, then transported on ice and stored in a freezer until analysis. During the 2024 season, soil samples were collected by auger from 0-15 cm, 15-25 cm, 25-35 cm, 35-55 cm, and 55-66 cm at each biweekly field visit. Soil samples were collected at all established monitoring sites in Fairfield and at Gallatin Field T24. Soils were transported on ice and then frozen until drying and analysis. Root depths were estimated by digging up approximately 2-3 individual plants per monitoring site and recording the deepest observed root on each plant. Observations were also made by scraping back soil from auger faces and making observations on deepest visible roots. Root observations during the growing season were made to limited depths to minimize destruction of crops, resulting in an underestimation of rooting depths. After harvest when disturbance concerns were reduced, deeper holes were dug to observe maximum rooting depths. Earlier observations were then scaled up with a ratio of the depths observed using the two different methods at the end of the season.

2.2.3: Hydrometer Analysis

Subsets of collected soil samples from all sites were analyzed for particle size distribution using hydrometers (Gee & Bauder, 1986). Soil samples were not treated to remove organic matter or carbonates. Samples were ground to pass through a 2-mm sieve, then 40 g of sieved soil was mixed with 100 mL of 50 mg L^{-1} sodium hexametaphosphate solution. Soils were shaken for five minutes to mix and allowed to soak overnight for sodium dispersion of clay aggregates. Graduated cylinders filled with 700 mL of water were also allowed to sit overnight to thermally equilibrate with ambient temperature in the lab. Soil solutions were added to graduated

cylinders and thoroughly mixed with a plunger, and additional water was added to cylinders to bring the volume to 1000 mL. Immediately after mixing the graduated cylinder, a hydrometer was placed in the solution and a timer was started. Hydrometer readings were taken at 40 seconds (assumed time for sand to settle out) and 2 hours (assumed time for silt to settle out). For the duration of the experiment, a second hydrometer in a graduated cylinder with water and sodium hexametaphosphate only was observed to obtain a reading on water density for corrections. Percentages of sand, silt, and clay were then calculated using the following equation:

$$\%\ \text{Sand} = \frac{\text{Concentration soil } \left(\frac{\text{g}}{\text{L}}\right) - (\text{sand reading } (\frac{\text{g}}{\text{L}}) - \text{blank}(\frac{\text{g}}{\text{L}}))}{\text{Concentration soil } (\frac{\text{g}}{\text{L}})} * 100 \quad (2.1)$$

$$\%\ \text{Silt} = = \frac{\text{Concentration soil } \left(\frac{\text{g}}{\text{L}}\right) - (\text{silt reading } (\frac{\text{g}}{\text{L}}) - \text{blank}(\frac{\text{g}}{\text{L}}))}{\text{Concentration soil } (\frac{\text{g}}{\text{L}})} * 100 - \%\ \text{Sand} \quad (2.2)$$

$$\%\ \text{Clay} = 100 - \%\ \text{Sand} - \%\text{Silt} \quad (2.3)$$

Soil concentration refers to the mass of dry soil added to the one-liter solution. ‘Sand reading’ in Equation 2.1 refers to the hydrometer measurement at 40 seconds, which is the density of the solution in grams per liter with sand settled out and silt and clay fractions still suspended. ‘Silt reading’ in Equation 2.2 is the density of water with both sand and silt settled out, which is then corrected to isolate the silt fraction by subtracting the previously determined sand percentage. In Equations 2.1 and 2.2, the water and sodium hexametaphosphate blank density is subtracted from the density of the solution without the particle fraction of interest. With the whole solution volume being one liter, the density in grams per liter can be interpreted as a mass in grams of only silt and clay (Equation 2.1) or only clay (Equation 2.2), which can then be subtracted from and then divided by the total soil mass to determine the fraction of the particle size of interest. Remaining particle sizes were assumed to be clay (Equation 2.3).

2.3: Soil Water Sensor Assessment and Corrections

Data collected by soil water sensors are critical to understanding irrigation responses and for calibrating models. It is therefore necessary to understand sensor behavior and be able to interpret measured values in a context of possible over- or under-estimation of actual soil water content and other possible inaccuracies. In this section, volumetric water content (VWC) data from sensors deployed in the field compared with each other and gravimetric data.

2.3.1: Gravimetric Water Comparisons

During select field visits, soil samples were collected and analyzed gravimetrically to determine volumetric water content. Samples were collected by driving 15-cm long PVC pipe pieces into soils to obtain small soil cores of known volumes. Three replicate samples were collected at intervals centered on soil water sensor depths (15, 30, and 90 cm). Soil samples were stored in paper bags inside plastic bags to minimize evaporative losses. Wet samples were weighed as soon as possible after returning from the field and dried at 100 ˚C for 24 hours or until a subset of soil sample masses stabilized based on periodic weight checks. Soils were then re-weighed after drying to obtain the mass of water in each sample by difference. Water mass was converted to volume (1 g = 1 cm^3) and divided by the volume of the PVC pipes (188 cm^3) to calculate VWC. Water contents determined with these methods will be referred to as gravimetric-calculated VWC throughout the rest of this section. Field soil samples were collected at the time of equipment removal in the Gallatin in 2023 and 2024. The silt soils with virtually no coarse fragments at the Gallatin sites facilitated precision in volume of sample collection and low uncertainty in gravimetric assessment of VWC. Field samples were collected in Fairfield in November 2023; however, due to the high coarse fragment content, volumes were

extremely inconsistent and so Fairfield data for gravimetric-calculated VWCs are not included here.

Gravimetric-calculated VWCs were compared to the VWCs logged by respective HOBO soil water sensors to gauge sensor performance. Results from the Gallatin data suggest that HOBO sensors generally overestimated water content relative to gravimetric methods, which has also been found in previous lab setting studies (Visconti et al., 2014; Mittelbach et al., 2011). The range of gravimetric-calculated VWCs was approximately 0.15 to 0.32 cm^3 cm^{-3}, with corresponding sensor VWC values ranging between 0.26 and 0.35 cm^3 cm^{-3}. This means that HOBO sensors generally measure a higher range of water contents than is found by field methods (Chp 2 - Figure 1). Gravimetric-calculated VWCs and sensors measured VWCs aligned more closely at higher water contents and diverged at lower water contents. This is reflected in the regression equation between the gravimetric-calculated and sensor VWC data, which has a relatively flat slope of 0.43 indicating less change in sensor VWC for a given increase in gravimetric data. The intercept of 0.205 suggests that HOBO sensors would estimate a water content of 0.205 cm^3 cm^{-3} in oven dried soils, further suggesting the overestimation of water content. The slope and intercept for all data (not the replicate averages) show a similar pattern, though with more scatter. While most data do follow a similar regression model fit, more noise is introduced when three individual data points per HOBO sensor are considered. This may be a result of slight differences in volume of samples due to error in collection techniques, or very small-scale variability in water content across replicated samples.

2.3.2: In-Field Sensor Comparisons

In Fairfield during the 2024 growing season, both METER T12 sensors and HOBO Decagon 10HS sensors were installed in the same field. Both sensors use capacitance technology. Sensor arrays were not co-located but were in close proximity (60 m or less) to one another and received the same irrigation. Two sets of METER sensors were installed in the field in addition to four HOBO sets. One METER site and two HOBO sites were installed under the GSP irrigation, and the remaining one METER and two HOBO sites were installed under RIR irrigation. Sensor comparisons presented here use closest pairs of METER and HOBO equipment under the GSP and RIR irrigation rates. For the GSP, monitoring site F143 (METER equipment) and monitoring site F133 (HOBO equipment) were located roughly 60 m apart and are used for comparison. For RIR, site F128 (METER equipment) and F123 (HOBO equipment) were located roughly 30 m apart and are compared. To mitigate against variability in soil texture and structure that may become more pronounced with depth, only the 15 cm sensor readings were considered to attempt to isolate sensor variability rather than spatial soil heterogeneity to the extent possible.

Field based comparisons suggest that HOBO sensors measured higher absolute values for VWC than METER sensors; however, magnitudes of responses and dynamic ranges of observed VWCs were generally very similar between sensors (Chp 2 - Figure 2). The range of observed values for the 15-cm METER sensor at F143 was 0.108 (0.195 to 0.303) $cm^3\ cm^{-3}$, lower than the 0.12 (0.299 to 0.419) $cm^3\ cm^{-3}$ observed by the HOBO at F133. This indicates a slightly larger dynamic range for the HOBO relative to the METER sensor. The average soil water content response to the 1.65 cm of irrigation per pivot pass was 0.032 $cm^3\ cm^{-3}$ (3.2% increase) at F143, similar to the 0.022 at F133. The difference between sites in the experimental treatment

showed comparable patterns, with the F128 METER sensor measuring a dynamic range of 0.123 (0.249 to 0.372) cm^3 cm^{-3}, while the observed range of 0.132 (0.031 to 0.458 cm^3 cm^{-3}) at the F123 HOBO sensor was slightly higher. Changes in soil water content in response to irrigation were 0.02 cm^3/cm^{-3} at F123 and 0.014 cm^3/cm^{-3} at F128. At both pairs of sites, the METER sensors measured slightly smaller dynamic ranges and a generally lower absolute range of values. Differences between response magnitudes to irrigation across pairs of sites were not consistent.

Regressions between datasets from sensors suggest some degree of variability in sensor relationships over time, particularly across different irrigation events. This is most pronounced for the F123-F128 pairing. At F123-128, the slopes of lines generally increase over the season, suggesting that METER and HOBO magnitudes of change gradually became more similar as the season progressed (Chp 2- Figure 2). The standard treatment F143-F133 showed more consistent behaviors over time (Chp 2 - Figure 3). Linear model fit regression slopes range from 0.60 to 0.78, with intercepts ranging from -0.04 to 0.02, depending on which period of the season was regressed. These slopes and intercepts support the finding that dynamic range of METER sensors VWCs appears to be roughly 75% of HOBO sensors VWCs, and that HOBO sensors measure higher water content relative to METERs at all observed VWC conditions. This field data comparison is limited in that equipment is not co-located, creating the possibility that slightly different moisture conditions between sites may account for some observed variability.

Co-located sets of HOBO and METER sensors were deployed during the 2025 growing season for site F121. While 2025 data are generally not included in this thesis, this sensor pairing provides further insight into sensor relationships with reduced uncertainty from spatial

variability. Results from this pairing show similar patterns in higher range of absolute values measured by the 15 cm HOBO sensor relative to the METER sensor. The METER at F121 detected more and larger magnitude VWC responses to input precipitation and irrigation, which is in contrast with the F143-F133 and F128-F123 pairings that did not find clear patterns in response magnitude differences. The slope of the linear regression for co-located equipment at F121is 2.41, suggesting that METER sensors have a much larger dynamic range (Chp 2- Figure 4). Overall, while absolute VWC ranges measured by sensors differ, data do support that comparing differences in response magnitudes between METER and HOBO sensors has merit.

2.4: Lysimeters and Nitrate Measurements

Soil water nitrate concentrations were characterized with samples collected from suction lysimeters. Lysimeter sample collection success appeared to be affected by soil texture, soil structure, and installation procedures. In this section, lysimeter and soil sample nitrate concentrations are compared to assess whether soil sampling could be an alternate method for understanding nitrate dynamics at times or places where lysimeter sample collection is not possible.

2.4.1: Controls on Lysimeter Sample Success

Soil texture appears to be a primary control on lysimeter sample success, but installation details also influenced lysimeter sample collection abilities. Texture-based controls may include the effective volume of soil that can propagate vacuum and draw water samples to a lysimeter, the capillary strength at which water is held in soils (Weihermüller et al., 2007), and how readily water moves through soils to lysimeters. Chp 2 - Figure 5 depicts lysimeter sample successes

across all sites. Success rates are highest at Fairfield, where lysimeters collect samples close to 70% of the time. This is driven by both a high number of lysimeters collecting samples at a given visit, and a relatively long duration of the season over which lysimeters can collect water samples. I hypothesize that this high success is due to a combination of easy water movement through structured clay soils and high capacity for clays to propagate the applied vacuum. On the sandy loam soils at NWARC, water samples were successfully collected approximately 52% of the time. Like Fairfield, most lysimeters at NWARC did collect samples; however, sample collection became more limited earlier in the summer apparently due to faster drying of soils. Ease of water extraction from sand-dominated soils and their high infiltration capacity may contribute to high lysimeter success rates early in the season, under wetter conditions. Lowest lysimeter sample collection rates were observed in the Gallatin Valley silt loam soils, where lysimeters only collected samples approximately 25% of the time. Sample collection was generally limited to a few individual lysimeters that possibly had more favorable micro-environments from soil texture, topographic position, or possible macropores.

Soil water content may be used to predict lysimeter sample collection likelihood and sample size, but relationships vary across soils and across individual installations. Wetter conditions generally yielded larger lysimeter samples (Chp 2 - Figure 6 Chp 2 – Table 2). The necessary VWC conditions and thresholds for sample collection were determined based on linear regressions between soil water content and sample size (Chp 2- Table 2). Soil water content thresholds for sample collection varied roughly by texture, but differences in absolute VWC measurements among sensor manufacturers precludes direct comparison of all water content thresholds in Chp 2 - Table 2.

In addition to texture-based variability in lysimeter performance, installation methods also impacted sample collection ability. Equipment manuals suggest that during lysimeter installations, silica slurry should be poured into the pilot hole and then lysimeters should be inserted into the slurry. At four sites in Fairfield (indicated in Chp 2 - Table 1), installations were conducted with the lysimeter inadvertently inserted first, with slurry poured in afterwards. One of these incorrectly installed sites collected very few samples, so it was hypothesized that the lack of slurry resulted in poor contact between the lysimeter and the soil matrix, preventing sample collection. Adjustments to installation techniques were necessary in sandy loam soils at NWARC. The sandy soils appeared to drain water from the silica slurry quickly, resulting in a plug of silica rather than a pool that the lysimeter could penetrate. After observing rapid slurry drying for two initial installations at NWARC (indicated in Chp 2 - Table 1), which appeared to prevent lysimeters from fully inserting into slurry using standard methods, the installation approach was adjusted. A more dilute slurry with approximately 20% more water relative to silica flour was prepared, and speed of inserting lysimeters into the slurry was prioritized over maximizing the quantity of slurry deposited into the pilot hole. All lysimeters installed under this revised protocol collected at least one sample during following visits, whereas neither lysimeter installed with standard methods ever did. In 2025, these two non-collecting lysimeters were removed and re-installed, and as hypothesized there were plugs of hardened slurry at the tip of the lysimeter with almost no silica surrounding the lysimeters (Chp 2 - Figure 7).

2.4.2: Lysimeter and Soil Nitrate Comparison

Lysimeter samples and bulk soil samples were collected biweekly at each monitoring site for the duration of the 2024 growing season, with the intention of comparing soil and water

sample nitrate. Lysimeter samples from the 30 cm depth were compared to bulk soil samples from the 25-35 cm increment, and 60 cm lysimeter samples were compared to 55-66 cm bulk soil samples. Relationships between lysimeters and soil samples both with and without VWC corrections for lysimeter samples are considered. Not all 60-cm lysimeters had co-located soil water sensors, resulting in only a subset of data where VWC corrections are possible. Additionally, it was identified that HOBO sensors overestimate VWC, qualifying the extent to which absolute VWC numbers can be trusted and creating an opportunity for discrepancies in nitrate concentration estimates across soil water sensor types. For soils samples collected at depths and locations with soil water sensors, bulk soil sample nitrate inventories were converted to soil water nitrate concentrations. The soil samples were converted from a mass per area to mass per volume of soil based on the sampling depth increment (Equation 2.4), and then divided by the average VWC over the 24-hour lysimeter sample collection period to achieve a mass per volume of water (Equation 2.5), which enabled comparison with lysimeter samples:

$$\frac{\text{Soil } NO_3^- \text{ (kg)}}{\text{Soil area (ha)}} * \frac{1x10^{-8} \text{ ha soil}}{1 \text{ cm}^2 \text{ soil}} * \frac{1}{10 \text{ cm depth soil}} = \frac{\text{Soil } NO_3^- \text{ (kg)}}{\text{Soil volume (cm}^3\text{)}} \quad (2.4)$$

$$\frac{\text{Soil } NO_3^- \text{ (kg)}}{\text{Soil volume (cm}^3\text{)}} * \frac{\text{Soil volume (cm}^3\text{)}}{\text{Water volume (cm}^3\text{)}} * \frac{1x10^6 \text{ mg}}{1 \text{ kg}} * \frac{1 \text{ cm}^3}{1 \text{ mL}} * \frac{1000 \text{ mL}}{1 \text{ L}} = \frac{\text{Nitrate (mg)}}{\text{water volume (L)}} \quad (2.5)$$

The relationship between nitrate concentrations from the two sampling methods was weak, indicating that soil water nitrate and bulk soil nitrate are not strongly correlated (Chp 2 - Figure 8). The smallest lysimeter samples show the most scatter and the least correlation with bulk soil nitrate concentrations. The generally poor relationships could suggest differences in the bulk volume of soil influencing lysimeter samples, and/or the likelihood that lysimeters draw from only a fraction of all soil pore space, whereas soil samples include nitrate held in micropores.

Logarithmic models resulted in improved model predictive abilities over linear models for lysimeter and soil sample nitrate comparisons, suggesting that small changes in lysimeter nitrate may be correlated with larger changes in bulk soil nitrate. Logarithmic models fit to non-VWC normalized lysimeter data have positive intercepts, implying that lysimeters continue to detect nitrate when bulk soil samples fall to zero. Lysimeter nitrate concentrations corrected for variable VWCs have a lower intercept and higher R^2 values, indicating that some of the poor model fit between non-VWC normalized lysimeter samples and bulk soil may be due to variability in water content. Corrections for VWC may be particularly relevant for more highly concentrated nitrate in lysimeter samples during dry periods. When separating comparisons based on sample collected depth, possible slight differences in model slopes emerged; however, relationships were generally weak and so it is inconclusive whether relationships between nitrate extracted by lysimeters and bulk nitrate vary with depth (Chp 2 – Figure 9). Nitrate concentrations estimated based on soil samples were generally much higher than those estimated by lysimeters, indicating that more nitrate is stored in pore space that is inaccessible to lysimeters at the applied vacuum (-60 kPa).

For relatively small lysimeter samples (~<3 mL), I hypothesize that one explanation for poor agreement between sampling approaches is that the soil volume from which the water samples were drawn was not representative of the 10 cm soil sample increment where the bulk sample was collected. Smallest water samples likely represent conditions more immediately adjacent to the lysimeter. For these small lysimeter samples, VWCs of the soils generally ranged from 0.234 to 0.308. For a lysimeter sample that is 3 mL, collected when VWC was initially 0.234 cm^3 cm^{-3} and assuming water content in the sphere of influence was drawn down to near

wilting point (~0.08 cm^3 cm^{-3}), the volume of soil needed to produce the sample (or the sphere of influence) is 19 cm^3. Interactions between the assumed sample size of 3 mL and assumed reduction in VWC as a result of the sample collection produced a range of sphere of influence scenarios from 22 to 214 mL, which are small relative to the 360 mL of soil collected (Chp 2 - Figure 10).

Another possible explanation for poor agreement between nitrate contents from different sampling approaches is that lysimeters collect water from different pore size fractions within the bulk soil and hence only collect a fraction of total nitrate stored in soil. The -60 kPa of applied vacuum is a relatively low tension in comparison to force exerted by roots, and by soils at wilting point (-1500 kPa). This may suggest that nitrate stored deeper in soil aggregates or with more tightly held water and is not readily captured by lysimeters. An implication of this finding is that treating lysimeter sample collection and bulk soil sample collection as interchangeable methods for understanding nitrate dynamics may not be appropriate. Lysimeter samples might be more characteristic of loosely held water which may be more susceptible to leaching, supporting the methodological approach of using suction lysimeters to understand solute leaching risk. Lysimeter samples likely do not capture all available nitrate. Bulk soil sampling may be a preferred method for understanding total nitrate inventories and assessing nitrogen use efficiency in instances where total quantities of nitrate in a soil relative to inputs and crop uptake information is needed.

2.5: Modeling Methods

To characterize the movement of water through soil and to estimate deep percolation and associated nitrate leaching rates, I used Hydrus 1D soil water modeling software (Šimůnek et al., 2013). Hydrus solves Richard's equation for unsaturated water flow through a porous substrate:

$$\frac{\partial \theta}{\partial t} = \frac{\partial}{\partial z}\left[K\left(\frac{\partial h}{\partial z} + 1\right)\right] - S \qquad (2.5)$$

Where θ is the volumetric water content of the soil ($cm^3\ cm^{-3}$), z is depth from the soil surface (cm), h is the pressure head (cm), $K()$ is the hydraulic conductivity for a given pressure head (cm d^{-1}), and S is a sink term representing root uptake ($cm^3\ cm^{-3}\ day^{-1}$).

Hydrus 1D was used to estimate deep percolation, runoff, and evapotranspiration for given meteorological conditions, irrigation schedules, and soil hydrologic parameters. Modeling enables the exploration of alternate irrigation schedules or variable water fate outcomes based on different soil parameters and weather years. It also allows quantification of possible deep percolation or runoff losses relative to irrigation and precipitation inputs to understand water use efficiency and leaching risk. Input boundary conditions for models include daily precipitation and Penman-Monteith estimated potential evapotranspiration (PET) from nearby Montana Climate Office Mesonet weather stations, and irrigation amounts and timing from cooperating producers. Crop rooting depth and the extent of canopy closure, crop water use coefficients for adjusting PET, and evaporation and transpiration partitioning were based on field observations and growing degree day-crop growth models (Allen et al., 2006). Soil profiles were described with van Genuchten parameters derived from soil texture characteristics and soil depths based on field observations and mapped soils. Soil samples collected at initial field visits were analyzed using standard hydrometer techniques (described in Chp 2.2.3), then van Genuchten parameters

were estimated with pedotransfer functions provided through the Rosetta neural network (Schaap et al., 2001) based on percentages of sand, silt, and clay from hydrometer analysis. Observation nodes for tracking water content over time were added to the Hydrus soil profile at the depths of field soil water sensors to compare between models and field data.

Field data were used for calibration and validation on model performance. For model calibration, data from the deepest soil water sensors (90 cm), which are best poised to characterize soil water dynamics associated with deep percolation (the primary objective for modeling), were used as opposed to shallower sensors that characterize dynamics associated with water input, evaporation, and root uptake. For 2024 in Fairfield, Hydrus predicted actual evapotranspiration (AET) were compared with field measured AET from the Licor 710. The R^2, root mean square error (RMSE) and Nash Sutcliffe Efficiency (NSE) (Nash & Sutcliffe, 1970) were calculated for each model. The NSE is widely used in hydrology and compares the model error to the variability within the dataset, and was the primary metric used for assessing model performance. NSE values range from -infinity to positive one. A model with an NSE greater than zero indicates that magnitudes of error are less than observational variation, and an NSE of one would be a perfect model fit. Model validation was primarily conducted with assessment of similarities in overall water budgets between field measurements and model predictions.

2.5.1: Single Porosity Models

In Hydrus 1D, multiple modeling options are available for characterizing water flow through soils. Single porosity refers to model types that assume all water transport occurs as equilibrium water flow through a soil matrix that can adequately be described by one soil water retention curve (Šimůnek et al., 2013). Single porosity models require six soil hydrological

parameters to describe water movement and retention: θr, θs, *alpha*, *n*, *l*, and *Ks*. θ_r is the residual water content of a soil at approximately -1500 kPa, or equivalent to the water that is most tightly bound to soil particles that cannot be removed by root extraction or gravity (commonly referred to as wilting point). θ_s is the saturated water content, equal to the porosity of a soil. *Alpha* is an empirical parameter related to the air entry value for a soil, or the matric pressure at which a soil drops below saturation. *N* is an empirical parameter based on pore size distribution that controls how sensitive changes in water content are to changes in matric pressure (Jiang et al., 2010). *L* is an empirical parameter linked to the tortuosity of soil pore networks, but is suggested to be treated as a constant value of 0.5 (van Genuchten, 1980). These parameters describe how water is retained in soils, and *Ks*, or the saturated hydraulic conductivity, describes the speed of water percolation through saturated soils. These parameters will be referred to as van Genuchten (VG) parameters throughout this methods section.

Single porosity models are beneficial due to their low complexity and relative ease of parameterization. Pedotransfer functions such as the Rosetta neural network used by Hydrus connect readily measured soil physical parameters such as texture or bulk density with more complex soil hydrological properties (Schaap et al., 2001). The Rosetta software in Hydrus allows users to estimate VG parameters used for single porosity models based on soil texture class, percentages of sand, silt, and clay in a soil sample, or with additional information including bulk density and known water contents at -1500 or -33 kPa. This makes single porosity an approachable method that can quickly be applied to scenarios of interest, even without complete knowledge of soil behavior. Single porosity models have high functionality in Hydrus and can be used for estimation of water flow and solute transport. In instances where preferential

flow is not a dominant factor for water movement, these models may predict water behavior with high accuracy (Šimůnek et al., 2013).

One major disadvantage to using single porosity models is the lack of incorporation of preferential flow that occurs in structured soils. Water moving through inter-aggregate macropores, earthworm tunnels, root channels, or soil cracks cannot be described by equilibrium flow for a single domain that is inherent in the assumptions of single porosity (Gerke & van Genuchten, 1993). For models based on soils were macropores have an important impact, single porosity models may fail to capture soil water content responses and underestimate water moving deep into a soil profile (Jarvis, 2007).

In this thesis, an assessment of the functionality of single porosity models is presented for Gallatin silt loam soils in Chapter 5. The silt loam soils were not observed to have any extensive structure or aggregation. This may be driven by a combined lack of structure development in soils with low clay content and soil disturbance from potato cultivation related activities. VG parameters for the Gallatin silt loams were derived from Rosetta predictions based on the percent sand, silt, and clay with bulk density as an additional factor. Details on model calibration and performances are included in Chapter 5.

2.5.2: Dual Porosity and Dual Permeability Models

Single porosity models are limited by their lack of capacity to model preferential flow. In Hydrus 1D, dual porosity and dual permeability models can be used to overcome these limitations. Dual porosity models assume two separate soil-water domains, including immobile soil matrix zones in which water can be stored but does not move, and mobile regions of macropore flow where water does move (Šimůnek et al., 2003). A coefficient characterizing the

exchange rate between the immobile matrix and the mobile macropores is central to the dual porosity model framework. Dual permeability models also assume two separate but interacting regions for the soil matrix and macropores; however, unlike dual porosity, water is mobile in both domains. Water is assumed to move slowly through the soil matrix and quickly through macropores (Šimůnek et al., 2003). A benefit to these two-region models is the simulation of water movement through macropores, which is necessary in some structured soils. Additionally, dual permeability models allow for separate water budgets and water flux modeling for the soil matrix and macropores.

Dual porosity and permeability models do have some drawbacks as well. Both models require more extensive parameters, eleven for dual porosity and seventeen for dual permeability. This makes parameterization more complex, and parameters for macropores can be difficult to obtain in field settings. The assumption that water is immobile in the soil matrix in dual porosity models is also limiting, in that upward potentiometric water movement is not possible. The lack of upwards water movement may be physically unrealistic, especially for fine textured soils.

Dual porosity model parameters include five VG parameters for the soil matrix (θ_r, θ_s, *alpha*, *n*, and *l*; *Ks* is excluded), five VG parameters for macropores including saturated hydraulic conductivity (θ_r, θ_s, *alpha*, *n*, and *Ks*; *l* is excluded), and a water transfer term between the soil matrix and macropores (ω) (Šimůnek et al., 2003). Dual permeability models are described with all six VG parameters for the soil matrix (θ_r, θ_s, *alpha*, *n*, *1*, and *Ks*), all six parameters for macropores, and a set of parameters to describe the interface of soil aggregates and macropore space. These parameters are *Ka*, or the hydraulic conductivity at the aggregate surface, *a*, or the average diffusion length of a soil aggregate, *beta*, or descriptor of macropore

geometries (where 15 is spherical), *gamma*, a scaling factor generally set to 0.4, and *w*, or the weight of macropores in the whole soil (Gerke & van Genuchten, 1993). In this thesis, the single porosity model is used for the relatively unstructured Gallatin silt loam soils and the dual permeability model is used for the more structured Fairfield clay loam soils. While this thesis does not include model results for the Creston sandy loam soils, it seems that a single porosity model is likely to be effective for those soils. Data and code for this chapter are available on Hydroshare (Robinson & Sigler, 2025).

Site	Field	Date Installed	Date Removed	Soil Water Sensor Depths (cm)	Soil Water Sensor Type	Notes
F113	Fairfield	2023-04-15	NA	15, 30, 90	HOBO	Sensor failures in 2024, Lysimeters installed incorrectly
F121	Fairfield	2023-06-29	NA	15, 30, 90	HOBO	Barley destroyed in 2023, Co-located METER and HOBO sensors in 2025
F123	Fairfield	2023-04-15	NA	15, 30, 90	HOBO	Lysimeters installed incorrectly
F128	Fairfield	2024-04-20	NA	15, 30, 60, 90	METER	
F133	Fairfield	2023-04-15	NA	15, 30, 90	HOBO	Sensor failure in 2024 at 90 cm
F143	Fairfield	2024-04-21	NA	15, 30, 60, 90	METER	
TC_North	Gallatin T23	2023-06-26	2023-09-13	15, 30, 90	HOBO	‘Experimental’ fertilizer treatment
TC_South	Gallatin T23	2023-06-21	2023-09-12	15, 30, 90	HOBO	‘Experimental’ fertilizer treatment
TT_Arable	Gallatin T23	2023-06-26	2023-09-13	15, 30, 90	HOBO	Kinks in lysimeter tube observed at removal, ‘standard’ fertilizer treatment
B_West	Gallatin B23	2023-06-07	2023-09-13	15, 30, 90	HOBO	
B_East	Gallatin B23	2023-06-07	2023-09-13	15, 30, 90	HOBO	Kinks in lysimeter tube observed at removal

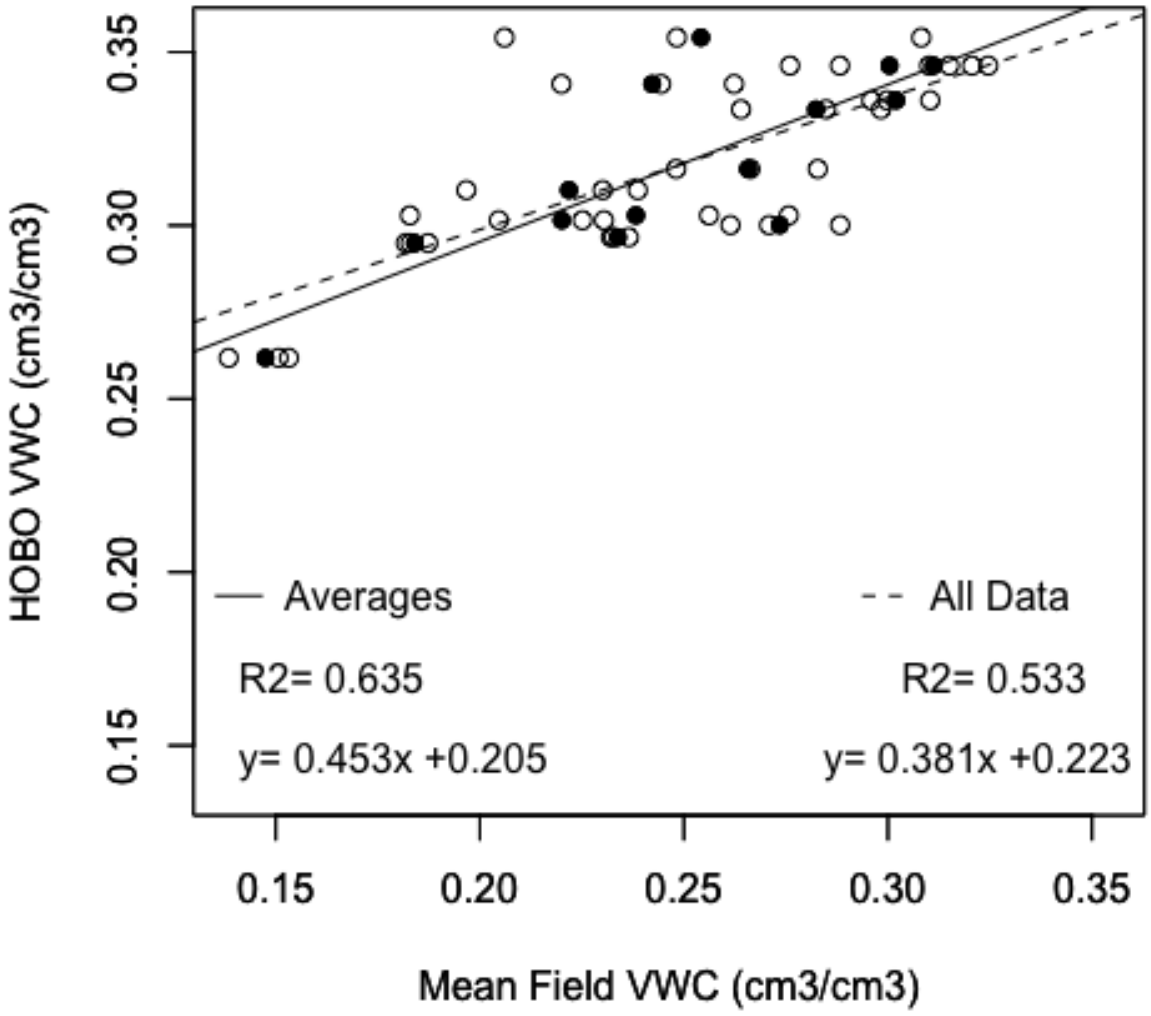
Chp 2 – Table 1 Continued.

Site	Field	Date Installed	Date Removed	Soil Water Sensor Depths (cm)	Soil Water Sensor Type	Notes
T191	Gallatin T24	2024-06-19	2024-09-14	15, 30, 90	HOBO	
T208	Gallatin T24	2024-06-19	2024-09-14	15, 30, 90	HOBO	Gaps in lysimeter backfill observed at removal, sensor failure issues
B10	Gallatin B24	2024-06-11	2024-09-14	15, 30, 90	HOBO	No lysimeters
B30	Gallatin B24	2024-06-11	2024-09-14	15, 30, 90	HOBO	No lysimeters, sensor failure issues
R5-01-350	NWARC	2024-04-04	NA	15, 30, 60, 90	METER	
R5-01-028	NWARC	2024-04-04	NA	15, 30, 60, 90	METER	Not sand method lysimeter installs
R5-07-002	NWARC	2024-04-04	NA	15, 30, 60, 90	METER	
R5-07-008	NWARC	2024-04-04	NA	15, 30, 60, 90	METER	

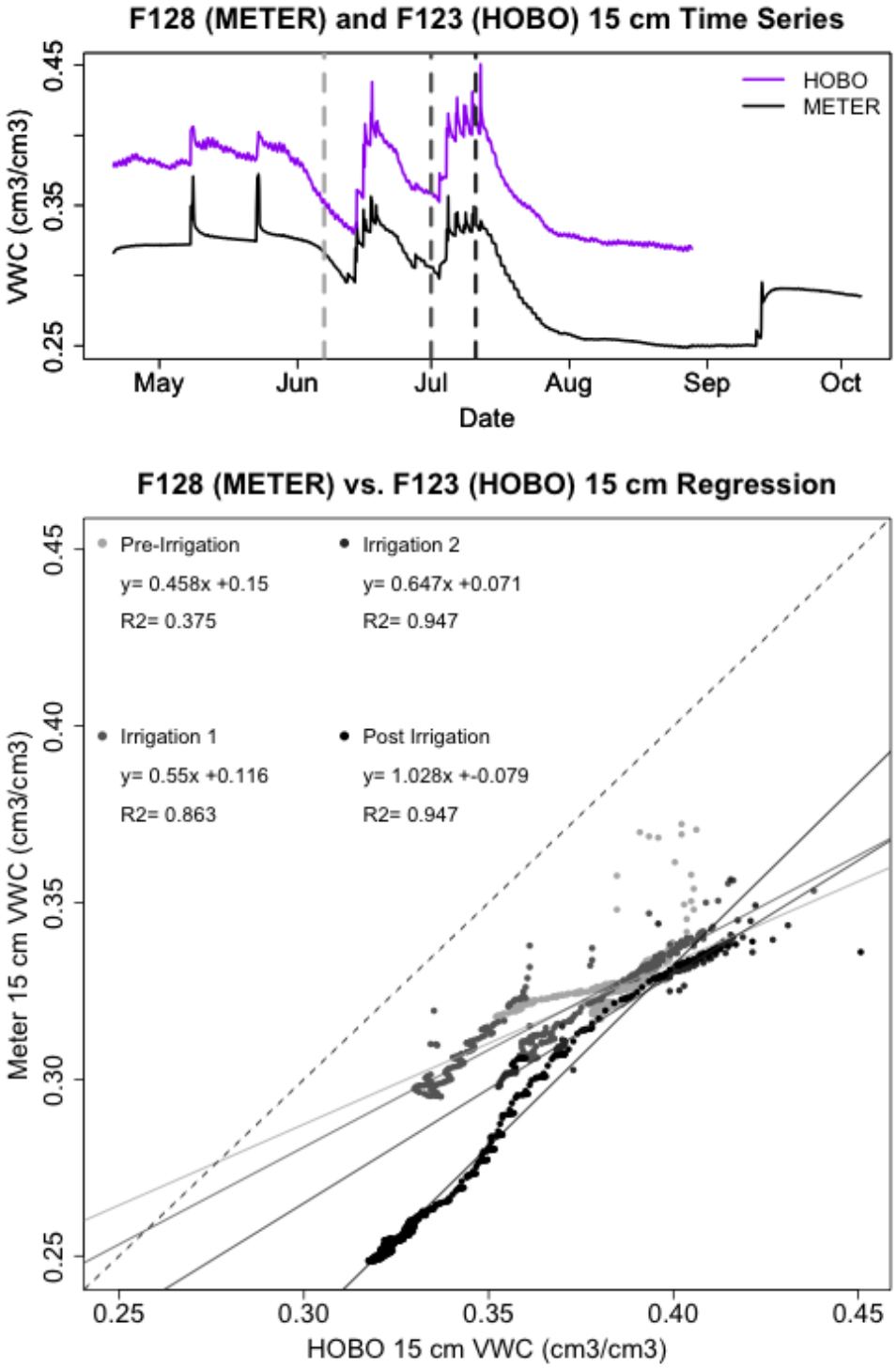
Chp 2 - Table 1: Sites Instrumentation and Issues. Site names, study locations, installation dates, soil water sensor depths (cm), instrument manufacturer, and sensor issues for all monitoring sites. NA in the ‘Date Removed’ column indicates sensors are still installed.

Lysimeter	Sample Collection Threshold (VWC)	Sample Volumes vs.VWC (mL / 1% VWC increase)
F113 30 cm*	0.30	13.7
F121 30 cm*	0.35	6.08
F123 30 cm*	0.34	5.05
F128 30 cm	0.26	9.12
F128 60 cm	0.28	2.74
F133 30 cm*	0.37	3.25
F143 60 cm	0.22	0.91
TT Arable 30 cm*	0.36	4.43
TC North 30 cm*	0.33	14.1
R5-01-350 30 cm	0.13	0.93
R5-01-350 60 cm	0.15	2.61
R5-07-002 30 cm	0.16	1.7
R5-07-008 30 cm	0.13	0.33
R5-07-008 60 cm	0.13	2.51

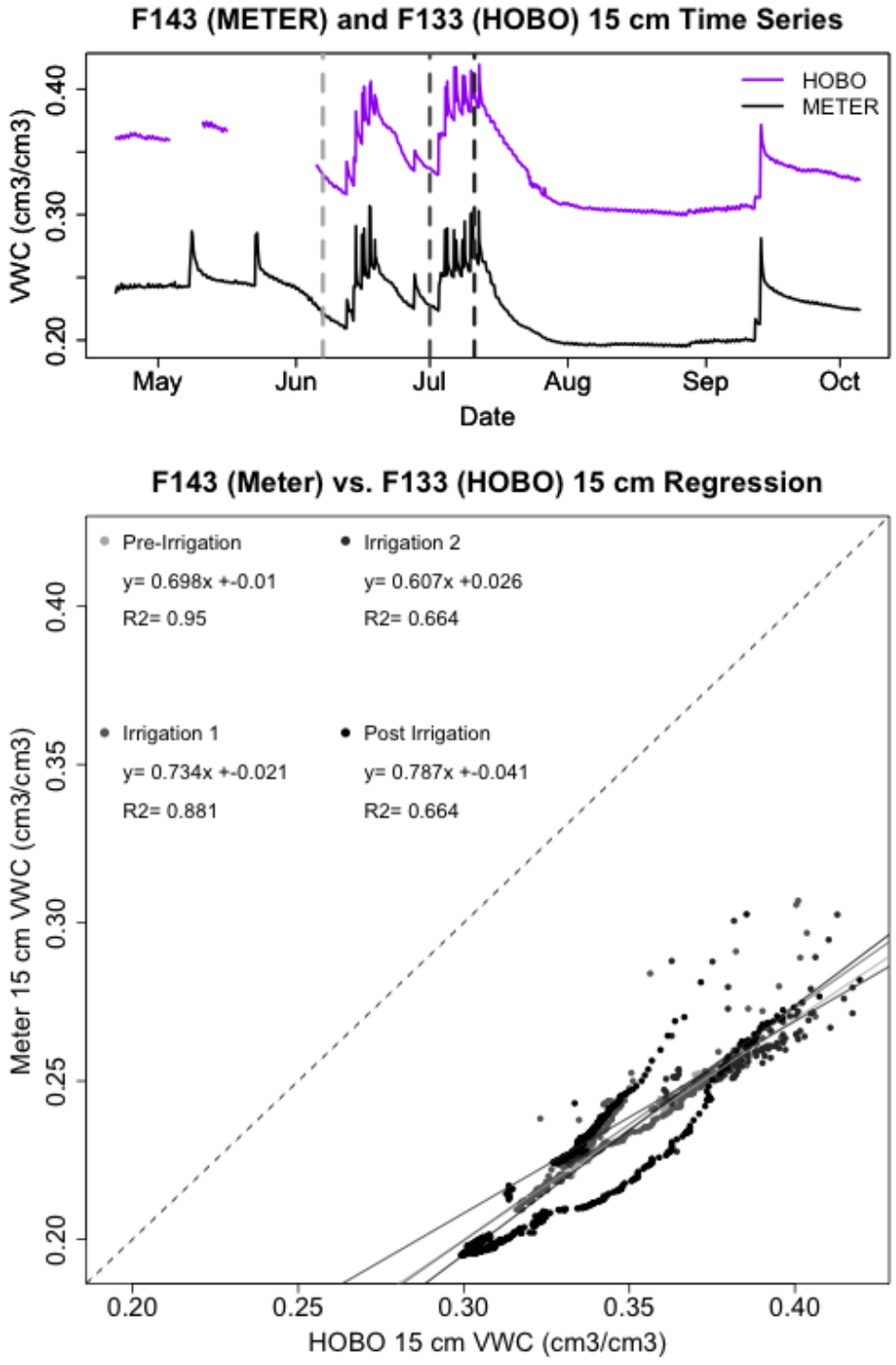
Chp 2 - Table 2: Lysimeter sample relationship to VWC. 'Lysimeter' describes the site location (full details in Chp 2 – Table 1) and depth. The 'Sample Collection Threshold' is the VWC value below which lysimeters did not produce samples. 'Sample Volume vs. VWC is the expected increase in sample volume (mL) for a 1% increase in VWC (slope of regression lines). Sites are only included in the table if more than three lysimeter samples were collected from the site. Stars indicate VWC is from HOBOs.



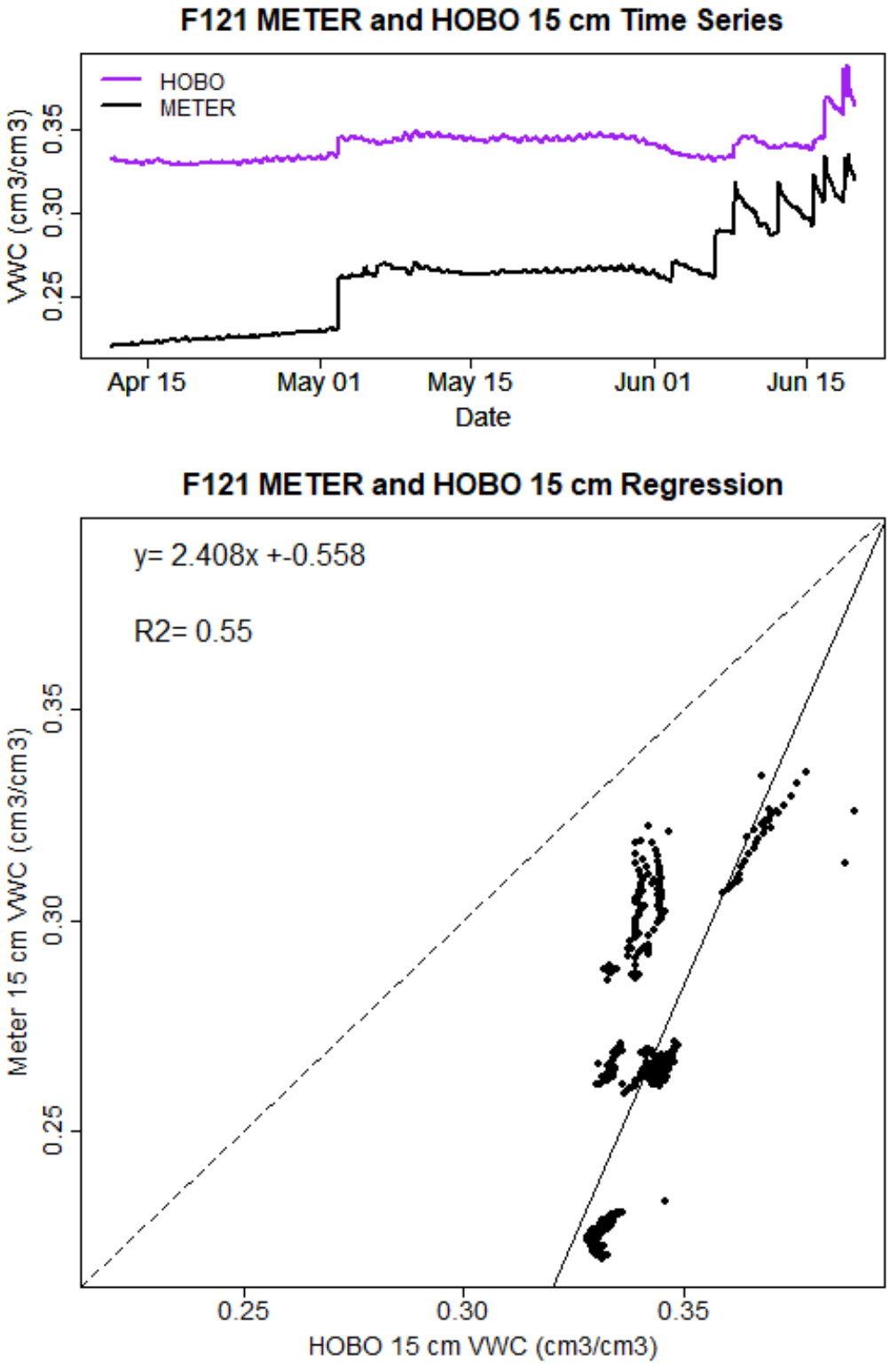
Chp 2 - Figure 1: Field and Sensor VWC Comparison. Field collected gravimetric water samples and HOBO sensor volumetric water content for Gallatin field sites in 2023. Open circles are individual replicates for gravimetric samples, closed dots are averages.



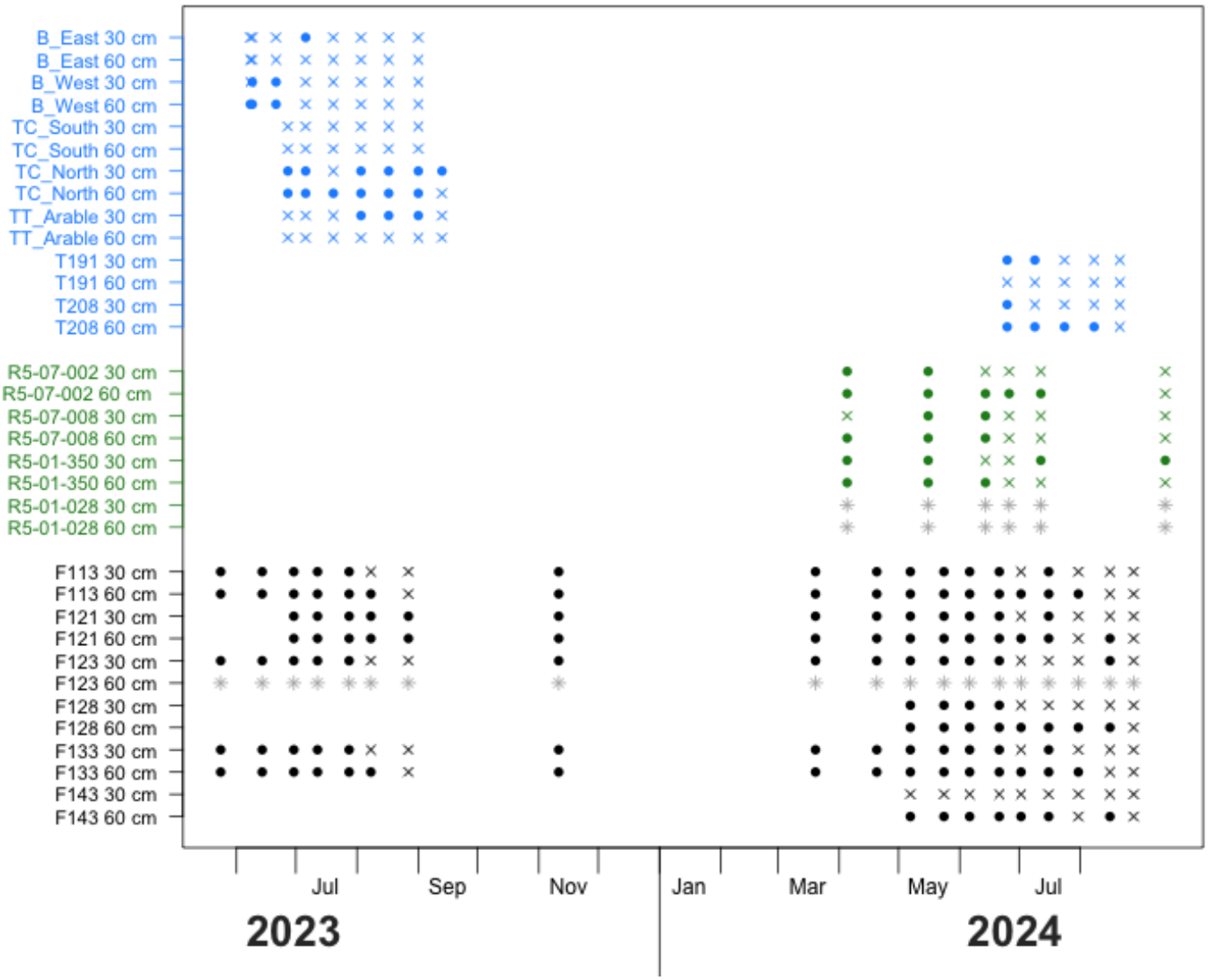
Chp 2 - Figure 2: RIR Field Sensor Comparison. Time series and regressions between HOBO and METER data for GSP sites F128 and F123. HOBO data is purple line in time series, METER is black line. Regressions are separated by time period, and darker grays and blacks are later in the summer. Data are from 2024.



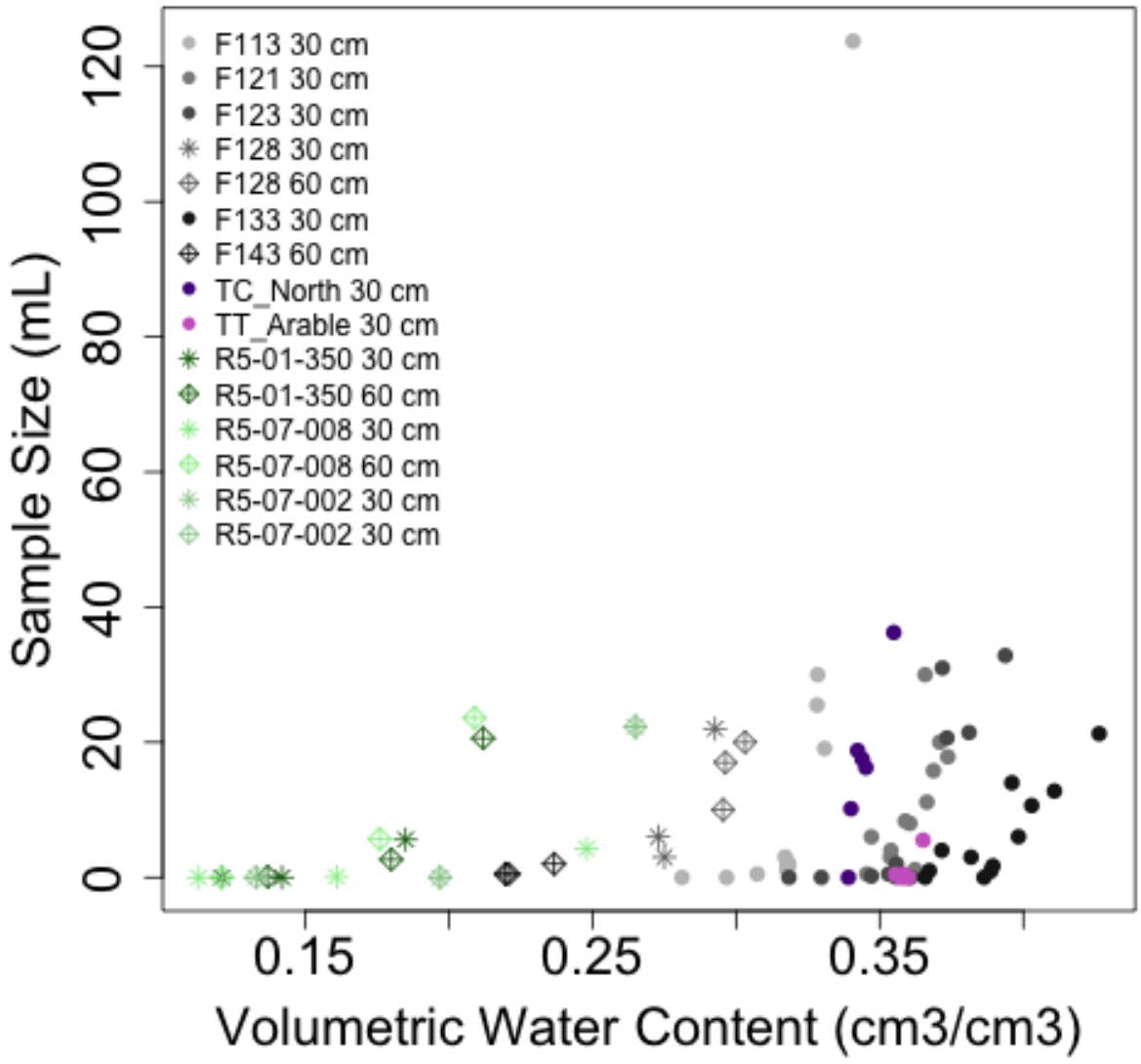
Chp 2 - Figure 3: GSP Field Sensor Comparison. Identical to Chp 2 – Figure 2, though comparing RIR sites F133 (HOBO) and F143 (METER). Data are from 2024.



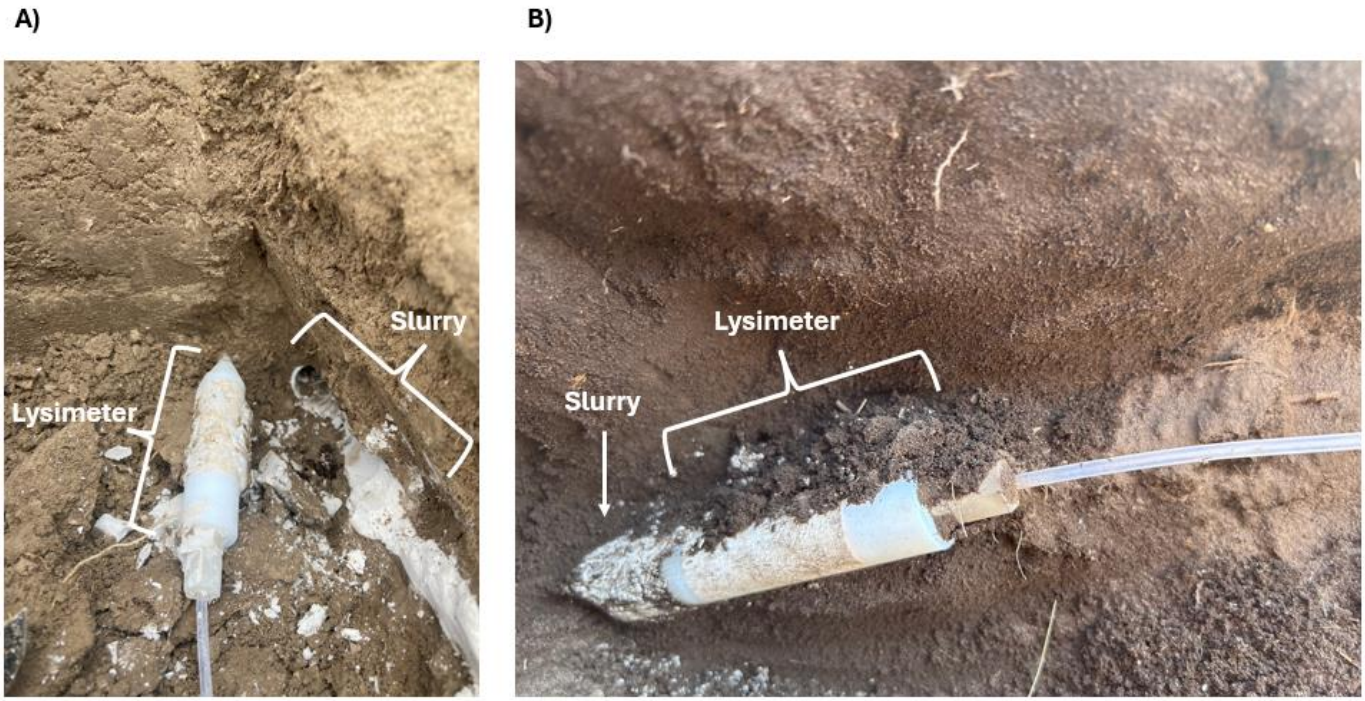
Chp 2 - Figure 4: F121 Field Sensor Comparison. Identical to Chp 2 – Figure 2, though comparing collocated equipment at site F121 during 2025.



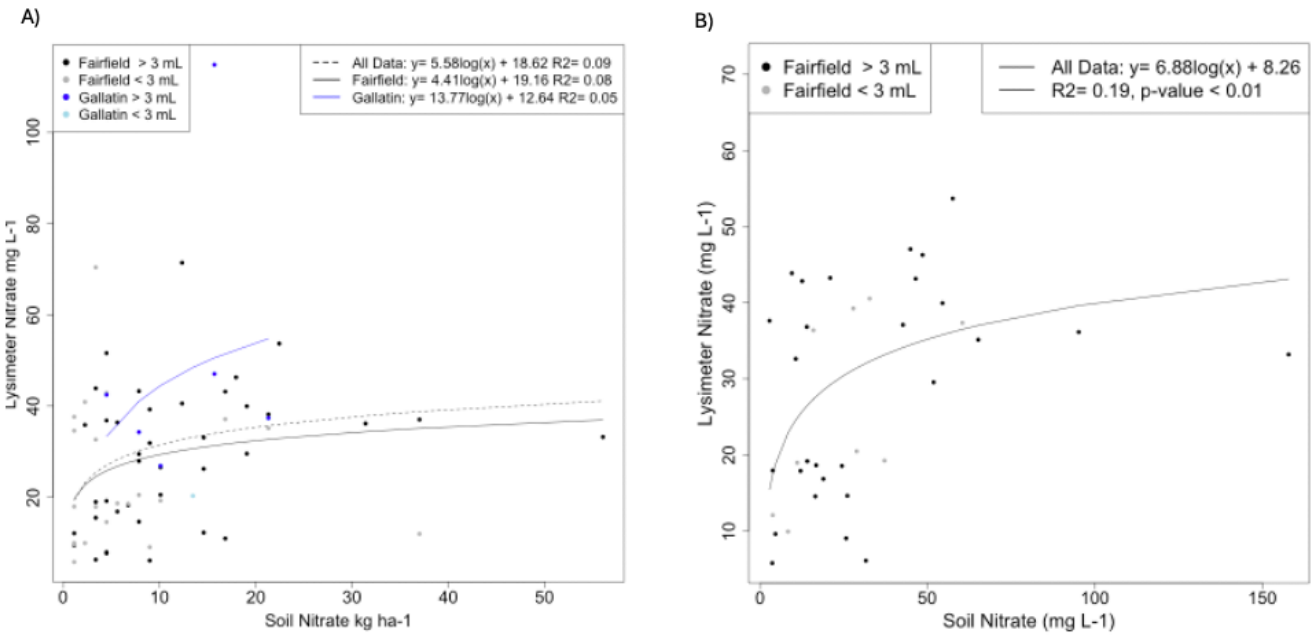
Chp 2 - Figure 5: Lysimeter Sample Successes. Closed points indicate a sample was collected, Xs indicate lysimeters were put under vacuum and no sample was collected. Vertical lines are field visits, horizontal lines are individual lysimeters. Black points are Fairfield (clay loam), blue points are Gallatin (silt loam) and green points are Creston (sandy loam) lysimeters. Light gray asterisks indicate sites with poor installations where no or very few samples were collected.



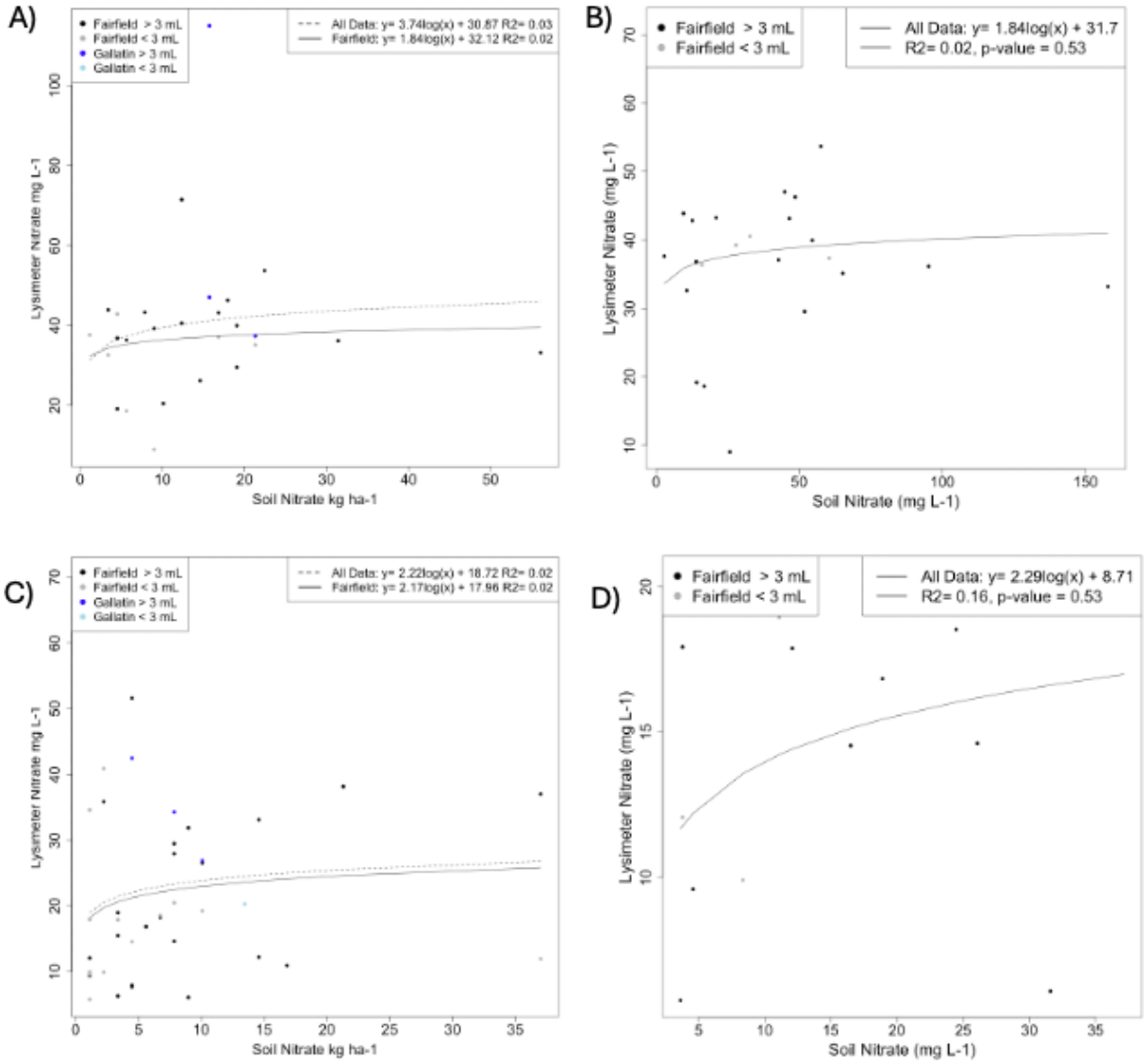
Chp 2 - Figure 6: Lysimeter Responses to VWC. Solid dots represent VWC from HOBO sensors, other symbols are VWC from METER sensors. Gray sites are Fairfield, purple sites are Gallatin, and green sites are Creston. Summaries of regression information are included in Chp 2 - Table 2.



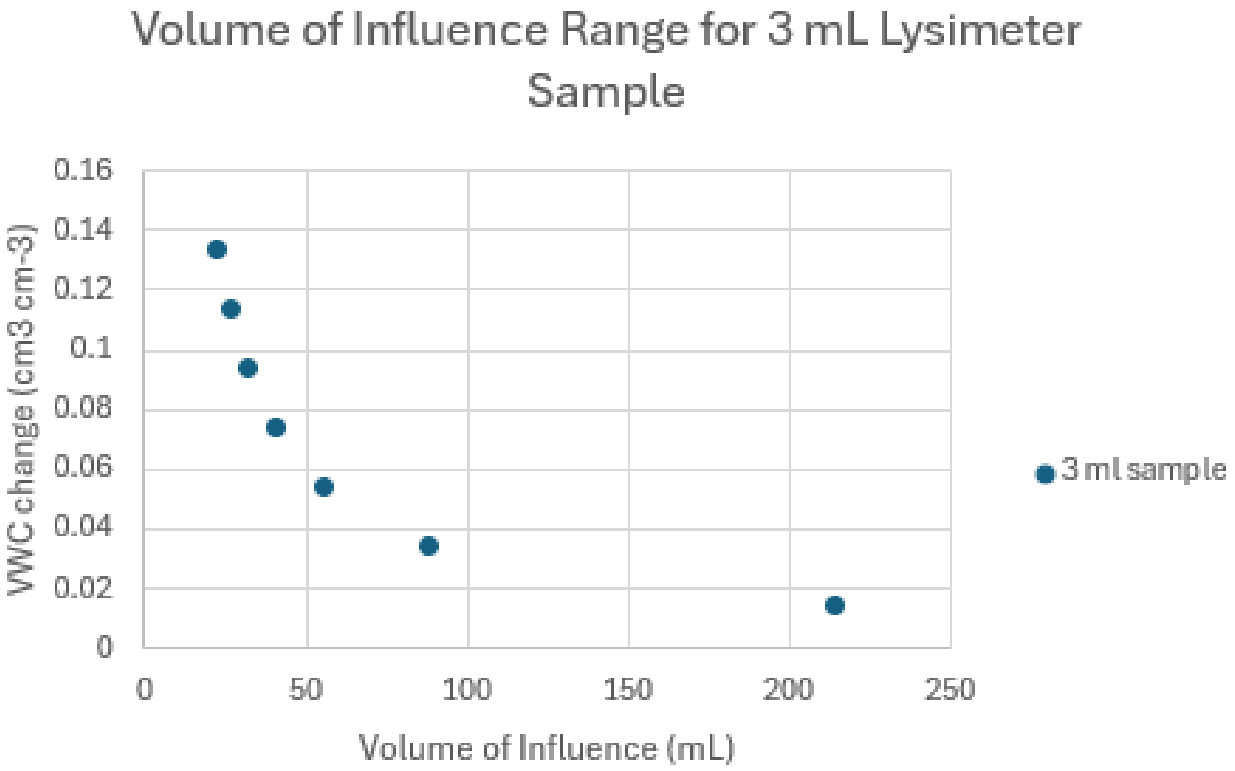
Chp 2 - Figure 7: Lysimeter Installation Photos. A) Lysimeter installed correctly with silica slurry filling area around lysimeter. B) Lysimeter installed without sand-adjusted techniques in Creston sandy loam soils. Lysimeter is not surrounded by slurry, but above a hardened block of slurry.



Chp 2 - Figure 8: Comparison of Lysimeter and Nitrate Soil Pools. Soil sample from 25-35 cm and lysimeter sample from 30 cm or soil sample from 55-66 cm and lysimeter sample from 60 cm for A) All data without VWC corrections applied and B) Data with VWC corrections applied, fewer points reflects that not all lysimeters had collocated soil water sensors. Black points are from Fairfield, blue points are from the Gallatin, and light grey or blue points indicate lysimeter samples were smaller than 3 mL.



Chp 2 - Figure 9: Lysimeter and Nitrate Soil Pools by Depth. A) Lysimeter and soil nitrate without VWC corrections for 30 cm lysimeters and 25-25 cm soil samples. B) Lysimeter and soil nitrate with lysimeters corrected for VWC for 30 cm lysimeter samples and 25-35 cm soil samples. C) Lysimeter and soil nitrate without VWC corrections for 60 cm lysimeters and 55-66 cm soil samples. D) Lysimeter and soil nitrate with VWC corrections for 60 cm lysimeters and 55-66 cm soil samples.



Chp 2 - Figure 10: Lysimeter Sphere of Influence. The volume from which water is extracted for a 3 mL lysimeter sample based on assumed drawdown in water content.

Literature Cited

Allen, R., Pereira, L. S., Raes, D., & Smith, M. (2006). *FAO Irrigation and Drainage Paper No. 56*.

Coleman, T., Boyd, K., Thatcher, T., & Sain, R. (2022, June). *Muddy Creek Master Plan*. https://static1.squarespace.com/static/6014bb1a9820e37481af89b6/t/62bb8583163e3f2f643eed6e/1656456599529/Muddy+Creek+Master+Plan+FINAL++06+28+2022.pdf

Gee, G. W., & Bauder, J. W. (1986). Particle-size Analysis. In *Methods of Soil Analysis* (pp. 383–411). John Wiley & Sons, Ltd. https://doi.org/10.2136/sssabookser5.1.2ed.c15

Gerke, H. H., & van Genuchten, M. T. (1993). A dual-porosity model for simulating the preferential movement of water and solutes in structured porous media. *Water Resources Research, 29*(2), 305–319. https://doi.org/10.1029/92WR02339

Jarvis, N. J. (2007). A review of non-equilibrium water flow and solute transport in soil macropores: Principles, controlling factors and consequences for water quality. *European Journal of Soil Science*, *58*(3), 523–546. https://doi.org/10.1111/j.1365-2389.2007.00915.x

Jiang, S., Pang, L., Buchan, G. D., Šimůnek, J., Noonan, M. J., & Close, M. E. (2010). Modeling water flow and bacterial transport in undisturbed lysimeters under irrigations of dairy shed effluent and water using HYDRUS-1D. *Water Research*, *44*(4), 1050–1061. https://doi.org/10.1016/j.watres.2009.08.039

Kendy, E., & Bredehoeft, J. D. (2006). Transient effects of groundwater pumping and surface-water-irrigation returns on streamflow. *Water Resources Research*, *42*(8). https://doi.org/10.1029/2005WR004792

Mittelbach, H., Casini, F., Lehner, I., Teuling, A. J., & Seneviratne, S. I. (2011). Soil moisture monitoring for climate research: Evaluation of a low-cost sensor in the framework of the Swiss Soil Moisture Experiment (SwissSMEX) campaign. *Journal of Geophysical Research: Atmospheres*, *116*(D5). https://doi.org/10.1029/2010JD014907

Montana Department of Agriculture. (2015). *Groundwater Monitoring for Pesticides and Nitrate in Greenfield Bench, Montana; Summary of Findings 1992-2015*. https://agr.mt.gov/_docs/groundwater-docs/GWR_GreenfieldBench1992-2015Final.pdf

Nash, J. E., & Sutcliffe, J. V. (1970). River flow forecasting through conceptual models part I — A discussion of principles. *Journal of Hydrology*, *10*(3), 282–290. https://doi.org/10.1016/0022-1694(70)90255-6

Robinson, M., W. A. Sigler (2025). Irrigation Management and Soils as Controls on Deep Percolation and Nitrate Leaching in Agricultural Systems: Thesis Data and Code, HydroShare, https://doi.org/10.4211/hs.2d6042efdc7944288ce486ae9a58da9e

Schaap, M. G., Leij, F. J., & van Genuchten, M. Th. (2001). rosetta: A computer program for estimating soil hydraulic parameters with hierarchical pedotransfer functions. *Journal of Hydrology*, *251*(3), 163–176. https://doi.org/10.1016/S0022-1694(01)00466-8

Sigler, W. A. (2011, January). *Upper Muddy Creek Water Quality Investigation 2010*.

Sigler, W. A. (2019, December 12). *Sun River Watershed Group Volunteer Monitoring Program Nutrient Data Summary*. https://static1.squarespace.com/static/6014bb1a9820e37481af89b6/t/619bcb0b5836c344bd16fd0c/1637600011621/2019+12+09+SunNutrientTrendReportFinal.pdf

Sigler, W. A., Ewing, S. A., Jones, C. A., Payn, R. A., Brookshire, E. N. J., Klassen, J. K., Jackson-Smith, D., & Weissmann, G. S. (2018). Connections among soil, ground, and surface water chemistries characterize nitrogen loss from an agricultural landscape in the upper Missouri River Basin. *Journal of Hydrology*, *556*, 247–261. https://doi.org/10.1016/j.jhydrol.2017.10.018

Sigler, W. A., Ewing, S. A., Jones, C. A., Payn, R. A., Miller, P., & Maneta, M. (2020). Water and nitrate loss from dryland agricultural soils is controlled by management, soils, and weather. *Agriculture, Ecosystems & Environment*, *304*, 107158. https://doi.org/10.1016/j.agee.2020.107158

Sigler, W. A., Ewing, S. A., Wankel, S. D., Jones, C. A., Leuthold, S., Brookshire, E. N. J., & Payn, R. A. (2022). Isotopic signals in an agricultural watershed suggest denitrification is locally intensive in riparian areas but extensive in upland soils. *Biogeochemistry*, *158*(2), 251–268. https://doi.org/10.1007/s10533-022-00898-9

Sigler, W., Kiekover, N., Roemmich, T., Dougher, F., & Krahn, B. (2024). *Gallatin County Groundwater Nitrate and Water Levels* [Dataset]. HydroShare. https://doi.org/10.4211/hs.7346a1e37bb04090bf8d8c1f5a4e2a4b

Šimůnek, J., Jarvis, N. J., van Genuchten, M. Th., & Gärdenäs, A. (2003). Review and comparison of models for describing non-equilibrium and preferential flow and transport in the vadose zone. *Journal of Hydrology*, *272*(1), 14–35. https://doi.org/10.1016/S0022-1694(02)00252-4

Šimůnek, J., Šejna, M., Saito, H., Sakai, M., & van Genuchten, M. Th. (2013, June). *The HYDRUS-1D Software Package for Simulating the One-Dimensional Movement of Water, Heat, and Multiple Solutes in Variably-Saturated Media: Version 4.17*. Department of Earth Sciences, University of California Riverside. chrome-extension://efaidnbmnnnibpcajpcglclefindmkaj/https://www.pc-progress.com/Downloads/Pgm_hydrus1D/HYDRUS1D-4.17.pdf

USDA National Agricultural Statistics Service (NASS), 2024, Cropland Data Layer, Accessed 2025-06-20 at https://nassgeodata.gmu.edu/CropScape.

USDA NASS, 2017. 2017 Census of Agriculture County Profile: Gallatin County Montana. (United States Department of Agriculture). https://www.nass.usda.gov/Publications/AgCensus/2017/Online_Resources/County_Profiles/Montana/cp30031.pdf

van Genuchten, M. Th. (1980). A Closed-form Equation for Predicting the Hydraulic Conductivity of Unsaturated Soils. *Soil Science Society of America Journal*, *44*(5), 892–898. https://doi.org/10.2136/sssaj1980.03615995004400050002x

Visconti, F., de Paz, J. M., Martínez, D., & Molina, M. J. (2014). Laboratory and field assessment of the capacitance sensors Decagon 10HS and 5TE for estimating the water content of irrigated soils. *Agricultural Water Management*, *132*, 111–119. https://doi.org/10.1016/j.agwat.2013.10.005

Vuke, S., Colton, R., & Fullerton, D. (2002). *Geologic Map of the Great Falls North 30’ x 60’ Quadrangle, Central Montana*. Montana Bureau of Mines and Geology. https://www.mbmg.mtech.edu/pdf_100k/greatFallsN-text.pdf

Water Quality Planning Bureau, Watershed Managment Section. (2004). *Water Quality Restoration Plan and Total Maximum Daily Loads for the Sun River Planning Area*. Montana Department of Environmental Quality. https://deq.mt.gov/files/Water/WQPB/TMDL/PDF/Sun/M13-TMDL-01a.pdf

Water Quality Planning Bureau, Watershed Managment Section. (2013). *Lower Gallatin Planning Area TMDLs & Framework Water Quality Improvement Plan*. Montana Department of Environmental Quality. https://deq.mt.gov/files/water/wqpb/CWAIC/TMDL/M05-TMDL-02a.pdf

Weihermüller, L., Siemens, J., Deurer, M., Knoblauch, S., Rupp, H., Göttlein, A., & Pütz, T. (2007). In Situ Soil Water Extraction: A Review. *Journal of Environmental Quality*, *36*(6), 1735–1748. https://doi.org/10.2134/jeq2007.0218

CHAPTER THREE

PERCOLATION METRIC TO QUANTIFY SOIL WATER RESPONSE TO WATER INPUT ON IRRIGATED AGRICULTURAL FIELDS

Contribution of Authors and Co-Authors

Manuscript in Chapter 3

Author: Meghan Robinson

Contributions: Field data collection; calculation development; data analysis; manuscript writing

Co-Author: W. Adam Sigler

Contributions: Initial research conceptualization; lead on funding acquisition; co-development of research ideas and methods; field work and data analysis oversight; calculation development; detailed editing and review of writing

Co-Author: Clain Jones

Contributions: Consultation on soil sampling methods; detailed editing and review of writing

Co-Author: Kent McVay

Contributions: Reviewed writing

Co-Author: Jasmine Neupane

Contributions: Reviewed writing

Manuscript Information

Meghan Robinson, W. Adam Sigler, Clain Jones, Kent McVay, Jasmine Neupane

Status of Manuscript: [Double click to put an X in one of the options below, then delete instruction in brackets. If you cannot double click to add an X, search for "Check Box Content Control."]

☒ Prepared for submission to a peer-reviewed journal
☐ Officially submitted to a peer-reviewed journal
☐ Accepted by a peer-reviewed journal
☐ Published in a peer-reviewed journal

Abstract

Understanding soil water infiltration and percolation dynamics are essential for water resource management, particularly in agricultural systems where concerns over water use efficiency and crop productivity are mounting. Water lost to deep percolation reduces water use efficiency in agricultural systems and creates risk for agrichemical leaching, which is a threat to downgradient water quality. Given the importance of understanding and managing for deep percolation and leaching, I ask how different soil physical properties control deep percolation risk across different soil types and irrigation management approaches. A soil water response metric is developed to quantify variability in soil water response to irrigation and precipitation inputs. The metric is calculated as a ratio with the change in soil water content during an input event as the numerator and net water input during the event as the denominator. This metric is applied across four irrigated fields instrumented with soil water sensors at 15 cm in three watersheds of western and central Montana. Results indicate that clay loam soils and low clay content sandy loam soils have the highest infiltration capacity. Sandy loams with higher clay contents and silt loams were found to be roughly ten times less responsive to irrigation and precipitation than soils with either high clay or high sand contents. Antecedent soil water content was also found to be an important control on responses. Findings may suggest that soil structure drives high responsiveness in clay loam soils, whereas coarse texture and limited water holding capacity likely produce large responses in sandy loam soils. The metric developed here provides insights into soil characteristics that enable efficient water infiltration, which is important in managing soil water. This metric can also be applied across different management and soil scenarios to understand variability in deep percolation and associated leaching risk.

3.1: Introduction

Soil water storage and transport characteristics are key drivers of water cycling and are important to understand for water resource management. Watershed behaviors such as surface runoff and streamflow generation (Scaife et al., 2020), groundwater recharge (Mathias et al., 2017), and patterns of evapotranspiration (Wang et al., 2019) are all driven by soil water dynamics. Understanding how soil water storage changes in response to water inputs can help develop an improved understanding of these processes. Networks of soil water sensors with high data logging frequencies have emerged as a mechanism for understanding soil water responses with a variety of applications including soil moisture-based drought identification (Osman et al., 2024), identification of preferential flow (Lin & Zhou, 2008), and improved understanding of watershed connectivity (Detty & McGuire, 2010). Utilizing sensor networks for the analysis of VWC responses to discrete precipitation events as an approach for assessing soil water behaviors has also become increasingly common, and allows for comparisons across agricultural management strategies (Ljutic et al., 2024), topographic positions (Singh et al., 2021), and storm types (Tymchak & Torres, 2007). Agricultural systems are understudied relative to natural systems with respect to soil water behavior, and quantifying VWC responses to water inputs including irrigation can contribute to understanding soil water transport behavior that plays a critical role in watershed function.

Building an understanding of soil infiltration and percolation capacity and the relative likelihood of deep percolation has benefits for assessing a range of hydrological processes. Water infiltration through the vadose zone may be advantageous when considering groundwater recharge and enhanced streamflow (Nazarieh et al., 2018; Ochoa et al., 2007). However, deep

percolation may also reduce water use efficiency, which is a concern particularly in agricultural systems where crop yields are closely correlated with water consumption, and water availability limits productivity (Pereira, 2017). Additionally, the loss of solutes such as nitrate with deep percolation can be a challenge for downgradient water quality, and may be mitigated by limiting excessive water percolation when leaching risk is high (Quemada et al., 2013). Existing tools such as geospatial models for assessing leaching potential can provide beneficial insights into general patterns of risk; however, coarse data resolution and limited availability for key data can confine the extent to which managers can use tools to make small scale decisions (Ki et al., 2015). Furthermore, many leaching and deep percolation risk models and management guides focus on soil texture (Andales et al., 2015; Jones & Olson-Rutz, 2018; Melvin & Yonts, 2009; Rieffenberger et al., 1989; Sharma, 2019), as texture is widely recognized for its control over water retention and infiltration properties (Saxton et al., 1986). However, other soil properties including structure, bulk density (Ruehlmann & Körschens, 2009), organic matter (Yang et al., 2014), and coarse fragments all contribute to water retention characteristics as well. Soil water management can be enhanced by understanding the aggregated effect of many soil properties on soil water infiltration and percolation behaviors.

Studying VWC responses to precipitation events has been conducted across systems to answer an array of questions, though a focus on mountain stream catchments has dominated literature (Nippgen et al., 2016). Previous work has focused on storm intensities and durations, as well as topographic and hillslope position variability as controls on VWC responses (Detty & McGuire, 2010; Kim, 2009; Singh et al., 2021). Antecedent soil water content (Singh et al., 2021; Wiekenkamp et al., 2016), vegetation type and seasonal water consumption patterns (Kim,

2009; Zhang & Schilling, 2006), and agricultural management (Ljutic et al., 2024) have all been recognized for their impacts on VWC responses as well. These previous studies have utilized methods for assessing responses such as changes in soil water storage following precipitation events, wetting front velocity between sensors in depth arrays, and identification of preferential flow through non-sequential sensor responses (Lin & Zhou, 2008; Ljutic et al., 2024; Wiekenkamp et al., 2016).While much of this previous work recognizes the importance of spatial and temporal variability, minimal work characterizes soil water responses in an explicit way that can be quantified and compared across time and space. Most work also focuses on VWC responses to precipitation, while irrigation has been studied less extensively.

Limited literature on quantifying VWC responses to precipitation or irrigation incorporates the nuances of water dynamics in semi-arid and water limited systems. Previous work has suggested that vegetation type impacts VWC responses due to different water use patterns, total water uptake, and variable canopy water interception (Dai et al., 2022; Kim, 2009; Zhang & Schilling, 2006). It has also been suggested that seasonal patterns of evapotranspiration demand may influence VWC response (Detty & McGuire, 2010). While these previous studies quantifying responses to rainfall events have been conducted across diverse vegetation settings, studies have generally focused on storm periods when evapotranspiration (ET) is suppressed. In systems where evaporative demands are high, recognizing that all precipitation or irrigation applied may not infiltrate or remain in soil long enough to be utilized by crops is essential (Bos et al., 2009; Muratoglu et al., 2023).

In this work, a method for quantifying variability in VWC responses to irrigation or precipitation events across soil textures and differences in irrigation management styles was

developed. This response metric addresses literature gaps around leveraging irrigation events in agricultural systems as well as the lack of direct incorporation of ET into VWC response characterization. Using the response metric, I ask what soil characteristics drive high responsiveness in infiltration and percolation to 15 cm (referred to as infiltration moving forwards) and a resulting high risk of deep percolation and leaching. I hypothesize that soil texture is a key driver of VWC responses to inputs, but that nuances in soil particle size composition and soil structure are also important controls on infiltration. To address these questions, it is necessary to compare response to water input at different times in the growing season and on different fields, highlighting the benefits of a metric that reflects soil characteristics and accounts for ET which is highly variable across space and time.

3.2: Methods

3.2.1: Site Locations and Descriptions

Field observations were made in cultivated, center pivot irrigated fields across three distinct soil types. All fields were managed by cooperating producers, including decisions on the timing and quantity of irrigation. Throughout this section, single irrigation events will be referred to as passes. Groups of irrigation passes that occur in immediate succession will be referred to as sets. Season total refers to the quantity of all irrigation added during the growing season. Study sites included one location on the Fairfield Bench of central Montana in the Sun River Watershed, two fields managed by separate producers in the Gallatin watershed of southwestern Montana, and one field at the Montana State University Northwestern Agricultural Research Center (NWARC) in the Flathead Lake watershed of northwestern Montana (Chp 3 - Figure 1). All fields are in generally semi-arid, water limited climates.

The Fairfield Bench site represents the highest clay content soil among our study soils. Hydrometer texture analysis (see Chp 2.2.3) indicates clay content ranges from 30-40%, and soils are classified as clay loams (Chp 3 - Figure 2). This aligns with the mapped Rothiemay and Niart clay loams soils (Chp 3 - Table 1). Soil VWC data were collected from three sites in 2023 and six sites in 2024. Barley (*Hordeum vulgare*) was planted in 2023, and spring wheat was (*Triticum aestivum L.*) planted in 2024. Weather data for precipitation and potential evapotranspiration (PET) are from a Montana Climate Office Mesonet site in Power, MT, 10 miles east of the study field (Montana Mesonet "mdapower" site). Irrigation management on this field included two irrigation rates. Three monitoring sites were located under the grower's standard practice (GSP), where irrigation was generally 1.7 cm (0.65 inches) per pass. Three monitoring sites were located under an experimental reduced irrigation rate (RIR), which received 75-80% of the GSP quantity. Irrigation frequency and total number of passes was equal between treatments. Season total irrigation quantities were 23.3 cm (9.1 inches) in 2023 and 23.9 cm (9.5 inches) in 2024 for GSP, and 18.24 cm (7.2 inches) and 20.32 cm (8.0 inches) for RIR in 2023 and 2024, respectively (Chp 3 - Table 2).

Gallatin Valley sites were situated on deep loess deposits with silt contents ranging from 60-75%. Research was conducted with two cooperating producers, both growing seed potatoes (*Solanum tuberosum*) in fields mapped as Brocko silt loams (Chp 3 - Table 1). Weather data were obtained from a Mesonet site in Manhattan, MT, approximately two miles north of the study fields (Montana Mesonet "mdamanha" site). Two sites were installed in each cooperator's field, for a total of four sites. Unlike Fairfield and Creston where sites were continuously installed for the duration of the project, Gallatin sites were installed over limited periods to avoid

equipment destruction during potato seeding and harvest. Data collected in 2024 were the focus for this analysis, as methods for tracking the times of irrigation water application were improved relative to 2023. Field B24 was irrigated based on our cooperator's standard practice, which was generally 1.3 cm (0.5 inches) per pass. Field T24 was irrigated based on ET loss replacements guided by a precision irrigation project led by the MSU Precision Agriculture Research Group, and applied quantities were approximately 0.75 to 1 cm (0.3 to 0.4 inches) per pass. Season total irrigation was 13.6 cm (5.4 inches) for Field B24 and 16.5 cm (6.5 inches) for Field T24 (Chp 3 - Table 2).

Spatial variability in soil texture was most pronounced at NWARC. Hydrometer texture analysis indicates that soils on the south end of the field were 70-75% sand with 10% clay content, whereas soils on the north end of the field were 60-65% sand with 20% clay content, generally matching expected patterns based on mapped soils (Chp 3 - Table 1). Monitoring equipment was installed at four sites under spring wheat. All sites were under a precision pivot, which enabled different irrigation treatments for discrete sectors across the field. Southern sites (R5-01 sites) were irrigated with ET-based prescriptions that varied spatially and temporally. Northern sites (R5-07 sites) were irrigated based on the NWARC farm manager's standard practice, generally 1.3 to 2.5 cm (0.5 to 1 inch) per pass. Season total irrigation for standard production sites was 4 cm (1.6 inches) and was 8.8 to 11.9 cm (3.5 to 4.7 inches) for ET replacement sites (Chp 3 - Table 2).

3.2.2: Site Instrumentation and Irrigation Events

All monitoring sites were equipped with arrays of soil water sensors at 15, 30, and 90 cm. Soil VWC was measured with HOBO Decagon 10HS capacitance sensors at locations with

equipment installed in 2023, and METER T12 capacitance sensors at locations with equipment installed in 2024. Sites instrumented with METER equipment (Chp 3 - Table 1) included sensors at 60 cm as well. For full assessment and comparison of sensor behaviors, see Chapter 2.3. Irrigation event timings were determined using hourly photographs from field cameras to monitor when the pivot passed over sites, and with water quantities captured in manual rain gauges at each monitoring site. At each field, at least one rain gauge was in the field of view of a camera, to allow tracking of irrigation accumulation. Mineral oil was added to rain gauges to prevent evaporation between field visits.

In Fairfield, 16 unique irrigation passes occurred in both 2023 and 2024. The number of irrigation passes that facilitated calculation of the percolation metric varied by site due to sensor failures and resulting data gaps (Chp 3 - Table 2). Data for site F121 in 2023 were not considered due to the destruction of the barley crop which caused abnormal soil water content responses. Numbers of irrigation passes varied across cooperators' management styles in the Gallatin, ranging from 14 to 22 irrigation passes. Site T208 had fewer passes considered due to data limitations from sensor failure. Only six irrigation passes were applied at NWARC, which motivated the inclusion of precipitation events as outlined in section 3.2.4. Due to uncertainty in pivot behavior and irrigation application to site R5-01-028, no irrigation passes for that site were considered for this metric.

3.2.3: Percolation Metric Calculation

The percolation metric for quantifying VWC response to irrigation or precipitation is calculated as:

$$\text{Metric}\left(\frac{\left(\frac{\text{cm}^3}{\text{cm}^3}\right)}{\text{cm}}\right) = \frac{\text{Peak 15 cm VWC}\left(\frac{\text{cm}^3}{\text{cm}^3}\right) - \text{Initial 15 cm VWC}\left(\frac{\text{cm}^3}{\text{cm}^3}\right)}{(\text{Irrigation (cm)} + \text{Precipitation (cm)}) - \text{PET (cm)}} \quad (3.1)$$

Metric values were calculated for individual irrigation or precipitation events. Initial soil water content was defined as the sensor VWC ($cm^3\ cm^{-3}$) recording that was most immediately prior (generally 30 to 90 minutes) to the irrigation event. Peak soil water content was defined as the highest observed VWC ($cm^3\ cm^{-3}$) in the 4 hours following an irrigation event. A four-hour search window was used because that was a sufficiently long period for water transport to 15 cm based on observation in all study fields; however, it was a short enough window to isolate individual irrigation passes (the shortest return intervals for irrigation passes were generally six hours). While each metric calculation focused on one specific irrigation pass or precipitation event, all irrigation and precipitation occurring between the start of the defining event and the time of peak observed VWC was summed. For example, if the focal event is a 1.5 cm irrigation pass but 0.05 cm of rain occur during the defined response window, then the cumulative water input would be 1.55 cm. Penman-Monteith PET occurring over the response window was then subtracted from the gross water input. PET is subtracted to account for variability in atmospheric demands across our sites spatially and across irrigation passes over the season temporally. PET is not adjusted with a crop coefficient. The resulting net water input addresses PET as a possibly confounding dynamic water loss variable and seeks to isolate VWC response associated with soil attributes.

The resulting metric normalizes the change in water content to the effective water input, producing a value that can be compared across soil types, crops, and irrigation management styles to quantitatively assess VWC response. All irrigation passes were visually assessed to ensure that peak VWC was captured by the algorithm (Example plot in Chp 3 - Figure 3). A

metric score of zero indicates that there was no change in soil water content over the four-hour window following irrigation. A larger positive value can be interpreted as a larger change in VWC relative to the inputs, whereas a more negative value indicates that soil dried out over the search window. A total of 277 metric scores for irrigation and precipitation events were calculated. Summaries of metric calculation inputs tabulated by site, field, and water type are included in Chp 3 - Table 2 (irrigation) and Chp 3 – Table 3 (precipitation).

To interpret metric values and understand patterns, antecedent soil water contents were considered. Conditions were classified based on how the value used for the initial 15 cm VWC compares to the full range of observed VWCs. Ranges of values reported by individual sensors were likely influenced by micro-environments surrounding sensors, including proximity to rocks. HOBO and METER sensors also read generally different VWC ranges (see Chapter 2.3). To combat this, absolute values were not used as thresholds for dividing VWC data, but rather antecedent water contents were grouped into quantiles for each sensor. Responses were then compared based on antecedent soil water content quantile group.

3.2.4: Precipitation Event Delineation

Metric value calculations focused on irrigation passes. This decision was motivated by the constrained and consistent quantities and intensities of irrigation passes and the lack of robust, proximal precipitation data at some field sites. At NWARC, on-site precipitation measured by a Montana Climate Office Mesonet site is available over the period of data collection. NWARC also received the fewest irrigation passes during the 2024 growing season, so to achieve a more comparable sample size, metric values were calculated for precipitation events at NWARC in addition to irrigation passes. Unique precipitation events were delineated

based on four consecutive hours without rain, which falls in a range consistent with previous studies (Meißl et al., 2020; Penna et al., 2011). This four-hour break in precipitation matches the four-hour search window for VWC responses included in the percolation metric definition. Further, 0.4 cm was defined as a threshold precipitation quantity for calculating metrics. This choice is also similar to previous literature (Singh et al., 2021), and while the threshold is smaller than standard irrigation events, it was generally large enough to induce a VWC response while being low enough to retain most summer precipitation events. At NWARC, a total of 15 events met these criteria and were used for metric calculation (Chp 3 - Figure 4). All data and code for analysis in this chapter are available on Hydroshare (Robinson & Sigler 2025).

3.3: Results

3.3.1: Site Weather Context

Average growing season precipitation (defined as April-September) for Fairfield was 14.5 cm based on 20-year data from the Greenfields AgriMet Station (Station GFMT). Precipitation was slightly above average in both 2023 (15.1 cm) and 2024 (18.4 cm). In 2023, precipitation was particularly high relative to normal between April and June. The 2024 growing season followed an extremely dry winter, but precipitation in April, May, and August was above average (Chp 3 – Figure 5). For the Gallatin, the 20-year average growing season precipitation at the Bozeman Agrimet Station (Station BOZM) was 18.3 cm, slightly higher than the Fairfield average. The 2024 growing season total precipitation of 20.4 cm was above the 20-year average, primarily reflecting a wetter than normal May (Chp 3 - Figure 5). NWARC received the most growing season precipitation (21.7 cm) among the sites in 2024. This total is just above the growing season average 20.1 cm at the Creston AgriMet Station (Station CRSM) and reflects

wetter than normal May, June, and July conditions (Chp 3 - Figure 5). Total monthly PET was generally similar between Fairfield and the Gallatin during the growing season but was consistently lower at Creston (Chp 3 – Figure 5).

3.3.2: Soil Water Content and Metric Results Across Soil Types

Patterns in soil VWC data found differences in responsiveness at 15 cm and variable frequency of water percolation to 90 cm across sites (Chp 3 – Figure 6). Clear responses to both the GSP and RIR irrigation rates were observed at 15 cm for all irrigation passes on the Fairfield clay loam soils (Chp 3 - Figure 7). The deepest observed VWC responses to irrigation on Fairfield soils were at 90 cm, though these responses were not always discretely linked to individual irrigation events (Chp 3 - Figure 6). Soil VWC data suggest that Gallatin silt loam soils represent the least responsive observed soil type. Fewer clear increases in 15 cm water content were observed at Gallatin monitoring sites, and responses generally occurred over a limited period in the late summer (Chp 3 - Figure 7). No changes in VWC in response to irrigation were observed deeper than 15 cm on either monitored silt loam field during the 2024 growing season (Chp 3 - Figure 6). Data for the sandy loam soils at NWARC suggested a separation of VWC response patterns within the field. Clear positive responses were measured for most irrigation passes at 15 cm on the southern sandy loam soils with 10% clay content. The two sites on the northern, less sandy (20% clay) soils were less responsive, and evidence of water transport to 15 cm was clearest when irrigation coincided with precipitation events (Chp 3 - Figure 7). Across the three study soils, the NWARC sandy loams had intermediate water transport to depth, as increases in water content were observed at 30 cm but not at 90 cm for any site during irrigation (Chp 3 - Figure 6).

Metric response differences were clear across study fields. Four soil texture groups emerged with distinctly variable infiltration and percolation: clay loams, sandy loams-10% clay, sandy loams-20% clay, and silt loams (Chp 3 - Figure 8). The median response metric score for Fairfield clay loams was 0.015 cm^3 cm^{-3} cm^{-1}, indicating that for every one centimeter of net water input (precipitation + irrigation - PET), volumetric water content increased by 0.015 cm^3 cm^{-3}. Site medians ranged from 0.01 (F128) to 0.024 (F143) cm^3 cm^{-3} cm^{-1}. When values for all Fairfield sites were considered together, the interquartile range (IQR) for metric values was 0.009 to 0.021 cm^3 cm^{-3} cm^{-1}, with no points considered statistical outliers and a maximum metric value of 0.038 cm^3 cm^{-3} cm^{-1}. The sandy loam soils with 10% clay content had a similarly high median metric score of 0.018 cm^3 cm^{-3} cm^{-1}, however with a wider IQR of 0.001 to 0.028 cm^3 cm^{-3} cm^{-1}, perhaps reflecting more variability in precipitation input characteristics. The maximum response metric calculated for sandy loams with 10% clay content was 0.146 cm^3 cm^{-3} cm^{-1}, which was the highest calculated for any event on any soil type. In contrast, sandy loam soils with 20% clay content had a median metric response score of 0.001 cm^3 cm^{-3} cm^{-1}, an order of magnitude lower than the slightly sandier soils. The IQR for sandy loams with 20% clay content was 0.00003 to 0.019 cm^3 cm^{-3} cm^{-1}, a similarly wide range as the sandy loams with 10% clay, though skewed towards lower values. The median metric score for Gallatin silt loam soils was 0.0005 cm^3 cm^{-3} cm^{-1}, and the IQR of -0.0007 to 0.001 cm^3 cm^{-3} cm^{-1} was the most limited range observed across soil types. The sandy loams with 20% clay had more high metric outliers than the silts, where metric response values were consistently low (Chp 3 - Figure 8).

3.3.3: Results Within Soil Types

In addition to response variability observed across soil textures, variability was observed within soil textures across monitoring sites and irrigation passes. Antecedent soil water content was identified as one driver of differences in response metric values for individual sites. In Fairfield, irrigation occurring on the wettest 25% of observed VWC conditions had an average metric score of 0.01 $cm^3\ cm^{-3}\ cm^{-1}$, roughly half of the 0.018-0.02 $cm^3\ cm^{-3}\ cm^{-1}$ for the driest 50% of soil conditions (Chp 3 - Figure 9). Drivers of variability in other soil types were less clearly pronounced. Higher responsiveness was observed during later phases of the growing season on silt loams. When considering precipitation events, intensity and storm length seem to impact response metrics. Longer and lower intensity storms generally resulted in higher metric values than shorter, high intensity storms that may have characteristics more closely aligned with irrigation events. The highest metric scores calculated for Creston sandy loam soils were in response to precipitation events of 2.6-3.4 cm over 36-81 hours.

3.4: Discussion

3.4.1: Irrigation Response Variability Across Soil Textures

The soil water response metric calculations presented here provide a method for comparing soil water infiltration capacity and responsiveness across soil textures, regions, and irrigation management. Results suggest that two soil texture characteristics emerge as causes of high water infiltration and percolation capacity, and hence imply a higher deep percolation risk: soils with high sand content and soils with relatively high clay content. In Fairfield clay loam soils, high response metrics are attributed to soil structure that facilitates rapid water transport. Preferential flow in aggregation-prone clay loam soils likely drives percolation and thus response

metrics reflect structure rather than being a function of texture alone. Previous work suggests clay content is the most important control on structure development, though exact thresholds for clay contents that facilitate aggregation depends on organic matter content (Koestel & Jorda, 2014). Other work has found that clay contents above 20% contribute to aggregate development, and that speed of soil crack formation is expedited for soils with clay content above 31% (Wagner et al., 2007), a threshold below the 30-40% clay measured in Fairfield clay loams. For the NWARC sandy loam soils with 10% clay content, in contrast, the high response metrics likely do reflect a texture-based control. The very high portion of coarse particles and the resulting high infiltration rate and limited water holding capacity likely caused high responsiveness at 15 cm. It is worth noting that on 10% clay sandy loam soils, irrigation responses below 30 cm were not observed. This may be a consequence of the more limited total irrigation quantity applied at NWARC relative to Fairfield, or it may suggest a lower deep percolation and leaching risk due to a lack of preferential flow paths that can increase water percolation to depth.

Analysis identified intermediate clay contents and high silt contents as soil characteristics associated with lower response metrics and hence more limited deep percolation and leaching risk. On the sandy loam soils with 65% sand content and 20% clay content, the response metric values were approximately ten times lower than the 10% clay content soils, indicating much less change in soil water content for given net water inputs. The difference in particle size distribution between the two sandy loams is primarily accounted for by a doubling in clay fraction for the 65% sand soils. This suggests that the increase from 10 to 20% clay content is sufficient to improve water holding capacity and greatly limit 15 cm water content responses, but

not so high that macropores and soil aggregates become dominant as they are in Fairfield. I hypothesize that the increase in clay content is the larger driver of differences in responses rather than the decrease in sand between the two sandy loam soils. The silt loam soils have clay contents ranging from 10-20% (similar to the NWARC sandy loams) but response metric values are low across silt loam sites. This suggests that unlike in sandy loam soils with 10% clay where water storage is limited due to the prevalence of coarser sand grains, silt loams with 10% clay have sufficient water holding capacity contributed by the intermediate particle size silt to produce high water holding capacity. At the same time, the 10-20% clay content in the silt loam is not sufficient to produce cracking or aggregation structure and high metric scores observed in clay rich (30-40%) soils.

3.4.2: Other Controls on Water Responses

After soil texture, antecedent soil water content emerges as a possible explanatory variable for differences in VWC responses across irrigation events. This behavior was most pronounced on Fairfield clay loams, where responsiveness was highest on drier soils. Lower response metrics for wetter soils could suggest that when conditions approach field capacity, soil potential for storing additional water is limited and incoming water percolates through water filled soil rather than being retained in storage. In contrast, high responsiveness on drier soils could reflect preferential flow through desiccation cracks, penetrating deeper into the soil quickly, but simultaneously producing more limited infiltration into the soil matrix. Low metric scores with high antecedent VWC imply necessity to focus on metric scores calculated with drier antecedent conditions to isolate soil behavior and accurately identify leaching risk. Findings on the importance of antecedent soil water content aligns with previous work that also identified

variable VWC responses depending on initial water contents (Ljutic et al., 2024; Singh et al., 2021; Wiekenkamp et al., 2016).

On other soil types, antecedent soil water contents do not appear to be a dominant control on infiltration and responsiveness. In sandy soils at NWARC, low water holding capacity may result in limited periods where antecedent VWC conditions are high enough to substantially impact metric calculations. In silty soils in the Gallatin, temporal variability in metric scores was observed, with events in late July and August causing larger responses than during the early growing season. This may reflect macropore development as roots develop. Alternatively, there could be plant physiology changes such as canopy closure affecting metric scores, in which case, non-soil related plant dynamics could be interfering with in intended metric purpose of inferring soil behavior.

For NWARC sites where precipitation was included in metric score calculation, storm duration and intensity also appeared to contribute to response metric values. The highest observed metric values were in response to longer and generally lower intensity storms. Shorter and higher intensity storms generally produced metric scores more similar to irrigation events. The larger IQRs calculated for NWARC also suggests that variable precipitation event characteristics may influence VWC response dynamics. Storm types have been found to control VWC responses in previous work (Detty & McGuire, 2010; Tymchak & Torres, 2007).

3.5: Conclusions and Future Work

In this chapter, I develop a metric for quantifying variable irrigation responses across agricultural systems. This work suggests that across our study field soils, Fairfield clay loams transport water to depth most readily. Deep percolation and nitrate leaching risk may therefore

be highest on clay loam soils, where blocky soil structure from aggregation or soil cracking enables preferential flow. Future work will expand to include monitoring sites in small grain fields on silt loams to further isolate whether VWC response behavior is linked to different crop types, and to provide continuity with crops in other soil types. Organic matter was not collected for study fields, though it may influence soil water holding capacity and infiltration behavior (Lal, 2020). Future work that explicitly characterizes organic matter content in addition to soil texture would improve understanding of soil property controls on infiltration and percolation. There is also opportunity to expand application of this metric to broader soil water sensing networks, including the Montana Mesonet network, to assess more variable soil textures and build a more robust understanding of soil infiltration and percolation behavior. Paired assessment of Mesonet station (installed in perennial vegetation) VWC data with nearby cultivated sites would allow for assessment of management influence on infiltration and percolation. Previous work has found that topography and landscape position are drivers of VWC response patterns as well. All field sites presented here have limited topographic variability. This choice was intentional to limit runoff opportunities and to isolate locations dominated by vertical soil water fluxes. Future research could expand to incorporate a wider range of landscapes and slope positions to identify the importance of topography for VWC responses in agricultural settings.

Site	Major Soil Series	Soil Taxonomy	Mapped Texture	Mapped Structure	Mapped Organic Matter	Soil Texture (Hydrometer)
Fairfield	Rothiemay-Niart (85%) (Map units 123B and 124B)	Fine-loamy, mixed, superactive frigid Aridic Calciustolls	Clay loam, 0-152 cm	Granular structure (0-18 cm), prismatic (18-78 cm), massive below 78 cm	1-2%, (0-18 cm), 0% (18-152 cm)	Clay: 35-40% Silt: 40% in the surface to 20% at depth Sand: 20% in the surface up to 40% at depth
Gallatin	Brocko (90%) (Map units 36B, 36C, and 36D)	Coarse-silty, mixed, superactive, frigid Aridic Calciustepts	Silt loam, 0-152 cm	Weak granular (0-18 cm) and prismatic (17-71 cm) structure, massive below 71 cm	Less than 1%, all depths	Clay: 10-20% Silt: 55% in the surface, 70% at depth Sand: 30% in the surface, 10% at depth
Creston-North	Creston (90%) (Map unit Ce)	NA	Silt loam, 0-152 cm	NA	NA	Clay: 20% Silt: 15% Sand: 65%; no notable variation by depth)
Creston-South	Flathead (90%) (Map unit Fa)	Coarse-loamy, mixed, superactive, frigid Pachic Haplustolls	Sandy loam, 0-86 cm, loamy sand 86-152 cm	Weak granular and subangular blocky structure (0-111 cm), single grain (below 111 cm)	2-4%, all depths	Clay: 10% Silt: 15% Sand: 75%; no notable variation by depth

Chp 3 - Table 1: Soils Across Sites. Mapped soils with percentage of map unit, texture, structure, and organic matter contents from the SSURGO database, as well as hydrometer textures for each study location.

Site	Location	Irrigation	Number of Events	Notes	Sensor
F113	Fairfield	Grower Standard- 1.65 cm per pass	26	Full 2023 data, periodic sensor failures in 2024	HOBO
F121	Fairfield	Reduced Experimental- 1.27 cm per pass	16	2023 data not considered (barley destruction), full 2024 data	HOBO
F123	Fairfield	Reduced Experimental- 1.27 cm per pass	32	Full 2023 and 2024 data	HOBO
F128	Fairfield	Reduced Experimental- 1.27 cm per pass	16	Installed in 2024, full season data	METER
F133	Fairfield	Grower Standard- 1.65 cm per pass	32	Full 2023 and 2024 data	HOBO
F143	Fairfield	Grower Standard- 1.65 cm per pass	16	Installed in 2024, full season data	METER
B10	Gallatin	Grower Standard- 1.27 per pass	14	Installed in 2024, full season data	HOBO
B30	Gallatin	Grower Standard- 1.27 cm per pass	14	Installed in 2024, full season data	HOBO
T191	Gallatin	ET Replacement- 0.75-1 cm per pass	22	Installed in 2024, full season data	HOBO
T208	Gallatin	ET Replacement- 0.75-1 cm per pass	15	Installed in 2024, periodic sensor failures	HOBO
R5-01-350	Creston	ET Replacement- variable	6	Installed in 2024, full season data	METER
R5-01-028	Creston	ET Replacement- variable	0	Installed in 2024, high uncertainty around irrigation quantities	METER

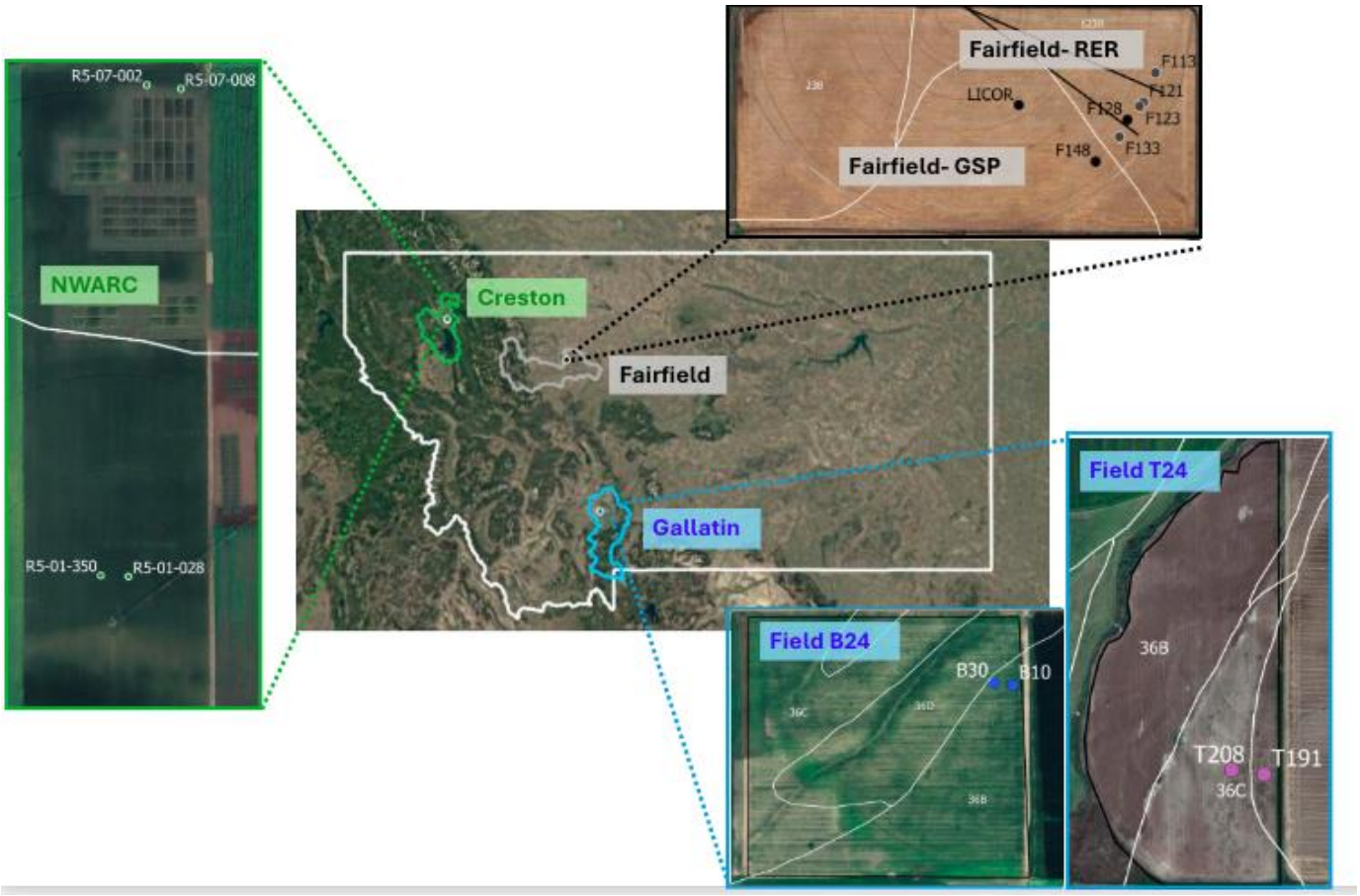
Chp 3 – Table 2 Continued.

Site	Location	Irrigation	Number of Events	Notes	Sensor
R5-07-002	Creston	Grower Standard-1.27-2.54 cm per pass	4	Installed in 2024, full season data	METER
R5-07-008	Creston	Grower Standard-1.27-2.54 cm per pass	4	Installed in 2024, full season data	METER

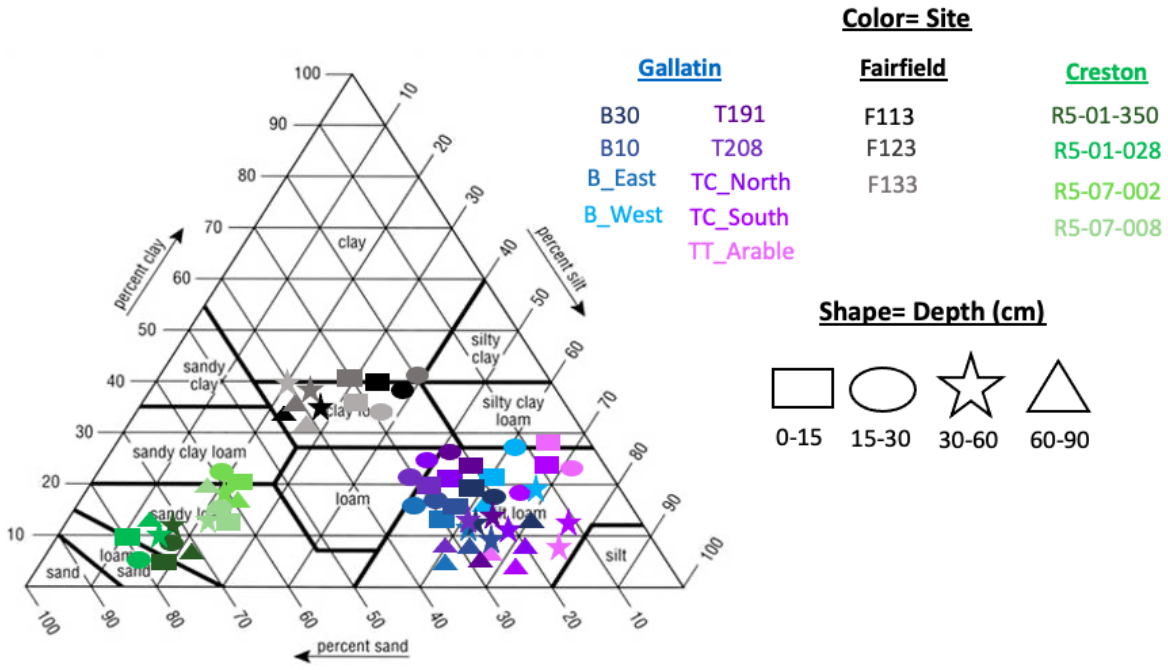
Chp 3 - Table 2: Irrigation Summary Across Sites. Monitoring site names, field locations, general irrigation management, total number of irrigations passes over each monitoring site, data included for metric calculations, and sensor type are summarized.

Event Number	Date	Quantity (cm)	Duration (hrs)	Peak Intensity (cm/hr)
1	4/5/2024	1.57	21	0.094
2	4/6/2024	0.46	11	0.053
3	4/27/2024	0.40	7	0.124
4	5/5/2024	2.13	25	0.109
5	5/7/2024	0.69	14	0.083
6	5/21/2024	0.89	18	0.079
7	5/25/2024	0.43	12	0.071
8	5/28/2024	0.61	9	0.122
9	6/2/2024	1.27	32	0.104
10	6/18/2024	1.02	16	0.094
11	6/26/2024	0.56	17	0.064
12	6/30/2024	2.59	36	0.142
13	7/16/2024	3.38	81	0.157
14	7/29/2024	0.76	50	0.038
15	8/4/2024	0.81	82	0.028

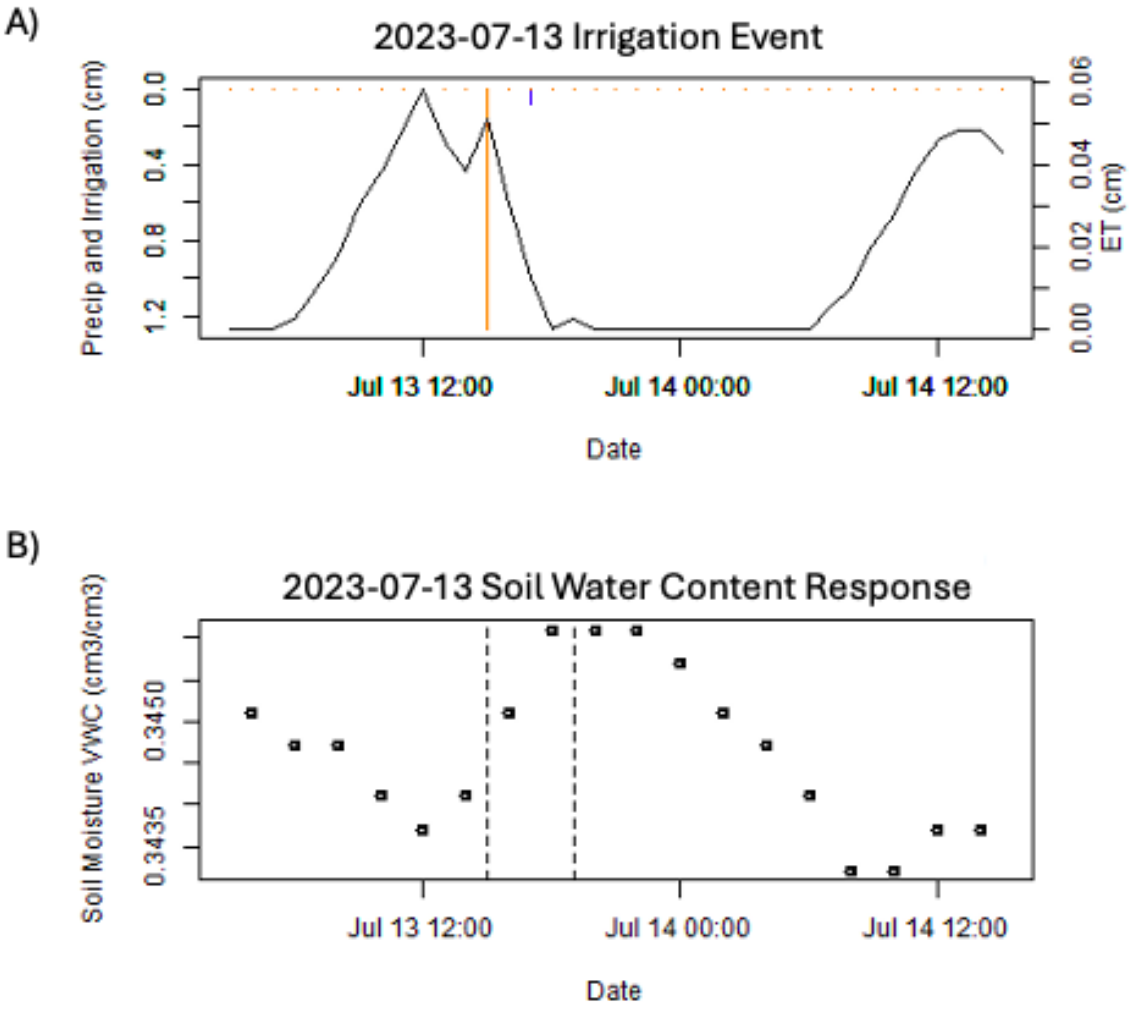
Chp 3- Table 3: Precipitation Event Summary for NWARC. Dates, quantities (cm), durations (hrs), and peak intensities (cm/hr) for precipitation events that metric values were calculated for. VWC data from all four NWARC sites were used in combination with these precipitation events for metric calculation.



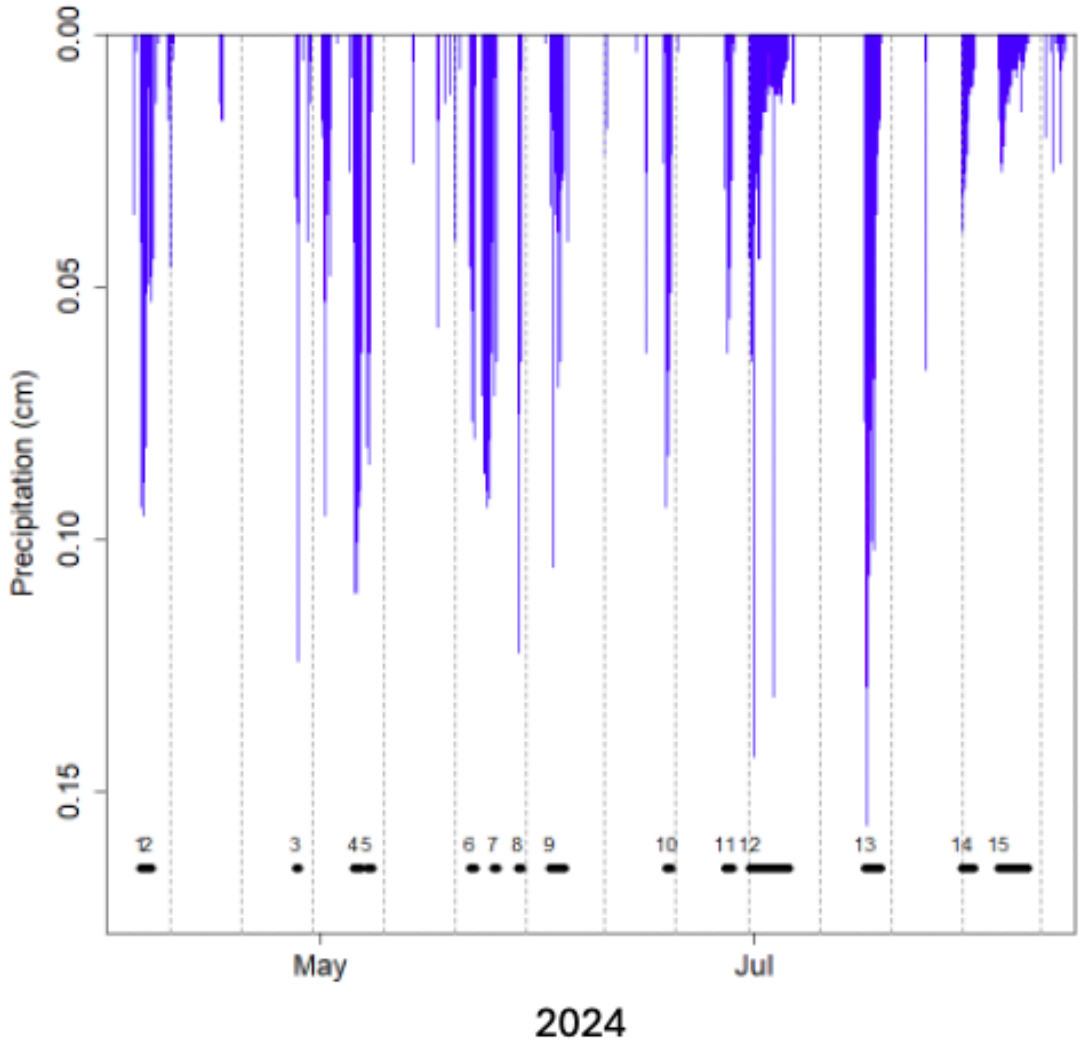
Chp 3 - Figure 1: Site Map. Field locations in watershed and state boundaries, and monitoring site locations within cooperator's fields.



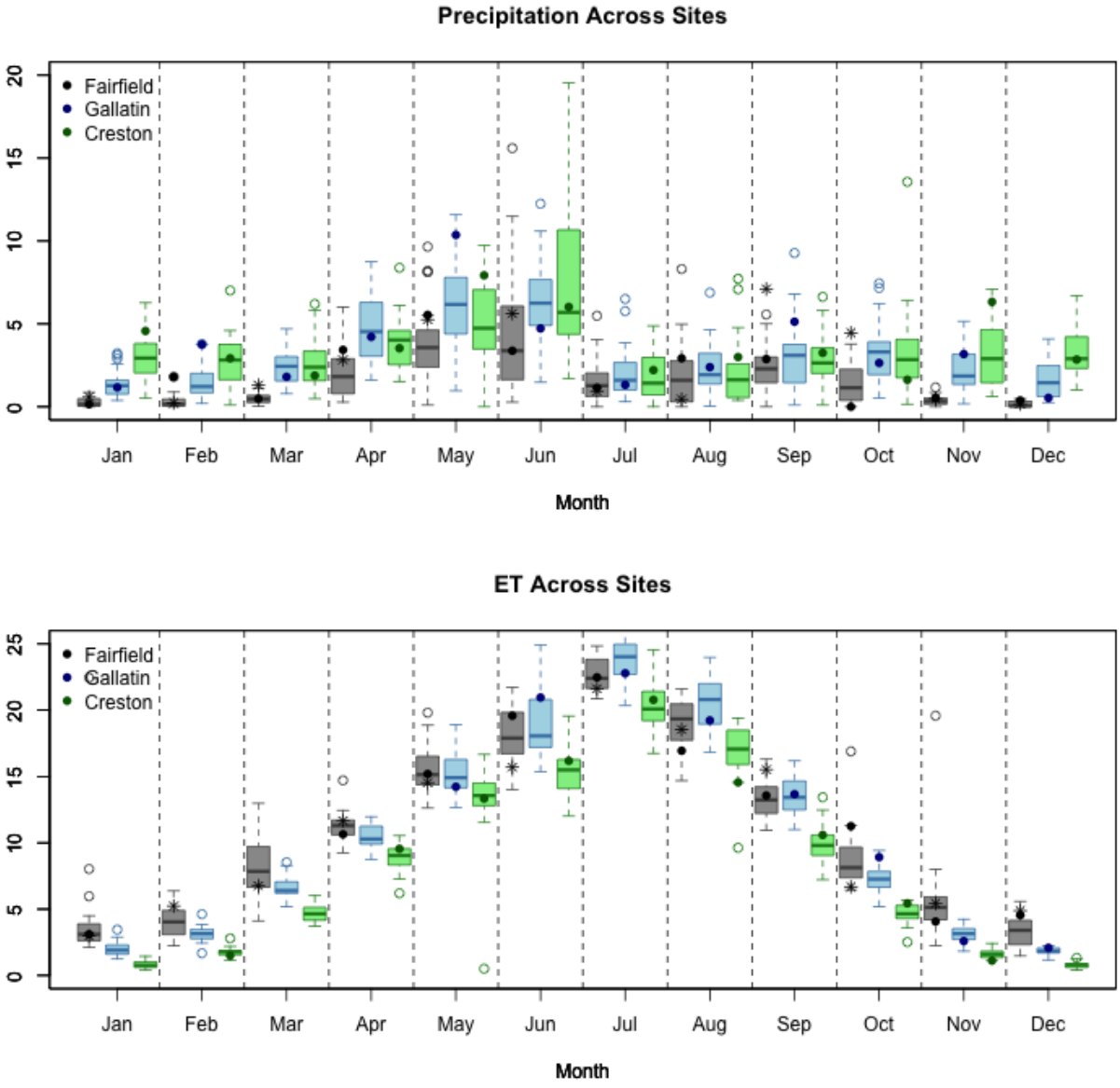
Chp 3 - Figure 2 Site Soil Textures. Hydrometer soil textures for Fairfield clay loams (black and gray points), Gallatin silt loams (blue and purple points), and Creston sandy loams (green points). Circles are 0-15 cm samples, squares are 15-30 cm samples, stars are 30-60 cm samples, and triangles are 60-90 cm samples.



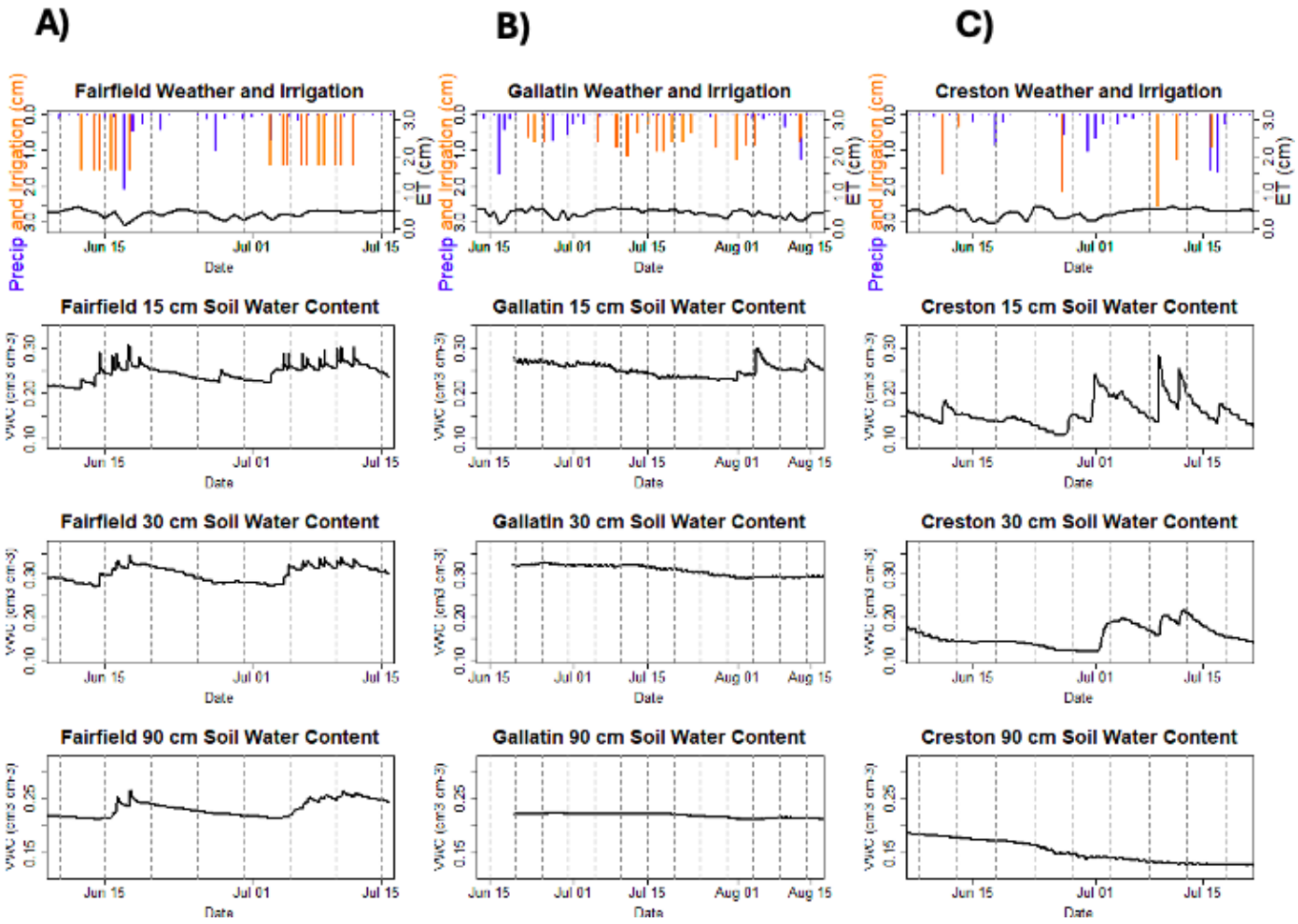
Chp 3 - Figure 3: Irrigation Response Example. A) Irrigation (orange), precipitation (blue), and ET (black) for the metric calculation period. B) 15-cm soil water content response. Dashed lines indicate the beginning and end of the four-hour response search window.



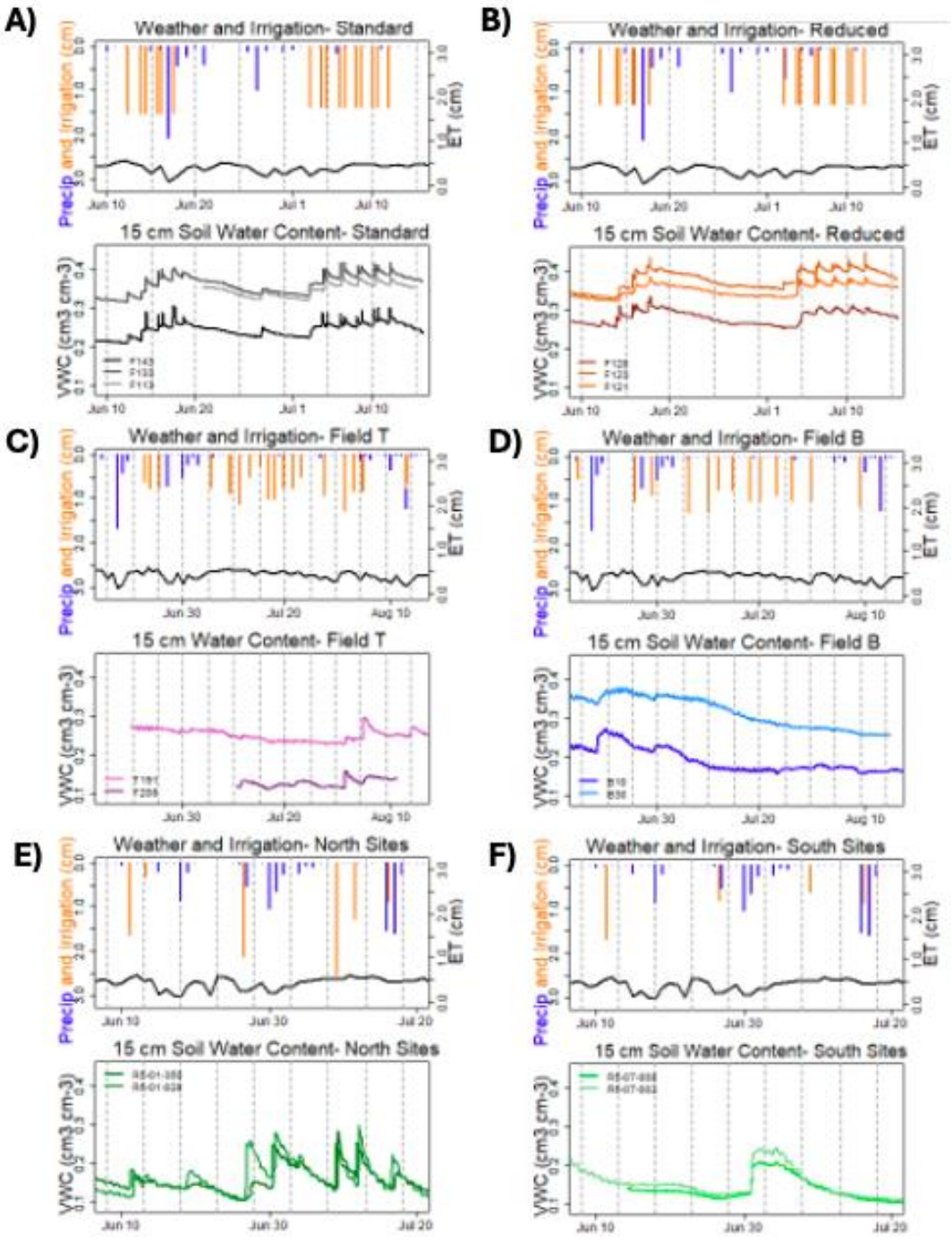
Chp 3 - Figure 4: Precipitation Event Delineation. Hourly precipitation (blue bars) from ‘kalispel’ Mesonet site located at NWARC during 2024, and defined precipitation events (black lines) for metric calculations. Vertical dashed lines are weeks.



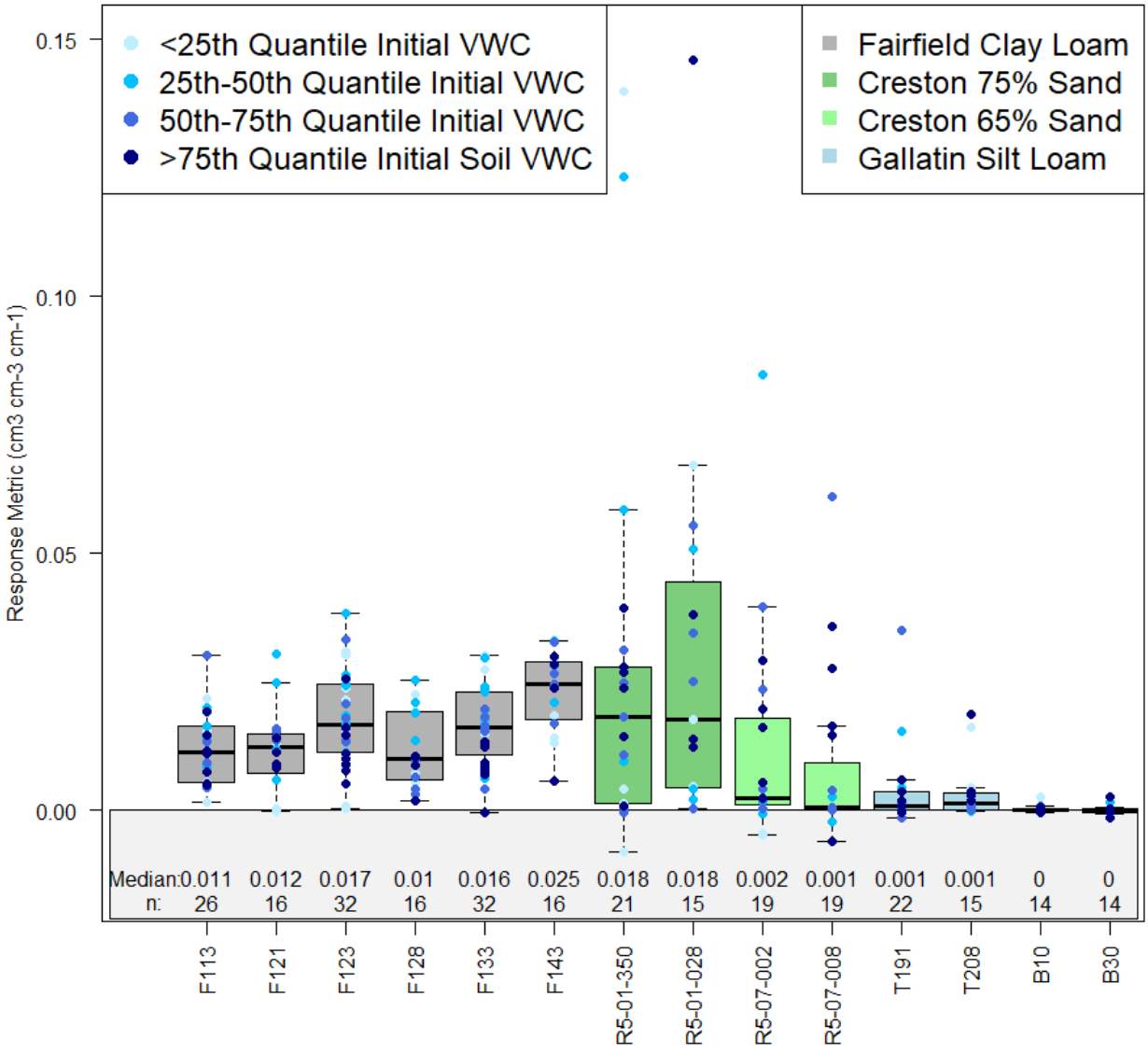
Chp 3 - Figure 5: Monthly Precipitation and ET. Boxplots indicating variability in monthly total precipitation and ET for the period of record at the gage for each study site. Grey is Fairfield, blue is Gallatin, green is Creston. All use data from 2000-2020. Solid points are 2024 totals for each site, stars are 2023 for Fairfield.



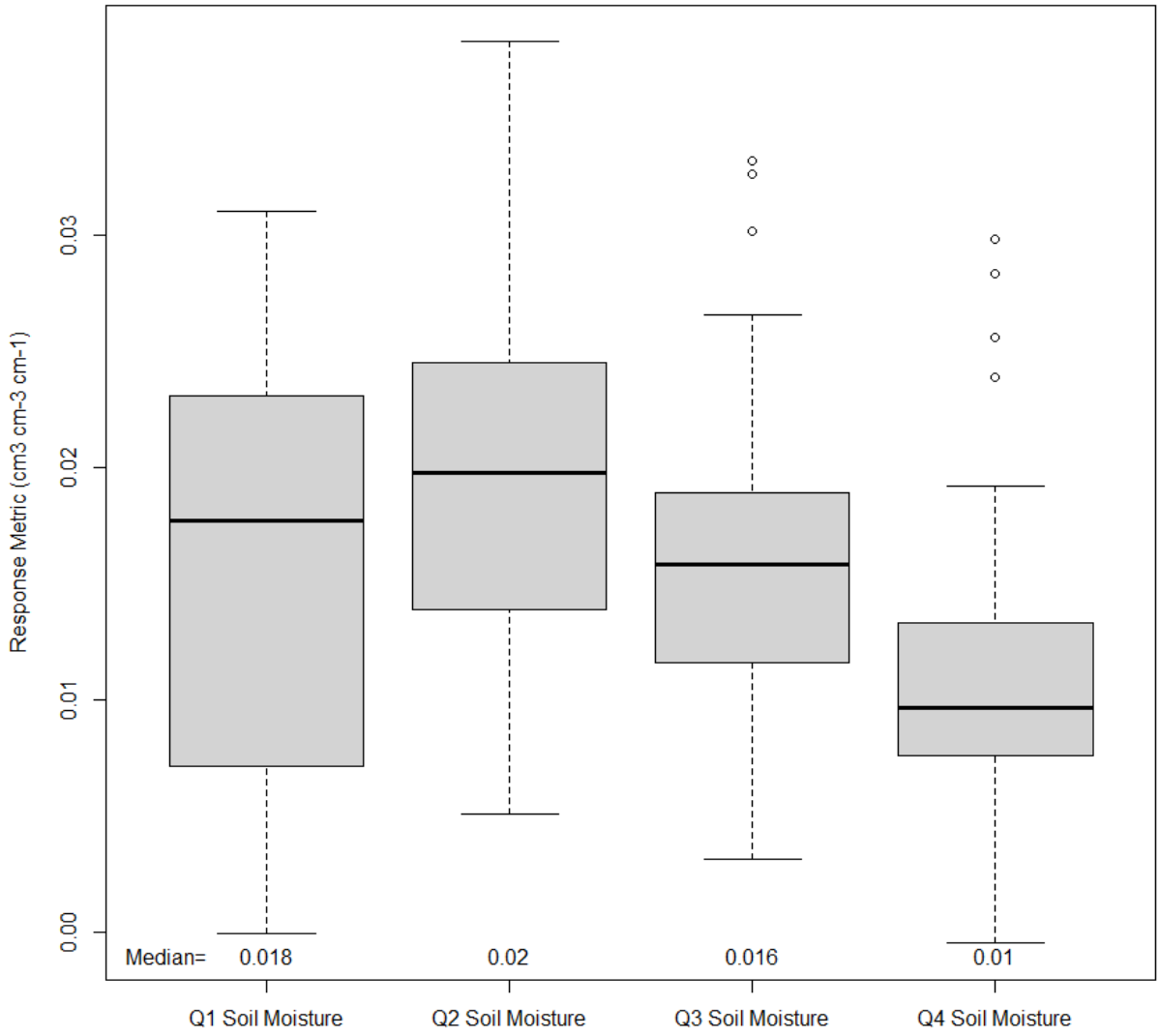
Chp 3 - Figure 6: Study Location Comparison of VWC by Depth. Precipitation, irrigation, and PET (top panels) for the 2024 growing season and soil VWC at 15, 30, and 90 cm for a single representative site for each study location: A) Fairfield, B) Gallatin and C) Creston.



Chp 3 - Figure 7: All Sites 15 cm Comparison. Soil 15 cm VWC responses for A) Fairfield- GSP, B) Fairfield- RIR, C) Gallatin- T24, D) Gallatin- B24, E) NWARC- North Sites and F) NWARC- South Sites for the 2024 growing season.



Chp 3 - Figure 8: Metric Values Across Sites. Metric values were calculated as change in VWC (cm3 cm-3) per cm of net water input. Grey boxes are Fairfield sites, dark green boxes are NWARC 75% sand/10% clay sites, light green boxes are NWARC 65%/20% clay sand sites, and blue boxes are Gallatin sites. Points are colored by antecedent soil water content, with darker indicating wetter conditions according to the legend.



Chp 3 - Figure 9: Fairfield Metric by Antecedent Soil Water Content. Metric scores grouped by antecedent soil VWC quantile. Only Fairfield sites are included.

Literature Cited

Andales, A., Chavez, J., & Bauder, T. (2015). *Irrigation Scheduling: The Water Balance Approach- Fact Sheet 4.707*. Colorado State University Extension. https://extension.colostate.edu/topic-areas/agriculture/irrigation-scheduling-the-water-balance-approach-4-707/

Bos, M. G., Kselik, R. A. L., Allen, R. G., & Molden, D. J. (Eds.). (2009). Effective Precipitation. In *Water Requirements for Irrigation and the Environment* (pp. 81–101). Springer Netherlands. https://doi.org/10.1007/978-1-4020-8948-0_3

Dai, L., Fu, R., Guo, X., Du, Y., Zhang, F., & Cao, G. (2022). Soil Moisture Variations in Response to Precipitation Across Different Vegetation Types on the Northeastern Qinghai-Tibet Plateau. *Frontiers in Plant Science*, *13*. https://doi.org/10.3389/fpls.2022.854152

Detty, J. M., & McGuire, K. J. (2010). Topographic controls on shallow groundwater dynamics: Implications of hydrologic connectivity between hillslopes and riparian zones in a till mantled catchment. *Hydrological Processes*, *24*(16), 2222–2236. https://doi.org/10.1002/hyp.7656

Jones, C., & Olson-Rutz, K. (2018). *Minimizing Nitrate Leaching From Cropland*. Montana State University Extension. https://store.msuextension.org/publications/AgandNaturalResources/EB0226.pdf

Ki, S. J., Ray, C., & Hantush, M. M. (2015). Applying a statewide geospatial leaching tool for assessing soil vulnerability ratings for agrochemicals across the contiguous United States. *Water Research*, *77*, 107–118. https://doi.org/10.1016/j.watres.2015.03.009

Kim, S. (2009). Characterization of soil moisture responses on a hillslope to sequential rainfall events during late autumn and spring. *Water Resources Research*, *45*(9). https://doi.org/10.1029/2008WR007239

Koestel, J., & Jorda, H. (2014). What determines the strength of preferential transport in undisturbed soil under steady-state flow? *Geoderma*, *217–218*, 144–160. https://doi.org/10.1016/j.geoderma.2013.11.009

Lal, R. (2020). Soil organic matter and water retention. *Agronomy Journal*, *112*(5), 3265–3277. https://doi.org/10.1002/agj2.20282

Lin, H., & Zhou, X. (2008). Evidence of subsurface preferential flow using soil hydrologic monitoring in the Shale Hills catchment. *European Journal of Soil Science*, *59*(1), 34–49. https://doi.org/10.1111/j.1365-2389.2007.00988.x

Ljutic, A., Moore, J., Ali, G., Van Eerd, L., Macrae, M. L., & Wagner-Riddle, C. (2024). Variable soil moisture responses to rainfall events in fields under different management practices. *Hydrological Processes*, *38*(7), e15242. https://doi.org/10.1002/hyp.15242

Mathias, S. A., Sorensen, J. P. R., & Butler, A. P. (2017). Soil moisture data as a constraint for groundwater recharge estimation. *Journal of Hydrology*, *552*, 258–266. https://doi.org/10.1016/j.jhydrol.2017.06.040

Meißl, G., Zieher, T., & Geitner, C. (2020). Runoff response to rainfall events considering initial soil moisture – Analysis of 9-year records in a small Alpine catchment (Brixenbach valley, Tyrol, Austria). *Journal of Hydrology: Regional Studies*, *30*, 100711. https://doi.org/10.1016/j.ejrh.2020.100711

Melvin, S., & Yonts, C. (2009). *Irrigation Scheduling: Checkbook Method*. University of Nebraska-Lincoln Extension. https://extensionpubs.unl.edu/publication/ec709/2009/pdf/view/ec709-2009.pdf

Muratoglu, A., Bilgen, G. K., Angin, I., & Kodal, S. (2023). Performance analyses of effective rainfall estimation methods for accurate quantification of agricultural water footprint. *Water Research*, *238*, 120011. https://doi.org/10.1016/j.watres.2023.120011

Nazarieh, F., Ansari, H., Ziaei, A. N., Izady, A., Davari, K., & Brunner, P. (2018). Spatial and temporal dynamics of deep percolation, lag time and recharge in an irrigated semi-arid region. *Hydrogeology Journal*, *26*(7), 2507–2520. https://doi.org/10.1007/s10040-018-1789-z

Nippgen, F., McGlynn, B. L., Emanuel, R. E., & Vose, J. M. (2016). Watershed memory at the Coweeta Hydrologic Laboratory: The effect of past precipitation and storage on hydrologic response. *Water Resources Research*, *52*(3), 1673–1695. https://doi.org/10.1002/2015WR018196

Ochoa, C. G., A. G. Fernald, S. J. Guldan, & M. K. Shukla. (2007). Deep Percolation and its Effects on Shallow Groundwater Level Rise Following Flood Irrigation. *Transactions of the ASABE*, *50*(1), 73–81. https://doi.org/10.13031/2013.22413

Osman, M., Zaitchik, B., Otkin, J., & Anderson, M. (2024). A global flash drought inventory based on soil moisture volatility. *Scientific Data*, *11*(1), 965. https://doi.org/10.1038/s41597-024-03809-9

Penna, D., Tromp-van Meerveld, H. J., Gobbi, A., Borga, M., & Dalla Fontana, G. (2011). The influence of soil moisture on threshold runoff generation processes in an alpine headwater catchment. *Hydrology and Earth System Sciences*, *15*(3), 689–702. https://doi.org/10.5194/hess-15-689-2011

Pereira, L. S. (2017). Water, Agriculture and Food: Challenges and Issues. *Water Resources Management*, *31*(10), 2985–2999. https://doi.org/10.1007/s11269-017-1664-z

Quemada, M., Baranski, M., Nobel-de Lange, M. N. J., Vallejo, A., & Cooper, J. M. (2013). Meta-analysis of strategies to control nitrate leaching in irrigated agricultural systems and their effects on crop yield. *Agriculture, Ecosystems & Environment*, *174*, 1–10. https://doi.org/10.1016/j.agee.2013.04.018

Rieffenberger, V., Kelley, P., Vichorek, D., Lien, B., Ames, G., & Beck, J. (1989). *The Montana Irrigator's Pocket Guide*. Energy Division, Montana Department of Natural Resources and Conservation.

Robinson, M., W. A. Sigler (2025). Irrigation Management and Soils as Controls on Deep Percolation and Nitrate Leaching in Agricultural Systems: Thesis Data and Code, HydroShare, https://doi.org/10.4211/hs.2d6042efdc7944288ce486ae9a58da9e

Ruehlmann, J., & Körschens, M. (2009). Calculating the Effect of Soil Organic Matter Concentration on Soil Bulk Density. *Soil Science Society of America Journal*, *73*(3), 876–885. https://doi.org/10.2136/sssaj2007.0149

Saxton, K. E., Rawls, W. J., Romberger, J. S., & Papendick, R. I. (1986). Estimating Generalized Soil-water Characteristics from Texture. *Soil Science Society of America Journal*, *50*(4), 1031–1036. https://doi.org/10.2136/sssaj1986.03615995005000040039x

Scaife, C. I., Singh, N. K., Emanuel, R. E., Miniat, C. F., & Band, L. E. (2020). Non-linear quickflow response as indicators of runoff generation mechanisms. *Hydrological Processes*, *34*(13), 2949–2964. https://doi.org/10.1002/hyp.13780

Sharma, V. (2019). *Basics of Irrigation Scheduling*. University of Minnesota Extension. extension.umn.edu/irrigation/basics-irrigation-scheduling#sources-1846810

Singh, N. K., Emanuel, R. E., McGlynn, B. L., & Miniat, C. F. (2021). Soil Moisture Responses to Rainfall: Implications for Runoff Generation. *Water Resources Research*, *57*(9), e2020WR028827. https://doi.org/10.1029/2020WR028827

Tymchak, M. P., & Torres, R. (2007). Effects of variable rainfall intensity on the unsaturated zone response of a forested sandy hillslope. *Water Resources Research*, *43*(6). https://doi.org/10.1029/2005WR004584

Wagner, S., Cattle, S. R., & Scholten, T. (2007). Soil-aggregate formation as influenced by clay content and organic-matter amendment. *Journal of Plant Nutrition and Soil Science*, *170*(1), 173–180. https://doi.org/10.1002/jpln.200521732

Wang, C., Fu, B., Zhang, L., & Xu, Z. (2019). Soil moisture–plant interactions: An ecohydrological review. *Journal of Soils and Sediments*, *19*(1), 1–9. https://doi.org/10.1007/s11368-018-2167-0

Wiekenkamp, I., Huisman, J. A., Bogena, H. R., Lin, H. S., & Vereecken, H. (2016). Spatial and temporal occurrence of preferential flow in a forested headwater catchment. *Journal of Hydrology*, *534*, 139–149. https://doi.org/10.1016/j.jhydrol.2015.12.050

Yang, F., Zhang, G.-L., Yang, J.-L., Li, D.-C., Zhao, Y.-G., Liu, F., Yang, R.-M., & Yang, F. (2014). Organic matter controls of soil water retention in an alpine grassland and its significance for hydrological processes. *Journal of Hydrology*, *519*, 3086–3093. https://doi.org/10.1016/j.jhydrol.2014.10.054

Zhang, Y.-K., & Schilling, K. E. (2006). Effects of land cover on water table, soil moisture, evapotranspiration, and groundwater recharge: A Field observation and analysis. *Journal of Hydrology*, *319*(1), 328–338. https://doi.org/10.1016/j.jhydrol.2005.06.044

CHAPTER FOUR

SEASONAL SOIL CRACKING AND DYNAMIC NITRATE CONCENTRATIONS CONTROL DEEP PERCOLATION AND LEACHING IN AN IRRIGATED SYSTEM: IMPLEMENTING TIME VARIABLE SOIL HYDROLOGICAL PARAMETERS FOR PROBABILISTIC MODELING

Contribution of Authors and Co-Authors

Manuscript in Chapter 4

Author: Meghan Robinson

Contributions: Data collection; model development; data analysis; manuscript writing

Co-Author: W. Adam Sigler

Contributions: Initial research conceptualization; lead on funding acquisition; field and study design; model development; detailed editing and review of writing

Co-Author: Clain Jones

Contributions: Feedback on nutrient management; detailed editing and review of writing

Co-Author: Kent McVay

Contributions: Reviewed writing

Co-Author: Jasmine Neupane

Contributions: Reviewed writing

Co-Author: Robert Payn

Contributions: Consulted on modeling approaches and concepts for characterizing uncertainty

Manuscript Information

Meghan Robinson, W. Adam Sigler, Clain Jones, Kent McVay, Jasmine Neupane, Robert Payn

Status of Manuscript: [Double click to put an X in one of the options below, then delete instruction in brackets. If you cannot double click to add an X, search for "Check Box Content Control."]

☒ Prepared for submission to a peer-reviewed journal
☐ Officially submitted to a peer-reviewed journal
☐ Accepted by a peer-reviewed journal
☐ Published in a peer-reviewed journal

Abstract

Water and nitrogen management are crucial for supporting adequate agricultural crop yields and mitigating environmental consequences from nitrate leaching. In irrigated systems, extended periods with high soil water content create prolonged opportunities for deep percolation (defined here as water drainage below 1.5 m) and nitrate leaching. We aim to understand mechanisms controlling deep percolation and nitrate leaching risk, as well as their temporal variability. Research was conducted in a center pivot irrigated field cultivated with small grains by a cooperating producer in central Montana. Six soil pits were instrumented with soil water sensors at four depths (15, 30, 60, and 90 cm) and suction lysimeters at two depths (30 and 60 cm). We characterized deep percolation with Hydrus 1D using the dual permeability module to account for preferential flow. Deep percolation predictions from Hydrus were multiplied by lysimeter nitrate concentrations to estimate nitrate leaching. Modeling efforts estimated that cumulative deep percolation was 2.6 to 5.2 cm in 2023 and 4.9 to 7.7 cm during the 2024 growing season. In 2023, we estimated 0.5 to 2.8 kg ha^{-1} total nitrate leaching losses, a low quantity reflecting that high nitrate concentrations coincided with a period of limited deep percolation following tillage. In 2024, we estimated 4.6 to 18.0 kg $ha^{-1}$of leached nitrate, which we attribute to the sustained nitrate concentrations from a slow-release fertilizer allowing the alignment of peak deep percolation periods and high nitrate concentrations. In both study years, periods of highest deep percolation occurred after the development of desiccation cracks at the soil surface. These findings have implications for soil water modeling efforts suggesting that the incorporation of dynamic soil structural parameters is important for quantifying the temporal

variability in risk of deep percolation and nitrate leaching. Variable deep percolation responses before and after desiccation crack formation has implications for irrigation management and emphasizes the need to understand seasonal patterns in soil and nitrate behaviors to improve water and nitrogen use efficiency.

4.1: Introduction

Water and nitrogen management are critical for balancing environmental and economic sustainability in agriculture (Mueller et al., 2012). In arid and semi-arid climates, water limits agricultural productivity; therefore, irrigation provides an opportunity for enhancing crop yields, particularly if water management minimizes deep percolation and runoff losses (Pereira, 2017). In recent decades, irrigated acreage has increased in the western US (Ketchum et al., 2020), and is forecast to continue to expand in efforts to meet agricultural intensification demands worldwide (Haile et al., 2024). The contributions of irrigated lands to food production and security are crucial, as they produce 40% of the global food supply while only accounting for 20% of cultivated lands (FAO, 2021). Enabling this high productivity is a significant impact on water resources, with irrigation representing the largest withdrawal of and consumptive use for water (Zhang et al., 2022). A challenging combination of increasing need for crop production (van Dijk et al., 2021) and competition for water resources as the population grows (Mancosu et al., 2015) coincides with climate change altering the timing, distribution, and quantities of precipitation, causing greater uncertainty in an already limited water supply (Lobell et al., 2011; Wang, 2005). Faced with these water supply limitations, pressure on agriculture - particularly in irrigated systems - to improve water use efficiency is imminent (Mehta et al., 2024; Wang et al., 2021).

Nitrate is vulnerable to leaching with deep percolation, posing challenges both for downgradient water quality and for the economic viability of agricultural operations (Quemada et al., 2013). Increasing nitrogen fertilizer inputs have been linked to heightened nitrate concentrations in groundwater (Puckett et al., 2011) and surface waters (Stets et al., 2015), which have consequences for both ecosystem and human health. Nitrogen (N) use efficiency is closely linked with water use efficiency, and improved irrigation scheduling has been identified as an ideal method for reducing nitrate leaching without detrimental impacts on crop yields (Quemada et al., 2013). Nitrogen may be the most limiting nutrient for crop production (Du et al., 2020), and a limiting growth factor alongside water (Mueller et al., 2012). In cultivated fields, nitrogen fertilizers are applied to mitigate against nutrient deficiencies and enhance crop yields. Nitrate leaching has previously been identified in Montana dryland agricultural systems, with the highest risk of deep percolation and associated nitrate losses occurring on the thinnest soils and during wet spring months following fallow cycles (Sigler et al., 2020).

Irrigation water inputs may extend periods when soil water content is near or exceeds field capacity, resulting in increased opportunity for water and nitrogen losses (Dzurella et al., 2015). Irrigation scheduling that improves water and nitrogen use efficiency depends on understanding soil water retention (Gu et al., 2020) and nitrate transport behaviors. Complexity in irrigation scheduling is exacerbated when considering seasonal variability in water availability, soil infiltration capacity (Guo et al., 2021), and solute concentrations. Bolstering methods for assessing deep percolation and nitrate leaching risk is critical for improving the capacity for efficient water and nitrogen management in irrigated agricultural systems.

The potential impacts of macropores on hydrologic processes such as deep percolation and solute leaching has long been recognized (Beven & Germann, 1982; Jarvis, 2007). Preferential flow through macropores has hydrologic implications including increased infiltration capacity, changed water storage distribution within a soil profile, and greater groundwater recharge (Nimmo, 2021). In irrigated systems, preferential flow may be beneficial for water infiltration in deep rooting crops; however, it may also reduce irrigation water use efficiency if deep percolation losses occur (Beyene et al., 2018). As preferential flow bypasses the soil matrix, solutes may have more limited opportunity for sorption and be prone to leaching (Zhang et al., 2018).

Soil-water modeling can be leveraged to predict hydrologic responses to changes in management and to scale point observations to field or landscape scales (Heinen et al., 2024; Šimůnek et al., 2003). The simplest soil water models assume equilibrium water flow through a single, uniform, porous soil substrate (Šimůnek et al., 2003). These single porosity models can utilize pedotransfer functions that describe relationships between readily characterized soil properties such as texture or bulk density and the soil's expected hydrologic behaviors, which facilitates relatively simple model parameterization (Schaap et al., 2001). Single porosity models do not capture water movement through preferential flow paths, which may be necessary in some systems.

Dual porosity and dual permeability models allow characterization of water movement through soils with both soil matrix and macropore regions. Parameterization for dual porosity and permeability models is more complex; however, due to the higher number of parameters required for describing water flow through domains with different water retentions. These

measurements may be difficult or impossible to determine non-destructively in the field (Šimůnek et al., 2003). Inverse modeling to estimate necessary parameters based on observed data is therefore common (Roulier & Jarvis, 2003). Previous studies have reported that benefits to inverse modeling may include the capturing of a field signal that integrates processes that are not explicitly considered in models (Graham et al., 2018). However, inverse modeling has also been criticized for its variability in parameter estimations based on type of input data (Köhne et al., 2006), production of non-unique parameter solutions and susceptibility to equifinality (Isch et al., 2019), and the potential for predicting physically unreasonable parameters (Haws et al., 2005). Uncertainty in inversely modeled parameter solutions may also result in error propagation when using forward models (Arora et al., 2012). While it has been recommended that future modeling efforts move towards independently derived macropore parameters determined with methods such as X-ray tomography, this requires equipment and computational resources that many model users may not have access to, contributing to the challenges of parameterizing dual porosity and permeability models (Jarvis et al., 2016).

In addition to challenges with parameterizing dual porosity and permeability models, spatial variability in macropore distribution and flow path heterogeneity complicates scaling point observations or single model runs to field and landscape levels that may be more relevant for hydrological and biogeochemical processes (Budhathoki et al., 2022). Efforts to link soil properties with potential for preferential flow path development has shown promise for identifying combinations of management, texture, and biotic activity that produce preferential flow, which could be applied at landscape levels (Jarvis et al., 2009). Continental scale modeling efforts have suggested that preferential flow may be important for groundwater recharge,

highlighting the importance of understanding macropore behavior at large scales (Kocian & Mohanty, 2024). However, small scale variability in the drivers of macropore development may result in non-constant modeling needs across proximate field sites (Fishkis et al., 2020). Bridging gaps between landscape behavior and single point models is important in expanding the understanding of contributions from preferential flow to processes like deep percolation and leaching (Beven & Germann, 2013).

Literature has also increasingly recognized the importance of temporal variability in soil structure (Heinen et al., 2024). Work in soil columns has supported that soil water retention, hydraulic conductivity, and relative abundance of macropores can all change as desiccation cracks develop in response to wetting and drying cycles (Coppola et al., 2015; Greve et al., 2010). Models reflecting time variability in potential for macropore flow may improve soil water content predictions, though are not widely incorporated into common water flux models (Luo et al., 2023). Work in field settings has supported that the dynamic nature of soil cracking can influence water infiltration behavior over time (Greve et al., 2011), and that macropore development from biotic drivers may vary seasonally (Bormann & Klaassen, 2008). However, soil column studies dominate the literature on temporal variability in cracking behavior and expansion to vegetated settings has been identified as a priority in preferential flow model development (Bordoloi et al., 2020).

Limited studies have linked dynamic soil structure with implications for solute transport. Variability in preferential flow and phosphorus leaching has been attributed to desiccation crack development in tilled, tile drained systems (Williams et al., 2016). Additionally, variable soil structure from both freeze-thaw cycles and desiccation crack formation has been hypothesized to

contribute to dynamic soil hydraulic conductivities and seasonal variability in nitrate concentrations in tile discharge (Kokulan et al., 2021). High clay content and irrigation scheduling that results in wetting and drying cycles have been found to exacerbate surface crack formation and increase the quantity of leached nitrate in greenhouse settings (Wang et al., 2022). This previous work suggests that links between soil cracking and solute transport exist and warrant further exploration.

Our research presented here broadly aims to understand how weather, soils, and irrigation management impact deep percolation and nitrate leaching risk. Nitrate leaching is controlled by the timing of downward water fluxes below the root zone and the concentration of soil water nitrate at that time. Given seasonal variations in both water inputs and nitrate concentrations, we ask how periods of deep percolation losses and soil nitrate concentrations interact to produce nitrate leaching risk. We hypothesize that neither periods of highest soil nitrate concentration nor the periods of highest deep percolation rates alone produce the highest nitrate leaching risk. Rather, we expect that periods of high nitrate leaching risk will vary based on alignment of both water movement and adequately high nitrate concentrations. Additionally, soil water fluxes are controlled by soil hydrologic characteristics that may vary over time due to structural changes in soils, such as desiccation crack formation or disturbance from tillage. We ask whether inclusion of time variable soil hydrologic parameters facilitates more accurate modeling of soil water dynamics. We hypothesize that for clay soils with observed dynamic soil structure, models that incorporate temporal changes in soil hydrologic parameters will simulate observed field data more accurately than models with static parameters. We assess these questions in the context of various sources of uncertainty including 1) known limitations of inverse modeling for

determining macropore hydrologic parameters; 2) spatial variability in the extent and connectivity of preferential flow paths; and 3) temporal variability in soil structure development.

4.2: Methods

4.2.1: Site Description and Field Management

Research was conducted at a field managed by a cooperating producer on the Fairfield Bench of north central Montana, in the Northern Great Plains. North central Montana is generally characterized by a semi-arid climate. The twenty-year mean annual precipitation for Fairfield is 31.4 cm, with approximately 50% of rainfall occurring between April and June (Western Regional Climate Center Station 242857). Annual potential evapotranspiration (PET) is 133 cm, with highest atmospheric demands during June, July, and August (Bureau of Reclamation Agrimet: Station GFMT). The Fairfield Bench is a gravel terrace with alluvial origins and a relatively shallow aquifer atop underlying shale (Vuke et al., 2002), with elevated nitrate in groundwater (Montana Department of Agriculture, 2015) and evidence of nitrate export in surface waters downstream (Water Quality Planning Bureau, Watershed Managment Section, 2004). Approximately 33,590 ha of the Fairfield Bench are irrigated with water diverted from the Sun River (HUC 10030104) and delivered to fields via a network of surface canals administered by the Greenfields Irrigation District (GID). Nitrate concentrations in irrigation water are less than 0.5 mg L^{-1}, as water is diverted at the mountain front before agricultural or other anthropogenic activities introduce nitrate. The Fairfield Bench is dominated by small grain production, and USDA CropScape estimates that between 2020 and 2024, 40-50% of acreage was planted as barley (*Hordeum vulgare*). Spring wheat, winter wheat, alfalfa, and canola are additional crops commonly grown on the Fairfield Bench. The GID estimates that 60% of

irrigation uses center pivots, reflecting ongoing conversion from historically dominant flood irrigation (Coleman et al., 2022).

The Soil Survey Geographic Database (SSURGO) suggests soils on the Fairfield Bench are primarily clay loams (Chp 4 – Figure 1). The Rothiemay-Niart complex, mapped as a clay loam soil with substantial gravel below 125 cm, is the single most widespread soil map unit on the Bench, accounting for 40% of all soils (Chp 4 - Table 1). In total, roughly 70% of all mapped soils on the Bench are clay loams (Chp 4 - Figure 1). Our field site is mapped as Rothiemay-Niart and Varney-Rothiemay clay loam soils (Chp 4 - Table 1). Hydrometer texture analysis (see Chapter 2.2.3 for methods) on field soil samples suggests that clay content is 30-40%, with increasing sand deeper in the soil profile. Substantial coarse fragments were noted at all depths at the field site. Soil structure from aggregation and cracking was observed during field visits. We note that extensive field leveling has been common on the Fairfield Bench in recent decades, perhaps limiting the extent to which mapped soils can be expected to align with field data.

Field monitoring equipment was installed in a center pivot irrigated field managed by a cooperating producer. Two irrigation treatments were applied to the field: the grower's standard practice (GSP), covering 170° of the total 180° pivot area, and an experimental reduced irrigation rate (RIR) over one 10-degree pivot section (Chp 4 - Figure 1). GSP and RIR were irrigated with the same frequency and spacing between irrigation events, though RIR received approximately 80% of the applied irrigation quantity relative to GSP (Chp 4 - Table 2). Individual passes of irrigation were generally applied in rapid succession (four to thirty hour spacing) for an irrigation set. Irrigation sets consisted of six to ten passes with each pass being 1.65 cm (GSP) or 1.3 cm (RIR), and irrigation sets were generally separated by ten to twenty

days. In both 2023 and 2024, the total irrigation quantity for GSP was 23-24 cm, and 18-19 cm for RIR (Chp 4 - Table 2). In 2023, the field was planted as barley, with a growing season from May 16th to August 26th. One application of 121 kg ha^{-1} N as urea fertilizer was broadcast and tilled for incorporation four days prior to seeding. An additional 13.5 kg ha^{-1} of N was applied with the seed using a no-till drill. In 2024, the field was planted as spring wheat, with a growing season from April 14th to September 4th. Fertilizer application included 143 kg ha^{-1} N as urea broadcast and incorporated immediately prior to seeding, and an additional 112 kg ha^{-1} N as ESN slow-release urea fertilizer (Nutrien, Saskatoon, Canada) on June 7th to sustain high soil nitrate concentrations with the goal of increasing wheat protein content. In both 2023 and 2024, the field was tilled to a depth of approximately 8 cm before seeding.

4.2.2: Field Instrumentation and Sampling

Monitoring sites were established under the center pivot and were instrumented with soil water sensor arrays and suction lysimeters. Four sets of monitoring equipment were installed in 2023, three of which were installed one month prior to seeding and one which was added during the first irrigation set. An additional two sets of equipment, for a total of six, were installed at seeding in 2024. Soil water sensor arrays installed in 2023 consisted of HOBO Decagon 10HS capacitance sensors at 15, 30, and 90 cm (Onset Computer Corp., Bourne, MA, USA). METER Teros-12 capacitance soil water sensors were installed at the same depths plus 60 cm in 2024 (METER Group, Pullman, WA, USA). All soil water sensors logged data every two hours, continuously from the time of installation to the end of the analyzed data period. Site equipment details and periods of data collection are noted in Appendix 1. Porous quartz suction lysimeters were installed following manufacturer specifications at 30 and 60 cm below ground surface,

using silica slurry to ensure lysimeter contact with the soil matrix (Prenart Equipment, Fredriksburg, Denmark). Soil water sensors were inserted horizontally into a soil pit face with the probe body in undisturbed soil. A steel rod was driven into soils at a 30-degree angle starting at the soil pit face to create a pilot hole, so lysimeters had an undisturbed soil profile directly above them. Holes were back filled with local soil to minimize artificial preferential flow to lysimeters.

Additional field instrumentation included one Licor-710 (LI-COR Environmental, Lincoln, NE, USA), installed two meters above soil height and logging actual evapotranspiration (AET) at 30-minute intervals from mid-May to November of 2024. The Licor was removed briefly for harvest, resulting in a data gap from August 28th to September 6th. Manual rain gauges were mounted on one-meter-tall wood posts under the pivot at all field monitoring sites. An additional manual rain gauge was installed at the edge of the field away from the pivot to provide a precipitation-only reading. This allowed partitioning precipitation and irrigation for each gauge, assuming constant precipitation across the field. Two sites included field cameras that took hourly photographs to document crop growth stage and irrigation timing. One camera was mounted facing the soil to allow visual assessment of crack development.

The field was visited biweekly during the 2023 and 2024 growing seasons. At each visit, lysimeters were put under -60 kPa vacuum and allowed to sit for 20-24 hours to collect samples. Lysimeters successfully collected samples for approximately 70% of attempts, with more samples collected earlier in the season and following irrigation events, when soils were sufficiently wet. Lysimeter samples were field filtered with 0.45-μm nylon filters, stored on ice, and frozen until analysis. All samples larger than 0.5 mL (range: 0.07-120 mL, 120 samples

collected) were analyzed for nitrate concentrations by cadmium reduction and colorimetry (Lachat QuickChem 8500). During 2024, soil samples were collected by hand auger at biweekly visits for 0-15, 15-25, 25-35, 35-55, and 55-66 cm depth increments at each of the six monitoring sites. Additional soil samples were collected from 0-15, 15-30, 30-60, and 60-90 cm prior to fertilizer application and at harvest. Soil samples were transported on ice, frozen and dried, and analyzed for nitrate at AGVISE laboratories using 0.12 M KCl extractions then cadmium reduction and colorimetry. Paired t-tests calculated for a 0.95 confidence level were used to determine whether there were statistically significant differences in mean 55-66 cm nitrate-N inventories between consecutive visits. During field visits, 2-3 plants were excavated to observe approximate root depth. To minimize disturbance and maintain a closed canopy over equipment, digging was limited. At harvest, when crop disturbance concerns were reduced, larger soil pits were dug and observations on maximum rooting depth were made. Earlier observations were then scaled based on these final observations. At all visits, manual rain gauge readings were recorded, and gauges were emptied. Mineral oil was added to prevent evaporative losses.

4.2.3: Model Inputs and Time Variable Model Framework

The Hydrus 1D dual permeability module was used to model soil water fluxes with a focus on estimating deep percolation. We find that for structured clay soils, the inclusion of a macropore domain is critical for satisfactory model performance. Dual permeability assumes two soil domains with separate water retention characteristics. One region represents the soil matrix in which water moves slowly, and one represents the macropore or fracture regions in which water moves quickly (Šimůnek & van Genuchten, 2008). Hydrus solves Richard's equation for

both domains, weighted to reflect the relative volumetric distribution of macropores and soil matrix:

$$\frac{\partial\,\theta_f(h_f)}{\partial t} = \frac{\partial}{\partial z}\left[K_f(h_f)\left(\frac{\partial h_f}{\partial z} + 1\right)\right] - S_f(h_f) - \frac{\Gamma_w}{w} \quad (4.1)$$

$$\frac{\partial\,\theta_m(h_m)}{\partial t} = \frac{\partial}{\partial z}\left[K_m(h_m)\left(\frac{\partial h_m}{\partial z} + 1\right)\right] - S_m(h_m) + \frac{\Gamma_w}{1-w} \quad (4.2)$$

In Equations 4.1 and 4.2, the m subscript indicates soil matrix, and f subscript indicates macropore or fracture region. θ is the soil volumetric water content ($cm^3\ cm^{-3}$), *h* is the pressure head (cm), *t* is the time (days), *z* is the depth coordinate (cm), *K* is the hydraulic conductivity for a given pressure head ($cm\ day^{-1}$), *S* is a sink term accounting for root water uptake over time ($cm^3\ cm^{-3}\ day^{-1}$), w is the ratio of macropores to soil matrix in the whole soil volume ($cm^3\ cm^{-3}$), and Γ_w is the exchange of water between macropores and the matrix ($cm\ day^{-1}$) (Šimůnek & van Genuchten, 2008). Water transfer rate between the soil matrix and macropore regions is determined by:

$$\Gamma_w = \frac{\beta}{a^2}\gamma_w K_a(h_f - h_m) \quad (4.3)$$

Where β is an aggregate geometry dependent scaling factor (dimensionless), *a* is the average soil aggregate length (cm), γ is an empirical scaling factor generally assumed to be 0.4 (dimensionless), and *Ka* is the saturated hydraulic conductivity at the aggregate-macropore interface ($cm\ day^{-1}$) (Gerke & van Genuchten, 1993). A Γ_w greater than 0 indicates that water moves from a macropore into the slow water movement soil matrix region.

In the study system, the top 8 cm of soil experience tillage in the early spring, which disrupts soil structure (Blanchy et al., 2023; Hellner et al., 2018). Shrink-swell clay behaviors prompted by wetting and drying cycles from irrigation then leads to cracking and dynamic soil

macropore conditions throughout the season (Greve et al., 2011; Luo et al., 2023). To capture these temporally variable soil surface conditions, we developed a modeling framework in which water retention parameters are not static over time. Models alternated between two sets of conditions: one 'tilled' scenario with minimal macropore structure present in the soil surface, and one 'cracked' scenario in which macropore water retention parameters are more distinctly separate from the soil matrix and macropores represent a larger volume of the soil. In this time-variable framework, an initial model with a first set of soil hydrologic parameters was executed, and then output pressure heads from the modeled soil profile discretized at 1 cm intervals were used as input pressure heads for the start of the subsequent model run. The next model was then executed using the second conditions' set of soil hydrologic parameters and starting pressure heads based on the previous model run. These changes in model parameters occurred on dates that represent an expected change in soil structure (1 - tillage, and 2 - VWC reaching a dryness threshold after irrigation events to induce cracking). Temporal changes in soil structure were confined to the top 10 cm of soil, representing a depth that is subject to both tillage and most intense drying. The soil profile in Hydrus was divided into two layers, and the lower layer (10-150 cm) has static structure over time to prevent erratic modeled soil water content behavior resulting from changing soil water retention curves. Soils were modeled as sand deeper than 150 cm to reflect an assumed gravel layer at depths lower than 150 cm.

Meteorological boundary condition inputs for Hydrus included precipitation from the nearest Montana Climate Office Mesonet station ("mdapower"), located 10 miles east of the field site. Water input was augmented by irrigation quantities from our cooperator, verified with on-field rain gauges. Reference potential evapotranspiration (PET) was calculated using Penman-

Monteith (Allen et al., 2006) with minimum and maximum daily temperature, relative humidity, and wind speed data from the Mesonet station, and solar radiation from GridMet (Abatzoglou, 2013). Data comparisons between Penman-Monteith weather parameters from our cooperating producer's personal weather station and the "mdapower" Mesonet station support that spatial variability in was minimal enough to justify data usage from the "mdapower" site (Appendix 2). We then used crop coefficients determined by the ratio of field observed AET to PET to inform evapotranspiration boundary conditions for Hydrus (Chp 4 - Figure 2).

Models were calibrated using field observations and validated by water budget assessment. Field-collected Licor AET data, soil VWC at 90 cm, and soil VWC at 15 cm were data sets used for calibration. Calibration efforts were focused on 90 cm VWC, as this data stream was most reflective of deep soil hydrologic conditions and opportunity for deep percolation. Transpiration is the primary water loss pathway in this system, so the comparison of modeled and measured AET was evaluated to ensure accuracy in the model's ability to estimate AET. Soil VWC at 15 cm was assessed to understand how well the dynamic surface wetting and drying behaviors were captured. For all model runs, root mean square error (RMSE) and Nash-Sutcliffe Efficiency (NSE) were calculated. NSE is the primary statistic for model selection, as it penalizes model error that exceeds observed data variability and is considered appropriate for hydrologic data. NSE values are bounded by -infinity < NSE < 1, with NSE values above zero indicating model error is less than observed variability and a value of 1 indicating a perfect fit (Nash & Sutcliffe, 1970). Models were validated by comparing deep percolation estimated by seasonal water budget with cumulative deep percolation estimated by the model. Field based seasonal water budget components were evaporation and transpiration from the Licor, changes in

soil storage estimated by soil water sensor arrays, and precipitation and irrigation based on manual rain gauge and nearby weather station data. Runoff was not observed on the field and is therefore assumed to be a minimal part of the water budget.

Using soil water sensors to calculate the wetting front velocity in response to precipitation or irrigation has gained traction as a method for identifying preferential flow in field settings (Guo & Lin, 2018; Lin & Zhou, 2008). The time between observed increases in soil water content at different sensors in a depth array can be divided by the total soil depth difference to understand how quickly water moves through soils. We implemented wetting front velocity calculations by assessing the difference in time for water content responses at 15 and 90 cm sensors in instances where a 90 cm VWC response could be directly linked to a single irrigation event. This method provides insights to field dynamics that support the decision to use the dual permeability module.

4.2.4: Modeling Deep Percolation and Quantifying Nitrate Leaching

To address our proposed questions on deep percolation and nitrate leaching risk and uncertainty of both across the growing season, we executed many model runs with an interface of R (R version 4.5.0, The R Foundation for Statistical Computing, Vienna, Austria) and Hydrus initially developed in Sigler et al. (2020). The first step in this process was solving for soil hydrologic parameters using Hydrus inverse modeling functionality, which applies the Marquardt-Levenberg optimization algorithm to estimate up to 15 soil hydrological parameter values based on field data observations (Šimůnek et al., 2013). We executed 200 inverse models for each monitoring site and used 90 cm VWC data as observation points for optimization. Inverse models had identical boundary conditions, but different initial hydrologic parameter

estimates. Input hydrologic parameters were randomly sampled from distributions based on literature values (Chp 4 - Table 3). Soil matrix hydrologic parameter predictions from ROSETTA based on percentages of sand, silt, and clay from hydrometer analysis (Schaap et al., 2001) were used, and these matrix parameters were held static and not adjusted during inverse modeling. All macropore water retention and aggregate-macropore interface parameters were optimized, except l (0.5) and γ (0.4) for which we used recommended literature values (Gerke & van Genuchten, 1993). Field data used for optimizations were divided into early season (tillage to the end of the first irrigation set), late season (crack emergence onwards), and whole season sets for inverse modeling. These enabled comparisons of model estimates that reflect time variable and static soil hydrologic parameters. Inverse models converged for approximately 65-75% of runs, resulting in 125-150 sets of inverse model predictions for each monitoring site during each time-period.

Forward models were then run with randomly paired early and late season parameter estimates, or with whole season parameter fits. This resulted in an ensemble of roughly 30 model runs with different soil hydrologic parameters for each monitoring site. Comparing daily and cumulative deep percolation estimates from the inverse model ensembles (with variable soil hydrologic parameters) was our approach for characterizing uncertainty in deep percolation for individual sites. Comparisons of deep percolation estimates across sets of models for different monitoring sites was used to assess spatial variability, as we assumed that differences in VWC responsiveness were primarily driven by macropore heterogeneity. Nitrate leaching estimates were then calculated by sampling from nitrate concentration distributions for each day during the growing season and multiplying the nitrate concentration by the daily modeled deep percolation

quantity for each model. For days when lysimeter samples were collected, nitrate distributions were developed by assuming a normal distribution centered on the median observed nitrate concentration and with one standard deviation equal to the distance between the median and most extreme observed nitrate concentration value. To characterize nitrate concentrations between field visits, a linear interpolation of median and standard deviation values was used. Relative water use efficiency across models was assessed by dividing the modeled deep percolation by total growing season precipitation and irrigation to understand the fraction of the water budget accounted for by deep percolation. Similarly, estimates on leached nitrate were divided by the total N in fertilizer application to assess the relative magnitude of leaching losses. All code and data for this chapter are available on Hydroshare (Robinson and Sigler, 2025).

4.3: Results

4.3.1: Weather Context

The 2023 growing season followed a typical winter snowpack and had slightly above average precipitation during the April to August growing season (12.7 cm in 2023 versus 12.2 average). April, May, and June of 2023 were all in or near the wettest 25% of monthly total rainfall for 2000-2020 period of record at the AgriMet GFMT station, while July and August were both drier than normal (Chp 4 - Figure 3). The GID irrigation season lasted from late May to mid-August, and a maximum irrigation allotment of 45 cm was allowed, only 52% of which (23.3 cm) was applied to the study field. The 2024 growing season followed a much drier winter, though growing season precipitation was above average at 16.4 cm, reflecting wetter than usual April, May, and August conditions. The irrigation season was more limited due to poor snowpack and lower resulting reservoir water storage. Maximum irrigation allotments were 30

cm (80% or 23.9 cm of which was applied to the study field), and irrigation was only possible between early June and late July.

4.3.2: Patterns in Soil Water Content

Soil VWC patterns suggest that across all monitoring sites and both irrigation treatments, irrigation water induced a response at 15 cm for all irrigation passes. During both the 2023 and 2024 growing seasons, 16 irrigation passes occurred for a total of 32 unique events. The mean increase in VWC at 15 cm across all passes for the three GSP sites (F113, F133, F143) was 0.023 $cm^3 cm^{-3}$. The mean increase in volumetric water content for the three RIR sites (F121, F123, F128) was slightly lower at 0.016 $cm^3 cm^{-3}$. While inter-sensor variability in exact ranges of measured VWC values varied, possibly driven by proximity to rocks or other influences on individual sensors, patterns in responses were consistent across sites and suggest more muted responses under the RIR (Chp 4 - Figure 4).

All 90-cm soil water sensors detected increases in VWC at least once during the irrigation season during both 2023 and 2024 (Chp 4 – Figure 4). Unlike 15 cm datasets, increases in deep soil water content were not always able to be linked to individual irrigation events. Magnitudes of response varied both spatially across monitoring sites and temporally throughout the growing season. During the first irrigation set, changes in 90 cm VWC ranged from zero (no indication of water inducing a response at 90 cm) to an increase of 0.03 $cm^3 cm^{-3}$ between the start of the set and the peak observed VWC. The second irrigation set occurred after desiccation cracks formed at the soil surface. Water content response magnitudes were larger, and occurrences of responses were more frequent. Across monitoring sites, we observed variability in the extent of response to the second irrigation set, ranging from increases in water content of

0.007 $cm^3\ cm^{-3}$ to 0.07 $cm^3\ cm^{-3}$ (Chp 4 - Figure 4). Differences in 90 cm VWC responses to the irrigation treatment rates were less clear than at 15 cm. This may suggest that initiation of macropore flow occurred for both irrigation rates after desiccation cracks formed. After desiccation crack formation, deep soil VWC responses to individual irrigation events were clearest. For irrigation events during the second irrigation set in 2024 with clear 90 cm responses, the average time between the irrigation application and the response at 90 cm was approximately 4 hours. This suggests a wetting front velocity of 540 cm/day, which greatly exceeds literature values for clay loam saturated hydraulic conductivity (18-40 cm/day) (Pachepsky & Park, 2015).

4.3.3: Lysimeter Nitrate Concentrations

During the summer of 2023, lysimeter soil water samples showed a clear signal of decreasing nitrate at both 30 and 60 cm (Chp 4 – Figure 5). Nitrate concentrations were highest immediately following N fertilizer application, and then decreased quickly before being consistently low after the first irrigation set. At 11 days after fertilizer application, 30 cm nitrate-N concentrations ranged from 26.6 to 44.4 mg L^{-1} and 60 cm nitrate ranged from 17.3 to 18.5 mg L^{-1}. Nitrate concentration ranges were obtained from three lysimeters at 30 cm, but only two lysimeters at 60 cm as the third failed to produce samples. At 32 days after fertilizer application and 11 days prior to the first irrigation set, nitrate-N concentrations ranged between 23.3 and 36.7 mg L^{-1} (30 cm) and 17.5 and 24.9 mg L^{-1} (60 cm), dropping to 0.7 to 2.5 mg L^{-1} (30 cm) and 0.1 to 1.4 mg L^{-1} (60 cm) by the end of irrigation set one. Nitrate-N concentrations above 3 mg L^{-1} were not detected for the remainder of the 2023 growing season and the median nitrate-N concentration was 0.27 mg L^{-1} following irrigation set two, apart from site F121. Installation of

F121 occurred during the first irrigation cycle, whereas all other monitoring sites were installed prior to seeding. This resulted in a complete destruction of the barley canopy over site F121 for most of the growing season. Without crop uptake, nitrate-N concentrations at F121 climbed to 28 mg L^{-1} (30 cm) and 17 mg L^{-1} (60 cm) by harvest in late August. In 2023, our deepest rooting depth observations were approximately 50 cm. During the period of most pronounced decreases in lysimeter nitrate concentrations, roots were observed to approximately 30 cm.

Between 2023 barley harvest and 2024 initial urea fertilizer application, soil water nitrate-N concentrations increased by 8.8 mg L^{-1} at 30 cm and 2.67 mg L^{-1} at 60 cm (Chp 4 – Figure 5). Following spring wheat seeding and eight days after urea fertilizer application in 2024, nitrate-N concentrations ranged from 17.6 to 43.5 mg L^{-1} (30 cm) and 5.4 to 6.2 mg L^{-1} (60 cm), excluding site F121. Unlike 2023, we did not observe a clear decrease in nitrate concentrations (Chp 4 - Figure 5). We primarily attribute this to the application of the ESN slow-release fertilizer in mid-June, which appears to have sustained heightened nitrate concentrations for the duration of the growing season. In late July, at the latest date that soils were wet enough to facilitate lysimeter sample collection, nitrate-N concentrations ranged from 9.9 to 34.5 mg L^{-1} at 60 cm. Nitrate-N at both 30 and 60 cm at F121 showed persistently high concentrations in 2024, peaking at 71.4 mg L^{-1}, suggesting that impacts of 2023 barley destruction had a multi-year effect (Chp 4 - Figure 6).

4.3.4: Soil Nitrate Inventories

In 2024, soil samples were collected as an additional mechanism for understanding nitrate dynamics and leaching risk (Chp 4 – Figure 7). The median nitrate-N inventory in the top 90 cm of soil one month prior to initial urea fertilizer application was 45.3 kg ha^{-1}, with 12.3 kg

ha^{-1} stored between 60 and 90 cm. At harvest, median nitrate-N stored in the top 90 cm of soil was 30.8 kg/ha, with 3.3 kg ha^{-1} nitrate stored between 60 and 90 cm. Among soil samples collected at biweekly field visits, we observed the highest nitrate-N inventory in the top 66 cm of the soil profile at 119.4 kg ha^{-1} 41 days after the urea fertilizer application. Nitrate-N inventories decreased by 41.5 kg ha^{-1} between this peak observed inventory on May 23rd and the next sampling event on June 5th. On June 7th the slow-release fertilizer was applied, resulting in a 14.6 kg ha^{-1} increase in nitrate-N inventories over the next two weeks. Nitrate then gradually decreased for the remaining eight weeks of the growing season (Chp 4 - Figure 7).

On multiple dates, changes in nitrate concentrations were detected below the rooting depth observed on that date. On May 23rd, following rainstorms totaling 4.3 cm of precipitation, median nitrate concentrations between 15 and 66 cm doubled to tripled relative to inventories for the same depth increments from on May 6th, and roots were only observed to 12 cm. At the 55-66 cm depth, mean nitrate-N inventories were roughly 5 kg ha^{-1} higher (t_5= 5.21, p value < 0.01) on May 23rd. This indicates a redistribution of nitrate into the deeper soil profile before roots depths were sufficiently deep to capture it. Between June 5th and June 20th, (the time period spanning irrigation set one), nitrate-N inventories at 35 to 55 cm increased by 3.9 kg ha^{-1}, and 55 to 66 cm nitrate-N inventories fell by 3.3 kg ha^{-1}. At the 55-66 cm increment, this numerical difference in means is not statistically significant (t_5= -0.76, p value= 0.48). Between our July 16th and July 31st visits, nitrate-N inventories at 55 to 66 cm fell by 4.5 kg ha^{-1}, which again is numerically but not statistically different (t_5= -1.45, p value= 0.20). This possible change was below maximum observed rooting depth. This drop followed the second irrigation set (Chp 4 - Figure 7). Total nitrate leaching estimated by subtracting final 60-90 cm nitrate-N inventories

(3.3 kg ha^{-1}) from pre-fertilizer 60-90 cm nitrate-N inventories (12.3 kg ha^{-1}) suggested 9 kg ha^{-1} losses (t_5= -2.06, p value= 0.13). Similarly, biweekly soil sampling found a decrease of 4.4 kg ha^{-1} (7.8 kg ha^{-1}– 3.4 kg ha^{-1}) at the 55-66 cm increment between highest nitrate inventories and final observations before slow-release fertilizer application, then a decrease of 5.1 kg ha^{-1} (6.2 kg ha^{-1}– 1.1 kg ha^{-1}) was observed after slow-release fertilizer application, for a total loss estimate of 9.5 3.4 kg ha^{-1}. These estimates assume negligible upward movement of nitrate dissolved in water transported up via matric potential.

Site F121 produced abnormal soil samples as well as soil water samples. Nitrate in bulk soil showed clear separation from all other sites, especially after mid-June. In the final biweekly soil sample set on August 15th, profile nitrate inventories ranged from 7.8 to 33.6 kg ha^{-1}, with a median of 21 kg $ha^{-1}$for the five sites that had been subject to continuous canopy closure. The nitrate inventory for F121 was 455 kg ha^{-1}, with all depth increments having nitrate concentrations two to three orders of magnitude higher than other sites (Chp 4 - Figure 7).

4.3.5: Inverse Modeling Parameter Distributions and Model Fits

Inverse model predictions suggested that different optimal soil hydrologic parameters best describe 90 cm soil water content responses across time and space. Temporal parameter variability compared across models optimized for early season data and late season data separately found that for the top 10 cm of soil, slightly lower θ_S, higher *w*, and higher *a* values were predicted for late season soil conditions when surface cracking was observed (Chp 4 - Figure 8). This implies that more responsive periods with developed cracks are better described by a lower saturated water content in macropore domains, a greater relative weight of macropores, and larger soil aggregate size. Among inverse models solved with the whole season

data (assuming no time variability), wider ranges for θ_S, *a*, *Ka*, and *Ks* were observed. Additionally, *n* values were generally higher. The contrast between generally narrow ranges for predicted parameters accounting for time variability and the larger ranges over the whole season may support the separation of parameters seasonally.

Inverse model parameters estimated for data from different monitoring sites were generally similar, however did suggest that more responsive sites were characterized by slightly higher *Ks* and *a* values, or faster water flow through macropore domains and larger soil aggregates. A pronounced bimodal distribution for *w* (the macropore weighting parameter), at site F128 was observed. Site F128 was a generally low-response site, so high weights of predicted macropores (high *w* values) were unexpected.

Implementing time variable macropore domain parameters may improve model fits relative to time static models (Chp 4 - Figure 10), but results are inconclusive. When comparing 90 cm soil water content, the average NSE for time variable model ensemble was -5.43, and the average RMSE was 0.02. Single parameter models resulted in a slightly improved average NSE of -4.92 and an RMSE of 0.02. However, the top three model NSE scores came from time variable models, and the lower mean appears to be driven by a subset of models with very low (< -10) NSE values. In contrast, single parameter time static models had more consistent NSE values in the -6 to -4 range, with no models performing as well as the best time variable models. A threshold NSE value of -10 was used to identify models with accuracy concerns which are excluded from the final suite of models presented here. A model-independent field water budget for 2024 found that Licor-measured growing season evapotranspiration was 39.4 cm, input precipitation and irrigation totaled 29.5 cm, and the decrease in soil water storage between the

beginning and end of the growing season was 8.6 cm. We assume that the remaining water balance was lost to deep percolation, so our water budget suggests -1.3 cm deep percolation, or a failure to close the water budget and a lack of physically possible deep percolation.

4.3.6: Modeled Deep Percolation Results

For the 2023 growing season, models predicted that peak daily deep percolation occurred in late July, in response to the second irrigation set. Patterns show that deep percolation drainage magnitudes increased at the start of the second irrigation cycle and continued until approximately ten days after the conclusion of irrigation. For our more responsive site F143, the range of peak daily deep percolation predictions was 0.11 to 0.16 cm. Estimated peak daily deep percolation at site F128 was a slightly more variable 0.08 to 0.27 cm (Chp 4 - Figure 11). Modeled deep percolation for the 2024 growing season peaked in mid-July, reflecting the earlier onset of irrigation set 2**.** The peak daily deep percolation estimates for F143 in 2024 were 0.12 to 0.36 cm, and for F128 were 0.05 to 0.24 cm. During the second irrigation cycle, separation between sites F143 and F128 was clearer, and models predicted more distinct and high magnitude deep percolation events, which aligns with its more responsive observed soil water content (Chp 4 - Figure 11).

The range of cumulative deep percolation predicted for F143 in 2023 was 5.22 to 6.03 cm, similar to the 4.35 to 5.58 cm predicted for F128 (Chp 4 - Figure 11). During the 2023 early season tilled period, cumulative deep percolation estimates were 0.02 to 0.59 cm (F143) and 0.04 to 0.58 cm (F128). Variation in deep percolation that occurred after soil cracking parameters were implemented ranged more widely, from 3.17 to 5.37 cm (F143) and 2.74 to 5.08 cm (F128). Cumulative deep percolation estimates for the 2024 growing season are generally higher, likely

reflecting the larger quantity of irrigation applied after soil cracks formed. Total deep percolation ranges were 5.60 to 7.74 cm (F143) and 4.88 to 7.49 cm (F128). Estimates of 2024 early season deep percolation found 0.01 to 0.80 cm (F143) and 0.04 to 0.79 cm (F128). Post-cracking cumulative deep percolation estimates found 3.16 to 5.37 cm at F143, and 2.72 to 7.52 cm estimated at F128.

4.3.7: Nitrate Leaching Estimates

Differences in seasonal patterns of nitrate concentrations resulted in divergent periods of highest nitrate leaching risk between 2023 and 2024. In 2023, we find that despite the larger quantity of deep percolation occurring later in the summer following irrigation set 2, the highest magnitude nitrate leaching events occurred in response to irrigation set 1, when nitrate concentrations were highest. In 2024, high nitrate concentrations were maintained due to slow-release fertilizer application, resulting in an alignment of later season peak deep percolation and high nitrate concentrations. This caused peak nitrate leaching losses during irrigation set 2 in 2024.

Variability in the peak daily nitrate leaching losses during 2023 ranges from 0.14 to 0.2 kg $ha^{-1}day^{-1}$, with variability between sites minimal relative to the combined uncertainty in macropore hydrologic parameters and nitrate concentrations (Chp 4 - Figure 12). In 2024, peak daily nitrate leaching estimates ranged from 1.5 to 3.2 kg $ha^{-1}day^{-1}$. In 2023, cumulative leached nitrate estimates for F143 were 0.5 to 1.6 kg ha^{-1}, similar to the 0.5 to 2.8 kg ha^{-1} predicted for F128. In 2024, cumulative leached nitrate estimated for F143 was 4.6 to 18.0 kg ha^{-1}, and 5.5 to 17.2 kg ha^{-1} at F128 (Chp 4 - Figure 12).

4.4: Discussion

4.4.1: Seasonal Development of Soil Cracks Drives Variable Deep Percolation Risk

Our findings suggest that preferential flow and incomplete aggregate saturation drive high water infiltration and percolation through the study field clay loam soils. Differences in change to peak VWC across irrigation treatment rates perhaps reflects the differing extents to which aggregates retained water based on irrigation quantities. The speed and magnitude of responses at 90 cm soil water sensors suggest that preferential flow occurs, because the observed infiltration rates cannot be explained by clay loam saturated hydraulic conductivities alone, and previous work has attributed unexpectedly high wetting front velocities to preferential flow (Lin & Zhou, 2008). We interpret the combination of rapid VWC responses at 90 cm and variable peak VWC following different irrigation quantities to suggest that not all irrigation water infiltrates through the soil matrix, but that macropore flow and crack networks are important infiltration conduits.

Temporal variability among 90 cm VWC responses further suggest that within a growing season, transitions from relatively limited macropore presence and blocky soil structure after tilling to higher connectivity and increased opportunity for preferential flow following desiccation crack formation results in variable soil infiltration and deep percolation risk. The relatively high clay content (30-40%) and mapped presence of 2:1 layer silicate clay with shrink swell capacity, supports that soil mineralogy and particle size distributions are conducive to crack formation. Static soil hydrological parameters may therefore be inadequate for describing the dynamic nature of soil crack development that occurs seasonally with wetting and drying cycles. We do not suggest that soil cracks need to extend to 90 cm to induce variable responses,

but instead that cracks need to penetrate the tilled layer and connect with an intact network of deeper macropores and aggregates that were not disturbed by tillage, a phenomenon documented by previous work (Shipitalo et al., 2004). This finding on the possible importance of seasonal variability in soil structure aligns with work that has suggested model performance may be improved with the implementation of different soil parameters before and after irrigation events (Jiang et al., 2010).

4.4.2: Time Variable Modeling Assessment

Possible improvements in model predictions with time variable soil parameters highlights the importance of seasonal soil macropore and crack development, which is consistent with soil column experiment findings (Luo et al., 2023). We recognize that the current modeling approach has limitations relative to mechanisms that cause variable soil structure conditions in the field, including the assumption of instantaneous changes from tilled to cracked conditions, and the assumption that the output pressure heads from an initial model are appropriate for subsequent model runs. Assuming sudden changes in soil structure on discrete days may be appropriate for events such as tillage; but may be less well suited for gradual processes such as soil crack formation. We implement changes reflecting soil cracking shortly after the conclusion of the first irrigation set to allow time for model equilibration during a dry period when deep percolation risks are minimal, and hope that in doing so, new model conditions will have stabilized by the second irrigation set where deep percolation concerns are heightened. Further development of models that explore impacts of slower transitions between structure conditions could be beneficial in better reflecting actual field processes. We also recognize that tillage does likely homogenize water content in the top 10 cm of soils and therefore the assumption that output

pressure heads from the first model scenario are completely applicable to the next scenario are not fully correct. However, we assume that the relatively small fraction of soil depths that experience tillage and the limited time over which homogenization persists before a matric gradient re-establishes is minimal enough that we do not expect this model assumption to impact deep percolation estimates. We therefore consider our modeling strategy to be sufficiently appropriate for addressing questions focused on deep percolation.

We deem model performance satisfactory based on alignment with field measured 90 cm VWC. Model validation by water budget suggests that deep percolation cannot occur, which is counter to our field observations on sharp increases in VWC at 90 cm. We hypothesize that the disconnect between field and modeled water budgets was influenced by possible overestimations of AET from the Licor. The Licor occasionally measured AET at ratios that exceeded the regular post-canopy closure observation of AET being 1.2 times higher than Penman-Monteith PET, a number we interpret as the crop coefficient for this system. For the seven days where ratios were unexpectedly high, cumulative measured AET was 7.2 cm (Chp 4 - Figure 2). Multiplying the PET over these periods by the assumed crop coefficient of 1.2 suggests total AET would be 5.5, resulting in a difference of 1.7 cm which is enough to close the water budget. The Licor does detect season total AET and patterns that are comparable with OpenET, though days with notable spikes in Licor AET are unexpected based on OpenET data (Chp 4 - Figure 13). Recognizing these possible concerns with Licor AET data, we do not consider the lack of alignment between the field water budget and modeled water budget to invalidate our model results.

4.4.3: Deep Percolation Patterns and Implications for Water Use Efficiency

Spatial variability in VWC patterns and best fit parameters across monitoring sites likely reflects heterogenous soil structure and macropore development. We assume that the inverse modeling parameters that characterize our most responsive site (F143) reflect high macropore connectivity. Among the three parameters with clear variability predicted across sites (*a*, *Ks*, *w*), two changed as expected for increased responsiveness driven by macropores. The slightly higher *Ks* predicted for F143 implies faster water infiltration through macropores, which aligns with rapid and high magnitude soil water content responses. The higher *a* indicates larger aggregate sizes, which causes slower water equilibration between macropores and soil matrix domains, and results in increased preferential flow (Gerke & van Genuchten, 1993). In contrast, the higher *w* cluster predicted for site F128 (a generally less responsive site) indicates a larger fraction of macropores, which is counter to expectations. Comparing early and late season parameter predictions, the higher *w* and *a* parameters for later season indicate a larger fraction of macropores and larger soil aggregates, and the slightly smaller θ_S may indicate a more limited water storage capacity that could contribute to more responsive behaviors. Whole season inverse models generally resulted in wider distributions of parameters, perhaps reflecting the range of conditions across the growing season. Whole season parameters do predict somewhat higher *Ks* and *n* values. The higher *n* suggests a pore size distribution skewed towards larger pores, suggesting networks that are dominated by more or larger macropores (Della Vecchia et al., 2015).

Overall, the modeled periods of highest deep percolation aligned with the wettest 90 cm soil water content conditions, providing field support for deep percolation timing predictions.

Modeling efforts find a more muted signal of deep percolation early in the season when soil structure is least developed, which corresponds with a period when limited VWC responses were observed at 90 cm sensors. Deep percolation accounted for 0.1 to 3.9% of the total model predicted water fate for irrigation and precipitation in the 2023 early season, and 0.06 to 5.4% in 2024. The periods with the highest predicted deep percolation occurred after cracked soil parameters were implemented. After crack formation, deep percolation accounted for 27.1% to 53.1% of water partitioning for irrigation set 2 in 2023 and 18.2% to 50.3% for irrigation set 2 in 2024. The cumulative deep percolation estimates compared to the 33.4 cm of combined growing season precipitation and irrigation result in an overall water budget contribution of 13.0 to 16.7% in 2023, and 12.5 to 19.9% of the total 38.9 cm precipitation and irrigation in 2024.

4.4.4: Variability in Nitrate Leaching Risk

In 2023, we identify the highest risk period for nitrate leaching during the first irrigation set in mid-June. Magnitudes of deep percolation were small following soil structure disruption from tillage during the critical early period when nitrate concentrations were high, resulting in only a cumulative 0.5-2.8 kg N ha^{-1} leached. Total nitrate leaching losses relative to N fertilizer inputs were minimal, with less than 1% of applied N estimated to have been lost to leaching. The peak periods of nitrate leaching and deep percolation were decoupled during the summer of 2023, with low nitrate concentrations during the period of most intense deep percolation in response to irrigation set 2. The inverted patterns between peak periods for daily deep percolation and nitrate leaching losses suggest an offset in most critical risk timings and suggest that irrigation set 2 deep percolation had low associated nitrate losses. This is consistent with previous findings that deep percolation on agricultural lands does not always result in nitrate

leaching (Reading et al., 2019). The offset in peak timings for predicted deep percolation and leaching highlight that management for optimized nitrogen use efficiency may be constrained to a limited period of the growing season, whereas management for water use efficiency may need to be more temporally extensive.

In 2024, the periods of highest deep percolation risk and nitrate leaching risk align. Daily rates for both deep percolation and nitrate leaching peaked in mid-July in response to irrigation set 2. Leaching losses contributed more substantially to nitrogen fertilizer fates in 2024. Lysimeter nitrate and modeled deep percolation based leaching estimates found 4.6 to 17.2 kg N ha^{-1} nitrate losses. Soil sample-based estimates comparing pre-fertilizer and harvest 60 to 90 cm nitrate inventories suggest that 9 kg ha^{-1} of nitrate was leached, which roughly aligns with the median 10.5 kg ha^{-1} (F128) or 12.2 kg ha^{-1} (F143) of leaching predicted by modeling. These estimates account for roughly 5-7% of applied N from fertilizers. While this is not a high percentage, it does indicate opportunities for improving nitrogen use efficiency during years when nitrate concentrations in soils are heightened after the development of soil cracks. The application of the slow-release fertilizer that resulted in prolonged periods of high nitrate concentrations was motivated by the goal of having sufficient nitrogen available to support high protein content in the wheat crop. Protein content is not a priority for barley, which was the 2023 crop. The different management practices implemented to meet these wheat crop-specific goals appear to have the implication that periods of high nitrate leaching risk may be extended, and precision irrigation management over a wider span of the growing season may be necessary to prevent excessive nitrate leaching.

Methods for estimating nitrate leaching assume that nitrate detected by 60 cm lysimeters is subject to leaching loss with deep percolation. While 60 cm lysimeters were below the observed rooting depths during both growing seasons, it is possible that some water and associated nitrate could have moved upwards along potentiometric gradients. Nitrate then may have been taken up by crop roots. This is particularly possible in 2024, when wheat roots were observed at 50 cm during periods when nitrate concentrations were high, and this implies that 2024 leaching quantities may be slightly overestimated. In 2023, roots were only observed to 30 cm at the timing of the observed decreases in nitrate concentrations and coinciding increases in 90 cm VWC that followed the first irrigation set, so leaching is more clearly implicated.

With water being the primary vehicle for nitrate movement, we assume that patterns of nitrate transport and accumulation mirror water movement. Irrigation inputs likely completely saturate the soil surface, allowing water to come into contact with the relatively abundant nitrate from soil organic matter mineralization or urea fertilizer nitrification in the top few centimeters of soil. Nitrate may then be moved deeper into the soil profile through preferential flow paths or partial saturation of aggregates (Chp 4 – Figure 14). The inadvertent barley canopy destruction during the 2023 growing season provides further insights to nitrate storage processes. The climbing nitrate concentrations in lysimeter samples at F121 (where barley was destroyed) during the summer of 2023 illustrate the importance of crop uptake, and that without uptake nitrate continues to mineralize and accumulate in soils. Nitrate mineralization was also likely greater at F121 than other sites, as conditions were generally wetter without root water uptake, and soil temperatures were likely higher without canopy closure. Previous work in Montana has estimated nitrate mineralization rates of 45 kg ha^{-1} annually (John et al., 2017), and this rate may

have been exceeded with warmer and wetter conditions at F121. We continued to find very high nitrate, particularly in bulk soil samples, for over a year and after approximately 30 cm of irrigation application following barley destruction. We interpret this to suggest that without uptake in 2023, nitrate had the opportunity to diffuse deeper into soil aggregates, where it was less accessible to crop roots and percolating water (Chp 4 – Figure 14). This could align with our finding that soil aggregates do not saturate completely following irrigation, because nitrate retention likely would have been more limited if aggregates had been regularly and completely saturated. The contrast between sites with and without canopy destruction could indicate that soil nitrate is not generally stored deep in soil aggregates, and with nitrate closer to aggregate surfaces (rather than intra-aggregate micropores), it is more susceptible to losses with preferential flow.

4.5: Conclusions

In this work, we aimed to understand combinations of water percolation and nitrate concentration patterns that result in high nitrate leaching risk. We find that seasonal development of desiccation cracks is an important control on water infiltration, and that irrigation after cracks have formed has a greater potential for ultimately being lost to deep percolation. Nitrate leaching risk varies based on fertilizer management. If nitrate concentrations are high for a limited window, as occurred in 2023 with a single fertilizer application, nitrate leaching risk may be highest early in the growing season and before deep percolation rates peak. When nitrate concentrations are sustained, the risk of larger nitrate leaching events with high magnitude deep percolation fluxes is increased. Our field observations and modeling efforts suggest the importance of temporal variability in the description of soil hydrologic parameters. In future

work, we plan to include more spatially extensive monitoring sites to develop an improved understanding of spatial variability in macropore characteristics and nitrate leaching risk. We suggest that continued work in developing models should recognize the importance of both spatial and temporal variability in soil behaviors and nitrate leaching risk. We find that understanding and managing for variability in potential deep percolation and nitrate leaching in irrigated systems is important in meeting goals serving agricultural productivity and water quality.

Soil Series	Map Unit and Percent	Taxonomic Class	Texture	Structure	pH	Organic Matter	Coarse fragments
Rothiemay	123B, 50%; 124B, 40%	Fine-loamy, mixed, superactive, frigid, Aridic Calciustolls	0-152 cm: Clay loam, 30% clay at all depths	0-18 cm: granular 18-78 cm: subangular blocky to prismatic 78-152: massive	0-152 cm: 7.9-8.2	0-13 cm: 2% 13-152 cm: <1%	5-10% gravel throughout profile
Niart	123B, 35%; 124B, 7%	Fine-loamy, carbonatic, frigid Aridic Calciustolls	0-76 cm: Clay loam, 30% clay 76-152 cm: Loam 20% clay	0-18 cm: granular 18-78 cm: subangular blocky to prismatic 78-152: massive	0-152 cm: 8.4	0-15 cm: 3% 15-152 cm: <1%	5-10% pebbles from 0-90 cm, 55% pebbles below 90 cm
Varney	123B, 5%; 124B, 50%	Fine-loamy, mixed, frigid, superactive Calcidic Argiustolls	0-40 cm: Clay loam, 28-30% clay 40-71 cm: Gravelly sandy clay loam, 33% clay, 71-152 cm: Gravelly sandy loam, 23% clay	0-18 cm: granular 18-78 cm: subangular blocky to prismatic 78-152: massive	0-25: 7-7.2 25-152 cm: 7.9	0-15 cm: 3% 15-152 cm: <1%	0-40 cm: 5-10% gravels 40-152 cm: 20-25% gravels and cobbles

Chp 4 - Table 1: Mapped Soil Summary. Mapped soil series name and associated map units, and mapped textures, structures, pH, organic matter, and coarse fragments. Data from SSURGO database.

Irrigation Set	Amount per Pass, GSP (cm)	Amount per Pass, RER (cm)	Number of Passes	Total Quantity, GSP (cm)	Total Quantity, RER (cm)
2023 Set 1-June	1.65	1.27	8	13.2	10.2
2023 Set 2-July	1.27	1	8	10.1	8.1
2024 Set 1-June	1.65	1.27	6	9.9	7.6
2024 Set 2-July	1.40	1.27	10	14	12.7

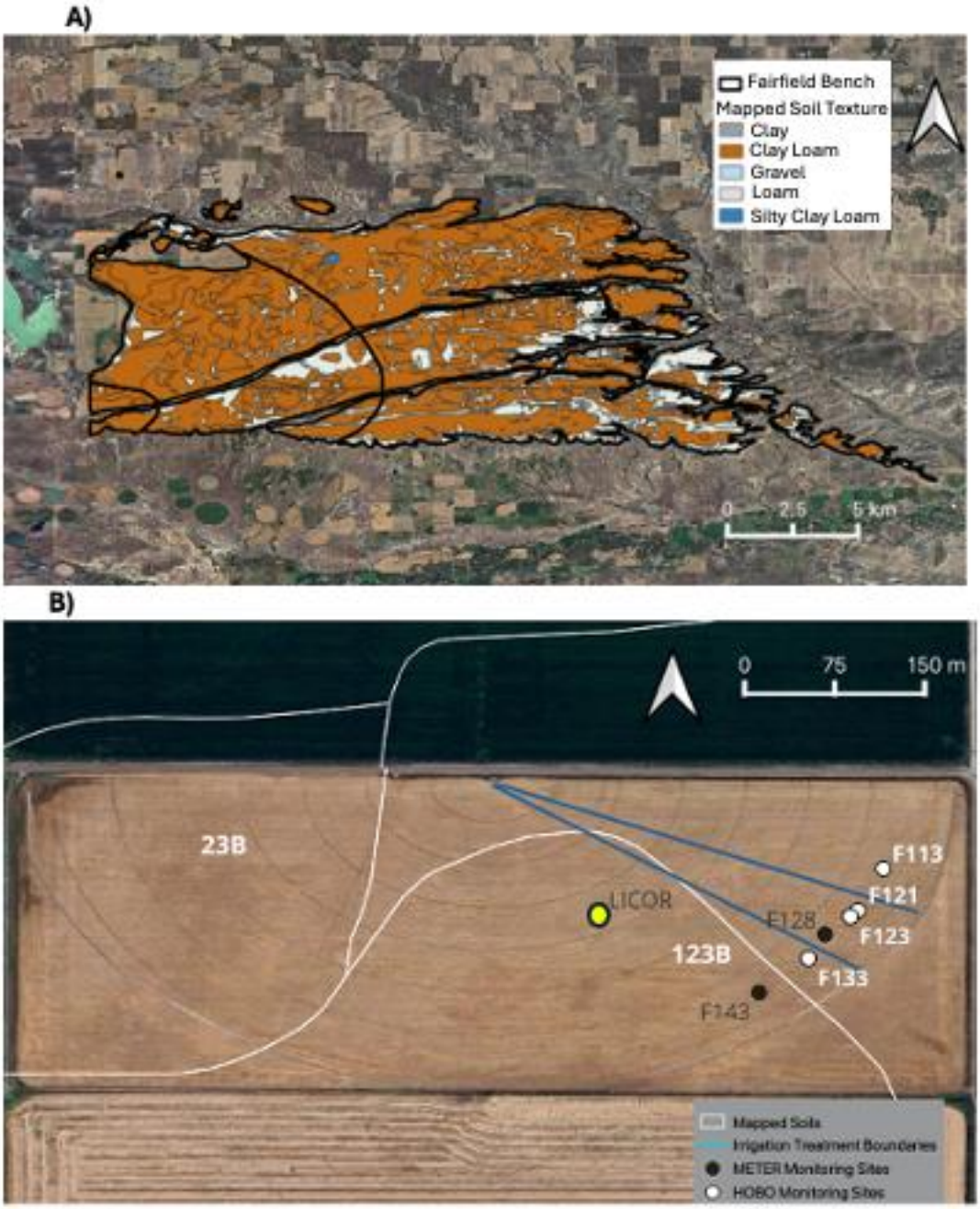
Chp 4 - Table 2: Irrigation Management Summary. Amount per pass and total irrigation quantities for GSP and RER irrigation treatments in 2023 and 2024.

Parameter	Optimized?	Starting Estimate Range	Allowed Solution Range	Description
Theta R-Matrix	No- ROSETTA prediction used	NA	NA	Residual water content for soil matrix ($cm^3\ cm^{-3}$)
Theta S-Matrix	No- ROSETTA prediction used	NA	NA	Saturated water content for soil matrix ($cm^3\ cm^{-3}$)
Alpha- Matrix	No- ROSETTA prediction used	NA	NA	Parameter related to air entry pressure for matrix (cm^{-1})
N- Matrix	No- ROSETTA prediction used	NA	NA	Parameter related to pore size distribution for matrix (dimensionless)
L- Matrix	No- 0.5 used	NA	NA	Parameter related to tortuosity matrix flowpaths (dimensionless)
Ks- Matrix	No- ROSETTA prediction used	NA	NA	Saturated hydraulic conductivity of soil matrix
Theta R-Macropore	Yes	0.001 to 0.02	0 to 0.1	Residual water content for macropores ($cm^3\ cm^{-3}$)
Theta S-Macropore	Yes	0.25 to 0.5	0.2 to 0.8	Saturated water content for macropores ($cm^3\ cm^{-3}$)
Alpha-Macropore	Yes	0.02 to 0.05	0.001 to 0.8	Parameter related to air entry pressure for macropores (cm^{-1})
N- Macropore	Yes	1.3 to 1.8	1.01 to 7	Parameter related to pore size distribution for macropores (dimensionless)
L- Macropore	No- 0.5 used	NA	NA	Parameter related to tortuosity of flowpaths for macropores(dimensionless)
Ks-Macropore	Yes	70 to 300	1 to 1000	Saturated hydraulic conductivity for macropores ($cm\ day^{-1}$)
W	Yes	0.03 to 0.09	0.001 to 0.25	Volumetric weight of macropores in whole soil ($cm^3\ cm^{-3}$)
Beta	Yes	1.5 to 5	1 to 20	Geometry based scaling factor (dimensionless)
Gamma	No- 0.4 used	NA	NA	Empirical scaling factor (dimensionless)
A	Yes	0.5 to 5	0.1 to 10	Soil aggregate length (cm)

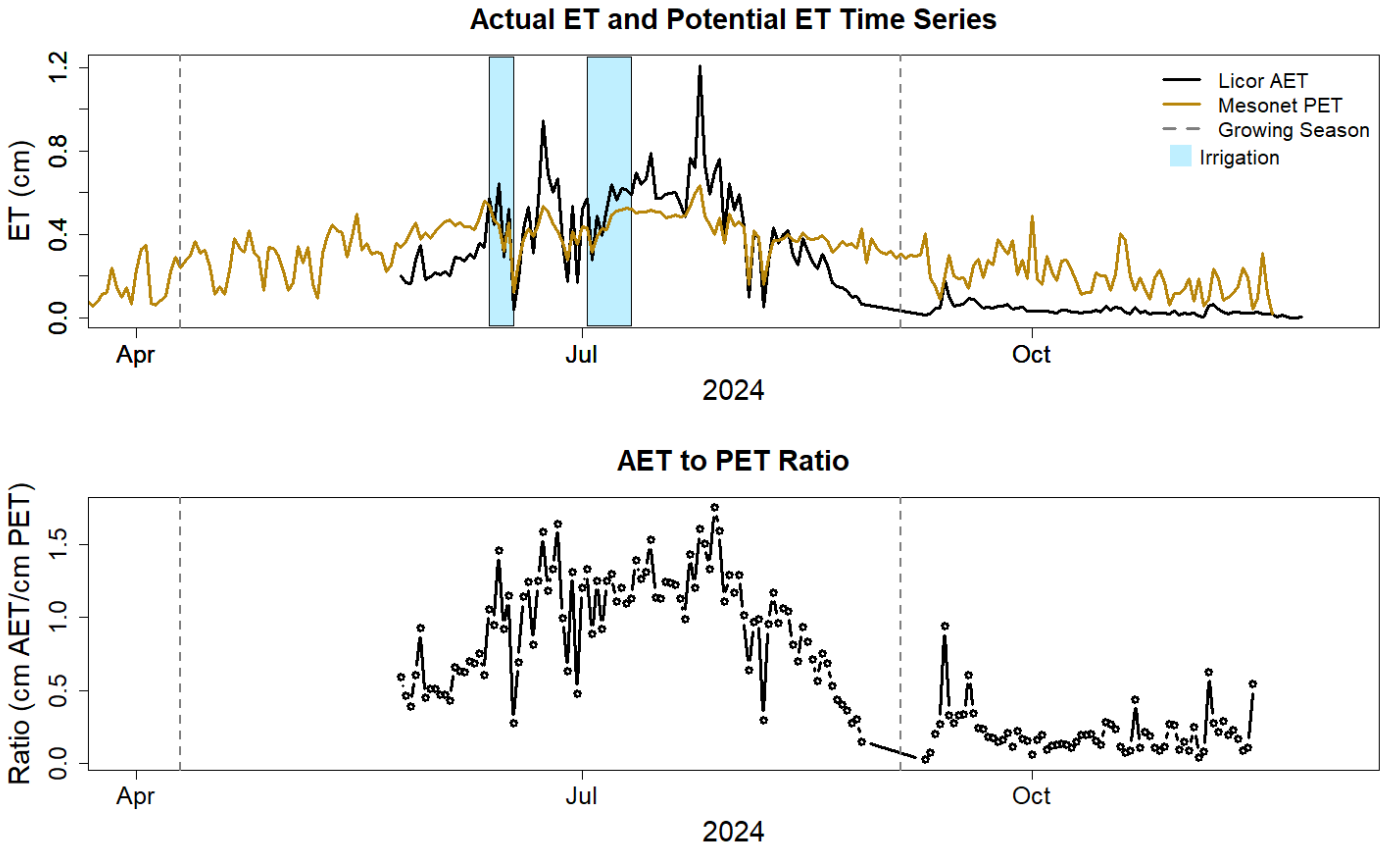
Chp 4 – Table 3 Continued.

Parameter	Optimized?	Starting Estimate Range	Allowed Solution Range	Description
Ka	Yes	0.001 to 2	0.00001 to 10	Saturated hydraulic conductivity at macropore-matrix interface (cm day^{-1})

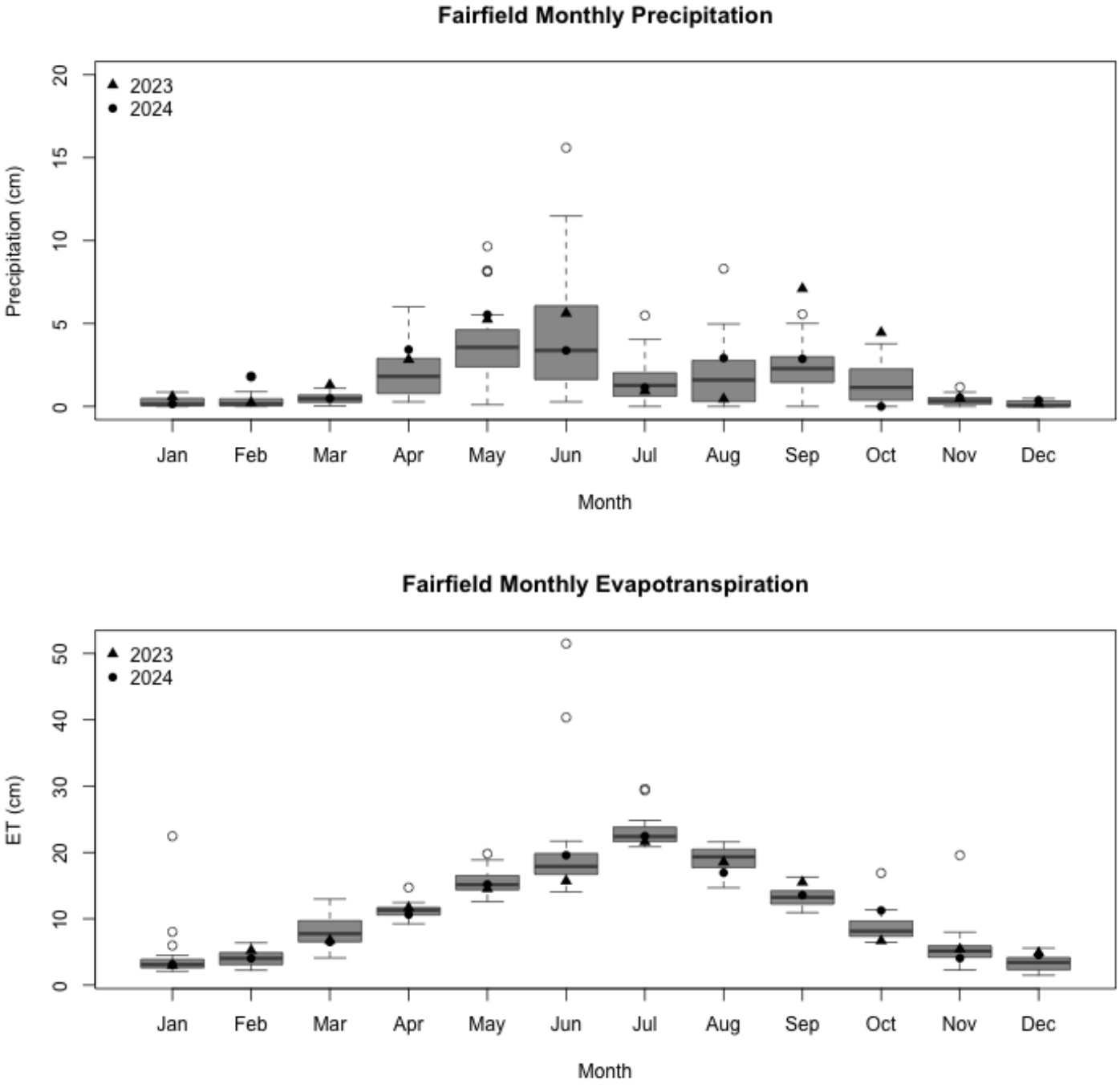
Chp 4 - Table 3: Inverse Modeling Summary. Input soil hydrological parameters for dual permeability, whether they were estimated using inverse modeling, inverse model starting parameter ranges, minimum and maximum allowed parameter values for convergence, and brief description of parameters.



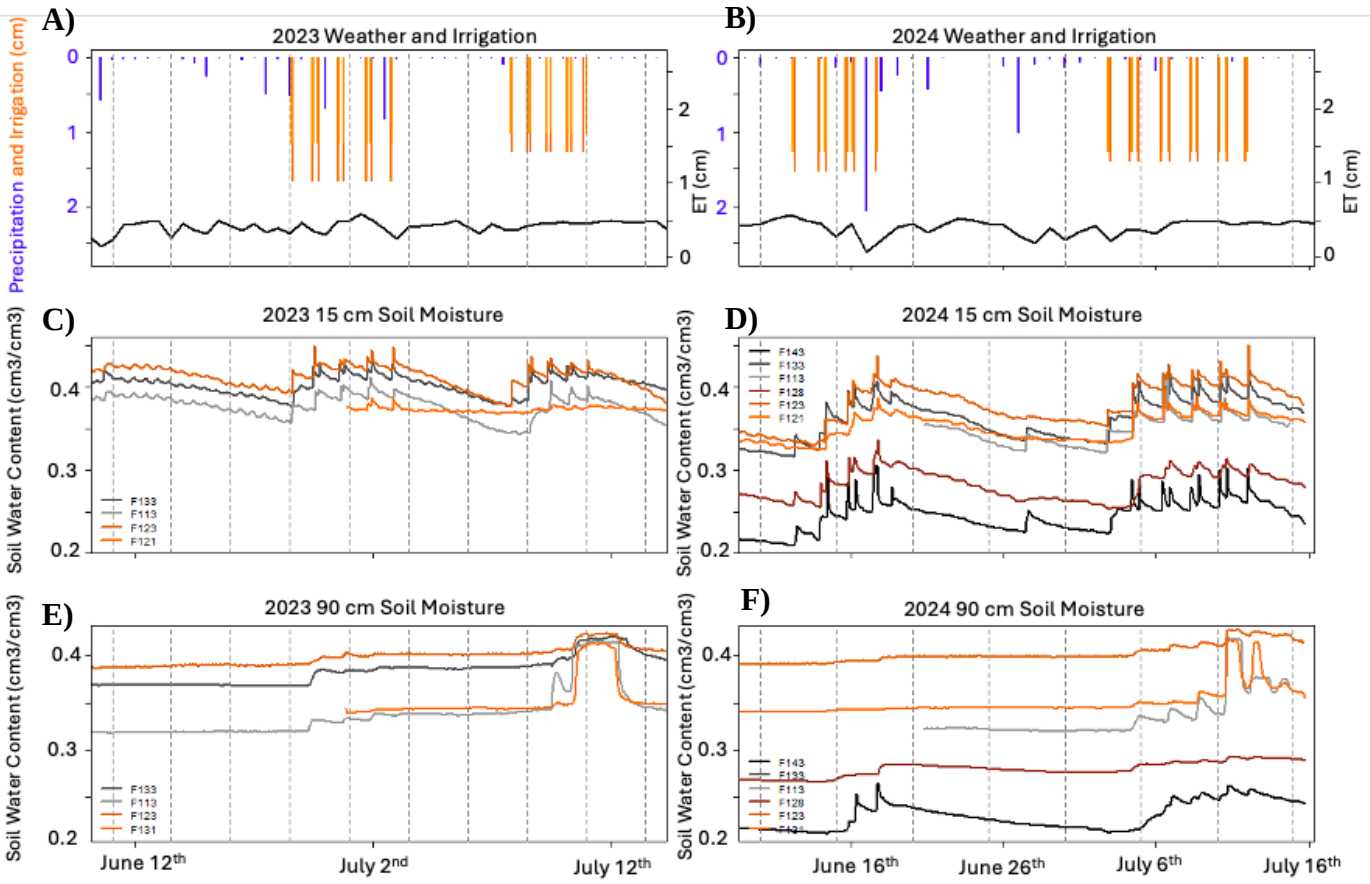
Chp 4 - Figure 1: Fairfield Site Maps. A) Fairfield bench soils: orange represents clay loams, white represents loams, and blue represents silty clay loams. B) Field sites, where white sites were installed in 2023 with HOBO equipment, and black sites were installed in 2024 with METER equipment. Yellow point is Licor 710, and blue lines indicate section of reduced rate treatment. Portion of field between blue lines is the reduced irrigation rate (RIR) and the remainder of the field is grower standard practice (GSP) irrigation rate.



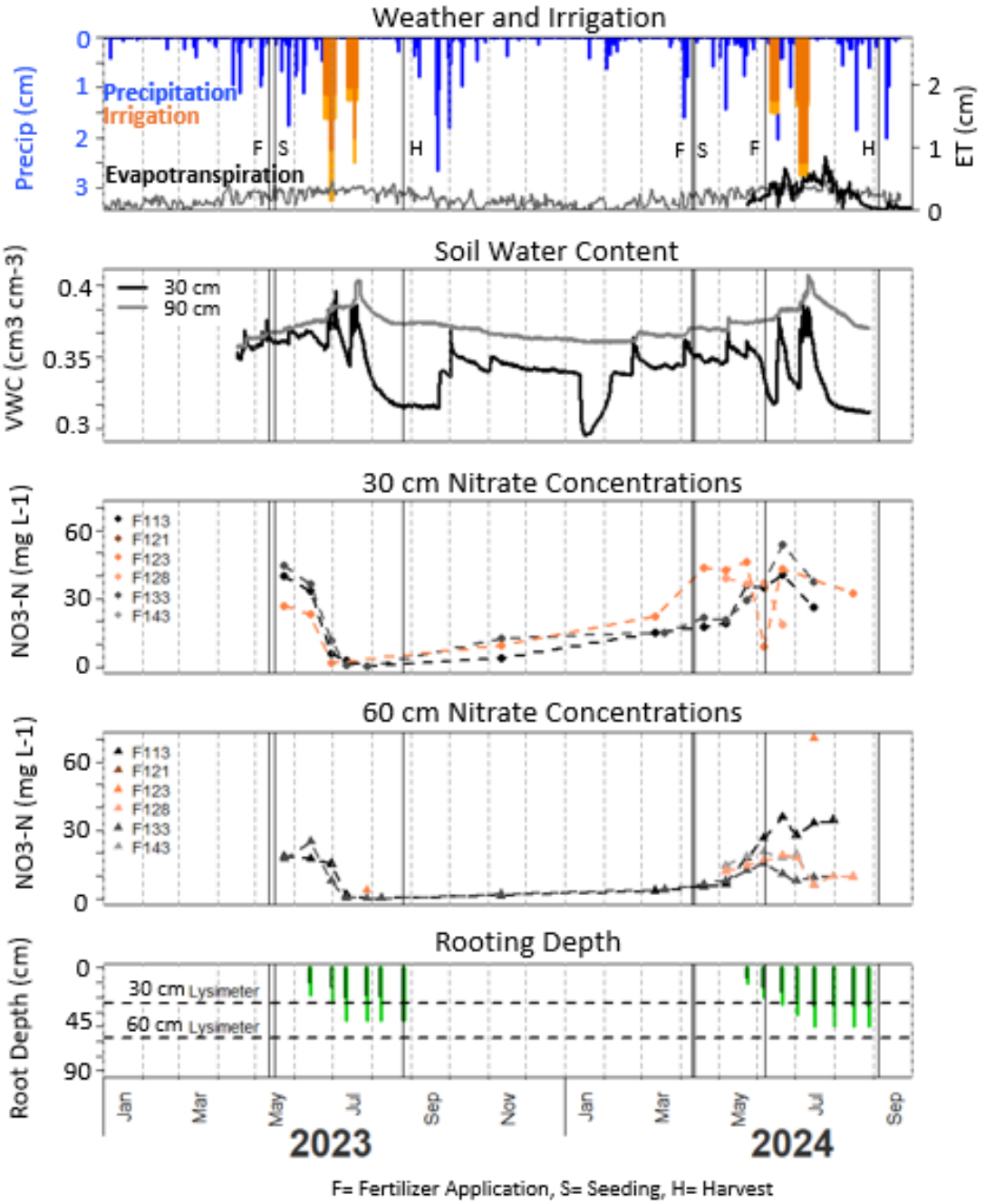
Chp 4 - Figure 2: Crop Coefficient Ratios Over 2024 Growing Season. Top panel- Licor AET in black and Mesonet PET in yellow for the 2024 growing season, with seeding and harvest indicated by vertical dashed lines and irrigation in blue boxes. Bottom panel- Ratio of AET to PET over the season.



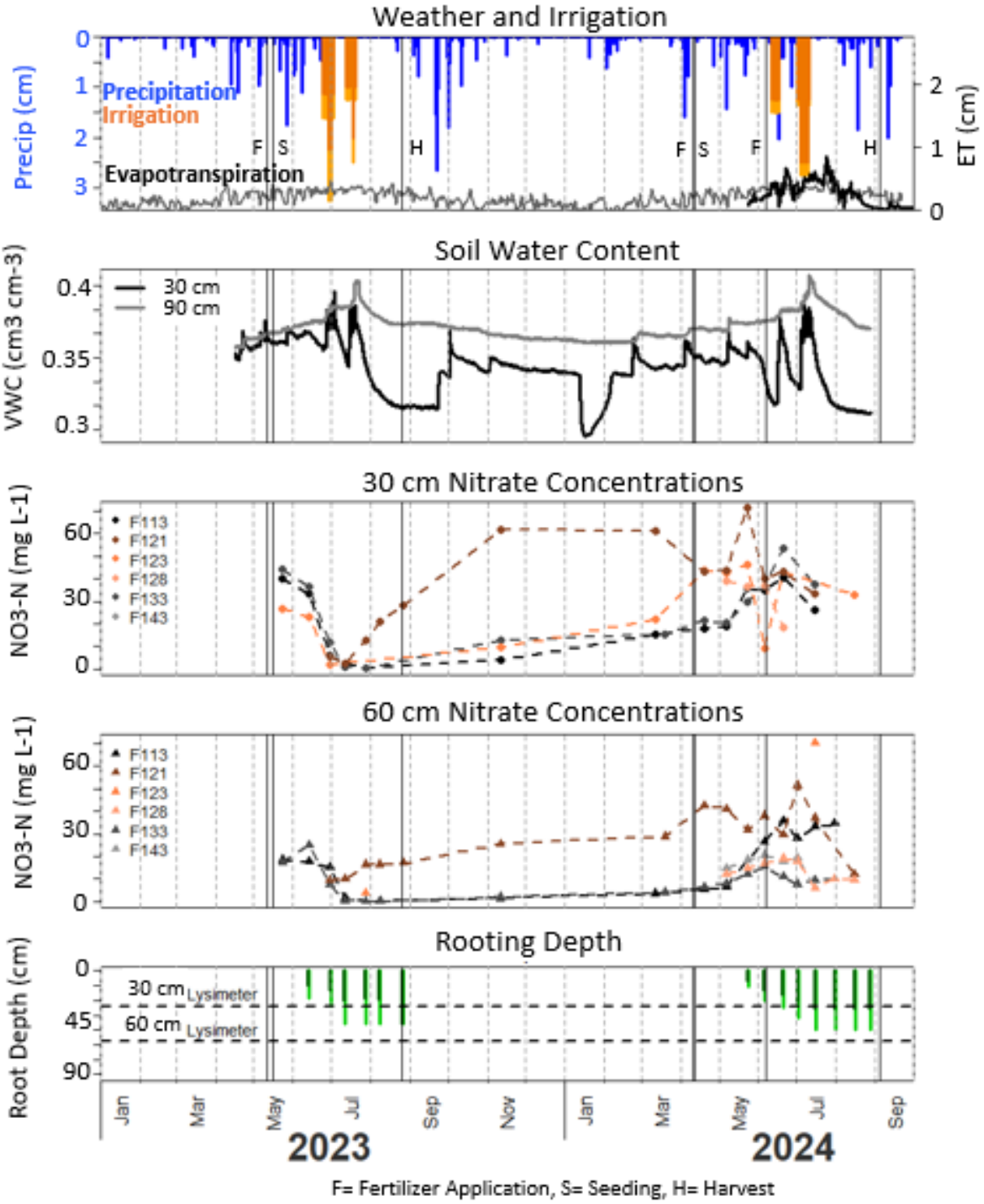
Chp 4 - Figure 3: Monthly Precipitation and Evapotranspiration. Ranges of precipitation and ET over a 20-year period (2000-2020) at Agrimet station GFMT. Triangles indicate 2023 data, and circles are 2024 data.



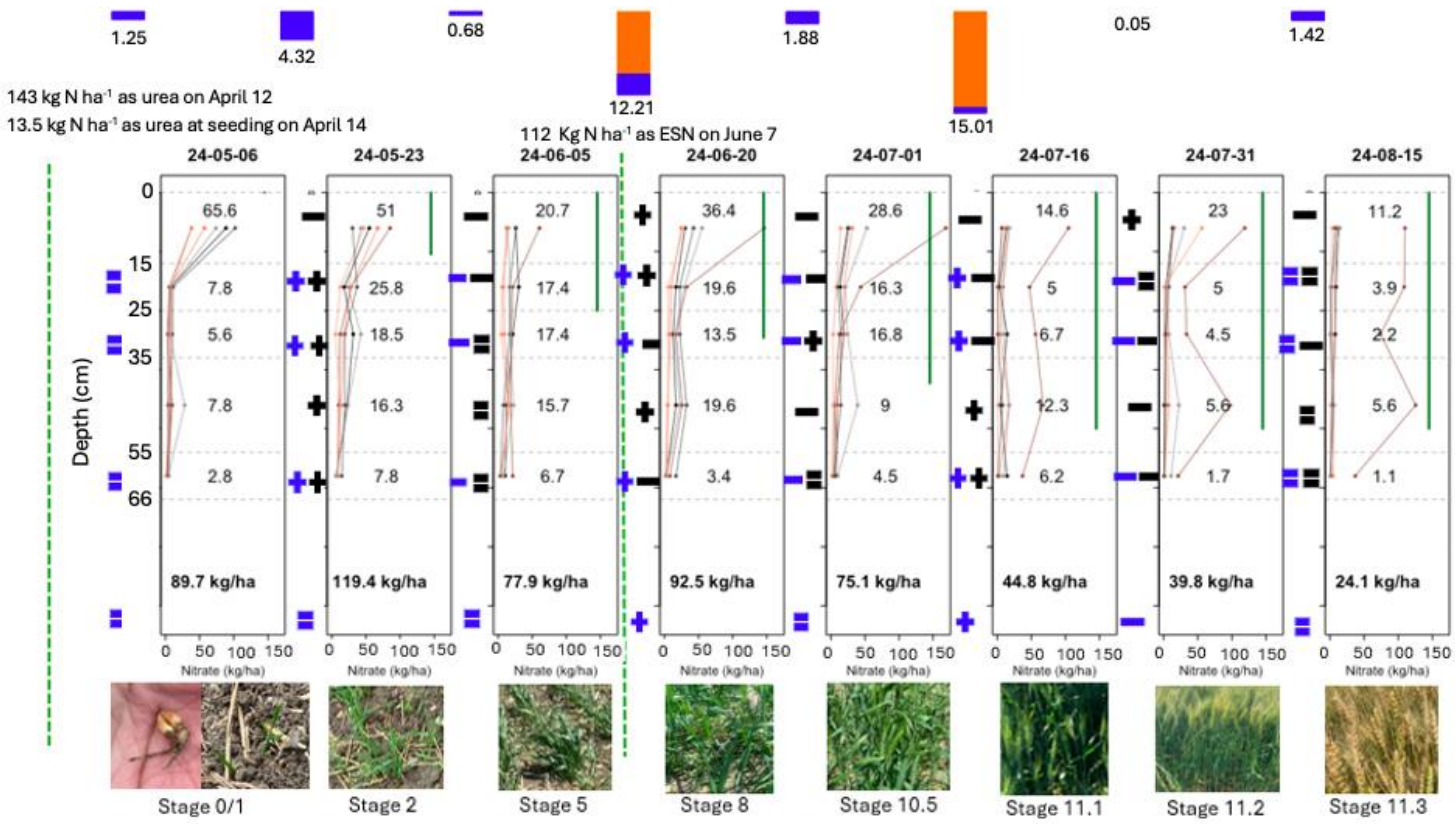
Chp 4 - Figure 4: Soil Water Content Irrigation Responses. A and B) Irrigation, precipitation, and ET for 2023 and 2024. C and D) Soil VWC responses at 15 cm for 2023 and 2024, black and gray sites are in GSP, and brown sites are in RIR. E and F) Soil VWC responses at 90 cm for 2023 and 2024, black and gray sites are in GSP, and brown sites are in RIR.



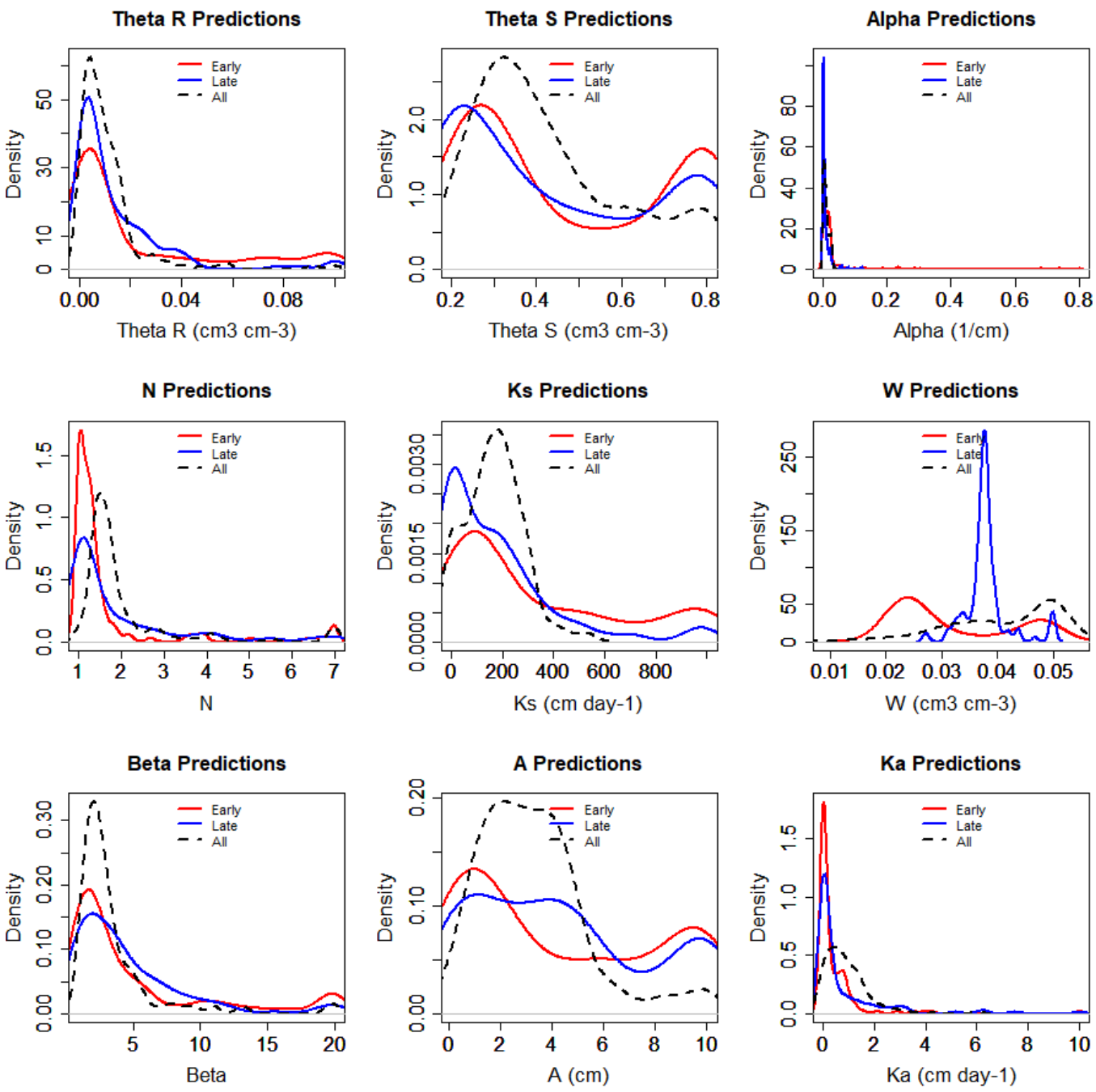
Chp 4 - Figure 5: Lysimeter Nitrate, No F121. A) Precipitation, irrigation, PET (gray) and LICOR AET (black, summer 2024 only) for full two-year study period. B) 30 cm (black) and 60 cm (gray) soil VWC from a representative site. C) 30 cm lysimeter nitrate concentrations, black and gray are GSP sites, brown are RIR sites. D) 60 cm lysimeter nitrate concentrations, black and gray are GSP sites, brown are RIR sites. E) Rooting depth- dark green is observed, light green is scaled. Lines labeled ‘F’ are fertilizer application, ‘S’ are seeding, and ‘H’ are harvest.



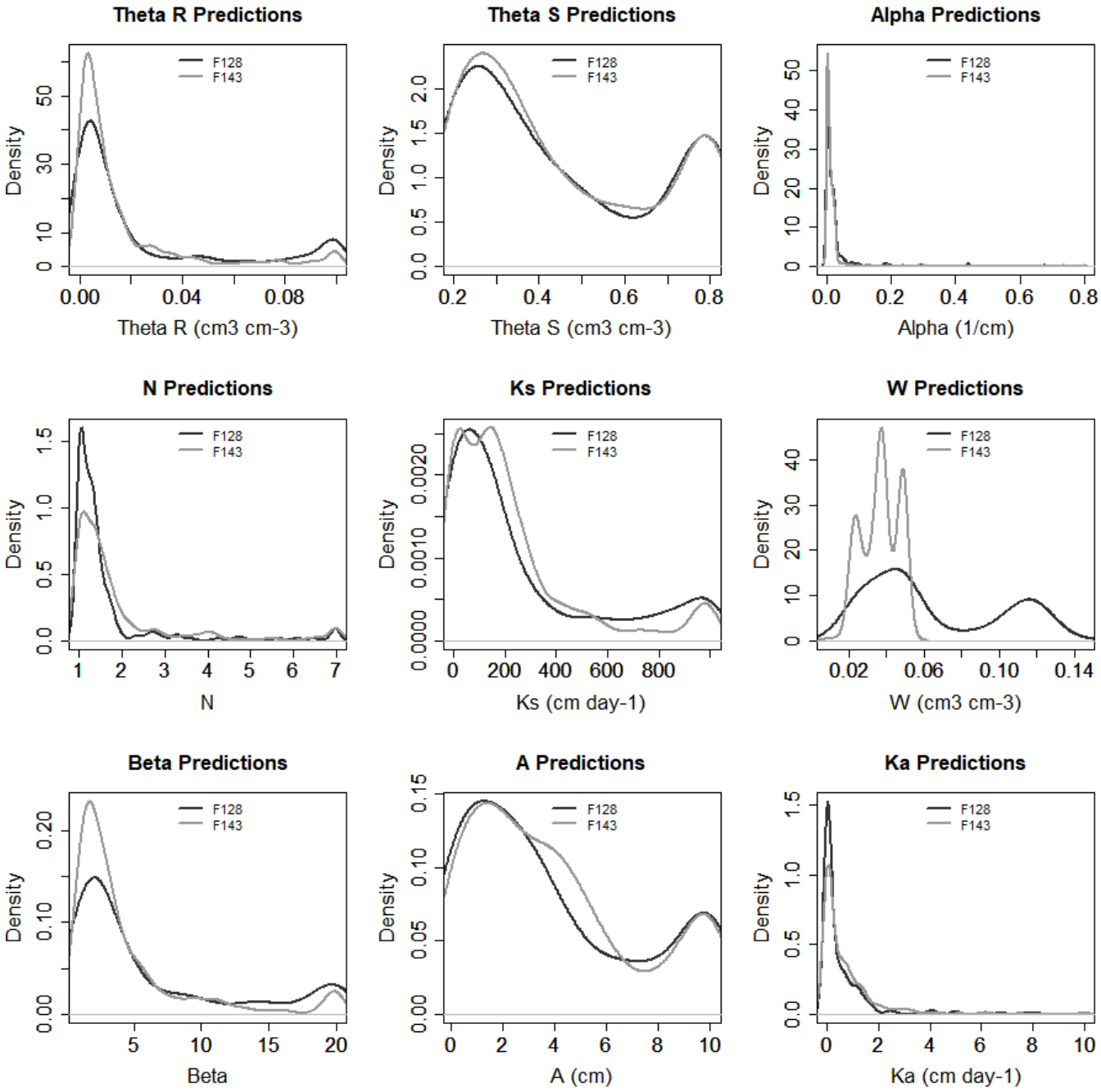
Chp 4 - Figure 6: Lysimeter Nitrate, Including F121. Figure identical to Chp 4- Figure 5, but with the inclusion of site F121 where barley was destroyed in 2023.



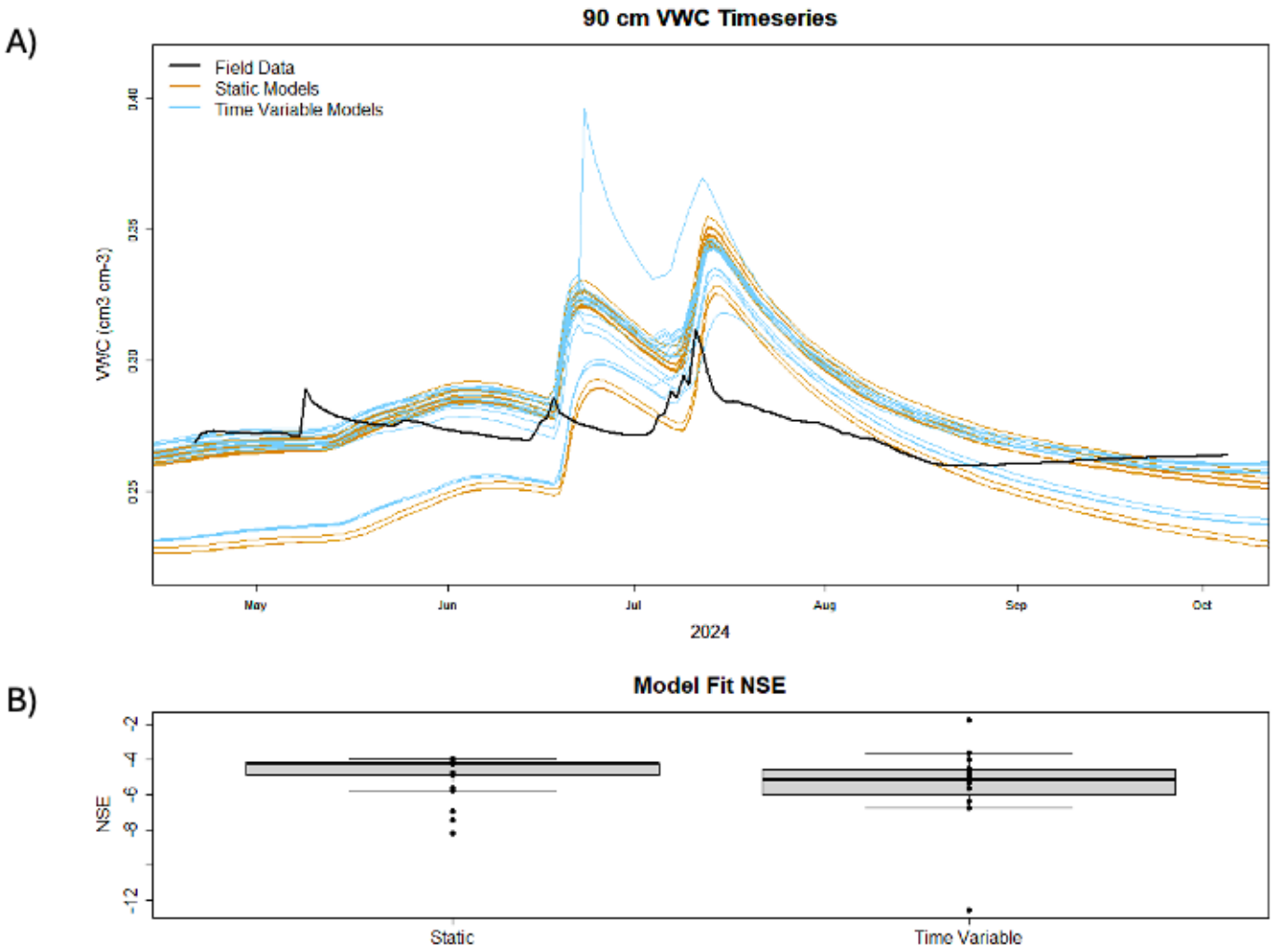
Chp 4 - Figure 7: Soil Nitrate Profiles to 66 cm. Black and gray sites are GSP, brown sites are RER, green lines along right sides of plots are root depths. Blue +/- signs represent water movement, black +/- signs indicate nitrate changes. Blue bars are aggregated precipitation, orange is irrigation. Green dashed lines indicate fertilizer application.



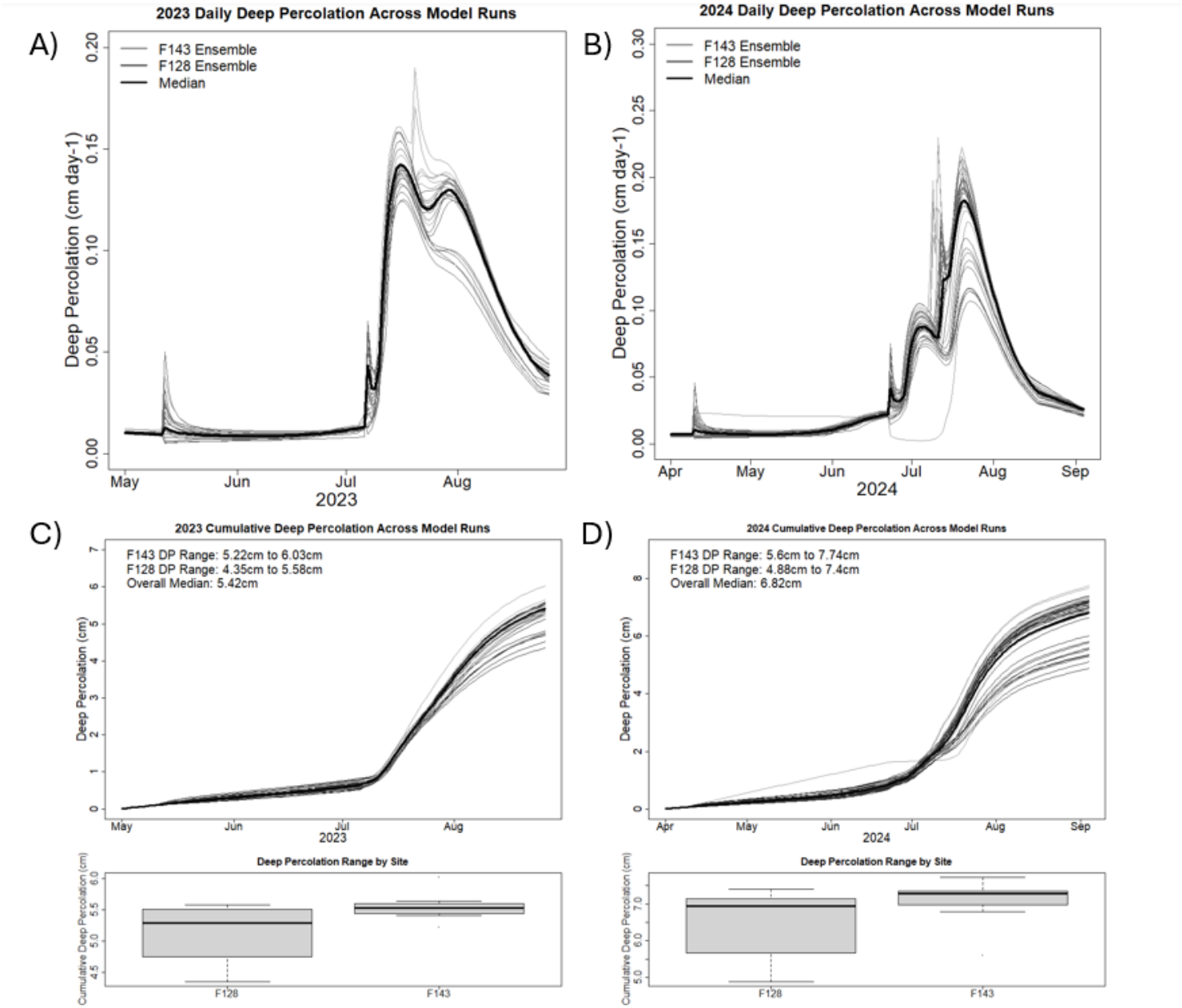
Chp 4 - Figure 8: Inverse Model Predictions Over Time. Distributions for each of the nine optimized parameters for site F143 for early season (red), late season (blue), and whole season (dashed black).



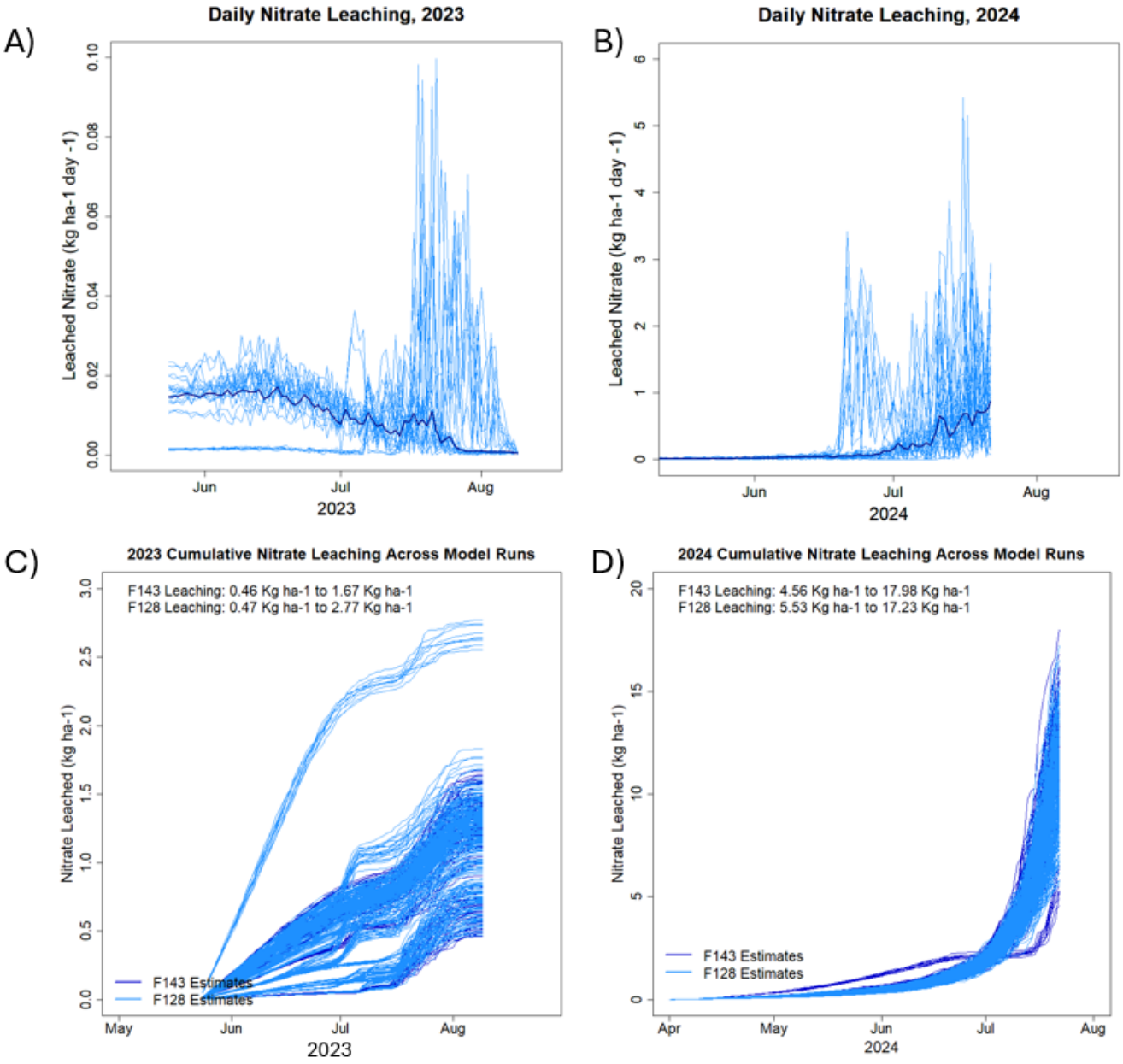
Chp 4 - Figure 9: Inverse Model Predictions Across Sites. Distributions for each of the nine optimized parameters for site F143 (higher response- gray) and site F128 (lower response- black).



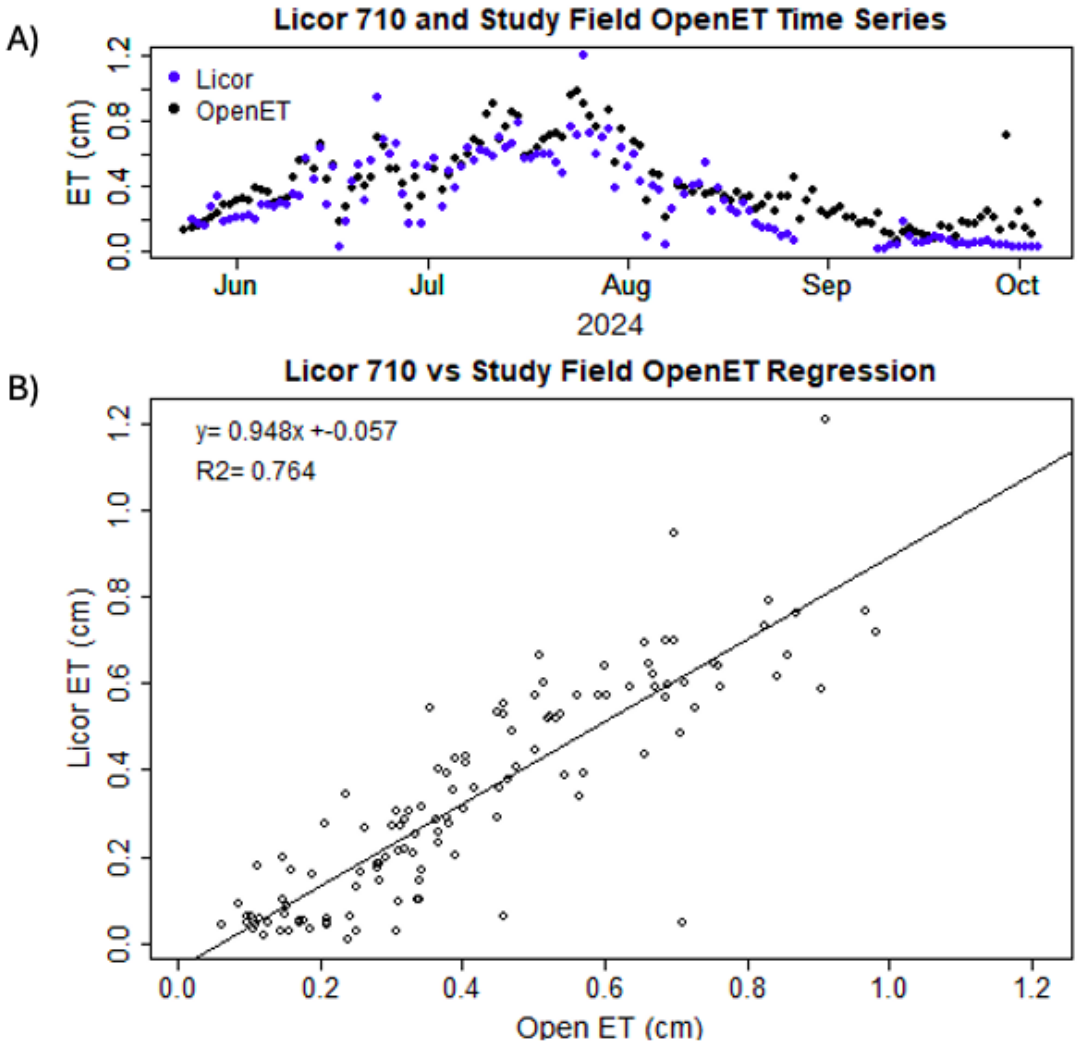
Chp 4 - Figure 10: Model Fit Summary. A) Time series comparison of observed 90 cm VWC data (black), time static parameter models (orange) and time variable parameter models (blue). B) Boxplots of NSE, where positive or less negative values indicates better model fit, distributions for time static and variable models.



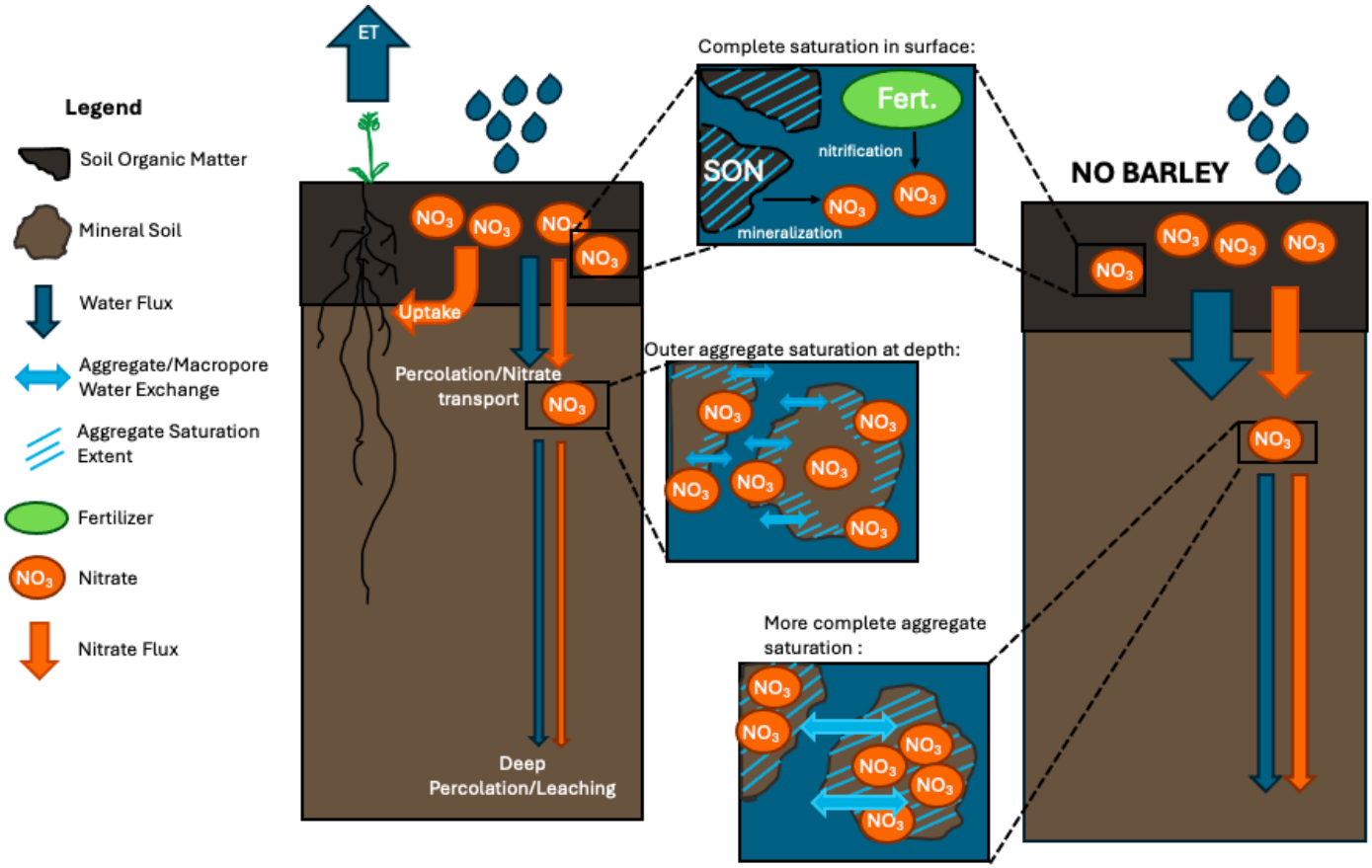
Chp 4 - Figure 11: Ranges of Deep Percolation Estimates. A) Daily deep percolation for 2023; B) Daily for 2024; C) Cumulative deep percolation for 2023 with boxplots of site totals; D) Cumulative deep percolation for 2024 with boxplots of site totals. Light gray lines are individual model runs, black like is median for a given day.



Chp 4 - Figure 12: Nitrate Leaching Estimates. A) Daily losses in 2023, B) Daily losses in 2024, C) Cumulative leaching for 2023 and D) Cumulative leaching for 2024. In daily plots, light blue lines are individual model scenarios, and the darker blue line is median daily nitrate leaching.



Chp 4 - Figure 13: Licor and OpenET Compare. A) Time series of Licor (blue) and OpenET (black) ET data during the 2024 growing season. B) Regression between ET data sources.



Chp 4 - Figure 14: Conceptual Water and Nitrate Movement. Left profile: Hypothesized surface saturation, water and nitrate uptake, and partial aggregate saturation at most sites with intact crop. Right profile: Hypothesized water and nitrate movement without barley uptake for site F121 during 2023. Thickness of arrows indicates hypothesized magnitude of flux (thicker arrow= larger flux).

Literature Cited

Abatzoglou, J. T. (2013). Development of gridded surface meteorological data for ecological applications and modelling. *International Journal of Climatology*, *33*(1), 121–131. https://doi.org/10.1002/joc.3413

Allen, R., Pereira, L. S., Raes, D., & Smith, M. (2006). *FAO Irrigation and Drainage Paper No. 56*.

Arora, B., Mohanty, B. P., & McGuire, J. T. (2012). Uncertainty in dual permeability model parameters for structured soils. *Water Resources Research*, *48*(1). https://doi.org/10.1029/2011WR010500

Beven, K., & Germann, P. (1982). Macropores and water flow in soils. *Water Resources Research*, *18*(5), 1311–1325. https://doi.org/10.1029/WR018i005p01311

Beven, K., & Germann, P. (2013). Macropores and water flow in soils revisited. *Water Resources Research*, *49*(6), 3071–3092. https://doi.org/10.1002/wrcr.20156

Beyene, A., Cornelis, W., Verhoest, N. E. C., Tilahun, S., Alamirew, T., Adgo, E., De Pue, J., & Nyssen, J. (2018). Estimating the actual evapotranspiration and deep percolation in irrigated soils of a tropical floodplain, northwest Ethiopia. *Agricultural Water Management*, *202*, 42–56. https://doi.org/10.1016/j.agwat.2018.01.022

Blanchy, G., Bragato, G., Di Bene, C., Jarvis, N., Larsbo, M., Meurer, K., & Garré, S. (2023). Soil and crop management practices and the water regulation functions of soils: A qualitative synthesis of meta-analyses relevant to European agriculture. *SOIL*, *9*(1), 1–20. https://doi.org/10.5194/soil-9-1-2023

Bordoloi, S., Ni, J., & Ng, C. W. W. (2020). Soil desiccation cracking and its characterization in vegetated soil: A perspective review. *Science of The Total Environment*, *729*, 138760. https://doi.org/10.1016/j.scitotenv.2020.138760

Bormann, H., & Klaassen, K. (2008). Seasonal and land use dependent variability of soil hydraulic and soil hydrological properties of two Northern German soils. *Geoderma*, *145*(3), 295–302. https://doi.org/10.1016/j.geoderma.2008.03.017

Budhathoki, S., Lamba, J., Srivastava, P., Malhotra, K., Way, T. R., & Katuwal, S. (2022). Temporal and spatial variability in 3D soil macropore characteristics determined using X-ray computed tomography. *Journal of Soils and Sediments*, *22*(4), 1263–1277. https://doi.org/10.1007/s11368-022-03150-x

Coleman, T., Boyd, K., Thatcher, T., & Sain, R. (2022, June). *Muddy Creek Master Plan*. https://static1.squarespace.com/static/6014bb1a9820e37481af89b6/t/62bb8583163e3f2f643eed6e/1656456599529/Muddy+Creek+Master+Plan+FINAL++06+28+2022.pdf

Coppola, A., Comegna, A., Dragonetti, G., Gerke, H. H., & Basile, A. (2015). Simulated Preferential Water Flow and Solute Transport in Shrinking Soils. *Vadose Zone Journal*, *14*(9), vzj2015.02.0021. https://doi.org/10.2136/vzj2015.02.0021

Della Vecchia, G., Dieudonné, A.-C., Jommi, C., & Charlier, R. (2015). Accounting for evolving pore size distribution in water retention models for compacted clays: EVOLVING PORE SIZE DISTRIBUTION IN WATER RETENTION MODELLING. *International Journal for Numerical and Analytical Methods in Geomechanics*, *39*(7), 702–723. https://doi.org/10.1002/nag.2326

Du, E., Terrer, C., Pellegrini, A. F. A., Ahlström, A., van Lissa, C. J., Zhao, X., Xia, N., Wu, X., & Jackson, R. B. (2020). Global patterns of terrestrial nitrogen and phosphorus limitation. *Nature Geoscience*, *13*(3), Article 3. https://doi.org/10.1038/s41561-019-0530-4

Dzurella, K. N., Pettygrove ,G.S., Fryjoff-Hung ,A., Hollander ,A., & and Harter, T. (2015). Potential to assess nitrate leaching vulnerability of irrigated cropland. *Journal of Soil and Water Conservation*, *70*(1), 63–72. https://doi.org/10.2489/jswc.70.1.63

FAO. (2021). AQUASTAT- FAO's Global Information System on Water and Agriculture. Food and Agriculture Organization of the United Nations.

Fishkis, O., Noell, U., Diehl, L., Jaquemotte, J., Lamparter, A., Stange, C. F., Burke, V., Koeniger, P., & Stadler, S. (2020). Multitracer irrigation experiments for assessing the relevance of preferential flow for non-sorbing solute transport in agricultural soil. *Geoderma*, *371*, 114386. https://doi.org/10.1016/j.geoderma.2020.114386

Gerke, H. H., & van Genuchten, M. T. (1993). A dual-porosity model for simulating the preferential movement of water and solutes in structured porous media. *Water Resources Research*, *29*(2), 305–319. https://doi.org/10.1029/92WR02339

Graham, S. L., Srinivasan, M. s., Faulkner, N., & Carrick, S. (2018). Soil Hydraulic Modeling Outcomes with Four Parameterization Methods: Comparing Soil Description and Inverse Estimation Approaches. *Vadose Zone Journal*, *17*(1), 170002. https://doi.org/10.2136/vzj2017.01.0002

Greve, A., Andersen, M. S., & Acworth, R. I. (2010). Investigations of soil cracking and preferential flow in a weighing lysimeter filled with cracking clay soil. *Journal of Hydrology*, *393*(1), 105–113. https://doi.org/10.1016/j.jhydrol.2010.03.007

Greve, A. K., Acworth, R. I., & Kelly, B. F. J. (2011). 3D Cross-hole resistivity tomography to monitor water percolation during irrigation on cracking soil. *Soil Research*, *49*(8), 661–669. https://doi.org/10.1071/SR11270

Gu, Z., Qi, Z., Burghate, R., Yuan, S., Jiao, X., & Xu, J. (2020). Irrigation Scheduling Approaches and Applications: A Review. *Journal of Irrigation and Drainage Engineering*, *146*(6), 04020007. https://doi.org/10.1061/(ASCE)IR.1943-4774.0001464

Guo, D., Olesen, J. E., Manevski, K., & Ma, X. (2021). Optimizing irrigation schedule in a large agricultural region under different hydrologic scenarios. *Agricultural Water Management*, *245*, 106575. https://doi.org/10.1016/j.agwat.2020.106575

Guo, L., & Lin, H. (2018). Addressing Two Bottlenecks to Advance the Understanding of Preferential Flow in Soils. In *Advances in Agronomy* (Vol. 147, pp. 61–117). Elsevier. https://doi.org/10.1016/bs.agron.2017.10.002

Haile, G. G., Tang, Q., Reda, K. W., Baniya, B., He, L., Wang, Y., & Gebrechorkos, S. H. (2024). Projected impacts of climate change on global irrigation water withdrawals. *Agricultural Water Management*, *305*, 109144. https://doi.org/10.1016/j.agwat.2024.109144

Haws, N. W., Rao, P. S. C., Simunek, J., & Poyer, I. C. (2005). Single-porosity and dual-porosity modeling of water flow and solute transport in subsurface-drained fields using effective

field-scale parameters. *Journal of Hydrology*, *313*(3), 257–273. https://doi.org/10.1016/j.jhydrol.2005.03.035

Heinen, M., Mulder, M., van Dam, J., Bartholomeus, R., de Jong van Lier, Q., de Wit, J., de Wit, A., & Hack - ten Broeke, M. (2024). SWAP 50 years: Advances in modelling soil-water-atmosphere-plant interactions. *Agricultural Water Management*, *298*, 108883. https://doi.org/10.1016/j.agwat.2024.108883

Hellner, Q., Koestel, J., Ulén, B., & Larsbo, M. (2018). Effects of tillage and liming on macropore networks derived from X-ray tomography images of a silty clay soil. *Soil Use and Management*, *34*(2), 197–205. https://doi.org/10.1111/sum.12418

Isch, A., Montenach, D., Hammel, F., Ackerer, P., & Coquet, Y. (2019). A Comparative Study of Water and Bromide Transport in a Bare Loam Soil Using Lysimeters and Field Plots. *Water*, *11*(6), Article 6. https://doi.org/10.3390/w11061199

Jarvis, N. J. (2007). A review of non-equilibrium water flow and solute transport in soil macropores: Principles, controlling factors and consequences for water quality. *European Journal of Soil Science*, *58*(3), 523–546. https://doi.org/10.1111/j.1365-2389.2007.00915.x

Jarvis, N. J., Moeys, J., Hollis, J. M., Reichenberger, S., Lindahl, A. M. L., & Dubus, I. G. (2009). A Conceptual Model of Soil Susceptibility to Macropore Flow. *Vadose Zone Journal*, *8*(4), 902–910. https://doi.org/10.2136/vzj2008.0137

Jarvis, N., Koestel, J., & Larsbo, M. (2016). Understanding Preferential Flow in the Vadose Zone: Recent Advances and Future Prospects. *Vadose Zone Journal*, *15*(12), vzj2016.09.0075. https://doi.org/10.2136/vzj2016.09.0075

Jiang, S., Pang, L., Buchan, G. D., Šimůnek, J., Noonan, M. J., & Close, M. E. (2010). Modeling water flow and bacterial transport in undisturbed lysimeters under irrigations of dairy shed effluent and water using HYDRUS-1D. *Water Research*, *44*(4), 1050–1061. https://doi.org/10.1016/j.watres.2009.08.039

John, A. A., Jones, C. A., Ewing, S. A., Sigler, W. A., Bekkerman, A., & Miller, P. R. (2017). Fallow replacement and alternative nitrogen management for reducing nitrate leaching in

a semiarid region. *Nutrient Cycling in Agroecosystems*, *108*(3), 279–296. https://doi.org/10.1007/s10705-017-9855-9

Ketchum, D., Jencso, K., Maneta, M. P., Melton, F., Jones, M. O., & Huntington, J. (2020). IrrMapper: A Machine Learning Approach for High Resolution Mapping of Irrigated Agriculture Across the Western U.S. *Remote Sensing*, *12*(14), Article 14. https://doi.org/10.3390/rs12142328

Kocian, L., & Mohanty, B. P. (2024). Characterizing large-scale preferential flow across Continental United States. *Vadose Zone Journal*, *23*(4), e20316. https://doi.org/10.1002/vzj2.20316

Köhne, J. M., Mohanty, B. P., & Šimůnek, J. (2006). Inverse Dual-Permeability Modeling of Preferential Water Flow in a Soil Column and Implications for Field-Scale Solute Transport. *Vadose Zone Journal*, *5*(1), 59–76. https://doi.org/10.2136/vzj2005.0008

Kokulan, V., Macrae, M. L., Ali, G. A., Lobb, D. A., Morison, M., & Brooks, B. C. (2021). Temporal variability in water and nutrient movement through vertisols into agricultural tile drains in the northern Great Plains. *Journal of Soil and Water Conservation*, *76*(4), 317–328. https://doi.org/10.2489/jswc.2021.00099

Lin, H., & Zhou, X. (2008). Evidence of subsurface preferential flow using soil hydrologic monitoring in the Shale Hills catchment. *European Journal of Soil Science*, *59*(1), 34–49. https://doi.org/10.1111/j.1365-2389.2007.00988.x

Lobell, D. B., Schlenker, W., & Costa-Roberts, J. (2011). Climate Trends and Global Crop Production Since 1980. *Science*, *333*(6042), 616–620. https://doi.org/10.1126/science.1204531

Luo, Y., Zhang, J., Zhou, Z., Aguilar-Lopez, J. P., Greco, R., & Bogaard, T. (2023). Effects of dynamic changes of desiccation cracks on preferential flow: Experimental investigation and numerical modeling. *Hydrology and Earth System Sciences*, *27*(3), 783–808. https://doi.org/10.5194/hess-27-783-2023

Mancosu, N., Snyder, R. L., Kyriakakis, G., & Spano, D. (2015). Water Scarcity and Future Challenges for Food Production. *Water*, *7*(3), Article 3. https://doi.org/10.3390/w7030975

Mehta, P., Siebert, S., Kummu, M., Deng, Q., Ali, T., Marston, L., Xie, W., & Davis, K. F. (2024). Half of twenty-first century global irrigation expansion has been in water-stressed regions. *Nature Water*, *2*(3), 254–261. https://doi.org/10.1038/s44221-024-00206-9

Montana Department of Agriculture. (2015). *Groundwater Monitoring for Pesticides and Nitrate in Greenfield Bench, Montana; Summary of Findings 1992-2015*. https://agr.mt.gov/_docs/groundwater-docs/GWR_GreenfieldBench1992-2015Final.pdf

Mueller, N. D., Gerber, J. S., Johnston, M., Ray, D. K., Ramankutty, N., & Foley, J. A. (2012). Closing yield gaps through nutrient and water management. *Nature*, *490*(7419), 254–257. https://doi.org/10.1038/nature11420

Nash, J. E., & Sutcliffe, J. V. (1970). River flow forecasting through conceptual models part I — A discussion of principles. *Journal of Hydrology*, *10*(3), 282–290. https://doi.org/10.1016/0022-1694(70)90255-6

Nimmo, J. R. (2021). The processes of preferential flow in the unsaturated zone. *Soil Science Society of America Journal*, *85*(1), 1–27. https://doi.org/10.1002/saj2.20143

Pachepsky, Y., & Park, Y. (2015). Saturated Hydraulic Conductivity of US Soils Grouped According to Textural Class and Bulk Density. *Soil Science Society of America Journal*, *79*(4), 1094–1100. https://doi.org/10.2136/sssaj2015.02.0067

Pereira, L. S. (2017). Water, Agriculture and Food: Challenges and Issues. *Water Resources Management*, *31*(10), 2985–2999. https://doi.org/10.1007/s11269-017-1664-z

Puckett, L. J., Tesoriero, A. J., & Dubrovsky, N. M. (2011). Nitrogen Contamination of Surficial Aquifers—A Growing Legacy. *Environmental Science & Technology*, *45*(3), 839–844. https://doi.org/10.1021/es1038358

Quemada, M., Baranski, M., Nobel-de Lange, M. N. J., Vallejo, A., & Cooper, J. M. (2013). Meta-analysis of strategies to control nitrate leaching in irrigated agricultural systems and their effects on crop yield. *Agriculture, Ecosystems & Environment*, *174*, 1–10. https://doi.org/10.1016/j.agee.2013.04.018

Reading, L. P., Bajracharya, K., & Wang, J. (2019). Simulating deep drainage and nitrate leaching on a regional scale: Implications for groundwater management in an intensively irrigated area. *Irrigation Science*, *37*(5), 561–581. https://doi.org/10.1007/s00271-019-00636-4

Robinson, M., W. A. Sigler (2025). Irrigation Management and Soils as Controls on Deep Percolation and Nitrate Leaching in Agricultural Systems: Thesis Data and Code, HydroShare, https://doi.org/10.4211/hs.2d6042efdc7944288ce486ae9a58da9e

Roulier, S., & Jarvis, N. (2003). Analysis of Inverse Procedures for Estimating Parameters Controlling Macropore Flow and Solute Transport in the Dual-Permeability Model MACRO. *Vadose Zone Journal*, *2*(3), 349–357. https://doi.org/10.2136/vzj2003.3490

Schaap, M. G., Leij, F. J., & van Genuchten, M. Th. (2001). rosetta: A computer program for estimating soil hydraulic parameters with hierarchical pedotransfer functions. *Journal of Hydrology*, *251*(3), 163–176. https://doi.org/10.1016/S0022-1694(01)00466-8

Shipitalo, M. J., Nuutinen, V., & Butt, K. R. (2004). Interaction of earthworm burrows and cracks in a clayey, subsurface-drained, soil. *Applied Soil Ecology*, *26*, 209–217. https://doi.org/10.1016/j.apsoil.2004.01.004

Sigler, W. A., Ewing, S. A., Jones, C. A., Payn, R. A., Miller, P., & Maneta, M. (2020). Water and nitrate loss from dryland agricultural soils is controlled by management, soils, and weather. *Agriculture, Ecosystems & Environment*, *304*, 107158-. https://doi.org/10.1016/j.agee.2020.107158

Šimůnek, J., Jarvis, N. J., van Genuchten, M. Th., & Gärdenäs, A. (2003). Review and comparison of models for describing non-equilibrium and preferential flow and transport in the vadose zone. *Journal of Hydrology*, *272*(1), 14–35. https://doi.org/10.1016/S0022-1694(02)00252-4

Šimůnek, J., Šejna, M., Saito, H., Sakai, M., & van Genuchten, M. Th. (2013, June). *The HYDRUS-1D Software Package for Simulating the One-Dimensional Movement of Water, Heat, and Multiple Solutes in Variably-Saturated Media: Version 4.17*. Department of Earth Sciences, University of California Riverside. chrome-extension://efaidnbmnnnibpcajpcglclefindmkaj/https://www.pc-progress.com/Downloads/Pgm_hydrus1D/HYDRUS1D-4.17.pdf

Šimůnek, J., & van Genuchten, M. Th. (2008). Modeling Nonequilibrium Flow and Transport Processes Using HYDRUS. *Vadose Zone Journal*, *7*(2), 782–797. https://doi.org/10.2136/vzj2007.0074

Stets, E. g., Kelly, V. j., & Crawford, C. g. (2015). Regional and Temporal Differences in Nitrate Trends Discerned from Long-Term Water Quality Monitoring Data. *JAWRA Journal of the American Water Resources Association*, *51*(5), 1394–1407. https://doi.org/10.1111/1752-1688.12321

van Dijk, M., Morley, T., Rau, M. L., & Saghai, Y. (2021). A meta-analysis of projected global food demand and population at risk of hunger for the period 2010–2050. *Nature Food*, *2*(7), Article 7. https://doi.org/10.1038/s43016-021-00322-9

Vuke, S., Colton, R., & Fullerton, D. (2002). *Geologic Map of the Great Falls North 30'x 60' Quadrangle, Central Montana*. Montana Bureau of Mines and Geology. https://www.mbmg.mtech.edu/pdf_100k/greatFallsN-text.pdf

Wang, G. (2005). Agricultural drought in a future climate: Results from 15 global climate models participating in the IPCC 4th assessment. *Climate Dynamics*, *25*(7), 739–753. https://doi.org/10.1007/s00382-005-0057-9

Water Quality Planning Bureau, Watershed Managment Section. (2004). *Water Quality Restoration Plan and Total Maximum Daily Loads for the Sun River Planning Area*. Montana Department of Environmental Quality.

Wang, X., Müller, C., Elliot, J., Mueller, N. D., Ciais, P., Jägermeyr, J., Gerber, J., Dumas, P., Wang, C., Yang, H., Li, L., Deryng, D., Folberth, C., Liu, W., Makowski, D., Olin, S., Pugh, T. A. M., Reddy, A., Schmid, E., … Piao, S. (2021). Global irrigation contribution to wheat and maize yield. *Nature Communications*, *12*(1), 1235. https://doi.org/10.1038/s41467-021-21498-5

Wang, Z., Liu, J., Hamoud, Y. A., Wang, Y., Qiu, R., Agathokleous, E., Hong, C., & Shaghaleh, H. (2022). Natural 15N abundance as an indicator of nitrogen utilization efficiency in rice under alternate wetting and drying irrigation in soils with high clay contents. *Science of The Total Environment*, *838*, 156528. https://doi.org/10.1016/j.scitotenv.2022.156528

Williams, M. R., King, K. W., Ford, W., Buda, A. R., & Kennedy, C. D. (2016). Effect of tillage on macropore flow and phosphorus transport to tile drains. *Water Resources Research*, *52*(4), 2868–2882. https://doi.org/10.1002/2015WR017650

Zhang, K., Li, X., Zheng, D., Zhang, L., & Zhu, G. (2022). Estimation of Global Irrigation Water Use by the Integration of Multiple Satellite Observations. *Water Resources Research*, *58*(3), e2021WR030031. https://doi.org/10.1029/2021WR030031

Zhang, Y., Zhang, Z., Ma, Z., Chen, J., Akbar, J., Zhang, S., Che, C., Zhang, M., & Cerdà, A. (2018). A review of preferential water flow in soil science. *Canadian Journal of Soil Science*, *98*(4), 604–618. https://doi.org/10.1139/cjss-2018-0046

CHAPTER FIVE

WATER AND NITROGEN USE EFFICIENCY IN LOW LEACHING RISK SYSTEMS- A GALLATIN VALLEY CASE STUDY

Contribution of Authors and Co-Authors

Manuscript in Chapter 5

Author: Meghan Robinson

Contributions: Field data collection; model calibration; data analysis; manuscript writing

Co-Author: W. Adam Sigler

Contributions: Initial research conceptualization; lead on funding acquisition; field and study design; model development; detailed editing and review of writing

Co-Author: Clain Jones

Contributions: Feedback on nutrient management; detailed editing and review of writing

Co-Author: Kent McVay

Contributions: Reviewed writing

Co-Author: Jasmine Neupane

Contributions: Reviewed writing

Manuscript Information

Meghan Robinson, W. Adam Sigler, Clain Jones, Kent McVay, Jasmine Neupane

Status of Manuscript: [Double click to put an X in one of the options below, then delete instruction in brackets. If you cannot double click to add an X, search for "Check Box Content Control."]

☒ Prepared for submission to a peer-reviewed journal
☐ Officially submitted to a peer-reviewed journal
☐ Accepted by a peer-reviewed journal
☐ Published in a peer-reviewed journal

Abstract

Water and nitrogen use efficiency are central in sustainable agriculture. In soils with low infiltration rates, risk of deep percolation and leaching are lower than in well drained soils. More than 50% of the irrigated soils in the Gallatin Valley of southwestern Montana are classified as silt loams. Seed potatoes are an important cash crop grown with irrigation on silt soils. This chapter summarizes findings on water and nitrogen movement conducted during the 2023 and 2024 growing seasons in the fields of two cooperators, both growing seed potatoes on silt loam soils. Soil VWC data was measured at 15, 30, and 90 cm, and water samples from lysimeters were collected at 30 and 60 cm and analyzed for nitrate. During 2024, soil samples were collected for bulk nitrate analysis early in the spring and at harvest, and biweekly during the growing season. Preliminary and relatively simple single porosity modeling was conducted in Hydrus 1D to quantify runoff and deep percolation for study fields. Results suggest that Gallatin silt loam soils where management includes extensive tillage for potato production have limited percolation and leaching risk is therefore minimal. Bulk soil samples also indicate a lack of growing season leaching risk in response to irrigation but do highlight the possibility of overwinter nitrate leaching depending on fertilizer application timing. Runoff was observed on all study fields in the Gallatin, which stands in contrast to all other study sites and suggests that runoff may be a larger challenge than leaching for managing water and nitrogen use efficiency on silt loams with limited infiltration capacities.

5.1: Introduction

The relative importance of different loss pathways for water and nitrogen is variable across soil and agricultural systems. Deep percolation and associated leaching drives water and nitrogen losses in some systems, whereas surface runoff may contribute more substantially to losses in others. Runoff may also cause soil erosion and result in the losses of nutrients and agrichemicals that are sorbed to the soil and less prone to leaching, allowing their entry into surface waterways (Pericherla et al., 2020). The importance of these different loss pathways is controlled by intensity and duration of precipitation and irrigation inputs (Xia et al., 2020), and soil hydrologic properties, soil management, compaction, and topography (Souchere et al., 1998). Losses to deep percolation and runoff can both result in challenges for optimizing water and nitrogen use efficiency, but require different management approaches to mitigate (Follett & Delgado, 2002).

Similarly, nitrogen processing and landscape storage may vary across systems. While certain soil types and agricultural practices may lead to conditions conducive for infiltration and nitrate flushing through soils, other systems may retain solutes in the vadose zone below root depths, leading to an accumulation of legacy nitrate (Xin et al., 2019). The lack of accounting for nitrogen that has accumulated in the agricultural soils has been identified as a challenge in solute modeling, and can result in long-term delay of agricultural management practice effects on water quality (Basu et al., 2022). In deep silt soils in agricultural regions of Oregon, fertilizer applied in a given year has been found to represent a low fraction of the total nitrate leached in that year, reflecting that gradual, multi-year nitrate leaching processes may contribute to nitrate accumulation in groundwater (Weitzman et al., 2024).

In this chapter, I present a case study for water and nitrogen dynamics in a lower leaching risk system. In contrast with the generally thin and structured clay loam soils in Fairfield, Gallatin Valley soils are deep, relatively fine textured, and have fewer macropores and aggregates in the potato study fields, leading to low infiltration rates. In this work, the risk of deep percolation, nitrate leaching, and runoff in response to irrigation was assessed and management approaches that may optimize water and nitrogen use efficiency were considered. I hypothesize that irrigation considering both soil water holding capacity and infiltration rates may be important in improving water use efficiency in soils with high silt fractions.

5.2: Methods

5.2.1: Site Descriptions, Equipment, and Field Visits

A detailed description of equipment installation protocols is provided in Chapter 2. This section will briefly elaborate on details specific to installations in the Gallatin potato fields. Four fields and nine sites were instrumented and monitored in the Gallatin over the two-year study period (Chp 5 - Figure 1). All equipment was installed in fields mapped as silt loams (55-70% silt), a texture that accounts for approximately 55% of all irrigated soils in the Gallatin Valley (Chp 5 - Figure 2). Equipment was installed following potato seeding, hilling, and re-hilling to avoid periods of high soil disturbance and minimize opportunity for equipment destruction. Similarly, equipment was removed ahead of potato harvest. This resulted in a data collection period that was more limited than field sites cultivated to small grains. Equipment was installed at Fields B23 from June 9th- September 13th, 2023, and B24 from June 7th – September 14th, 2024. Fields T23 and T24 had equipment installed from June 26th - September 14th, 2023, and June 19th - September 14th, 2024. Data collected covers the majority of both growing seasons

(Chp 5 - Table 1), as instruments were installed as shortly after seeding and removed as shortly before harvest as possible. Fields T23 and T24 had more limited monitoring periods due to the more extensive amount of work that disturbs soils after seeding, based on that cooperator's standard practices. Field B24 was installed without lysimeters, due to the low sample success rates observed on silt loam soils. Soils at both fields were sampled in the early season- before first fertilizer application at Field T24, and at the time of equipment installation but after fertilization at Field B24. Soils were sampled again in mid-September, just before harvest. Field T24 was the focus of more extensive soil sampling during the summer of 2024 and included biweekly sampling through the growing season as well.

All farm operations were controlled by cooperators, resulting in variable conditions across fields. Fields B23 and B24 were fertilized approximately six months prior to seeding with ammonium nitrate, and soils were tilled to 20-30 cm for fertilizer incorporation. In 2023, Field T23 was the site of a cooperator's fertilizer experiment. Two monitoring sites received an experimental fertilizer treatment, while the other one site received the cooperator's standard fertilizer. In 2024, Field T24 fertilizer was broadcast prior to seeding, and then nitrogen fertilizer was added periodically through the growing season via center pivot fertigation. At all fields, a desiccant was sprayed approximately three weeks before harvest to reduce above ground biomass. Fields B23 and B24 were "devined" by mechanically thrashing plants as an additional means to remove biomass, while Fields T23 and T24 were "rolled" to aid in mechanical breakdown of biomass. Irrigation was generally managed according to cooperator's standard practices. Field T24 was irrigated based on modeled evapotranspiration loss replacements, resulting in a lower than typical quantity of applied irrigation water.

5.2.2: Modeling Methods

With a lack of developed soil structure, single porosity models were appropriate for characterizing water movement in Gallatin silt loam soils. Parameterization for van Genuchten soil hydrologic parameters compared three approaches. One used single, depth-integrated, hydrometer-based percentages of sand, silt, and clay for estimation parameter estimation. A second approach used the same percentages of particle sizes with the average bulk density determined from known volumes of dried field soils included. Finally, a third approach divided soils into two depth increments, one from 0-30 cm and one from 30-90 cm, based on an increase in silt content below 30 cm. Models use weather data from the Manhattan Mesonet station ("mdamanha"), located two miles north of study fields. Alignment between precipitation and Penman-Monteith potential evapotranspiration (PET) parameters between fields and the Mesonet site was satisfactory (Appendix 3). Irrigation schedules were developed from a combination of hourly photographs taken by field cameras at monitoring sites, rain gauges, and cooperator's pivot software interface. Irrigation applications were modeled at 5-, 10-, and 30-minute application times to assess runoff across different pivot speeds and understand differential water partitioning based on runoff risk. These times were selected based on the estimated times for one meter of travel for a nozzle 10, 150, and 300 m from the pivot tower.

5.2.3: Water Use Efficiency and Nitrate Leaching

Water use efficiency was assessed by comparing total quantities of modeled deep percolation and runoff with total quantities of irrigation water applied by cooperators. Data collected were insufficient for closing a nitrogen budget and fully quantifying nitrogen use efficiency using standard literature methods (John et al., 2017); however, changes in soil nitrate

and predicted leaching losses were used to roughly approximate how different managements influence risk of nitrogen loss. Differences in nitrate inventories in the top 90 cm of soil from early season and post-harvest measurements were calculated to assess what remains after harvest. Biweekly soil samples collected to 66 cm and analyzed for nitrate-N by KCl extraction and cadmium reduction colorimetry at AGVISE are the focus for nitrogen loss risk estimations because lysimeter samples were too limited to provide nitrate ranges that can be confidently assumed to capture spatial or temporal variability in nitrate behavior. All data and code for this chapter are available on Hydroshare (Robinson & Sigler, 2025).

5.3: Results

5.3.1: Field Results

The 2023 growing season followed an exceptionally wet winter and spring, and cumulative growing season precipitation exceeded average. During 2024, a milder winter with below average precipitation preceded the season, however spring and summer precipitation were above normal (Chp 3 – Figure 5). VWC data collected in both fields and during both years found limited evidence of water percolation to 90 cm in soils. At 15 cm, occasional increases in soil VWC following irrigation or precipitation events were observed in all study fields. The clearest responses generally occurred in August, and frequently when precipitation and reduced evapotranspiration aligned with irrigation events (Chp 5 - Figures 3, 4, 5, and 6). Soil VWC was observed to increase at 30 cm in both Field T23 and Field B23, also during the limited late season period (Chp 5 - Figure 3 and 5). In 2023, small increases in 90 cm VWC were observed at all monitoring sites in Field T23. From antecedent to peak observed conditions, VWC at 90 cm rose an average of 0.0103 cm^3cm^{-3} (1.03%). This was in contrast with the other three monitored

fields, where responses at 90 cm were never observed and only Field B23 had mild evidence of increasing VWC at 30 cm. The total irrigation application on Field T23 was 35.1 cm (13.8 in), or approximately twice the irrigation quantity applied to any other study field during the period of data collection.

Over the two years of data collection and 14 individual lysimeters installed, more than two samples were collected from only four lysimeters, constraining the ability to understand soil water nitrate behavior. In 2023 in Field T23, three lysimeters produced adequate samples for assessing time series data, including two 30 cm lysimeters and one 60 cm lysimeter. Both 30 cm lysimeters followed an expected pattern with nitrate concentrations that peaked immediately after N fertilizer application and then gradually decreased over the growing season, likely reflecting crop uptake (Chp 5 - Figure 7). Nitrate-N concentrations between the two lysimeters differed greatly early in the season, with TT_Arable recording a maximum concentration of 394.7 mg L^{-1} on August 4th, and TC_North recording a peak concentration of 196.2 mg L^{-1} on July 7th. At the last date of successful sample collection, nitrate-N concentrations were more similar between the sites, at 18.8 mg L^{-1} (TT_Arable) and 21.9 mg L^{-1} (TC_North). The 60 cm TC_North lysimeter also collected repeated samples, though after an initial increase following fertilizer application, nitrate concentrations varied minimally. Concentrations consistently ranged from 76.0 mg L^{-1} to 79.0 mg L^{-1} between July 7th and September 1st (Chp 5 - Figure 7). During the 2024 growing season, more than two samples were collected from only one lysimeter at 60 cm at site T208. Nitrate concentrations show a similar pattern to those observed in 2023, with a highest concentration of 42.5 mg L^{-1} observed on July 9th, and then gradual decreases to a final observed concentration of 20.3 mg L^{-1} on August 8th (Chp 5 - Figure 8). Potato roots were

observed as deep or deeper than all lysimeters that produced samples in the Gallatin during both study years (Chp 5 - Figures 7 and 8).

Soil samples collected from Field T23 in 2023 approximately one month after fertilizer application had 317 kg ha^{-1} nitrate-N in the top 90 cm of the soil for the monitoring site under conventional fertilizer management compared to 156 kg ha^{-1} for the two monitoring sites under the alternative fertilizer management (Chp 5 - Figure 9). This aligns with lysimeter results that found much higher nitrate concentrations in the samples collected by TT_Arable lysimeters as opposed to TC_North lysimeters. In Field B23, soil samples were collected approximately eight months following fertilizer application the previous October. The average nitrate-N inventory to 90 cm for the two monitoring sites was 123 kg ha^{-1}, with 24 to 28 kg ha^{-1} in the top 15 cm of the soil, and the largest nitrate inventory of 46 to 52 kg ha^{-1} at 30 to 60 cm (Chp 5 - Figure 9).

To compensate for limited lysimeter sample collection, more extensive bulk soil samples were collected during the 2024 growing season. Biweekly soil sampling in Field T24 found relatively dynamic nitrate concentrations in the top 15 cm of soils, perhaps reflecting interactions between regular nitrogen applications via fertigation and crop uptake (Chp 5 - Figure 10). The highest nitrate-N inventory in the soil profile to 66 cm was an average of 130.6 kg ha^{-1} (range: 111.2 to 150 kg ha^{-1}) on June 24th. The lowest observed profile nitrate-N inventory was 67.3 kg ha^{-1} (range: 52.9 to 81.7 kg ha^{-1}) on August 21st, the final sampling date for the season. Clear decreases in nitrate inventories were observed at depth increments 0-15 cm, 15-25 cm, and 25-35 cm over the six sampling events. Nitrate inventories were more constant deeper in the profile. At the 55-66 cm depth increment, only 1.6 kg ha^{-1} of variability in nitrate-N concentrations across

the six visits and two sampling sites were observed. All increases in nitrate concentrations occurred within the root zone observed for a particular sampling date (Chp 5 - Figure 10).

Pre-fertilizer and post-harvest nitrate inventories show different patterns on Field T24, where fertilizer was applied in the spring, and Field B24, where fertilizer was applied in the fall. The median nitrate-N inventory to 90 cm on field T24 was 66.1 kg ha^{-1} on April 16th, roughly one week prior to fertilizer application. At harvest, the median nitrate-N inventory was 55.5 kg ha^{-1}. Median nitrate inventories in the top 30 cm of soil were very similar between sampling dates, with 21.9 kg ha^{-1} on April 16th and 21.3 kg ha^{-1} on September 14th. Nitrate-N concentrations from 30 to 90 cm decreased from 44.8 kg ha^{-1} on April 16th to 33.6 kg ha^{-1} on September 14th. In Field B24, the median early season (but post-fertilizer, applied the previous October) 90 cm nitrate-N inventory was 314.4 kg ha^{-1}. The median nitrate-N inventory on September 14th was 168.7 kg ha^{-1}. Nitrate-N inventories in the upper 30 cm fell from 153 kg ha^{-1} in June to 23 kg ha^{-1} in September, representing 130 kg ha^{-1} of uptake or other losses. Nitrate-N inventories between 30 and 90 cm dropped only slightly, from 161.4 kg ha^{-1} in April to 145.7 kg ha^{-1} in September, a reduction of 15.7 kg ha^{-1} that is similar to the decrease observed in Field T24, but reflecting the much higher initial nitrate concentrations (Chp 5 - Figure 11).

5.3.2: Modeling Results

Hydrus models generally predicted much more responsive 15 cm soil VWC patterns than were observed in the field. The model predicted more fluctuations in 90 cm VWC as well; however, soil water content predictions were somewhat smoothed and less dynamic when bulk density was included in van Genuchten parameter predictions. Model alignment with field data was improved when bulk density was included for soil hydrologic parameter estimation and was

further improved when separate textures for surface and deeper soils were included (Chp 5 – Figure 12). and model fits for Field B23 have the highest NSE: -0.96 using a two-depth approach, -8.94 using single depth texture and bulk density, and -4.71 using only texture percentages. The 90 cm VWC model fit for B23 using two depths for calibration resulted in the best model fit across all fields (Chp 5 - Figure 12). Model improvements based on NSE were found across fields when using additional data beyond percentages of sand, silt, and clay: -8.66 (sand, silt, and clay only) to -3.18 (bulk density and two depths) at B24, -541.39 to -191.97 at T23, and -73.21 to -29.88 for T24.

Hydrus predicted effectively no deep percolation on Field B23 for either depth averaged parameterization approach; however, predicted 3.2 cm of losses with the best fit two depth approach. For Field B24, Hydrus models over-predicted drying at depth and suggest a larger range of soil water contents throughout the season than were observed in the field. All models for Field B24 predicted approximately 7 cm (6.54-7.63 cm) of deep percolation, though deep percolation primarily occurred earlier in the season following early spring increases in soil water content, which due to limited data periods cannot be fully validated with field data (Chp 5 - Figure 13). Field T23, which received 35 cm of irrigation, is the only field where the model predicted that irrigation caused deep percolation. Hydrus estimated 14.23-14.68 cm of deep percolation; however, VWC are over-predicted by Hydrus relative to field data, and alignment between field data and the model is poor based on NSE criteria (Chp 5 - Figure 14). Field T24 and Field B24 behaved similarly, with deep percolation predicted early in the season before field equipment was installed, and the model over- predicting early season water contents while also suggesting more intense drying than observed (Chp 5 - Figure 15). Modeled deep percolation

estimates for Field T23 suggest that 25% of the total 58.3 cm of combined irrigation (35.0 cm) and precipitation (23.3 cm) was lost as deep percolation. On other fields, deep percolation in response to irrigation was negligible.

Modeling results suggest that increasing the rate of irrigation water application resulted in higher cumulative runoff. Predicted runoff quantities for different irrigation application rates were calculated for Field B23, as model performance relative to field data was best. Season runoff decreased from a total of 11.2 cm and peak daily losses of 1 cm day^{-1} with 5-minute irrigation times, to 9.1 cm and approximately 0.8 cm day^{-1} losses with 30-minute irrigation (Chp 5 - Figure 16). For irrigation events modeled with 1.27 cm applied in 5 minutes, the 11.2 cm of predicted runoff accounts for 27% of total of irrigation and precipitation (11.2 cm/41.6 cm). A pivot speed resulting in the application of the same 1.27 cm over 30 minutes predicts 9.1 cm of runoff, a smaller 21% (9.1 cm /41.6 cm) of the total water input. Without field data, these predictions cannot be validated. Runoff was observed at all study fields, particularly along rows that were driven regularly by sprayers and at areas of fields with steeper slopes.

5.4: Discussion

5.4.1: Limited Nitrate Leaching Risk in Silt Soil

Soil water content data suggest that minimal percolation occurs on silt loam soils. With water movement being a necessary condition for nitrate leaching, the lack of observed deep percolation implies that nitrate leaching risk in response to irrigation is low. Data are limited by the short period of VWC data collection, and leaching is possible in response to precipitation or snowmelt outside of the growing season when water inputs are relatively high and PET is low. Periods of heightened responsiveness in VWC in late summer periods do suggest opportunity for

water and nitrogen losses; however, only with total irrigation quantities above 30 cm were VWC responses at 90 cm observed. Increased 15 cm soil water content responsiveness later in the growing season could reflect changing soil conditions and possible macropore development as the season progresses and roots grow, or perhaps could result from canopy closure and reduced evaporation from furrows, allowing conditions more conducive for infiltration. These variable responses could also reflect changes in potato water uptake patterns. Exploring late season responsiveness could help develop an understanding of deep percolation risk during the growing season and implications for irrigation decisions. Limited water movement is corroborated by low success rates for lysimeter sample collection, suggesting low water infiltration into the soil profile.

Modeling results suggest that some deep percolation occurs; however, deep percolation is dominated by early season losses that cannot be validated with the current field data. Hydrus only predicted clear deep percolation in response to irrigation under the highest irrigation rates observed across study fields. In other model runs, the lack of deep percolation predictions is logical given field data patterns that show drying at depth over the growing season.

Soil nitrate patterns generally support a lack of water movement during the growing season as well. The relatively stable bulk soil nitrate inventories at 55-66 cm are consistent with a lack of water moving to this depth, and a limited opportunity for nitrate leaching. Low lysimeter sample collection success in the Gallatin allows for limited interpretation, but low sample collection rates do further support low leaching risk. In the summer of 2024, nitrate concentrations were observed to decrease at the 60 cm lysimeter. Roots were observed to 90 cm, so this decreasing pattern in concentrations is likely partially attributed to root uptake.

Findings suggest that fertilizer application timing may be an important driver of leaching risk outside the growing season. Higher quantities of nitrate remained in the soil after harvest in the fall-fertilized Field B24. Fall fertilizer application has historically been the primary management approach on Fields B23 and B24, so nitrate has had an opportunity to accumulate at depth over many crop rotation cycles. If overwinter and early spring deep percolation do occur as Hydrus models suggest, nitrate stored deep in the soil profile is poised for leaching. Data also suggest that potato roots are not efficient at nitrate uptake below approximately 30 cm. While roots were observed to 90 cm in both Fields B24 and T24, relatively small (< 16 kg N ha^{-1}) changes in 30-90 cm nitrate inventories were found over the season in both fields. This finding suggests that if nitrate moves deeper into soils and towards the boundaries of the root zone, it could be vulnerable to leaching. This aligns with previous work in silt loam soils that found leached fertilizer was gradually pushed past roots over multiple years (Weitzman et al., 2024), and that nitrate remaining in soils after harvest was at risk for leaching in potato production (Peralta & Stockle, 2002). Fertilizer applied in the fall appears to allow for higher risk of this gradual leaching process relative to spring applied nitrogen, because wet winter conditions can move nitrate to depths of less effective root extraction before the growing season starts.

Runoff may present a larger challenge than deep percolation for growing season water and nitrogen losses on silt loam soils, particularly if cultivation practices result in limited infiltration capacity. Runoff was observed at all field sites, and while field methods did not quantify runoff, Hydrus models do predict that runoff occurs at the range of speeds possible for pivot travel. Results imply that runoff risk may be higher along the edges of fields, where the pivot circumference and travel distance is longer, resulting in sprinkler nozzles traveling faster.

At faster travel speeds, nozzles must apply an equivalent quantity of water at a faster rate. This may result in application rate exceeding infiltration capacity for soils, and runoff risk increasing with distance from the center tower. The modeled differences in water budget were primarily reflected in lower cumulative transpiration predictions for faster pivot speeds, suggesting water that was lost as runoff at high application intensities would be consumed by the crop if applied at lower intensity (longer duration to apply same amount of water). This work suggests that efforts to improve water use efficiency in irrigated silt loams should focus on ensuring that infiltration rates are not exceeded by irrigation rates, and that considering total water holding capacity to limit deep percolation is important but perhaps a less immediate concern where infiltration and deep percolation are limited.

5.5: Conclusions

Gallatin silt loam soils have limited deep percolation and leaching risk relative to clay loam soils in Fairfield. Runoff may result in greater water and nutrient losses than deep percolation, and therefore reducing runoff is likely key to improving agricultural resource efficiency and managing for water quality. These results are most relevant to silt loam soils, which account for over half of all irrigated soils in the Gallatin Valley. Further work should incorporate observations in non-potato crops on silt loam soils, to isolate soil water responses that are unique to potatoes as opposed to processes that result from soil characteristics. Working under crops that require lower disturbance, such as small grains, would also allow for data collection during wet, early spring periods where deep percolation and leaching risk may be highest. Additional work in quantifying deep soil nitrate storage across fertilizer management

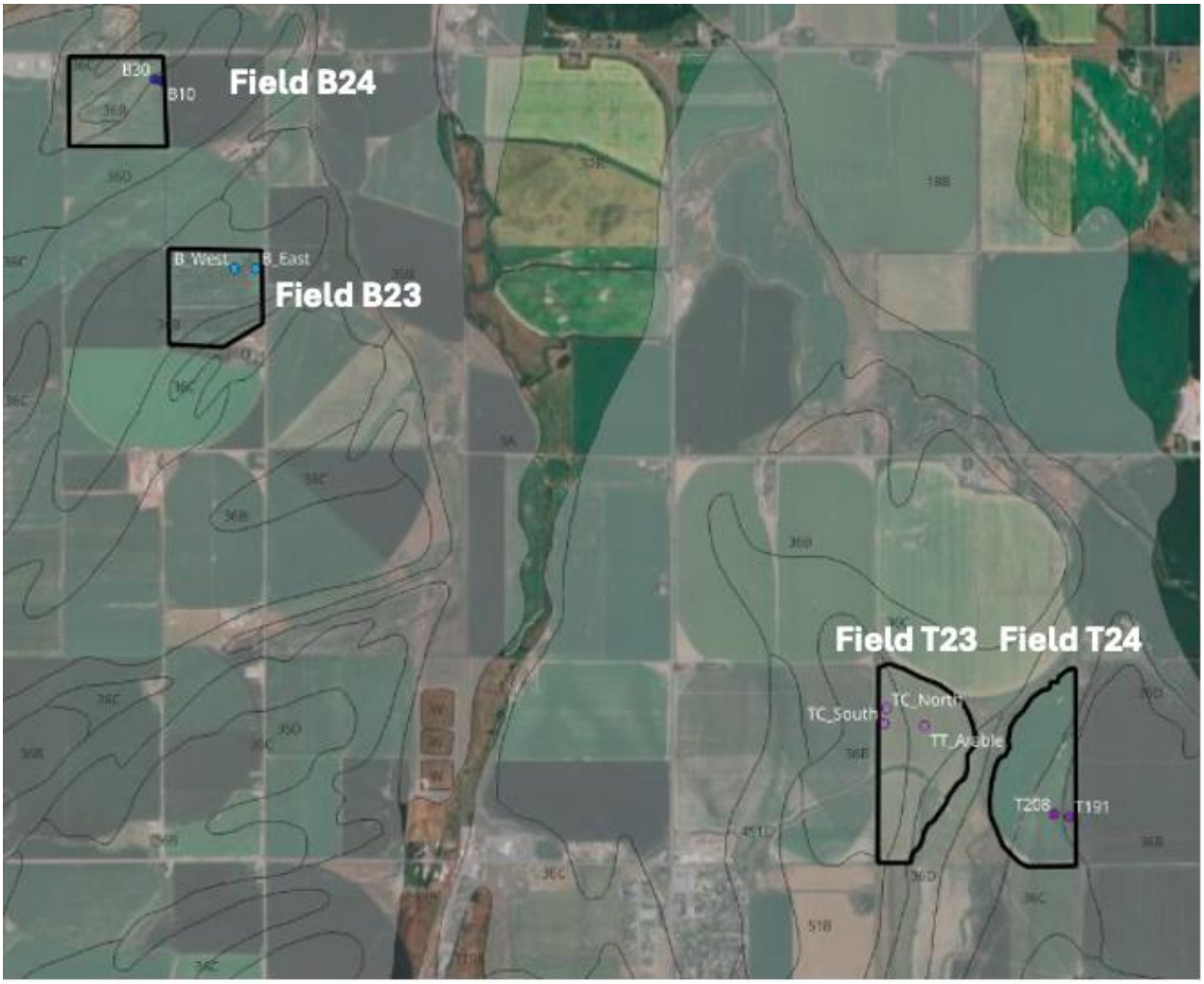
strategies to understand implications for nitrogen use efficiency and leaching risk is also recommended.

Field	Seeding	Harvest	Equipment Install	Equipment Removal	Growing Season	Monitoring Period
B23	2023-06-02	2023-10-01	2023-06-07	2023-09-13	121 days	98 days
B24	2024-05-30	2024-09-23	2024-06-11	2024-09-14	116 days	95 days
T23	2023-05-28	2023-09-28	2023-06-26	2023-09-13	123 days	79 days
T24	2024-05-25	2024-09-18	2024-06-19	2024-09-14	116 days	87 days

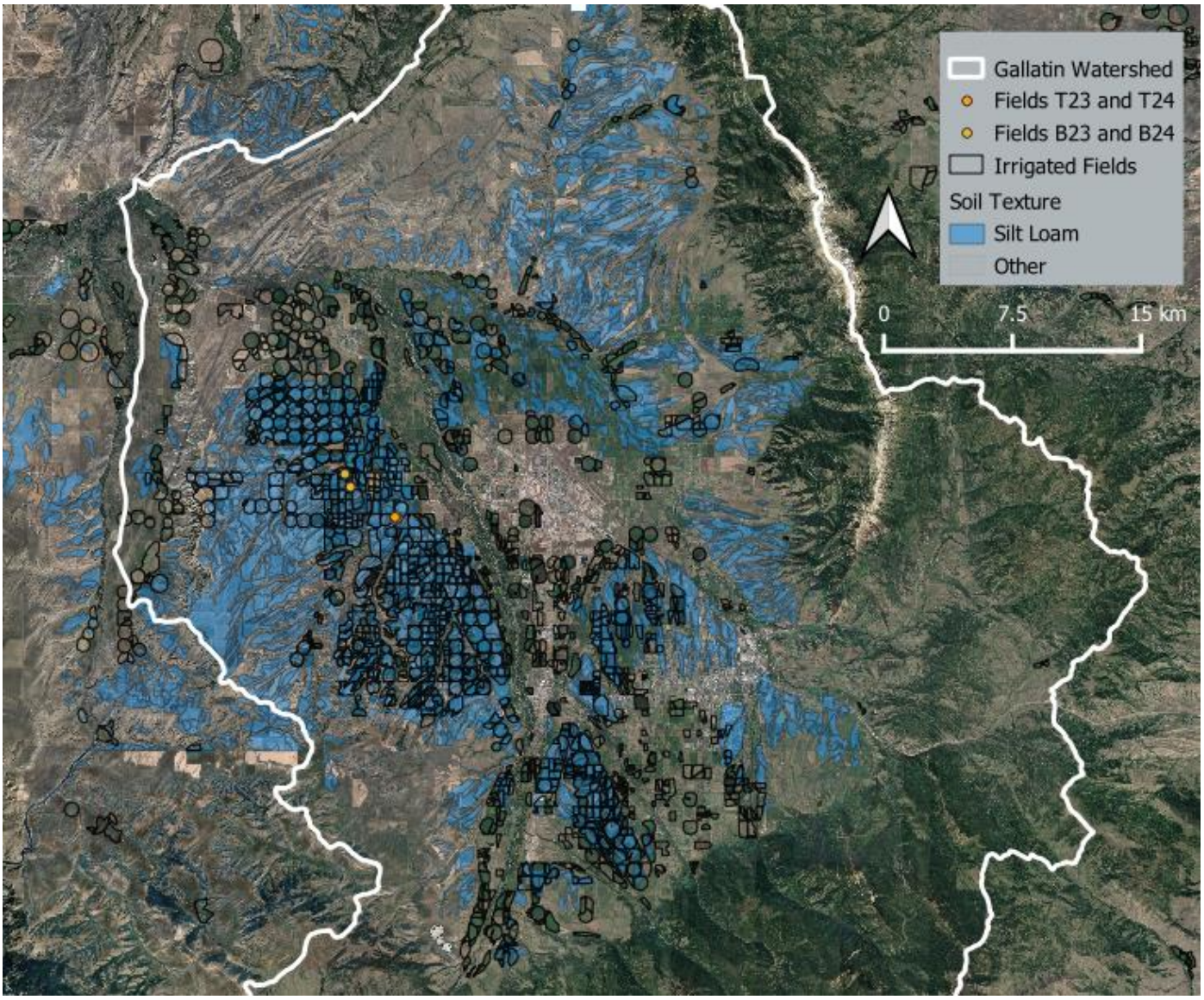
Chp 5 - Table 1: Monitoring Periods and Growing Season. Comparison of growing seasons and monitoring periods for all instrumented fields.

Site	Field	Lysimeter Samples Collected	Fertilizer and Irrigation	Other Notes
B_East	B23	2	Fall fertilizer, grower standard irrigation: 18.23 cm	Kinked lysimeter tube
B_West	B23	1	Fall fertilizer, grower standard irrigation: 18.23 cm	
TC_North	T23	10	Experimental fertilizer, grower standard irrigation: 35.07 cm	Soil water water sensor damaged by rodents
TC_South	T23	0	Experimental fertilizer, grower standard irrigation: 35.07 cm	
TT_Arable	T23	3	Conventional fertilizer, grower standard irrigation: 35.07 cm	Kinked lysimeter tube
B10	B24	NA- no lysimeters	Fall fertilizer, grower standard irrigation: 13.59 cm	Soil water sensor failures
B30	B24	NA- no lysimeters	Fall fertilizer, grower standard irrigation: 13.59 cm	
T191	T24	2	Spring fertilizer and fertigation, ET replacement irrigation: 16.51 cm	
T208	T24	5	Spring fertilizer and fertigation, ET replacement irrigation: 16.51 cm	Soil water sensor failures

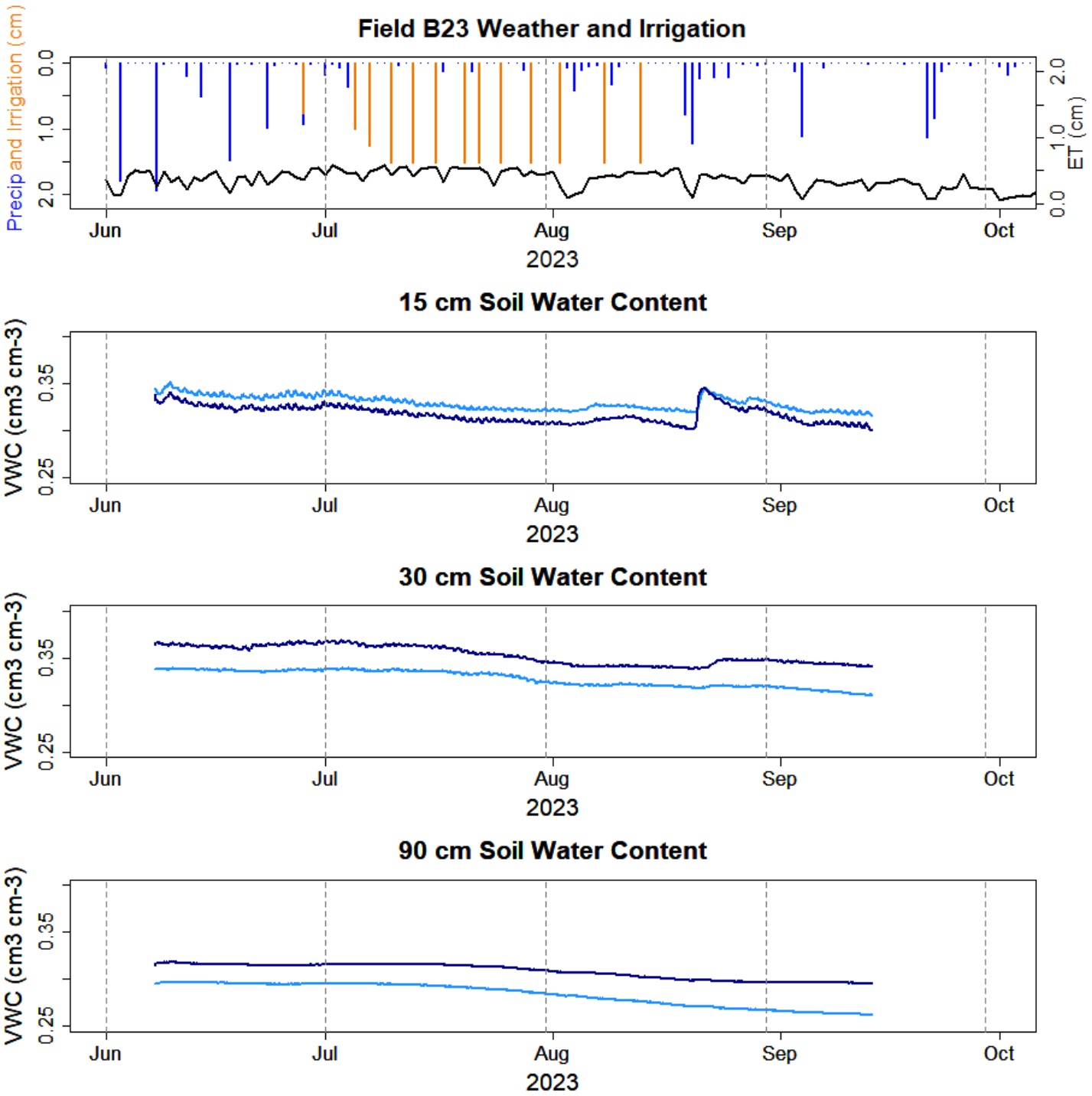
Chp 5 - Table 2: Site Summary. Summary of field sites, locations, lysimeter sample success, management practices, and other notes.



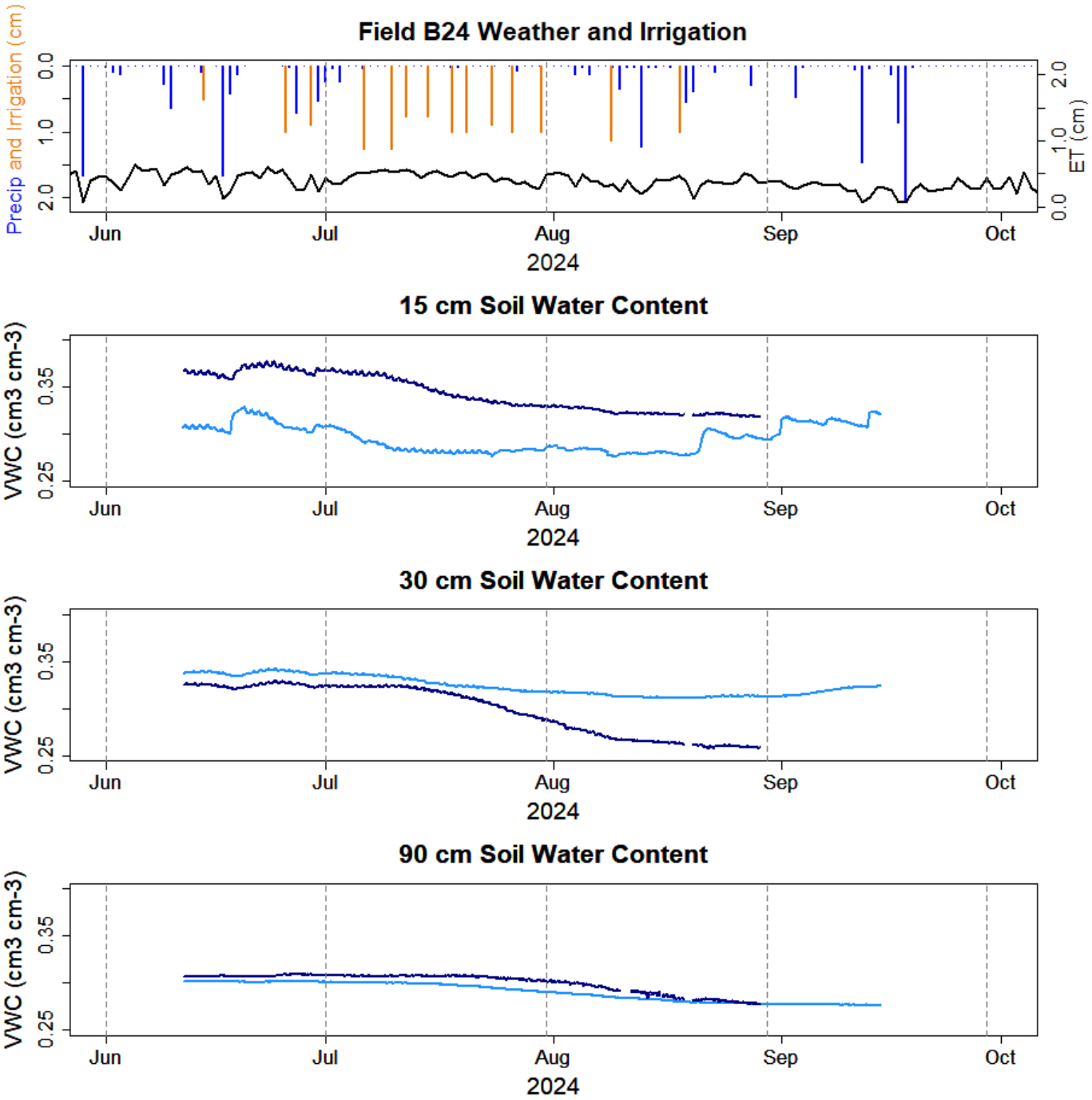
Chp 5 - Figure 1: Gallatin Field Sites. Field locations (outlined in black) and field sites (labeled points within field boundaries). Light grey shading shows soils mapped as silt loams.



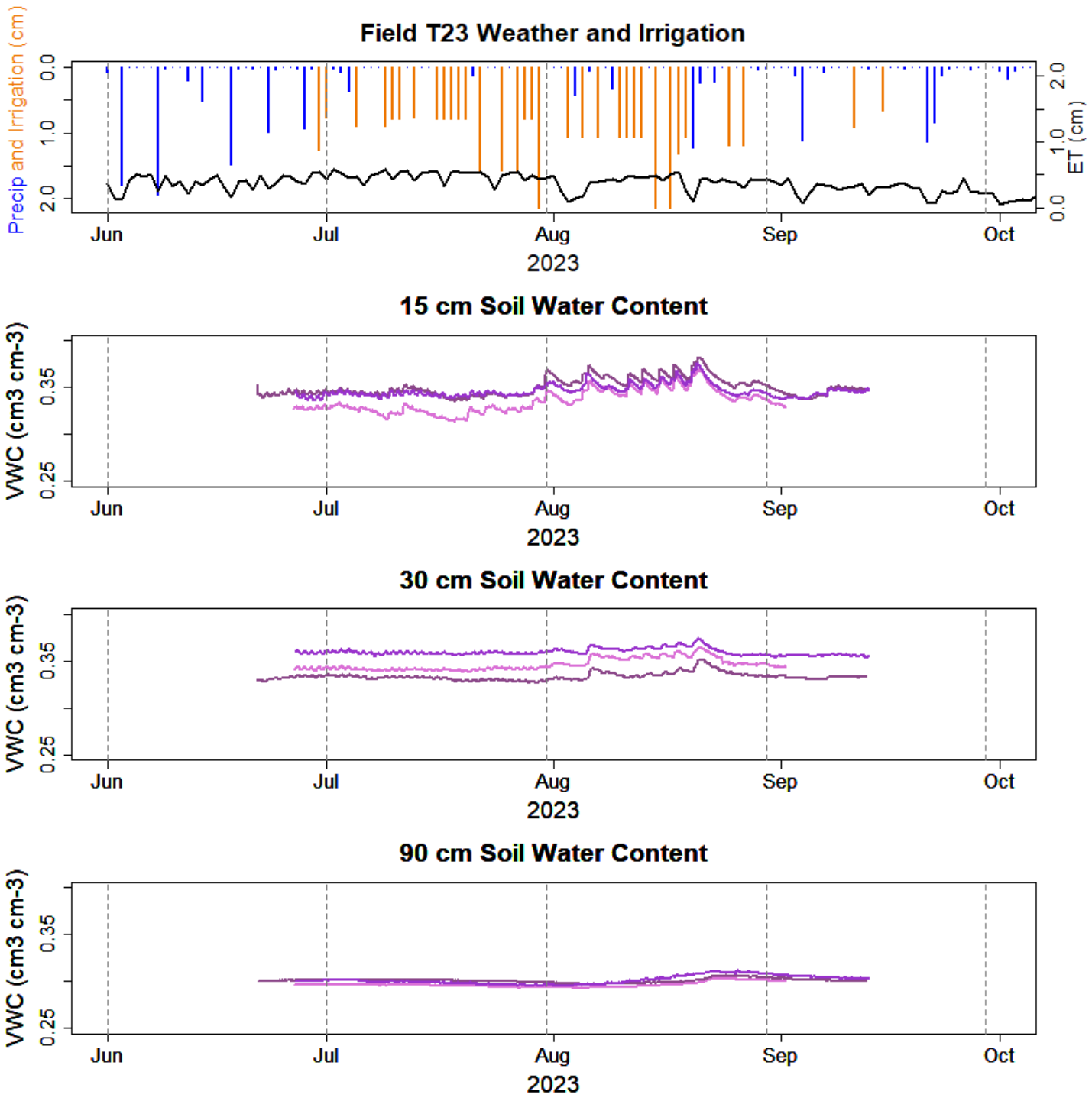
Chp 5 - Figure 2: Map of Gallatin Valley Silt Loams and Irrigation. Soils mapped as silt loams (blue) and mapped irrigation (black) for the Gallatin Valley.



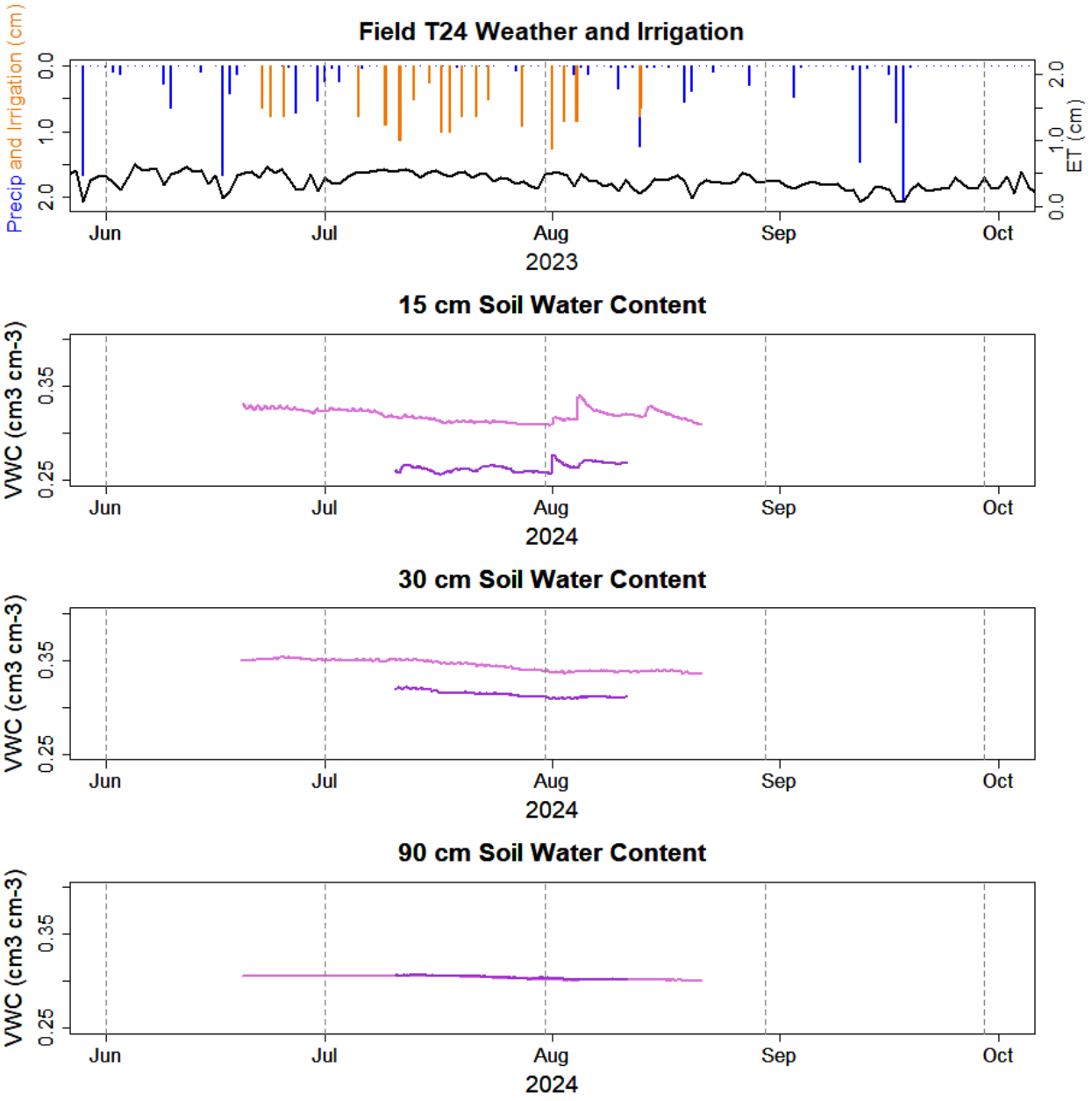
Chp 5 - Figure 3: Soil Water Content Responses for B23. Top panel: Precipitation, irrigation, and ET during 2023. Panels 2, 3, and 4: Soil water content for B_East (light blue) and B_West (dark blue) at 15, 30, and 90 cm.



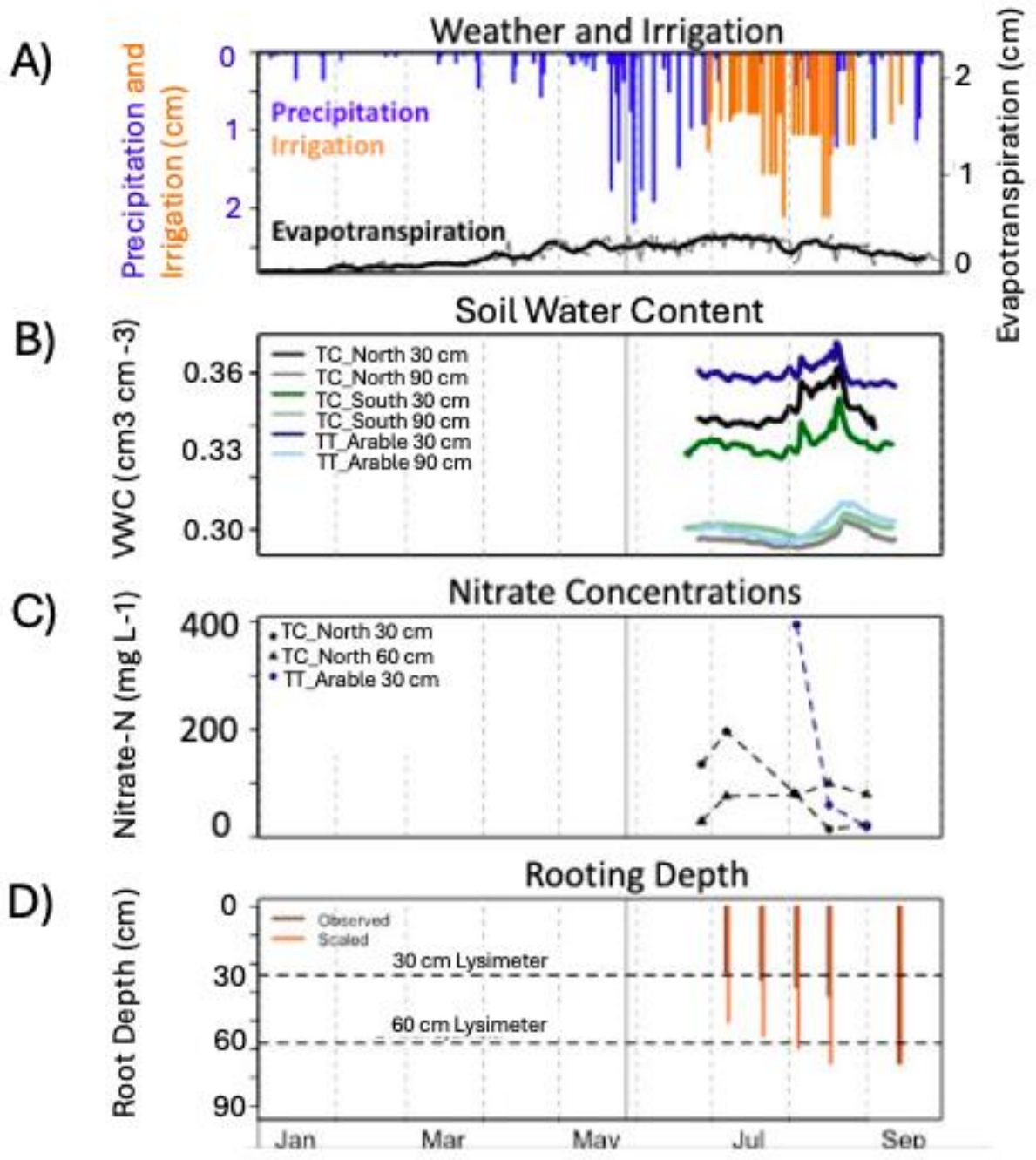
Chp 5 - Figure 4: Soil Water Content Responses for B24. Top panel: Precipitation, irrigation, and ET during 2024. Panels 2, 3, and 4: Soil water content for B10 (light blue) and B30 (dark blue) at 15, 30, and 90 cm.



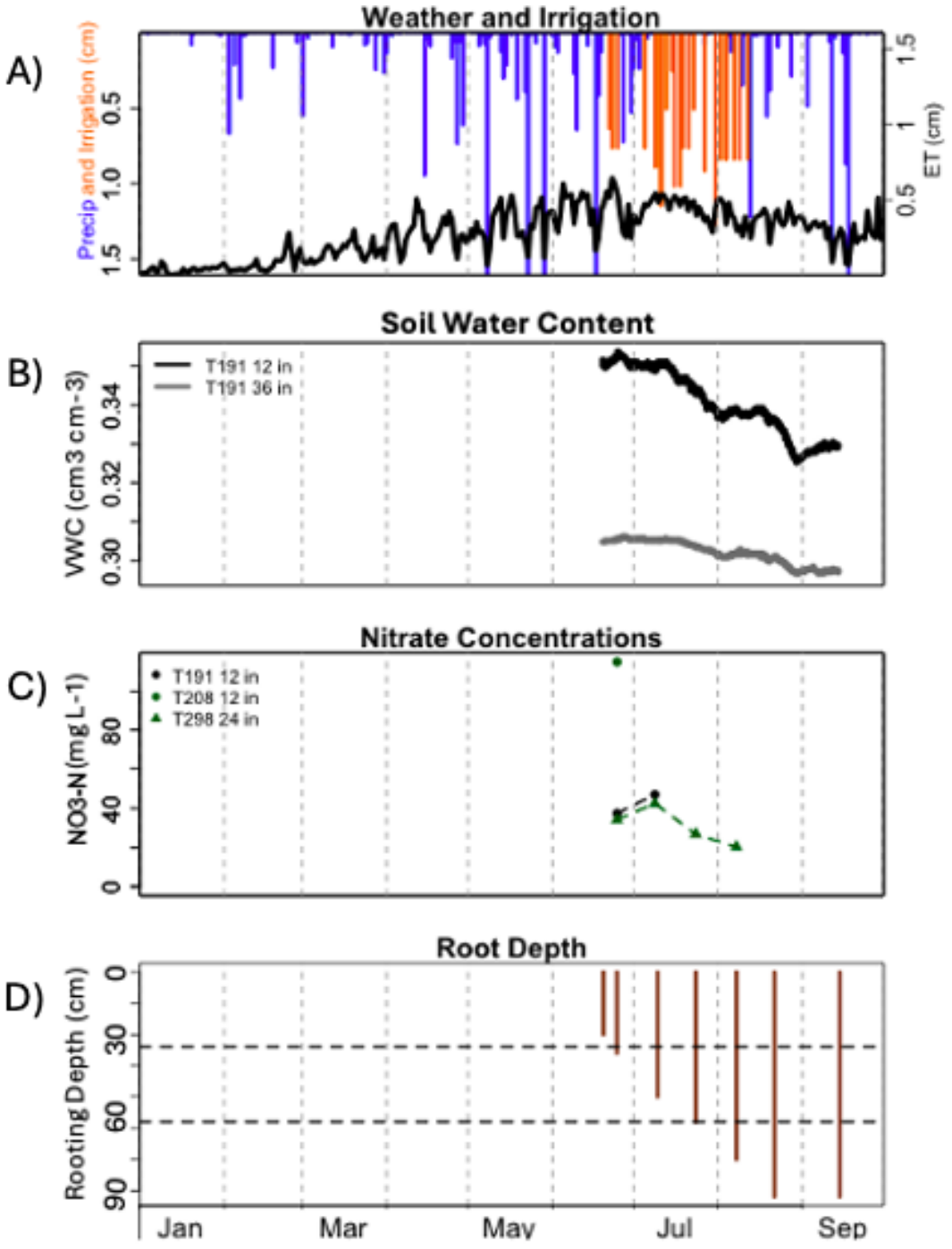
Chp 5 - Figure 5: Soil Water Content Responses for T23. Top panel: Precipitation, irrigation, and ET during 2023. Panels 2, 3, and 4: Soil water content for TT_Arable (lightest purple) and TC_South (medium purple), and TC_North (darkest purple) at 15, 30, and 90 cm.



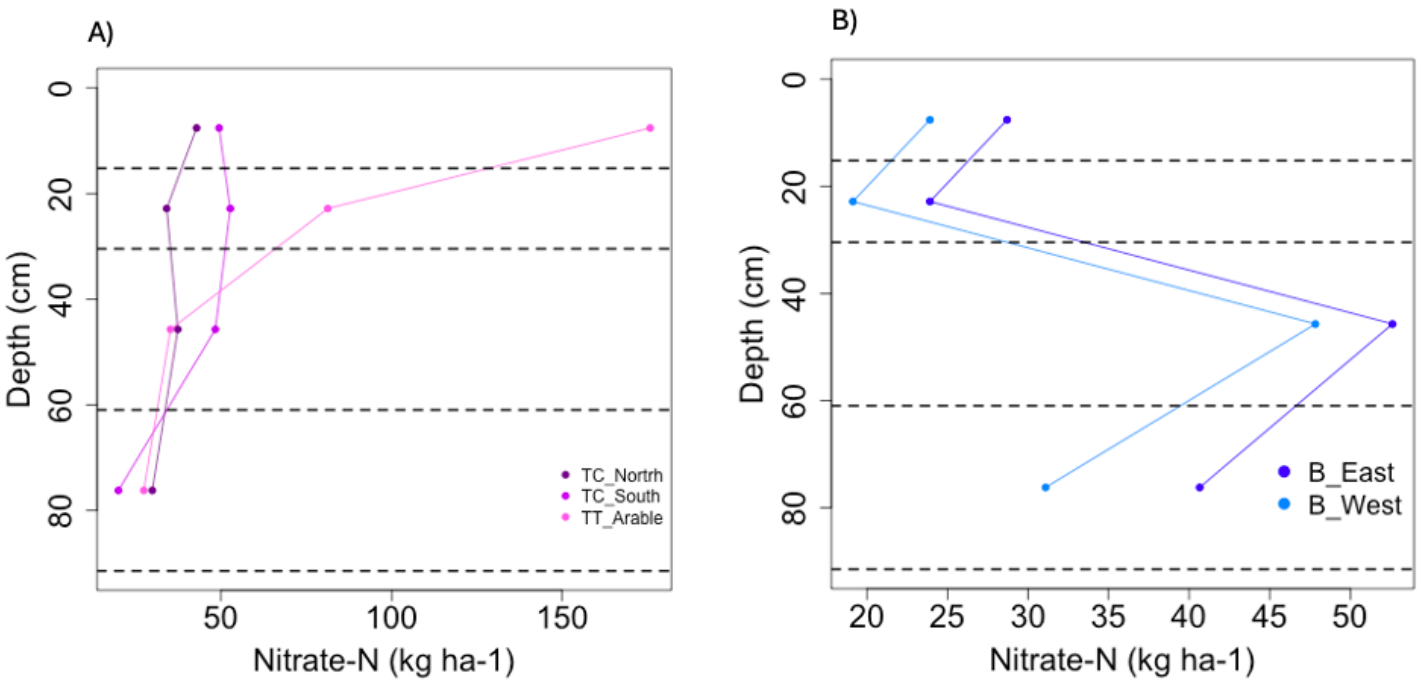
Chp 5 - Figure 6: Soil Water Content Responses for T24. Top panel: Precipitation, irrigation, and ET during 2024. Panels 2, 3, and 4: Soil water content for T191 (light purple) and T208 (dark purple) at 15, 30, and 90 cm.



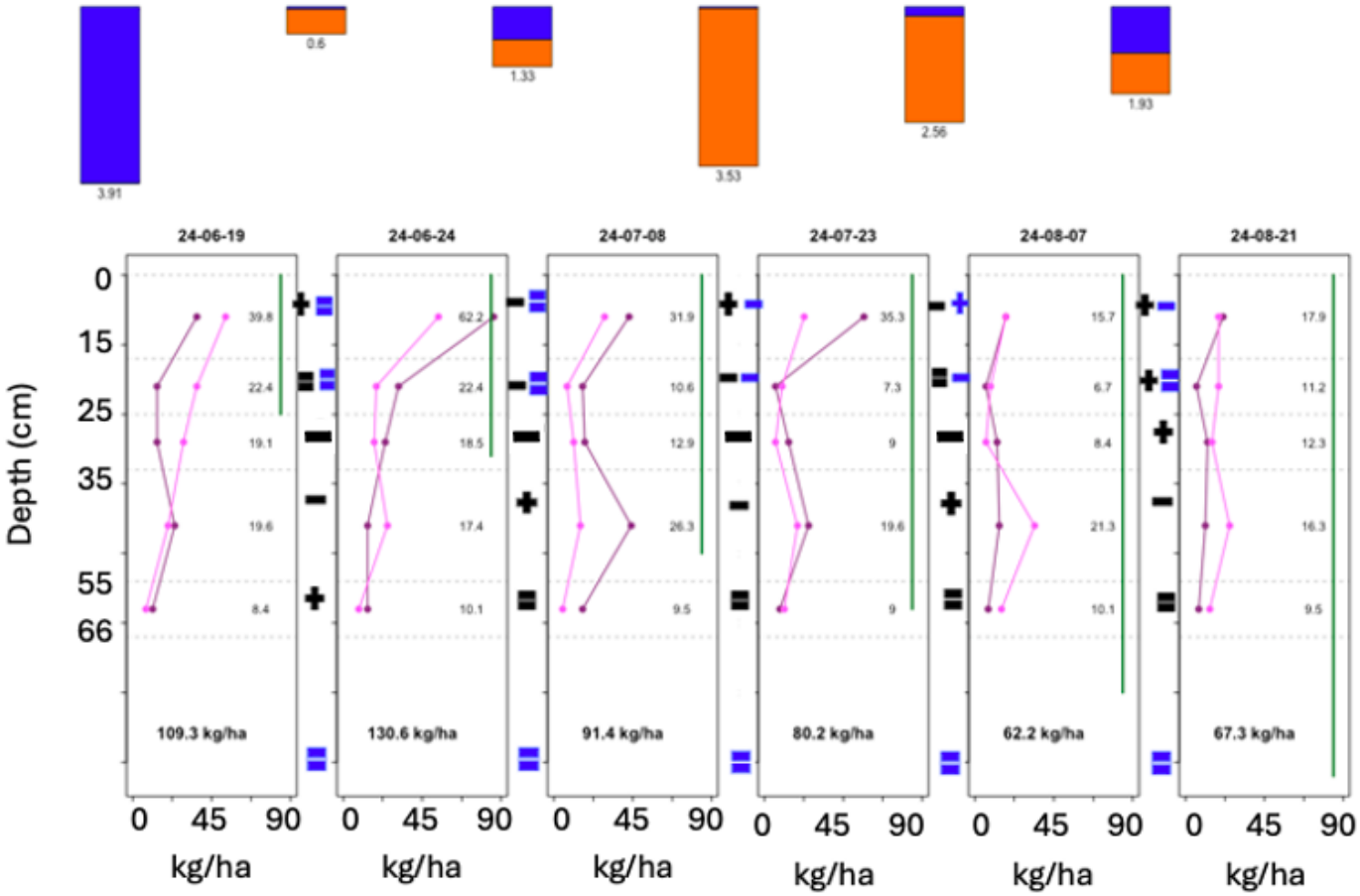
Chp 5 - Figure 7: 2023 Lysimeter Nitrate Patterns. A) Weather and irrigation for the T23 during the 2023 growing season. B) VWC at 30 and 90 cm for three monitoring sites. C) Nitrate concentrations from lysimeter samples. D) Potato rooting depths.



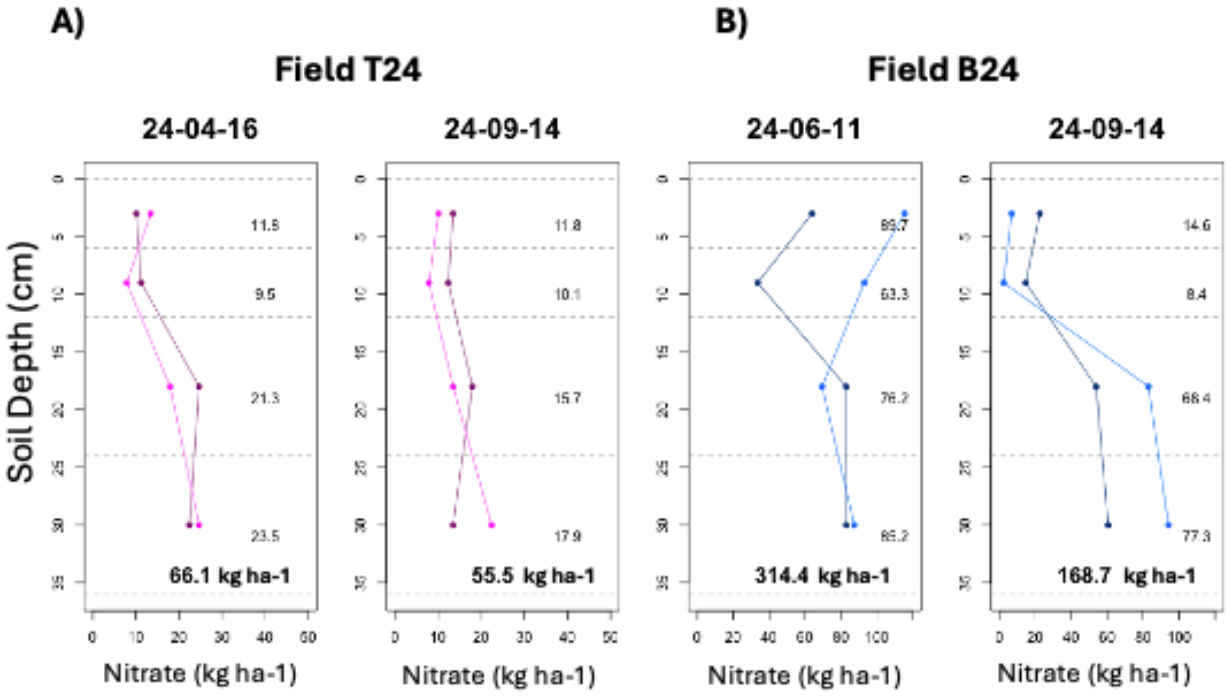
Chp 5 - Figure 8: 2024 Lysimeter Patterns. A) Weather and irrigation for T24 during the 2024 growing season. B) Representative site soil VWC data at 30 and 90 cm. C) Lysimeter nitrate concentrations. D) Potato rooting depth.



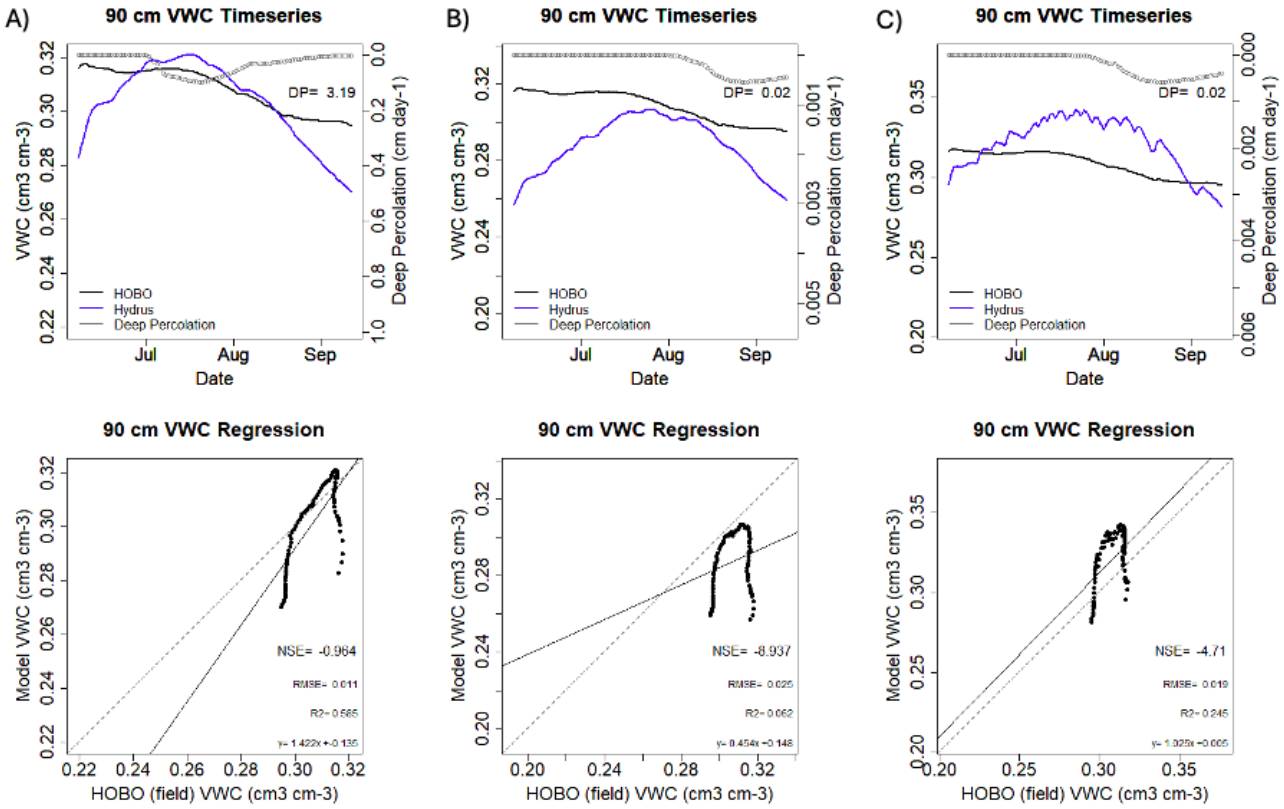
Chp 5 - Figure 9: 2023 Soil Samples. Soil nitrate inventories at A) Field T23, and B) Field B23. Both are from mid-June, after fertilizer application.



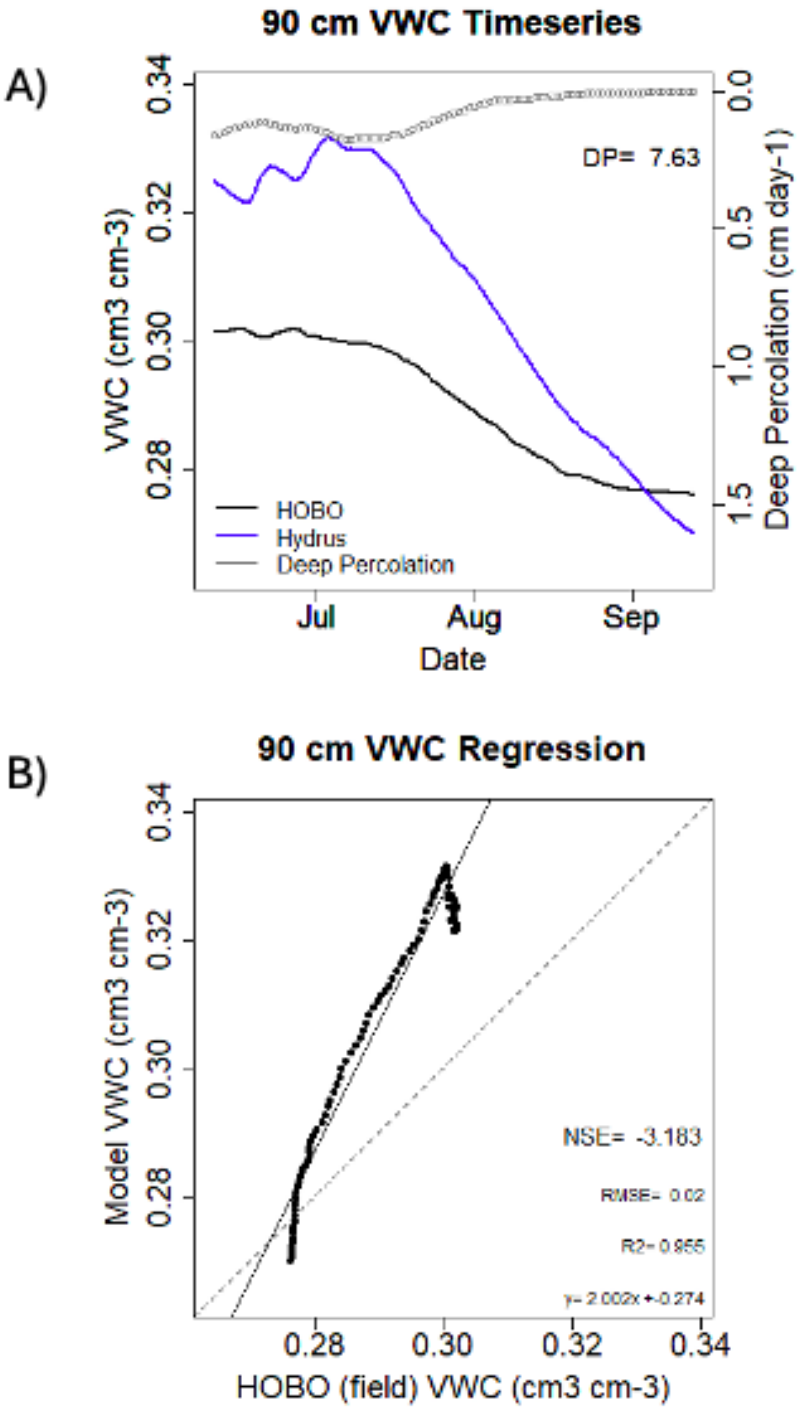
Chp 5 - Figure 10: 2024 Biweekly Soil Sampling. Nitrate from soil samples at two sites on six dates. Dark purple points are nitrate concentrations from monitoring site T191, light purple points are from monitoring site T208. Green lines along right side of plot indicate rooting depth. Bars are aggregated precipitation (blue) and irrigation (orange) between visits. Black +,-, and = signs show differences in nitrate concentrations between visits. Blue +, -, and = signs show differences in VWC patterns between visits.



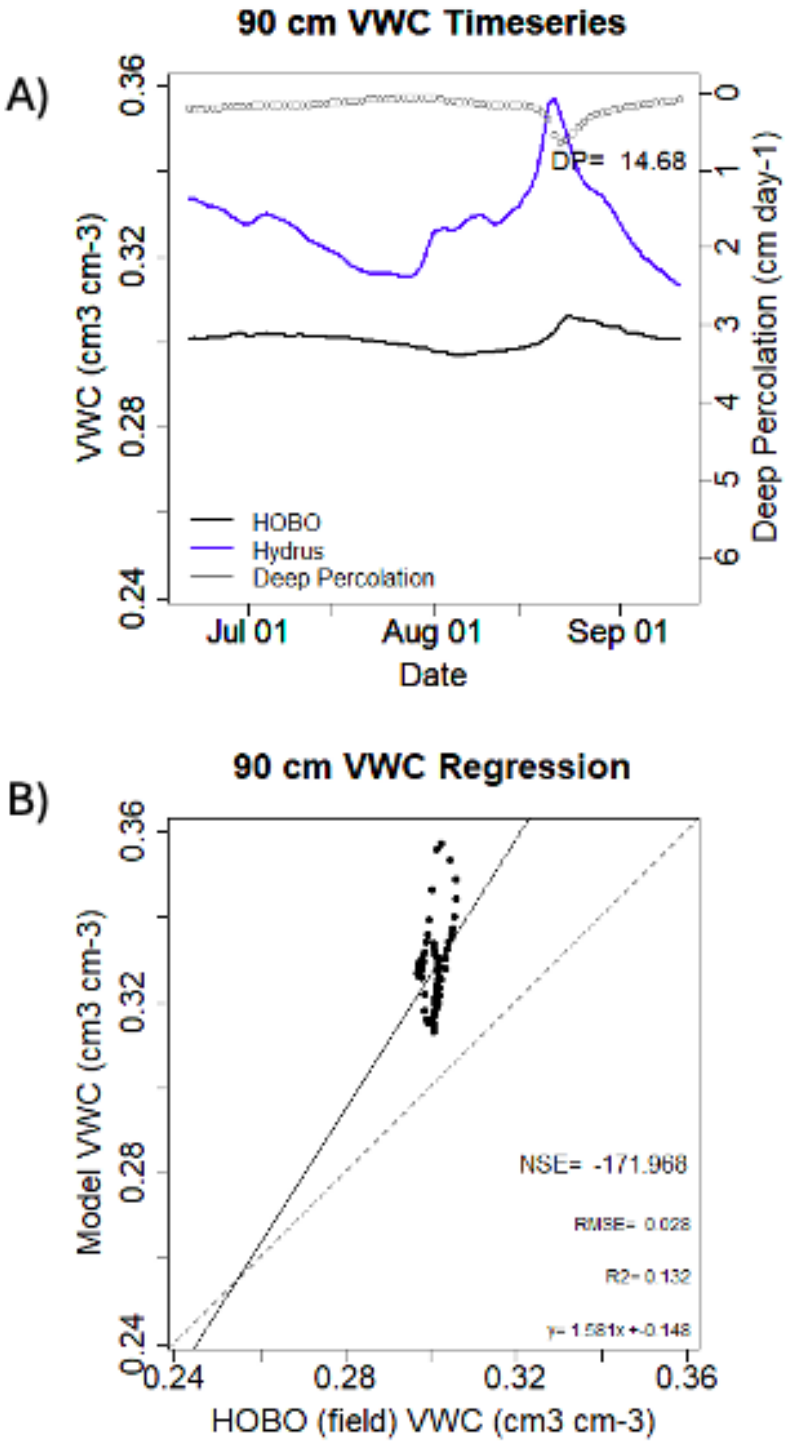
Chp 5 - Figure 11: 2024 Early and Late Season Soil Samples. A) Pre-fertilizer and harvest nitrate inventories for Field T24. B) Early season (post fertilizer) and harvest nitrate inventories for Field T24.



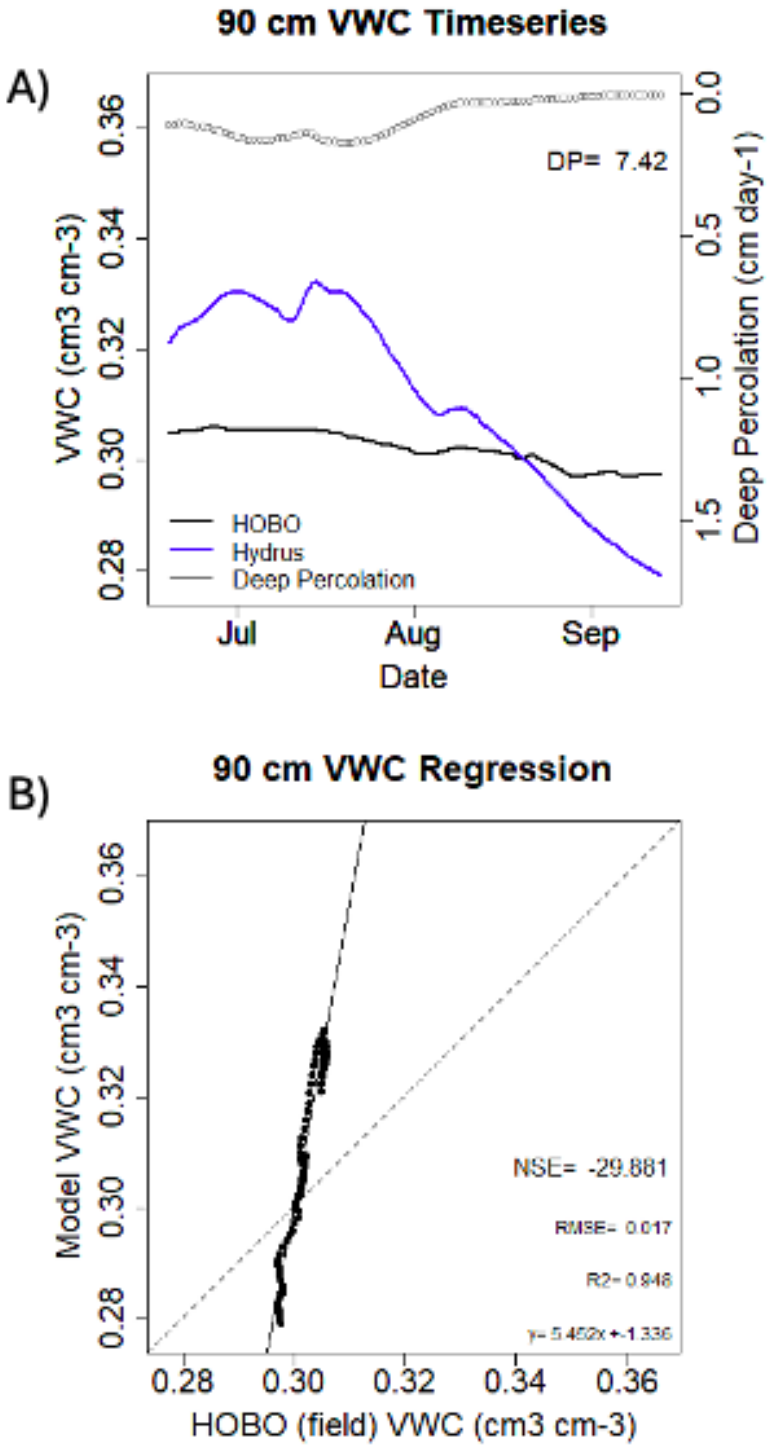
Chp 5 - Figure 12: B23 Model Calibrations. Model calibrations for 90 cm VWC data at B23 A) with two depths, bulk density, and percentages of sand, silt, and clay; B) with one depth bulk density, and percentages of sand, silt, and clay; C) Percentages of sand, silt, and clay only. Blue lines in time series are model predictions, black lines are field HOBO data, and gray lines along the tops of plots are deep percolation estimates.



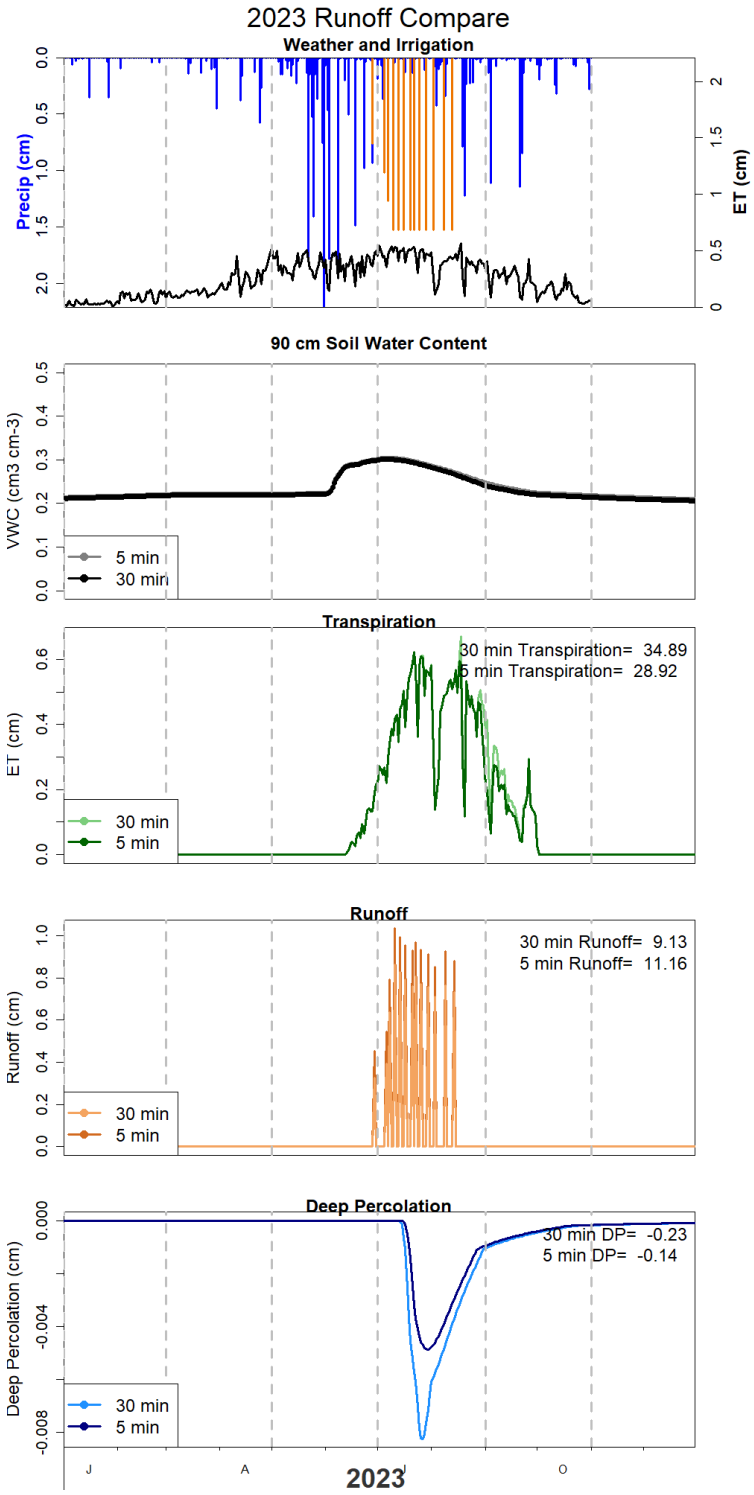
Chp 5 - Figure 13: B24 Model Calibration and Deep Percolation. Best model fit for Field B24 90 cm VWC data with A) Time series comparison of model (blue) and field (black) VWC data and predicted deep percolation (gray circles) and B) Regression between field and modeled data.



Chp 5 - Figure 14: T23 Model Calibration and Deep Percolation. Best model fit for Field T23 90 cm VWC data with A) Time series comparison of model (blue) and field (black) VWC data and predicted deep percolation (gray circles) and B) Regression between field and modeled data.



Chp 5 - Figure 15: T24 Model Calibration and Deep Percolation. Best model fit for Field T24 with A) Time series comparison of model (blue) and field (black) VWC data and predicted deep percolation (gray circles) and B) Regression between field and modeled data.



Chp 5 - Figure 16: B23 Runoff Assessment. A) Weather and irrigation for Field B23. B) Hydrus predicted 90 cm soil VWC. C) Hydrus predicted transpiration. D) Hydrus predicted runoff. E) Hydrus predicted deep percolation. All comparing 5- and 30-minute irrigation rates.

Literature Cited

Basu, N. B., Van Meter, K. J., Byrnes, D. K., Van Cappellen, P., Brouwer, R., Jacobsen, B. H., Jarsjö, J., Rudolph, D. L., Cunha, M. C., Nelson, N., Bhattacharya, R., Destouni, G., & Olsen, S. B. (2022). Managing nitrogen legacies to accelerate water quality improvement. *Nature Geoscience*, *15*(2), 97–105. https://doi.org/10.1038/s41561-021-00889-9

Follett, R. F., & and Delgado, J. A. (2002). Nitrogen fate and transport in agricultural systems. *Journal of Soil and Water Conservation*, *57*(6), 402–408. https://doi.org/10.1080/00224561.2002.12457472

John, A. A., Jones, C. A., Ewing, S. A., Sigler, W. A., Bekkerman, A., & Miller, P. R. (2017). Fallow replacement and alternative nitrogen management for reducing nitrate leaching in a semiarid region. *Nutrient Cycling in Agroecosystems*, *108*(3), 279–296. https://doi.org/10.1007/s10705-017-9855-9

Peralta, J. M., & Stockle, C. O. (2002). Dynamics of nitrate leaching under irrigated potato rotation in Washington State: A long-term simulation study. *Agriculture, Ecosystems & Environment*, *88*(1), 23–34. https://doi.org/10.1016/S0167-8809(01)00157-8

Pericherla, S., Karnena, M. K., & Vara, S. (2020). *A Review on Impacts of Agricultural Runoff on Freshwater Resources*.

Robinson, M., W. A. Sigler (2025). Irrigation Management and Soils as Controls on Deep Percolation and Nitrate Leaching in Agricultural Systems: Thesis Data and Code, HydroShare, https://doi.org/10.4211/hs.2d6042efdc7944288ce486ae9a58da9e

Souchere, V., King, D., Daroussin, J., Papy, F., & Capillon, A. (1998). Effects of tillage on runoff directions: Consequences on runoff contributing area within agricultural catchments. *Journal of Hydrology*, *206*(3), 256–267. https://doi.org/10.1016/S0022-1694(98)00103-6

Weitzman, J. N., Brooks, J. R., Compton, J. E., Faulkner, B. R., Peachey, R. E., Rugh, W. D., Coulombe, R. A., Hatteberg, B., & Hutchins, S. R. (2024). Vadose zone flushing of fertilizer tracked by isotopes of water and nitrate. *Vadose Zone Journal*, *n/a*(n/a), e20324. https://doi.org/10.1002/vzj2.20324

Xia, Y., Zhang, M., Tsang, D. C. W., Geng, N., Lu, D., Zhu, L., Igalavithana, A. D., Dissanayake, P. D., Rinklebe, J., Yang, X., & Ok, Y. S. (2020). Recent advances in control technologies for non-point source pollution with nitrogen and phosphorous from agricultural runoff: Current practices and future prospects. *Applied Biological Chemistry*, *63*(1), 8. https://doi.org/10.1186/s13765-020-0493-6

Xin, J., Liu, Y., Chen, F., Duan, Y., Wei, G., Zheng, X., & Li, M. (2019). The missing nitrogen pieces: A critical review on the distribution, transformation, and budget of nitrogen in the vadose zone-groundwater system. *Water Research*, *165*, 114977. https://doi.org/10.1016/j.watres.2019.114977

CHAPTER SIX

CONCLUSION

In this thesis, I assessed the risk of deep percolation and nitrate leaching across varied Montana irrigated agricultural systems. Across these study systems, risk of deep percolation and nitrate leaching was found to be highest for structured clay loam soils. Soil texture emerged as a clear control on the potential for percolation. Other important drivers of soil water responsiveness, including soil structure and antecedent water content, were identified as well. In the higher leaching risk clay loam systems, temporal variability in both soil structure development and nitrate concentrations were found to contribute to seasonal patterns in deep percolation and nitrate leaching risk. The development of desiccation cracks following irrigation cycles resulted in increased capacity for infiltration and greater risk of deep percolation during the later growing season. In instances where nitrate concentrations are high for a short period following a single fertilizer application, the time over which irrigation management is most critical for reducing nitrate leaching is limited, and peak periods of deep percolation and nitrate losses are offset. Management strategies that apply fertilizers with the intent of maintaining high nitrate concentrations throughout the growing season (such as for meeting wheat protein goals), may expand periods of high nitrate leaching risk. In contrast, on silt loam soils cultivated for potatoes, growing season percolation is limited, leaching concerns are low, and management to prevent nutrient losses via runoff may be most important. One exception to the observation on generally low leaching risk on Gallatin silt soils is the possibility of overwinter leaching

associated with fall applied nitrogen. An accumulation of nitrate at depths that are outside of zones of efficient root extraction creates a possibility of a gradual leaching process to contrast with the faster flushing of nitrate in Fairfield clay loams.

Working with cooperating producers made this research possible. Maintaining equipment and collecting data on actively managed fields required working in the same conditions that cooperators make their decisions in. This approach did result in limitations for research, including reduced periods when data collection was possible and a lack of control over all decisions made, including on irrigation and fertilizer applications. While this variability in field management did to some extent limit data replication and confidence in findings, it allowed for observations across management styles that piqued my and our cooperators curiosity and have motivated continued work. Further exploration into deep soil nitrate under spring and fall fertilized fields, efforts to understand drivers of limited infiltration on silt loam fields, and irrigation experiments to manage against deep percolation on cracked clay loam soils are all ongoing projects catalyzed by intriguing and/or unexpected patterns in data. Working in diverse settings and with cooperators who have different management approaches but share the goal of managing resources efficiently has allowed for these explorations. Work with cooperators also provided insights into the myriad management decisions made by irrigators and allows for context on how scientific findings fit into landscape management. Recognizing that most optimal methods for irrigating may be challenged by limitations on water rights or water delivery and constrained by the capabilities of pivots and other farm management activities provide insights into the complexity of irrigation decision making and the obstacles that must be considered when striving for improved water use efficiency. This is important to consider for Extension goals on

supporting producers in decision making that is feasible to implement. Determining methods that strike a balance between providing the most beneficial information on field conditions while retaining flexibility for irrigation management may be most practical and approachable for producer adoption. Helping producers interpret data from soil water sensors to understand how irrigation causes responses at different depths is one approach that may provide this flexibility in management while also improving awareness of potential for deep percolation.

This work does suggest that irrigation management based on soil texture alone may not be most appropriate in meeting water and nitrogen use efficiency goals. Soil macropores and aggregated structure observed on clay loam soils resulted in increased water percolation and higher magnitude responses in deep soil than were observed on other soils with lower texture-based water holding capacities. Conversely, low infiltration rates on silt loams perhaps reflecting impacts of soil disturbance from potato cultivation suggest that soil water percolation may be lower than rates expected based on texture in some systems. Recognizing that soil structure and agricultural management practices are additional controls beyond texture that influence soil water responses to irrigation has emerged as an important finding from this work. In meeting goals for improved water resource management, preserved water quality, and agricultural sustainability for farmers, understanding both the drivers of deep percolation and nitrate leaching as well as the on-farm applicability of information is key. I hope that work presented in this thesis is a step towards that improved sustainability.

REFERENCES CITED

Andales, A., Chavez, J., & Bauder, T. (2015). *Irrigation Scheduling: The Water Balance Approach- Fact Sheet 4.707*. Colorado State University Extension. https://extension.colostate.edu/topic-areas/agriculture/irrigation-scheduling-the-water-balance-approach-4-707/

Abatzoglou, J. T. (2013). Development of gridded surface meteorological data for ecological applications and modelling. *International Journal of Climatology*, *33*(1), 121–131. https://doi.org/10.1002/joc.3413

Allen, R., Pereira, L. S., Raes, D., & Smith, M. (2006). *FAO Irrigation and Drainage Paper No. 56*.

Arora, B., Mohanty, B. P., & McGuire, J. T. (2012). Uncertainty in dual permeability model parameters for structured soils. *Water Resources Research*, *48*(1). https://doi.org/10.1029/2011WR010500

Basu, N. B., Van Meter, K. J., Byrnes, D. K., Van Cappellen, P., Brouwer, R., Jacobsen, B. H., Jarsjö, J., Rudolph, D. L., Cunha, M. C., Nelson, N., Bhattacharya, R., Destouni, G., & Olsen, S. B. (2022). Managing nitrogen legacies to accelerate water quality improvement. *Nature Geoscience*, *15*(2), 97–105. https://doi.org/10.1038/s41561-021-00889-9

Berthold, T. A., Ajaz, A., Olsovsky, T., & Kathuria, D. (2021). Identifying barriers to adoption of irrigation scheduling tools in Rio Grande Basin. *Smart Agricultural Technology*, *1*, 100016. https://doi.org/10.1016/j.atech.2021.100016

Beven, K., & Germann, P. (1982). Macropores and water flow in soils. *Water Resources Research*, *18*(5), 1311–1325. https://doi.org/10.1029/WR018i005p01311

Beven, K., & Germann, P. (2013). Macropores and water flow in soils revisited. *Water Resources Research*, *49*(6), 3071–3092. https://doi.org/10.1002/wrcr.20156

Beyene, A., Cornelis, W., Verhoest, N. E. C., Tilahun, S., Alamirew, T., Adgo, E., De Pue, J., & Nyssen, J. (2018). Estimating the actual evapotranspiration and deep percolation in

irrigated soils of a tropical floodplain, northwest Ethiopia. *Agricultural Water Management*, *202*, 42–56. https://doi.org/10.1016/j.agwat.2018.01.022

Blanchy, G., Bragato, G., Di Bene, C., Jarvis, N., Larsbo, M., Meurer, K., & Garré, S. (2023). Soil and crop management practices and the water regulation functions of soils: A qualitative synthesis of meta-analyses relevant to European agriculture. *SOIL*, *9*(1), 1–20. https://doi.org/10.5194/soil-9-1-2023

Bordoloi, S., Ni, J., & Ng, C. W. W. (2020). Soil desiccation cracking and its characterization in vegetated soil: A perspective review. *Science of The Total Environment*, *729*, 138760. https://doi.org/10.1016/j.scitotenv.2020.138760

Bormann, H., & Klaassen, K. (2008). Seasonal and land use dependent variability of soil hydraulic and soil hydrological properties of two Northern German soils. *Geoderma*, *145*(3), 295–302. https://doi.org/10.1016/j.geoderma.2008.03.017

Bos, M. G., Kselik, R. A. L., Allen, R. G., & Molden, D. J. (Eds.). (2009). Effective Precipitation. In *Water Requirements for Irrigation and the Environment* (pp. 81–101). Springer Netherlands. https://doi.org/10.1007/978-1-4020-8948-0_3

Budhathoki, S., Lamba, J., Srivastava, P., Malhotra, K., Way, T. R., & Katuwal, S. (2022). Temporal and spatial variability in 3D soil macropore characteristics determined using X-ray computed tomography. *Journal of Soils and Sediments*, *22*(4), 1263–1277. https://doi.org/10.1007/s11368-022-03150-x

Coleman, T., Boyd, K., Thatcher, T., & Sain, R. (2022, June). *Muddy Creek Master Plan*. https://static1.squarespace.com/static/6014bb1a9820e37481af89b6/t/62bb8583163e3f2f643eed6e/1656456599529/Muddy+Creek+Master+Plan+FINAL++06+28+2022.pdf

Coppola, A., Comegna, A., Dragonetti, G., Gerke, H. H., & Basile, A. (2015). Simulated Preferential Water Flow and Solute Transport in Shrinking Soils. *Vadose Zone Journal*, *14*(9), vzj2015.02.0021. https://doi.org/10.2136/vzj2015.02.0021

Dai, L., Fu, R., Guo, X., Du, Y., Zhang, F., & Cao, G. (2022). Soil Moisture Variations in Response to Precipitation Across Different Vegetation Types on the Northeastern

Qinghai-Tibet Plateau. *Frontiers in Plant Science*, *13*. https://doi.org/10.3389/fpls.2022.854152

Della Vecchia, G., Dieudonné, A.-C., Jommi, C., & Charlier, R. (2015). Accounting for evolving pore size distribution in water retention models for compacted clays: EVOLVING PORE SIZE DISTRIBUTION IN WATER RETENTION MODELLING. *International Journal for Numerical and Analytical Methods in Geomechanics*, *39*(7), 702–723. https://doi.org/10.1002/nag.2326

Detty, J. M., & McGuire, K. J. (2010). Topographic controls on shallow groundwater dynamics: Implications of hydrologic connectivity between hillslopes and riparian zones in a till mantled catchment. *Hydrological Processes*, *24*(16), 2222–2236. https://doi.org/10.1002/hyp.7656

Du, E., Terrer, C., Pellegrini, A. F. A., Ahlström, A., van Lissa, C. J., Zhao, X., Xia, N., Wu, X., & Jackson, R. B. (2020). Global patterns of terrestrial nitrogen and phosphorus limitation. *Nature Geoscience*, *13*(3), Article 3. https://doi.org/10.1038/s41561-019-0530-4

Dzurella, K. N., Pettygrove ,G.S., Fryjoff-Hung ,A., Hollander ,A., & and Harter, T. (2015). Potential to assess nitrate leaching vulnerability of irrigated cropland. *Journal of Soil and Water Conservation*, *70*(1), 63–72. https://doi.org/10.2489/jswc.70.1.63

Erisman, J. W., Sutton, M. A., Galloway, J., Klimont, Z., & Winiwarter, W. (2008). How a century of ammonia synthesis changed the world. *Nature Geoscience*, *1*(10), 636–639. https://doi.org/10.1038/ngeo325

FAO. (2021). AQUASTAT- FAO's Global Information System on Water and Agriculture. Food and Agriculture Organization of the United Nations.

Fishkis, O., Noell, U., Diehl, L., Jaquemotte, J., Lamparter, A., Stange, C. F., Burke, V., Koeniger, P., & Stadler, S. (2020). Multitracer irrigation experiments for assessing the relevance of preferential flow for non-sorbing solute transport in agricultural soil. *Geoderma*, *371*, 114386. https://doi.org/10.1016/j.geoderma.2020.114386

Follett, R. F., & and Delgado, J. A. (2002). Nitrogen fate and transport in agricultural systems. *Journal of Soil and Water Conservation*, *57*(6), 402–408. https://doi.org/10.1080/00224561.2002.12457472

Gee, G. W., & Bauder, J. W. (1986). Particle-size Analysis. In *Methods of Soil Analysis* (pp. 383–411). John Wiley & Sons, Ltd. https://doi.org/10.2136/sssabookser5.1.2ed.c15

Genius, M., Koundouri, P., Nauges, C., & Tzouvelekas, V. (2014). Information Transmission in Irrigation Technology Adoption and Diffusion: Social Learning, Extension Services, and Spatial Effects. *American Journal of Agricultural Economics*, *96*(1), 328–344. https://doi.org/10.1093/ajae/aat054

Gerke, H. H., & van Genuchten, M. T. (1993). A dual-porosity model for simulating the preferential movement of water and solutes in structured porous media. *Water Resources Research*, *29*(2), 305–319. https://doi.org/10.1029/92WR02339

Graham, S. L., Srinivasan, M. s., Faulkner, N., & Carrick, S. (2018). Soil Hydraulic Modeling Outcomes with Four Parameterization Methods: Comparing Soil Description and Inverse Estimation Approaches. *Vadose Zone Journal*, *17*(1), 170002. https://doi.org/10.2136/vzj2017.01.0002

Greve, A., Andersen, M. S., & Acworth, R. I. (2010). Investigations of soil cracking and preferential flow in a weighing lysimeter filled with cracking clay soil. *Journal of Hydrology*, *393*(1), 105–113. https://doi.org/10.1016/j.jhydrol.2010.03.007

Greve, A. K., Acworth, R. I., & Kelly, B. F. J. (2011). 3D Cross-hole resistivity tomography to monitor water percolation during irrigation on cracking soil. *Soil Research*, *49*(8), 661–669. https://doi.org/10.1071/SR11270

Gu, Z., Qi, Z., Burghate, R., Yuan, S., Jiao, X., & Xu, J. (2020). Irrigation Scheduling Approaches and Applications: A Review. *Journal of Irrigation and Drainage Engineering*, *146*(6), 04020007. https://doi.org/10.1061/(ASCE)IR.1943-4774.0001464

Guo, D., Olesen, J. E., Manevski, K., & Ma, X. (2021). Optimizing irrigation schedule in a large agricultural region under different hydrologic scenarios. *Agricultural Water Management*, *245*, 106575. https://doi.org/10.1016/j.agwat.2020.106575

Guo, L., & Lin, H. (2018). Addressing Two Bottlenecks to Advance the Understanding of Preferential Flow in Soils. In *Advances in Agronomy* (Vol. 147, pp. 61–117). Elsevier. https://doi.org/10.1016/bs.agron.2017.10.002

Haile, G. G., Tang, Q., Reda, K. W., Baniya, B., He, L., Wang, Y., & Gebrechorkos, S. H. (2024). Projected impacts of climate change on global irrigation water withdrawals. *Agricultural Water Management*, *305*, 109144. https://doi.org/10.1016/j.agwat.2024.109144

Haws, N. W., Rao, P. S. C., Simunek, J., & Poyer, I. C. (2005). Single-porosity and dual-porosity modeling of water flow and solute transport in subsurface-drained fields using effective field-scale parameters. *Journal of Hydrology*, *313*(3), 257–273. https://doi.org/10.1016/j.jhydrol.2005.03.035

Heinen, M., Mulder, M., van Dam, J., Bartholomeus, R., de Jong van Lier, Q., de Wit, J., de Wit, A., & Hack - ten Broeke, M. (2024). SWAP 50 years: Advances in modelling soil-water-atmosphere-plant interactions. *Agricultural Water Management*, *298*, 108883. https://doi.org/10.1016/j.agwat.2024.108883

Hellner, Q., Koestel, J., Ulén, B., & Larsbo, M. (2018). Effects of tillage and liming on macropore networks derived from X-ray tomography images of a silty clay soil. *Soil Use and Management*, *34*(2), 197–205. https://doi.org/10.1111/sum.12418

Isch, A., Montenach, D., Hammel, F., Ackerer, P., & Coquet, Y. (2019). A Comparative Study of Water and Bromide Transport in a Bare Loam Soil Using Lysimeters and Field Plots. *Water*, *11*(6), Article 6. https://doi.org/10.3390/w11061199

Jarvis, N. J. (2007). A review of non-equilibrium water flow and solute transport in soil macropores: Principles, controlling factors and consequences for water quality. *European Journal of Soil Science*, *58*(3), 523–546. https://doi.org/10.1111/j.1365-2389.2007.00915.x

Jarvis, N. J., Moeys, J., Hollis, J. M., Reichenberger, S., Lindahl, A. M. L., & Dubus, I. G. (2009). A Conceptual Model of Soil Susceptibility to Macropore Flow. *Vadose Zone Journal*, *8*(4), 902–910. https://doi.org/10.2136/vzj2008.0137

Jarvis, N., Koestel, J., & Larsbo, M. (2016). Understanding Preferential Flow in the Vadose Zone: Recent Advances and Future Prospects. *Vadose Zone Journal*, *15*(12), vzj2016.09.0075. https://doi.org/10.2136/vzj2016.09.0075

Jiang, S., Pang, L., Buchan, G. D., Šimůnek, J., Noonan, M. J., & Close, M. E. (2010). Modeling water flow and bacterial transport in undisturbed lysimeters under irrigations of dairy shed effluent and water using HYDRUS-1D. *Water Research*, *44*(4), 1050–1061. https://doi.org/10.1016/j.watres.2009.08.039

John, A. A., Jones, C. A., Ewing, S. A., Sigler, W. A., Bekkerman, A., & Miller, P. R. (2017). Fallow replacement and alternative nitrogen management for reducing nitrate leaching in a semiarid region. *Nutrient Cycling in Agroecosystems*, *108*(3), 279–296. https://doi.org/10.1007/s10705-017-9855-9

Jones, C., & Olson-Rutz, K. (2018). *Minimizing Nitrate Leaching From Cropland*. Montana State University Extension. https://store.msuextension.org/publications/AgandNaturalResources/EB0226.pdf

Kendy, E., & Bredehoeft, J. D. (2006). Transient effects of groundwater pumping and surface-water-irrigation returns on streamflow. *Water Resources Research*, *42*(8). https://doi.org/10.1029/2005WR004792

Ketchum, D., Jencso, K., Maneta, M. P., Melton, F., Jones, M. O., & Huntington, J. (2020). IrrMapper: A Machine Learning Approach for High Resolution Mapping of Irrigated Agriculture Across the Western U.S. *Remote Sensing*, *12*(14), Article 14. https://doi.org/10.3390/rs12142328

Ki, S. J., Ray, C., & Hantush, M. M. (2015). Applying a statewide geospatial leaching tool for assessing soil vulnerability ratings for agrochemicals across the contiguous United States. *Water Research*, *77*, 107–118. https://doi.org/10.1016/j.watres.2015.03.009

Kim, S. (2009). Characterization of soil moisture responses on a hillslope to sequential rainfall events during late autumn and spring. *Water Resources Research*, *45*(9). https://doi.org/10.1029/2008WR007239

Kocian, L., & Mohanty, B. P. (2024). Characterizing large-scale preferential flow across Continental United States. *Vadose Zone Journal*, *23*(4), e20316. https://doi.org/10.1002/vzj2.20316

Koestel, J., & Jorda, H. (2014). What determines the strength of preferential transport in undisturbed soil under steady-state flow? *Geoderma*, *217–218*, 144–160. https://doi.org/10.1016/j.geoderma.2013.11.009

Köhne, J. M., Mohanty, B. P., & Šimůnek, J. (2006). Inverse Dual-Permeability Modeling of Preferential Water Flow in a Soil Column and Implications for Field-Scale Solute Transport. *Vadose Zone Journal*, *5*(1), 59–76. https://doi.org/10.2136/vzj2005.0008

Kokulan, V., Macrae, M. L., Ali, G. A., Lobb, D. A., Morison, M., & Brooks, B. C. (2021). Temporal variability in water and nutrient movement through vertisols into agricultural tile drains in the northern Great Plains. *Journal of Soil and Water Conservation*, *76*(4), 317–328. https://doi.org/10.2489/jswc.2021.00099

Lal, R. (2020). Soil organic matter and water retention. *Agronomy Journal*, *112*(5), 3265–3277. https://doi.org/10.1002/agj2.20282

Levidow, L., Zaccaria, D., Maia, R., Vivas, E., Todorovic, M., & Scardigno, A. (2014). Improving water-efficient irrigation: Prospects and difficulties of innovative practices. *Agricultural Water Management*, *146*, 84–94. https://doi.org/10.1016/j.agwat.2014.07.012

Lin, H., & Zhou, X. (2008). Evidence of subsurface preferential flow using soil hydrologic monitoring in the Shale Hills catchment. *European Journal of Soil Science*, *59*(1), 34–49. https://doi.org/10.1111/j.1365-2389.2007.00988.x

Ljutic, A., Moore, J., Ali, G., Van Eerd, L., Macrae, M. L., & Wagner-Riddle, C. (2024). Variable soil moisture responses to rainfall events in fields under different management practices. *Hydrological Processes*, *38*(7), e15242. https://doi.org/10.1002/hyp.15242

Lobell, D. B., Schlenker, W., & Costa-Roberts, J. (2011). Climate Trends and Global Crop Production Since 1980. *Science*, *333*(6042), 616–620. https://doi.org/10.1126/science.1204531

Luo, Y., Zhang, J., Zhou, Z., Aguilar-Lopez, J. P., Greco, R., & Bogaard, T. (2023). Effects of dynamic changes of desiccation cracks on preferential flow: Experimental investigation and numerical modeling. *Hydrology and Earth System Sciences*, *27*(3), 783–808. https://doi.org/10.5194/hess-27-783-2023

Mancosu, N., Snyder, R. L., Kyriakakis, G., & Spano, D. (2015). Water Scarcity and Future Challenges for Food Production. *Water*, *7*(3), Article 3. https://doi.org/10.3390/w7030975

Mathias, S. A., Sorensen, J. P. R., & Butler, A. P. (2017). Soil moisture data as a constraint for groundwater recharge estimation. *Journal of Hydrology*, *552*, 258–266. https://doi.org/10.1016/j.jhydrol.2017.06.040

Mehta, P., Siebert, S., Kummu, M., Deng, Q., Ali, T., Marston, L., Xie, W., & Davis, K. F. (2024). Half of twenty-first century global irrigation expansion has been in water-stressed regions. *Nature Water*, *2*(3), 254–261. https://doi.org/10.1038/s44221-024-00206-9

Meißl, G., Zieher, T., & Geitner, C. (2020). Runoff response to rainfall events considering initial soil moisture – Analysis of 9-year records in a small Alpine catchment (Brixenbach valley, Tyrol, Austria). *Journal of Hydrology: Regional Studies*, *30*, 100711. https://doi.org/10.1016/j.ejrh.2020.100711

Melvin, S., & Yonts, C. (2009). *Irrigation Scheduling: Checkbook Method*. University of Nebraska-Lincoln Extension. https://extensionpubs.unl.edu/publication/ec709/2009/pdf/view/ec709-2009.pdf

Mittelbach, H., Casini, F., Lehner, I., Teuling, A. J., & Seneviratne, S. I. (2011). Soil moisture monitoring for climate research: Evaluation of a low-cost sensor in the framework of the Swiss Soil Moisture Experiment (SwissSMEX) campaign. *Journal of Geophysical Research: Atmospheres*, *116*(D5). https://doi.org/10.1029/2010JD014907

Montana Department of Agriculture. (2015). *Groundwater Monitoring for Pesticides and Nitrate in Greenfield Bench, Montana; Summary of Findings 1992-2015*. https://agr.mt.gov/_docs/groundwater-docs/GWR_GreenfieldBench1992-2015Final.pdf

Montana Department of Natural Resources and Conservation. (2015). *State Water Plan Regional Basin Plans*. https://dnrc.mt.gov/Water-Resources/Water-Planning-Implementation-and-Communications/State-Water-Plan-Regional-Basin-Plans/

Mueller, N. D., Gerber, J. S., Johnston, M., Ray, D. K., Ramankutty, N., & Foley, J. A. (2012). Closing yield gaps through nutrient and water management. *Nature*, *490*(7419), 254–257. https://doi.org/10.1038/nature11420

Muratoglu, A., Bilgen, G. K., Angin, I., & Kodal, S. (2023). Performance analyses of effective rainfall estimation methods for accurate quantification of agricultural water footprint. *Water Research*, *238*, 120011. https://doi.org/10.1016/j.watres.2023.120011

Nash, J. E., & Sutcliffe, J. V. (1970). River flow forecasting through conceptual models part I — A discussion of principles. *Journal of Hydrology*, *10*(3), 282–290. https://doi.org/10.1016/0022-1694(70)90255-6

Nazarieh, F., Ansari, H., Ziaei, A. N., Izady, A., Davari, K., & Brunner, P. (2018). Spatial and temporal dynamics of deep percolation, lag time and recharge in an irrigated semi-arid region. *Hydrogeology Journal*, *26*(7), 2507–2520. https://doi.org/10.1007/s10040-018-1789-z

Nimmo, J. R. (2021). The processes of preferential flow in the unsaturated zone. *Soil Science Society of America Journal*, *85*(1), 1–27. https://doi.org/10.1002/saj2.20143

Nippgen, F., McGlynn, B. L., Emanuel, R. E., & Vose, J. M. (2016). Watershed memory at the Coweeta Hydrologic Laboratory: The effect of past precipitation and storage on hydrologic response. *Water Resources Research*, *52*(3), 1673–1695. https://doi.org/10.1002/2015WR018196

Ochoa, C. G., A. G. Fernald, S. J. Guldan, & M. K. Shukla. (2007). Deep Percolation and its Effects on Shallow Groundwater Level Rise Following Flood Irrigation. *Transactions of the ASABE*, *50*(1), 73–81. https://doi.org/10.13031/2013.22413

Osman, M., Zaitchik, B., Otkin, J., & Anderson, M. (2024). A global flash drought inventory based on soil moisture volatility. *Scientific Data*, *11*(1), 965. https://doi.org/10.1038/s41597-024-03809-9

Pachepsky, Y., & Park, Y. (2015). Saturated Hydraulic Conductivity of US Soils Grouped According to Textural Class and Bulk Density. *Soil Science Society of America Journal*, *79*(4), 1094–1100. https://doi.org/10.2136/sssaj2015.02.0067

Penna, D., Tromp-van Meerveld, H. J., Gobbi, A., Borga, M., & Dalla Fontana, G. (2011). The influence of soil moisture on threshold runoff generation processes in an alpine headwater catchment. *Hydrology and Earth System Sciences*, *15*(3), 689–702. https://doi.org/10.5194/hess-15-689-2011

Peralta, J. M., & Stockle, C. O. (2002). Dynamics of nitrate leaching under irrigated potato rotation in Washington State: A long-term simulation study. *Agriculture, Ecosystems & Environment*, *88*(1), 23–34. https://doi.org/10.1016/S0167-8809(01)00157-8

Pereira, L. S. (2017). Water, Agriculture and Food: Challenges and Issues. *Water Resources Management*, *31*(10), 2985–2999. https://doi.org/10.1007/s11269-017-1664-z

Pericherla, S., Karnena, M. K., & Vara, S. (2020). *A Review on Impacts of Agricultural Runoff on Freshwater Resources*.

Puckett, L. J., Tesoriero, A. J., & Dubrovsky, N. M. (2011). Nitrogen Contamination of Surficial Aquifers—A Growing Legacy. *Environmental Science & Technology*, *45*(3), 839–844. https://doi.org/10.1021/es1038358

Quemada, M., Baranski, M., Nobel-de Lange, M. N. J., Vallejo, A., & Cooper, J. M. (2013). Meta-analysis of strategies to control nitrate leaching in irrigated agricultural systems and their effects on crop yield. *Agriculture, Ecosystems & Environment*, *174*, 1–10. https://doi.org/10.1016/j.agee.2013.04.018

Reading, L. P., Bajracharya, K., & Wang, J. (2019). Simulating deep drainage and nitrate leaching on a regional scale: Implications for groundwater management in an intensively irrigated area. *Irrigation Science*, *37*(5), 561–581. https://doi.org/10.1007/s00271-019-00636-4

Robinson, M., W. A. Sigler (2025). Irrigation Management and Soils as Controls on Deep Percolation and Nitrate Leaching in Agricultural Systems: Thesis Data and Code, HydroShare, https://doi.org/10.4211/hs.2d6042efdc7944288ce486ae9a58da9e

Rieffenberger, V., Kelley, P., Vichorek, D., Lien, B., Ames, G., & Beck, J. (1989). *The Montana Irrigator's Pocket Guide*. Energy Division, Montana Department of Natural Resources and Conservation.

Roulier, S., & Jarvis, N. (2003). Analysis of Inverse Procedures for Estimating Parameters Controlling Macropore Flow and Solute Transport in the Dual-Permeability Model MACRO. *Vadose Zone Journal*, *2*(3), 349–357. https://doi.org/10.2136/vzj2003.3490

Ruehlmann, J., & Körschens, M. (2009). Calculating the Effect of Soil Organic Matter Concentration on Soil Bulk Density. *Soil Science Society of America Journal*, *73*(3), 876–885. https://doi.org/10.2136/sssaj2007.0149

Saxton, K. E., Rawls, W. J., Romberger, J. S., & Papendick, R. I. (1986). Estimating Generalized Soil-water Characteristics from Texture. *Soil Science Society of America Journal*, *50*(4), 1031–1036. https://doi.org/10.2136/sssaj1986.03615995005000040039x

Scaife, C. I., Singh, N. K., Emanuel, R. E., Miniat, C. F., & Band, L. E. (2020). Non-linear quickflow response as indicators of runoff generation mechanisms. *Hydrological Processes*, *34*(13), 2949–2964. https://doi.org/10.1002/hyp.13780

Schaap, M. G., Leij, F. J., & van Genuchten, M. Th. (2001). rosetta: A computer program for estimating soil hydraulic parameters with hierarchical pedotransfer functions. *Journal of Hydrology*, *251*(3), 163–176. https://doi.org/10.1016/S0022-1694(01)00466-8

Sharma, V. (2019). *Basics of Irrigation Scheduling*. University of Minnesota Extension. extension.umn.edu/irrigation/basics-irrigation-scheduling#sources-1846810

Shipitalo, M. J., Nuutinen, V., & Butt, K. R. (2004). Interaction of earthworm burrows and cracks in a clayey, subsurface-drained, soil. *Applied Soil Ecology*, *26*, 209–217. https://doi.org/10.1016/j.apsoil.2004.01.004

Sigler, W. A. (2011, January). *Upper Muddy Creek Water Quality Investigation 2010*.

Sigler, W. A. (2019, December 12). *Sun River Watershed Group Volunteer Monitoring Program Nutrient Data Summary*. https://static1.squarespace.com/static/6014bb1a9820e37481af89b6/t/619bcb0b5836c344bd16fd0c/1637600011621/2019+12+09+SunNutrientTrendReportFinal.pdf

Sigler, W. A., Ewing, S. A., Jones, C. A., Payn, R. A., Brookshire, E. N. J., Klassen, J. K., Jackson-Smith, D., & Weissmann, G. S. (2018). Connections among soil, ground, and surface water chemistries characterize nitrogen loss from an agricultural landscape in the upper Missouri River Basin. *Journal of Hydrology*, *556*, 247–261. https://doi.org/10.1016/j.jhydrol.2017.10.018

Sigler, W. A., Ewing, S. A., Jones, C. A., Payn, R. A., Miller, P., & Maneta, M. (2020a). Water and nitrate loss from dryland agricultural soils is controlled by management, soils, and weather. *Agriculture, Ecosystems & Environment*, *304*, 107158. https://doi.org/10.1016/j.agee.2020.107158

Sigler, W. A., Ewing, S. A., Jones, C. A., Payn, R. A., Miller, P., & Maneta, M. (2020b). Water and nitrate loss from dryland agricultural soils is controlled by management, soils, and weather. *Agriculture, Ecosystems & Environment*, *304*, 107158-. https://doi.org/10.1016/j.agee.2020.107158

Sigler, W. A., Ewing, S. A., Wankel, S. D., Jones, C. A., Leuthold, S., Brookshire, E. N. J., & Payn, R. A. (2022). Isotopic signals in an agricultural watershed suggest denitrification is locally intensive in riparian areas but extensive in upland soils. *Biogeochemistry*, *158*(2), 251–268. https://doi.org/10.1007/s10533-022-00898-9

Sigler, W., Kiekover, N., Roemmich, T., Dougher, F., & Krahn, B. (2024). *Gallatin County Groundwater Nitrate and Water Levels* [Dataset]. HydroShare. https://doi.org/10.4211/hs.7346a1e37bb04090bf8d8c1f5a4e2a4b

Šimůnek, J., Jarvis, N. J., van Genuchten, M. Th., & Gärdenäs, A. (2003). Review and comparison of models for describing non-equilibrium and preferential flow and transport in the vadose zone. *Journal of Hydrology*, *272*(1), 14–35. https://doi.org/10.1016/S0022-1694(02)00252-4

Šimůnek, J., Šejna, M., Saito, H., Sakai, M., & van Genuchten, M. Th. (2013, June). *The HYDRUS-1D Software Package for Simulating the One-Dimensional Movement of Water, Heat, and Multiple Solutes in Variably-Saturated Media: Version 4.17*. Department of Earth Sciences, University of California Riverside. chrome-extension://efaidnbmnnnibpcajpcglclefindmkaj/https://www.pc-progress.com/Downloads/Pgm_hydrus1D/HYDRUS1D-4.17.pdf

Šimůnek, J., & van Genuchten, M. Th. (2008). Modeling Nonequilibrium Flow and Transport Processes Using HYDRUS. *Vadose Zone Journal*, *7*(2), 782–797. https://doi.org/10.2136/vzj2007.0074

Singh, N. K., Emanuel, R. E., McGlynn, B. L., & Miniat, C. F. (2021). Soil Moisture Responses to Rainfall: Implications for Runoff Generation. *Water Resources Research*, *57*(9), e2020WR028827. https://doi.org/10.1029/2020WR028827

Souchere, V., King, D., Daroussin, J., Papy, F., & Capillon, A. (1998). Effects of tillage on runoff directions: Consequences on runoff contributing area within agricultural catchments. *Journal of Hydrology*, *206*(3), 256–267. https://doi.org/10.1016/S0022-1694(98)00103-6

Stets, E. g., Kelly, V. j., & Crawford, C. g. (2015). Regional and Temporal Differences in Nitrate Trends Discerned from Long-Term Water Quality Monitoring Data. *JAWRA Journal of the American Water Resources Association*, *51*(5), 1394–1407. https://doi.org/10.1111/1752-1688.12321

Tymchak, M. P., & Torres, R. (2007). Effects of variable rainfall intensity on the unsaturated zone response of a forested sandy hillslope. *Water Resources Research*, *43*(6). https://doi.org/10.1029/2005WR004584

USDA National Agricultural Statistics Service (NASS), 2024, Cropland Data Layer, Accessed 2025-06-20 at https://nassgeodata.gmu.edu/CropScape.

USDA NASS 2019. 2018 Irrigation Water and Management Survey (United States Department of Agriculture). https://www.nass.usda.gov/Publications/AgCensus/2017/Online_Resources/Farm_and_Ranch_Irrigation_Survey/fris.pdf

van Dijk, M., Morley, T., Rau, M. L., & Saghai, Y. (2021). A meta-analysis of projected global food demand and population at risk of hunger for the period 2010–2050. *Nature Food*, *2*(7), Article 7. https://doi.org/10.1038/s43016-021-00322-9

van Genuchten, M. Th. (1980). A Closed-form Equation for Predicting the Hydraulic Conductivity of Unsaturated Soils. *Soil Science Society of America Journal*, *44*(5), 892–898. https://doi.org/10.2136/sssaj1980.03615995004400050002x

Visconti, F., de Paz, J. M., Martínez, D., & Molina, M. J. (2014). Laboratory and field assessment of the capacitance sensors Decagon 10HS and 5TE for estimating the water content of irrigated soils. *Agricultural Water Management*, *132*, 111–119. https://doi.org/10.1016/j.agwat.2013.10.005

Vuke, S., Colton, R., & Fullerton, D. (2002). *Geologic Map of the Great Falls North 30'x 60' Quadrangle, Central Montana*. Montana Bureau of Mines and Geology. https://www.mbmg.mtech.edu/pdf_100k/greatFallsN-text.pdf

Wagner, S., Cattle, S. R., & Scholten, T. (2007). Soil-aggregate formation as influenced by clay content and organic-matter amendment. *Journal of Plant Nutrition and Soil Science*, *170*(1), 173–180. https://doi.org/10.1002/jpln.200521732

Wang, C., Fu, B., Zhang, L., & Xu, Z. (2019). Soil moisture–plant interactions: An ecohydrological review. *Journal of Soils and Sediments*, *19*(1), 1–9. https://doi.org/10.1007/s11368-018-2167-0

Wang, G. (2005). Agricultural drought in a future climate: Results from 15 global climate models participating in the IPCC 4th assessment. *Climate Dynamics*, *25*(7), 739–753. https://doi.org/10.1007/s00382-005-0057-9

Wang, X., Müller, C., Elliot, J., Mueller, N. D., Ciais, P., Jägermeyr, J., Gerber, J., Dumas, P., Wang, C., Yang, H., Li, L., Deryng, D., Folberth, C., Liu, W., Makowski, D., Olin, S., Pugh, T. A. M., Reddy, A., Schmid, E., … Piao, S. (2021). Global irrigation contribution to wheat and maize yield. *Nature Communications*, *12*(1), 1235. https://doi.org/10.1038/s41467-021-21498-5

Wang, Z., Liu, J., Hamoud, Y. A., Wang, Y., Qiu, R., Agathokleous, E., Hong, C., & Shaghaleh, H. (2022). Natural 15N abundance as an indicator of nitrogen utilization efficiency in rice under alternate wetting and drying irrigation in soils with high clay contents. *Science of The Total Environment*, *838*, 156528. https://doi.org/10.1016/j.scitotenv.2022.156528

Water Quality Planning Bureau, Watershed Managment Section. (2004). *Water Quality Restoration Plan and Total Maximum Daily Loads for the Sun River Planning Area*. Montana Department of Environmental Quality. https://deq.mt.gov/files/Water/WQPB/TMDL/PDF/Sun/M13-TMDL-01a.pdf

Water Quality Planning Bureau, Watershed Managment Section. (2013). *Lower Gallatin Planning Area TMDLs & Framework Water Quality Improvement Plan*. Montana Department of Environmental Quality. https://deq.mt.gov/files/water/wqpb/CWAIC/TMDL/M05-TMDL-02a.pdf

Weihermüller, L., Siemens, J., Deurer, M., Knoblauch, S., Rupp, H., Göttlein, A., & Pütz, T. (2007). In Situ Soil Water Extraction: A Review. *Journal of Environmental Quality*, *36*(6), 1735–1748. https://doi.org/10.2134/jeq2007.0218

Weitzman, J. N., Brooks, J. R., Compton, J. E., Faulkner, B. R., Peachey, R. E., Rugh, W. D., Coulombe, R. A., Hatteberg, B., & Hutchins, S. R. (2024). Vadose zone flushing of fertilizer tracked by isotopes of water and nitrate. *Vadose Zone Journal*, *n/a*(n/a), e20324. https://doi.org/10.1002/vzj2.20324

Wiekenkamp, I., Huisman, J. A., Bogena, H. R., Lin, H. S., & Vereecken, H. (2016). Spatial and temporal occurrence of preferential flow in a forested headwater catchment. *Journal of Hydrology*, *534*, 139–149. https://doi.org/10.1016/j.jhydrol.2015.12.050

Williams, M. R., King, K. W., Ford, W., Buda, A. R., & Kennedy, C. D. (2016). Effect of tillage on macropore flow and phosphorus transport to tile drains. *Water Resources Research*, *52*(4), 2868–2882. https://doi.org/10.1002/2015WR017650

Xia, Y., Zhang, M., Tsang, D. C. W., Geng, N., Lu, D., Zhu, L., Igalavithana, A. D., Dissanayake, P. D., Rinklebe, J., Yang, X., & Ok, Y. S. (2020). Recent advances in control technologies for non-point source pollution with nitrogen and phosphorous from agricultural runoff: Current practices and future prospects. *Applied Biological Chemistry*, *63*(1), 8. https://doi.org/10.1186/s13765-020-0493-6

Xin, J., Liu, Y., Chen, F., Duan, Y., Wei, G., Zheng, X., & Li, M. (2019). The missing nitrogen pieces: A critical review on the distribution, transformation, and budget of nitrogen in the vadose zone-groundwater system. *Water Research*, *165*, 114977. https://doi.org/10.1016/j.watres.2019.114977

Yang, F., Zhang, G.-L., Yang, J.-L., Li, D.-C., Zhao, Y.-G., Liu, F., Yang, R.-M., & Yang, F. (2014). Organic matter controls of soil water retention in an alpine grassland and its significance for hydrological processes. *Journal of Hydrology*, *519*, 3086–3093. https://doi.org/10.1016/j.jhydrol.2014.10.054

Zhang, K., Li, X., Zheng, D., Zhang, L., & Zhu, G. (2022). Estimation of Global Irrigation Water Use by the Integration of Multiple Satellite Observations. *Water Resources Research*, *58*(3), e2021WR030031. https://doi.org/10.1029/2021WR030031

Zhang, Y., Zhang, Z., Ma, Z., Chen, J., Akbar, J., Zhang, S., Che, C., Zhang, M., & Cerdà, A. (2018). A review of preferential water flow in soil science. *Canadian Journal of Soil Science*, *98*(4), 604–618. https://doi.org/10.1139/cjss-2018-0046

Zhang, Y.-K., & Schilling, K. E. (2006). Effects of land cover on water table, soil moisture, evapotranspiration, and groundwater recharge: A Field observation and analysis. *Journal of Hydrology*, *319*(1), 328–338. https://doi.org/10.1016/j.jhydrol.2005.06.044

APPENDICES

APPENDIX A

SITE EQUIPMENT SUMMARIES

Appendix 1 - Table 1: Equipment Summary**.** Irrigation rates, periods of data, and sensor or lysimeter issues noted at monitoring sites.

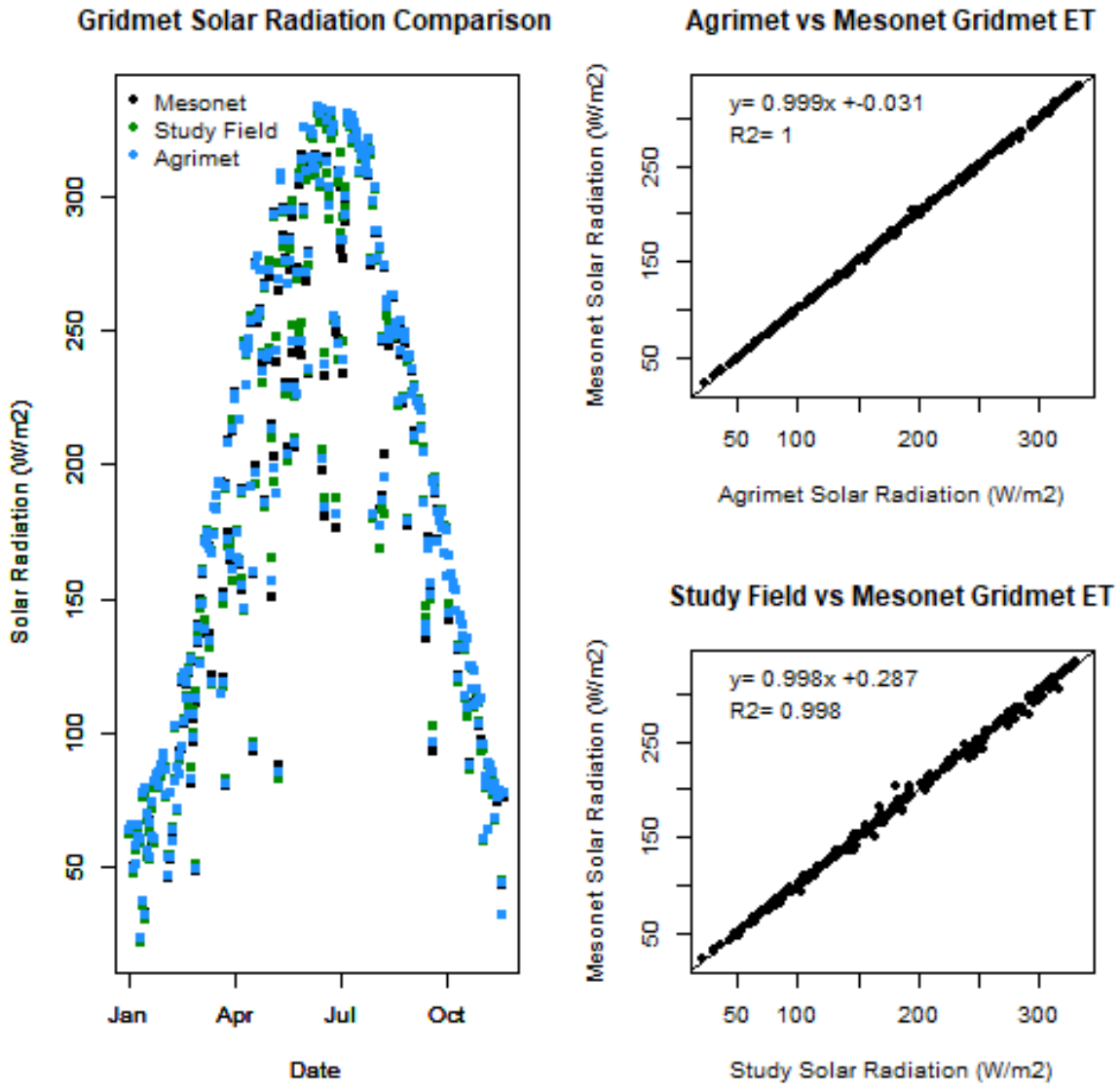
Name	Irrigation	Installation Date	Removal Date	Sensor Type	Data Gaps	Other Notes
F113	GSP	2023-04-15	NA	HOBO	2023-12-16 to 2024-04-20, 2024-06-13 to 2024-06-20, 2024-07-15 to 2024-07-30, 2024-09-08 to 2024-10-05, 2024-11-05 to 2025-04-12	Replaced HOBO sensors with METER on 2025-04-12
F121	RER	2023-06-30	NA	HOBO	None	Barley destruction in 2023, collocated METER and HOBO sensors
F123	RER	2023-04-15	2025-04-12	HOBO	2024-08-28 to 2024-09-09	60 cm lysimeter did not produce samplees
F128	RER	2024-04-20	NA	METER	None	
F133	GSP	2023-04-15	NA	HOBO	2024-01-14 to 2024-04-20, 2024-05-03 to 2024-05-07, 2024-05-16 to 2024-05-23,	No 90 cm soil VWC data in 2024, replaced with METER sensors on 2025-04-12

					2024-05-28 to 2024-06-05	
F143	GSP	2024-04-20	NA	METER	None	

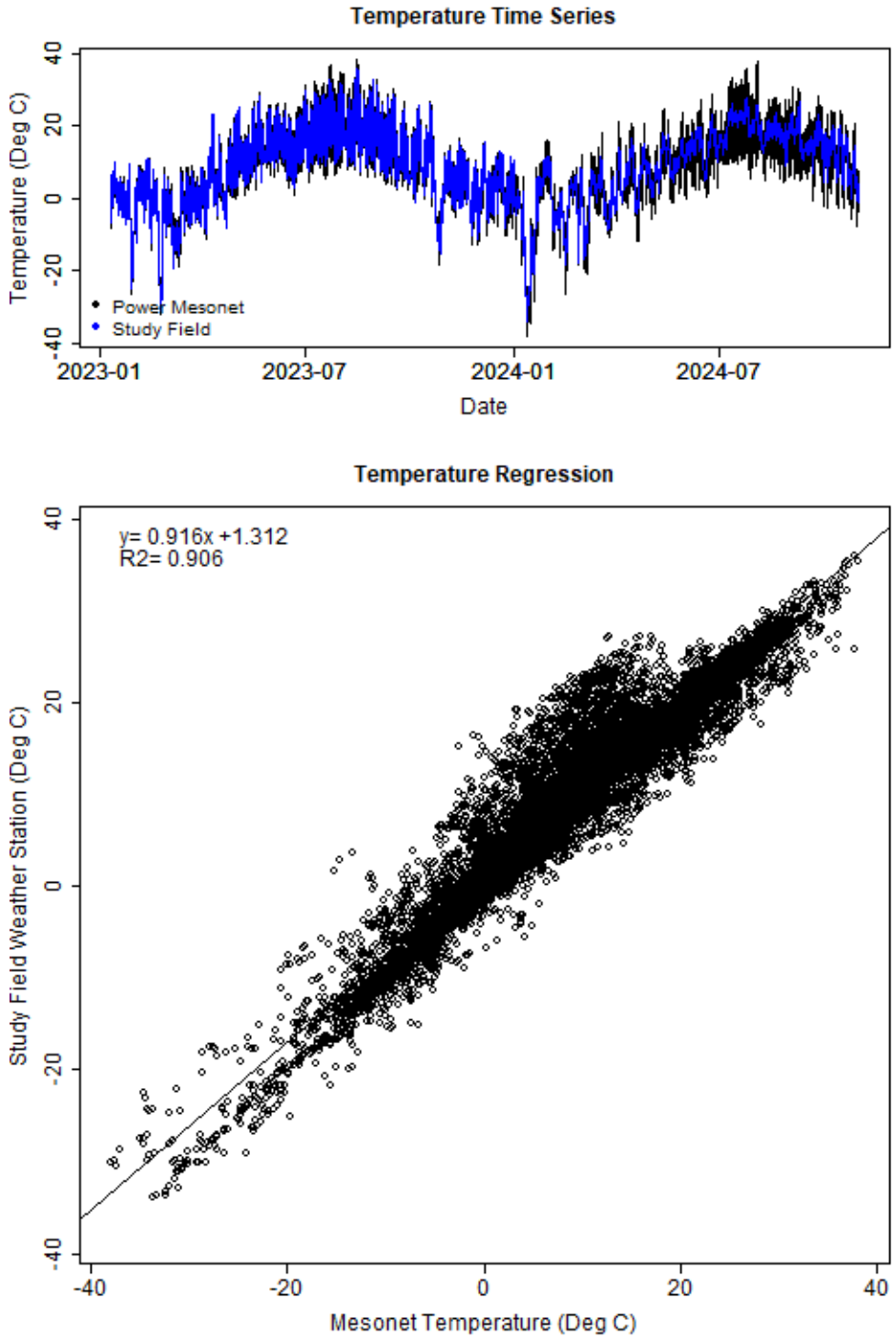
Sites F113, F123, and F133 were all installed prior to seeding in 2023, and F121 was added during the first irrigation cycle. The barley crop over F121 was pressed into the mud from the recent irrigation and completely destroyed for the remainder of the 2023 growing season. Sites F113 and F133 both experienced sensor shorting and resulting data gaps during the summer of 2024. Sites F128 and F143 were installed one week after seeding in 2024 with METER sensors. At both sites, recently seeded wheat was protected with an elevated wood board and canopy closure was satisfactory. Sensors at sites F113 and F133 were replaced with METER sensors prior to seeding in 2025. METER sensors were added in addition to HOBO sensors, which were still fully functional at F121, to facilitate in-field sensor assessment. Site F123 was removed before seeding in 2025 due to the lack of lysimeter samples collected by the 60 cm lysimeter and the fact that HOBO sensors had died over the winter.

APPENDIX B

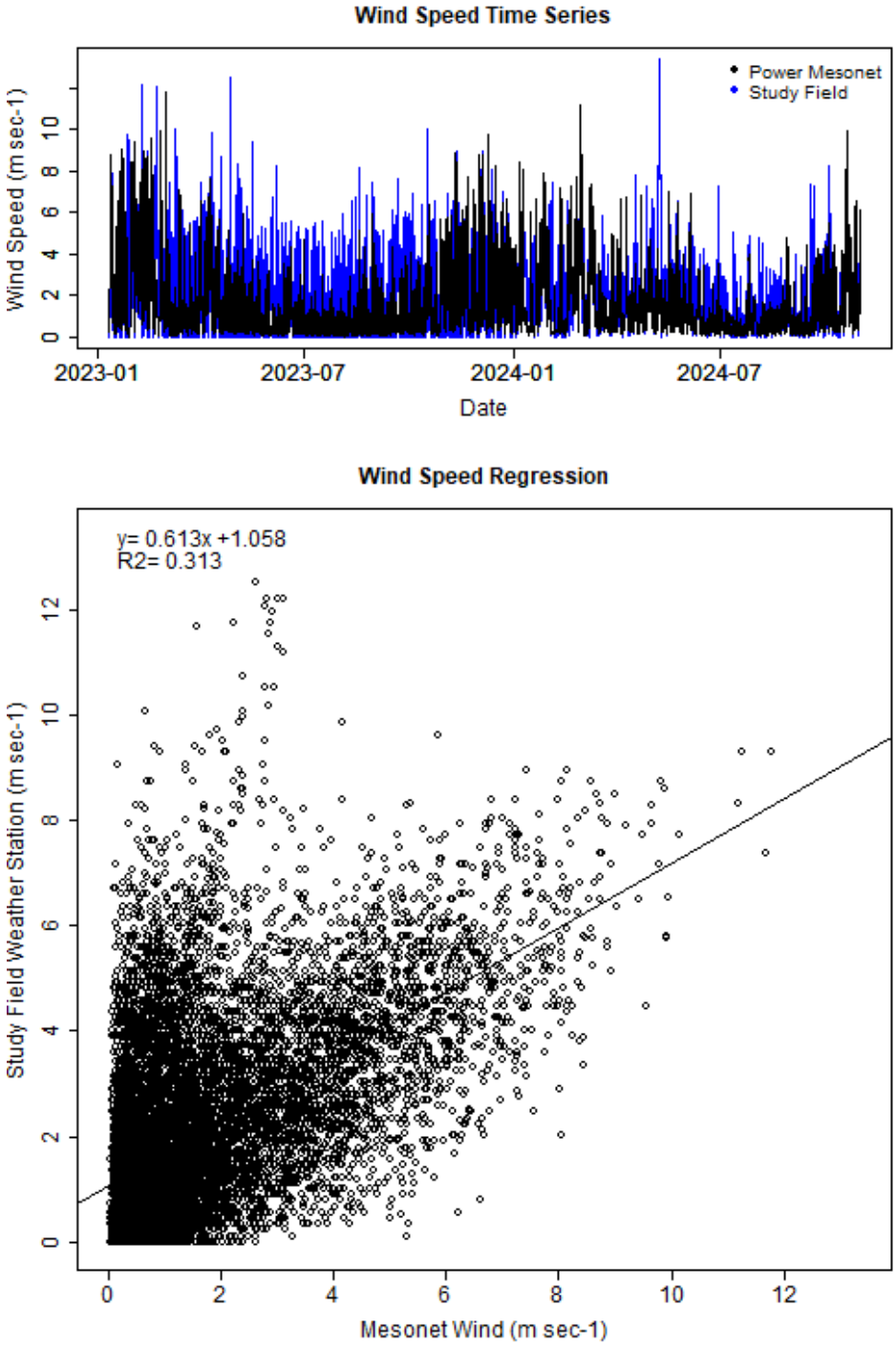
FAIRFIELD WEATHER PARAMETER VARIABILITY ASSESSMENT



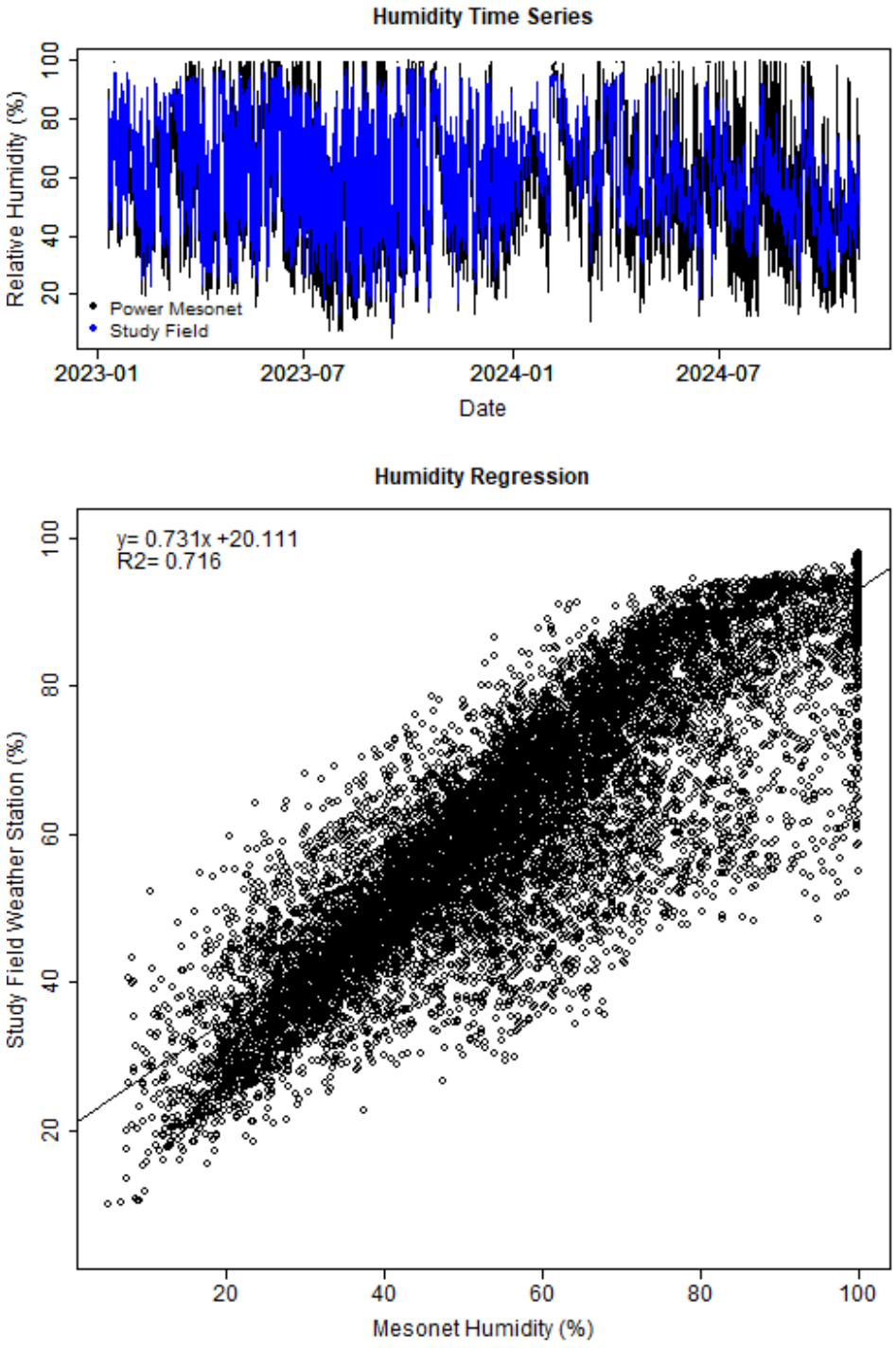
Appendix 2 – Figure 1: Solar Radiation Variability. Left panel- Summer time series solar radiation using Gridmet data for Mesonet site (black), study field (green), and Agrimet site (blue). Upper right panel- regression between Agrimet and Mesonet sites' solar radiation. Lower right panel- regression between study field and Mesonet site solar radiation.



Appendix 2 – Figure 2: Temperature Variability. Top panel- Time series temperature data for 2023 and 2024 from Mesonet "mdapower" site and study field. Lower panel- Temperature regression, with slope of 0.91 and R^2 of 0.90.



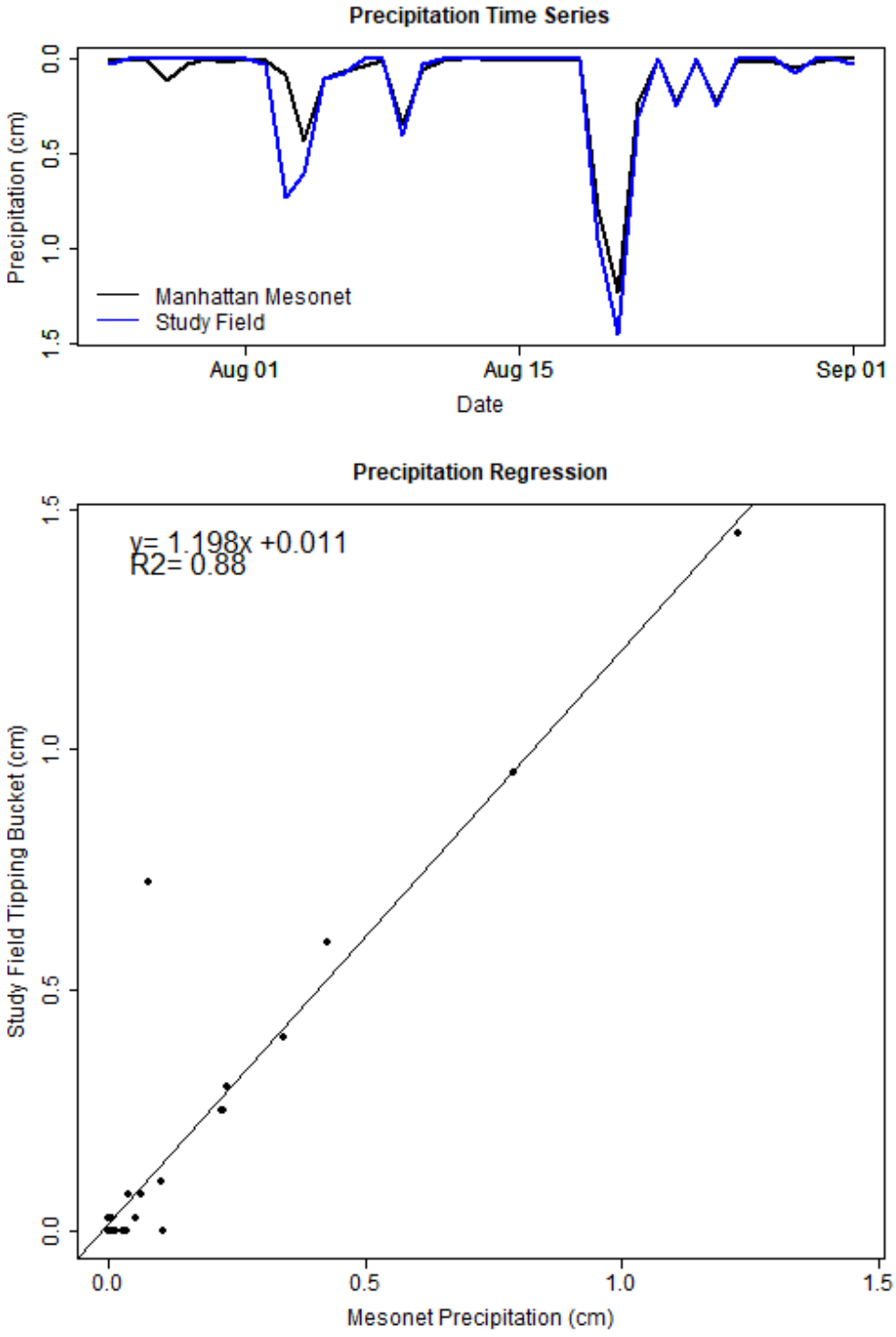
Appendix 2 – Figure 3: Wind Variability. Top panel- Time series wind data for 2023 and 2024 from Mesonet "mdapower" site and study field. Lower panel- Wind regression, with slope of 0.61 and R^2 of 0.31.



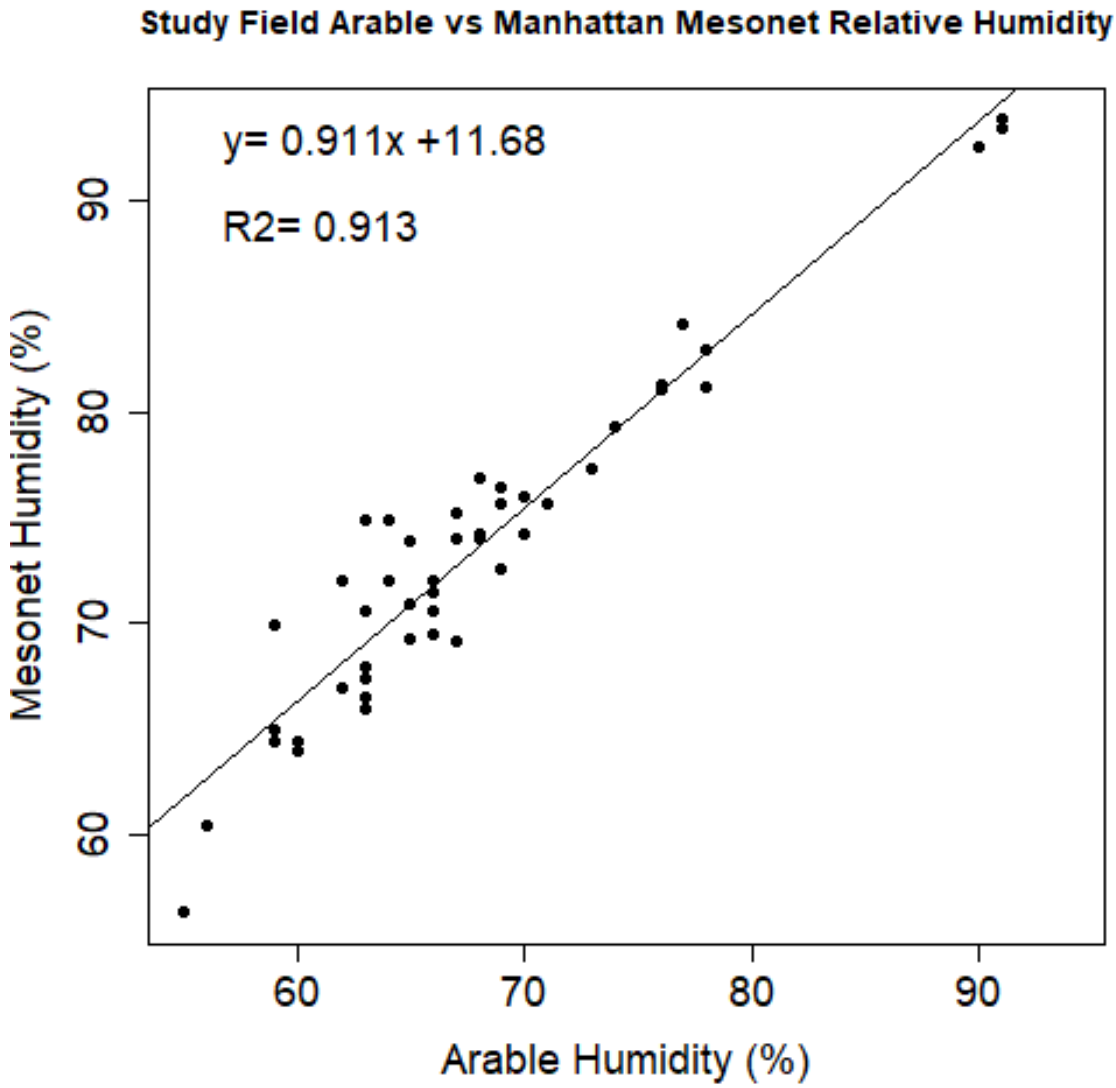
Appendix 2 – Figure 4: Humidity Variability. Top panel- Time series humidity data for 2023 and 2024 from Mesonet "mdapower" site and study field. Lower panel- Humidity regression, with slope of 0.73 and R^2 of 0.71.

APPENDIX C

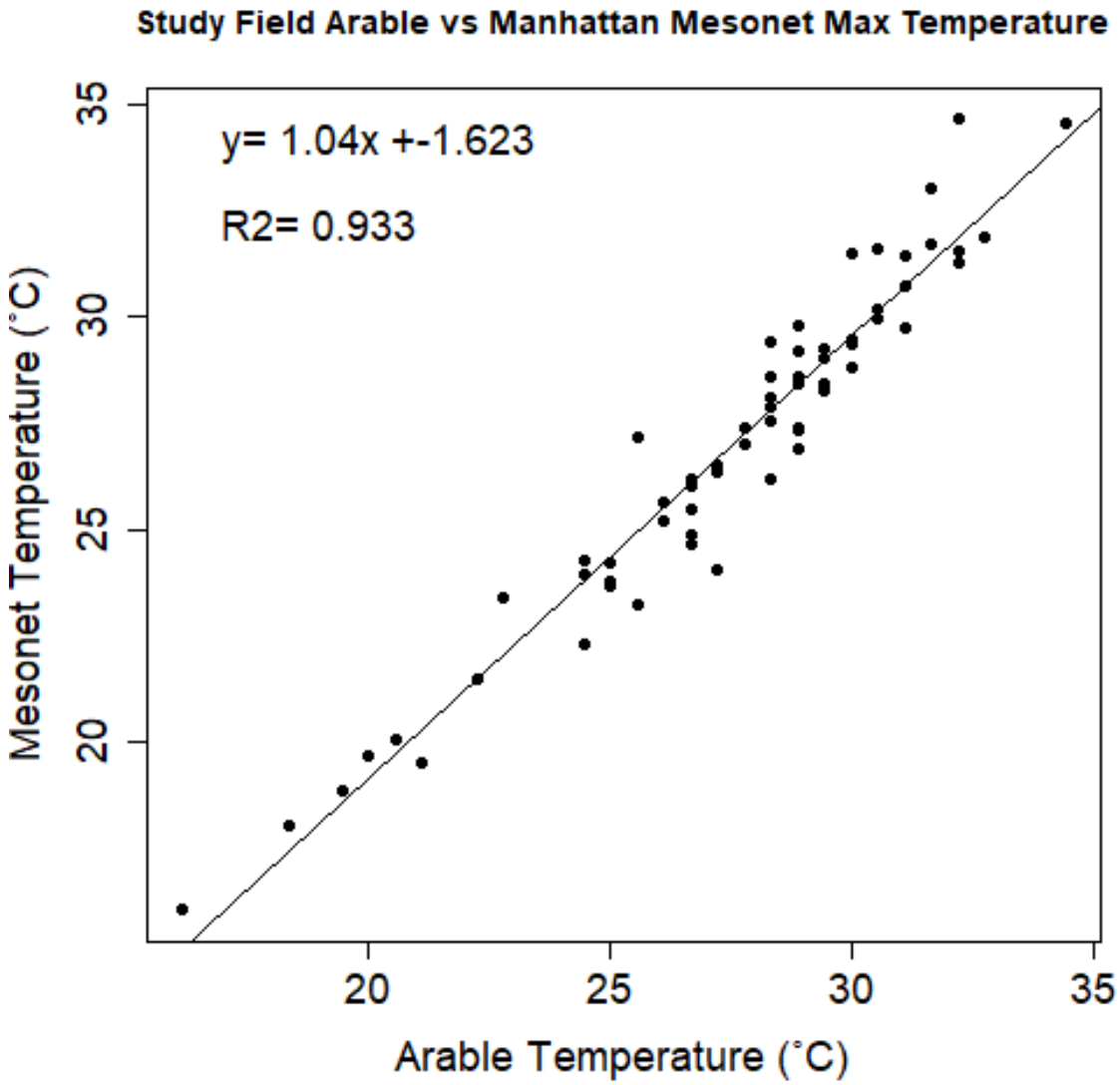
GALLATIN WEATHER PARAMETER VARIABILITY ASSESSMENT



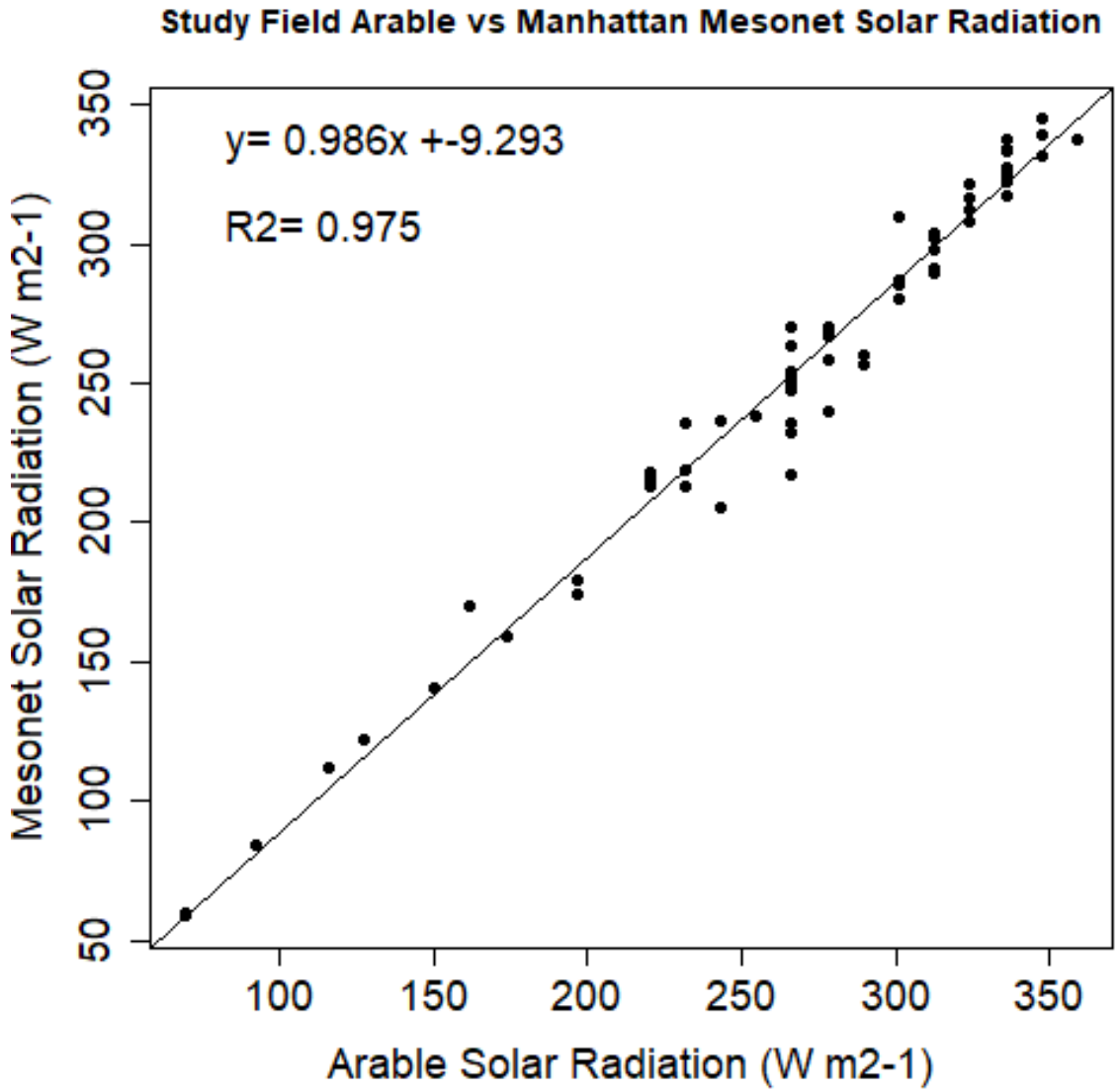
Appendix 3 - Figure 1: Precipitation Variability**.** Top panel- Time series precipitation data for 2023 from Mesonet "mdamanha" site and study field. Right panel- Precipitation regression, with slope of 1.19 and R^2 of 0.88.



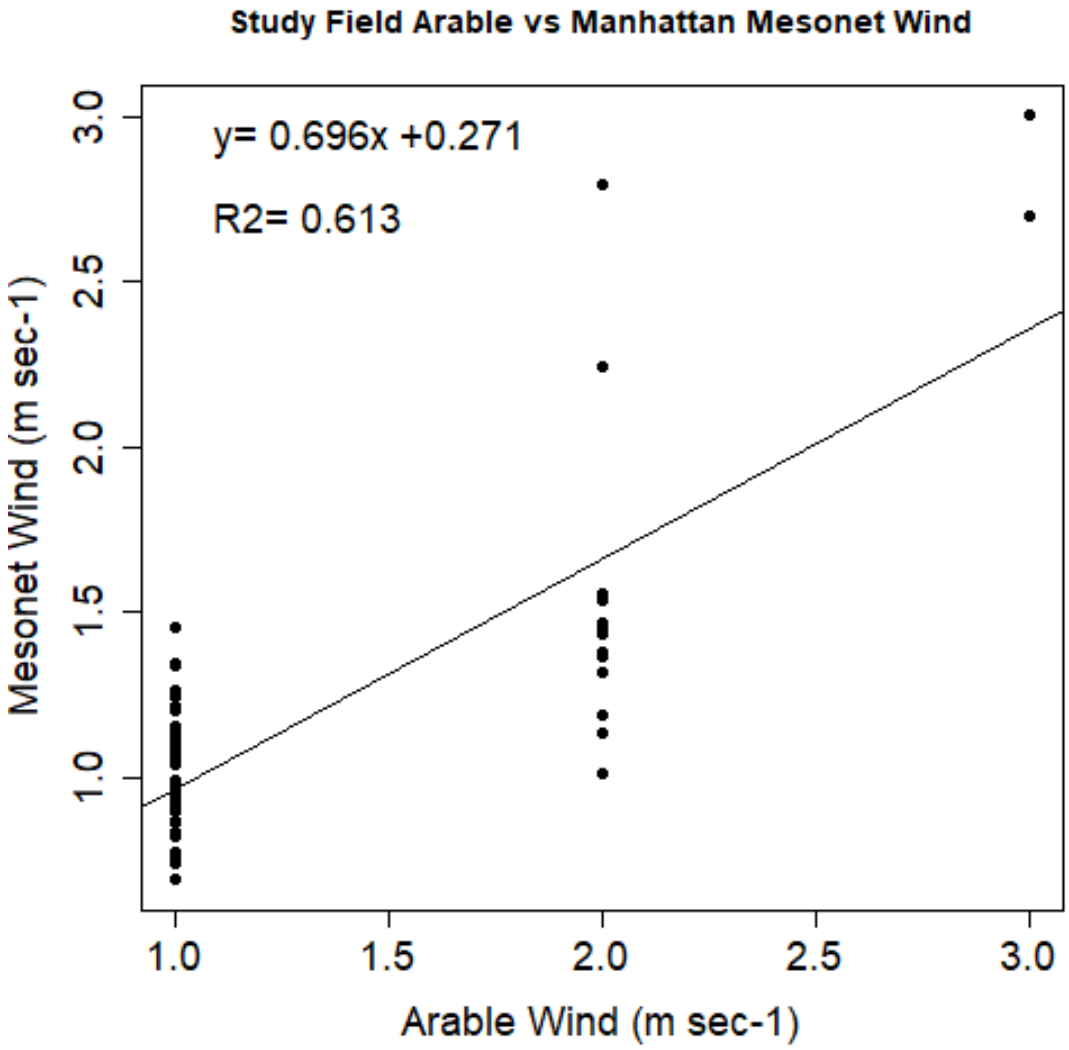
Appendix 3 - Figure 2: Humidity Variability. Humidity data for 2023 Mesonet "mdamanha" site and Arable sensor at study field, with a slope of 0.91 and an R^2 of 0.91.



Appendix 3 - Figure 3: Temperature Variability. Temperature data for 2023 Mesonet "mdamanha" site and Arable sensor at study field, with a slope of 1.04 and a R^2 of 0.93.



Appendix 3 - Figure 4: Solar Radiation Variability. Solar radiation data for 2023 Mesonet "mdamanha" site and Arable sensor at study field, with a slope of 0.99 and an R^2 of 0.98.



Appendix 3 - Figure 5: Wind Variability. Wind data for 2023 Mesonet “mdamanha” site and Arable sensor at study field, with a slope of 0.7 and an R^2 of 0.61.